# MASS SPECTROMETRY STUDIES

# OF PEPTIDES CATIONIZED BY TRIVALENT METAL IONS

by

JULIETTE JOAN COMMODORE

CAROLYN J. CASSADY, COMMITTEE CHAIR

GREGORY J. SZULCZEWSKI
JOHN B. VINCENT
MARTIN BAKKER
MATTHEW JENNY

A DISSERTATION

Submitted in partial fulfillment of the requirements
for the degree of Doctor of Philosophy
in the Department of Chemistry
in the Graduate School of
The University of Alabama

TUSCALOOSA, ALABAMA

2018

Copyright Juliette Joan Commodore 2018
ALL RIGHTS RESERVED

ABSTRACT

The field of proteomics is dedicated to understanding how a protein's structure and function relates to human health and disease. Peptide sequencing by mass spectrometry is important to the proteomics movement. Unfortunately, sequencing of many peptides and proteins, such as those with residues containing acidic and neutral side chains, can be difficult. Acidic side chains undergo facile deprotonation that make analysis challenging and can hinder formation of positive mode ions. New methods of sample preparation and dissociation techniques are needed to increase sequence information. This dissertation includes an extensive study of the effects on electron transfer dissociation (ETD) mass spectrometry of biological and model acidic non-phosphorylated and phosphorylated peptides adducted to trivalent lanthanide metal cations. Mass spectra contained herein provide abundant information about the primary structure of peptides.

The ETD process requires multiply positively charged ions that can be difficult to obtain with acidic peptides. This work demonstrates that addition of trivalent lanthanide metal cations allows highly acidic peptides to be analyzed by ETD by forming multiply positively charged precursor ions by electrospray ionization (ESI).

Using trivalent lanthanide cations as ionizing agents yields extensive sequence information for highly acidic peptides including definitive identification of phosphorylation sites. Peptides forming $[M + Met + H]^{4+}$ and $[M + Met]^{3+}$ generate full sequence coverage in many cases, but $[M + Pr - H]^{2+}$ generates less sequence coverage. (Met is the trivalent metal cation.)

The spectra contain primarily a mix of non-metallated and metal adducted c- and z- ions. All metallated product ions incorporate at least two acidic sites or a highly acidic phosphoresidue, which strongly suggests that the trivalent metal cation coordinates with residues that contain highly acidic side chains. All trivalent lanthanide cations are suitable for sequencing highly acidic peptides except europium and radioactive promethium. ETD spectra contain high signal-to-noise ratios making identification of product ions straightforward. Sequence coverage generally improves with increasing peptide chain length.

Trivalent chromium enhances protonation of neutral peptides, which is important to ETD analysis. ESI conditions, particularly drying and nebulizing gas pressures are critical to formation of $[M + 2H]^{2+}$ by neutral peptides.

.

# DEDICATION

This dissertation is dedicated to my family especially my parents, Jones and Ursula Commodore, my sister, Jo-Anne Kethline Commodore, and my husband and son Senyo and Israel Botoklo. Their love and support provided me with the strength that I needed to maintain my sanity while completing this important chapter of my life.

# LIST OF ABBREVIATIONS AND SYMBOLS

| | |
|---|---|
| AC | alternating current |
| ACN | acetonitrile |
| AI | absolute intensity |
| Ala | alanine (A) |
| Arg | arginine (R) |
| Asn | asparagine (N) |
| Asp | aspartic acid (D) |
| bar | unit of pressure |
| cal | calorie |
| c | centi (prefix) |
| $Cr^{3+}$ | chromium trivalent cation |
| CID | collision-induced dissociation |
| Cys | cysteine (C) |
| Da | Dalton |
| DC | direct current |
| DIC | 1,3-diisopropylcarbodiimide |
| DMF | N, N-dimethylformamide |
| e-* | low energy electron |
| eV | electron volt |
| EGF | epidermal growth factor |

| | |
|---|---|
| ESI | electrospray ionization |
| ECD | electron capture dissociation |
| ETD | electron transfer dissociation |
| ETnoD | electron transfer no dissociation |
| ExD | electron-based dissociation |
| FA | formic acid |
| Fmoc | 9-fluoroenylmethoxycarbonyl |
| FT | Fourier transform |
| FWHM | full width half maximum |
| g | grams |
| GA | gas-phase acidity |
| GB | gas-phase basicity |
| Glu | glutamic acid (E) |
| Gln | glutamine (Q) |
| Gly | glycine (G) |
| HCT | high capacity trap |
| His | histidine (H) |
| HOBt | 1-hydroxybenxotriazole |
| HPLC | high performance liquid chromatography |
| HPP | human proteome project |
| HUPO | human proteome organization |
| hr | hour |
| hsp | heat shock protein fragment |
| ICC | ion charge control |
| ICR | ion cyclotron resonance |

| | |
|---|---|
| IE | ionization energy |
| Ile | isoleucine (I) |
| I/M | ion/molecule |
| IRMPD | infrared radiation multiphoton dissociation |
| J | joule |
| k | kilo (prefix) |
| KE | kinetic energy |
| L | liter |
| LC | liquid chromatography |
| Leu | leucine (L) |
| LMWCr | low-molecular-weight chromium-binding peptide |
| Lys | lysine (K) |
| MALDI | matrix-assisted laser desorption ionization |
| Met | methionine (M) |
| MS | mass spectrometry (or mass spectrometer) |
| μ | micro (prefix) |
| m | milli (prefix) |
| m | meter |
| $[M + H]^+$ | protonated peptide ion |
| $[M + Met]^{n+}$ | metallated peptide ion |
| $[M + Met + H]^{n+}$ | metallated peptide ion with extra proton |
| $[M + Met – H]^{n+}$ | metallated peptide ion lacking a hydrogen |
| M | moles/liter (concentration) |
| MeOH | methanol |
| Met | methionine (M) |

| | |
|---|---|
| mol | mole(s) |
| MS | mass spectrometry |
| MS/MS | tandem mass spectrometry |
| $MS^n$ | tandem mass spectrometry |
| *m/z* | mass-to-charge ratio |
| n | nano (prefix) |
| NETD | negative electron transfer dissociation |
| $–NH_2$ | amide |
| NMP | n-methylpyrrolidinone |
| NMR | nuclear magnetic resonance |
| Ω | angular frequency |
| p | pico (prefix) |
| pE | pyroglutamate |
| Phe | phenylalanine (F) |
| PIP | piperidine |
| $Pr^{3+}$ | praseodymium trivalent cation |
| Pro | proline (P) |
| pSer | phosphoserine (pS) |
| pThr | phosphothreonine (pT) |
| pTyr | phosphotyrosine (pY) |
| PA | proton affinity |
| PTM | post-translational modification |
| QIT | quadrupole ion trap |
| rf | radio frequency |
| s | second |

| | |
|---|---|
| Ser | serine (S) |
| S/N | signal-to-noise ratio |
| SPPS | solid-phase peptide synthesis |
| TFA | trifluoroacetic acid |
| Thr | threonine (T) |
| TIPS | triisopropyl silane |
| TOF | time-of-flight |
| Trp | tryptophan (W) |
| Tyr | tyrosine (Y) |
| UW | Utah-Washington |
| Val | valine (V) |
| V | volt |

# ACKNOWLEDGMENTS

I would like to thank my research advisor, Dr. Carolyn J. Cassady, for her willingness to take me under her wing and shape me into a better chemist. I was able to succeed because of her continued support and extreme patience in molding me into the chemist that I am at present. Her chemistry knowledge leaves much to be envied, and she has taught me how to operate in an ethical and professional manner despite personal issues. She is by far the best mentor and advisor that I have ever encountered, and I will truly miss being her student.

Many thanks also to the members of my committee, Dr. John B. Vincent, Dr. Gregory Szulczewski, Dr. Martin Bakker, and Dr. Matthew Jenny for their invaluable input during my academic progress. Special thanks to Dr. Vincent for providing me with my first samples of lanthanide salts as well as continued discussions about my projects involving the trivalent metal compounds. I would also like to thank Dr. Qiaoli Liang for training me on the use and maintenance of the departmental mass spectrometers. Her input in spectral interpretation was very valuable.

Throughout my years in graduate school, I have been fortunate to be fully funded. Thank you to the National Institutes of Health (grant number 1R15GM109401A) and the National Science Foundation (grant number CHE-1609764). I would also like to thank the National Science Foundation CRIF program for providing the funds for the Bruker HCTultra PTM discovery system (CHE 0639003), which was my main instrument of use for my research projects.

I would like to thank the members of the Cassady group, past and present. Dr. Changgeng Feng, Dr. Chelsea Plummer, Nnenna Dieke, Ranelle Duke, Chelsea McMillen, Can Cui, Xinyao Jing, and Matt Mireles have provided a comfortable and professional environment to allow me to flourish. I will cherish our memories of all the conferences that we have attended and all the new places and sites we have experienced together. The many discussions when writing manuscripts or preparing for conferences allowed me to think critically and constructively in presenting my research information.

No amount of thanks will suffice when expressing my gratitude to my family. They never stopped encouraging me from so far away, and never doubted my ability to succeed even after not having physically visited them for almost 8 years. I would jokingly tell my friends that I am surviving off my parents' prayers because they always told me that God would take care of me no matter how trying or depressing my situation became. I would like to add a special dedication to my sister, Jo-Anne Kethline Commodore, who has supported me financially by taking on some of my debt. She is my number one fan. No amount of words can express how grateful I am for having her in my corner.

Last, but certainly not least, I would like to thank my husband, Senyo Komi Botoklo, and my son, Israel Sessime Botoklo. They came into my life at the time when I had hit a low point. They kept me afloat and supported me the rest of the way through my years in graduate school. I am excited to start the next phase of my life with them when I will be able to dedicate all my time to the growth of our family.

CONTENTS

ABSTRACT ……ii

DEDICATION……iv

LIST OF ABBREVIATIONS AND SYMBOLS ……v

ACKNOWLEDGMENTS ……...x

LIST OF TABLES……xvi

LIST OF FIGURES…….xvii

CHAPTER 1: AN OVERVIEW OF THE DISSERTATION…….1

References…….12

CHAPTER 2: INSTRUMENTATION, EXPERIMENTAL PROCEDURES AND THEORY..23

2.1 Overview…….23

2.2 Electrospray ionization ……..23

2.3 Quadrupole ion trap ……...26

2.4 Dissociation methods…….32

2.4.1 Collision-induced dissociation.……32

2.4.2 Electron transfer dissociation……...33

2.5 Peptide sequencing nomenclature……..40

2.6 Peptide synthesis……42

2.7 Amino acid structure……..46

References…….51

CHAPTER 3: THE EFFECTS OF TRIVALENT LANTHANIDE CATIONIZATION ON THE ELECTRON TRANSFER DISSOCIATION OF ACIDIC FIBRINOPEPTIDE B AND ITS ANALOGS ……55

3.1 Overview……55

3.2 Introduction……56

3.3 Experimental……..59

3.3.1 Mass spectrometry ……...59

3.3.2 Peptides……59

3.4 Results……60

3.4.1 Adduction of trivalent metal cations to peptides ……60

3.4.2 Electron transfer dissociation on $[M + Met - H]^{2+}$ ……..62

3.4.3 Electron transfer dissociation on $[M + Met]^{3+}$ ……66

3.4.4 Electron transfer dissociation on $[M + Met + H]^{4+}$ ……..71

3.5 Discussion……..71

3.5.1 Impact of metal ion properties ……71

3.5.2 Dissociation trends and sequence information ……85

3.6 Conclusions……89

References……91

CHAPTER 4: EFFECTS OF ACIDIC PEPTIDE SIZE AND SEQUENCE ON TRIVALENT PRASEODYMIUM ADDUCTION AND ELECTRON TRANSFER DISSOCIATION MASS SPECTROMETRY ……99

4.1 Overview……99

4.2 Introduction……..100

4.3 Experimental……103

4.3.1 Mass spectrometry ……103

4.3.2 Peptides……..104

4.4 Results and discussion ……104

4.4.1 Biological peptides……105

4.4.2 Model peptides……...114

4.5 Conclusions……..130

References……...132

CHAPTER 5: ELECTRON TRANSFER DISSOCIATION MASS SPECTROMETRY OF ACIDIC PHOSPHORYLATED PEPTIDES CATIONIZED WITH TRIVALENT PRASEODYMIUM…….140

5.1 Overview……..140

5.2 Introduction……..141

5.3 Experimental……145

5.3.1 Mass spectrometry…….145

5.3.2 Peptides……..146

5.4 Results and discussion ……146

5.4.1 Biological peptides……147

5.4.1.1. ESI ion formation…….147

5.4.1.2 Electron transfer dissociation of biological peptides……151

5.4.2 Model peptides……...169

5.4.2.1 Ion formation for model peptides ……172

5.4.2.2 Electron transfer dissociation of model peptides……..172

5.4.3 Dissociation trends and structural effects ……..174

5.5 Conclusions……195

References……196

CHAPTER 6: OPTIMIZATION OF ELECTROSPRAY IONIZATION CONDITIONS TO ENHANCE FORMATION OF DOUBLY PROTONATED PEPTIDE IONS WITH AND WITHOUT ADDITION OF CHROMIUM(III)……..205

6.1 Overview……...205

6.2 Introduction……...206

6.3 Experimental……207

6.3.1 Mass spectrometry……..207

6.3.2 Peptides……...208

6.4 Results and discussion ……208

6.4.1 Effects of ESI gases……...210

6.4.2 Effects of ESI potentials……214

6.4.3 Effects of sample preparation and storage container……223

6.5 Conclusions……228

References……..235

CHAPTER 7: CONCLUDING REMARKS ……..239

References……..244

LIST OF TABLES

4.1. ESI ion formation and corresponding ETD product ions for acidic biological peptides cationized by $Pr^{3+}$ ..... 106

4.2. ESI ion and corresponding ETD product ions for acidic model peptides cationized by $Pr^{3+}$. ..... 115

4.3. ESI ion formation and corresponding ETD product ions for model tri- and hexapeptides cationized by $Pr^{3+}$. ..... 118

5.1. Experimental GAs ($\Delta G_{acid}$) for acid and phosphorylated amino acid amides ..... 143

5.2. ESI ion formation and corresponding ETD product ions for acidic phosphorylated biological peptides cationized by $Pr^{3+}$. ..... 148

5.3. ESI ion formation and corresponding ETD product ions for phosphorylated model peptides cationized by $Pr^{3+}$. ..... 170

LIST OF FIGURES


2.1. Schematic of desolvation of ions in ESI source……..25

2.2. Schematic of ESI source for the Bruker HCTultra PTM Discovery System……..25

2.3. Schematic showing transfer of ions from ion source to ion trap.……27

2.4. Mathieu stability diagram (used with permission from reference 15).……31

2.5. Diagram showing overlap of ions in a spherical vs. a linear ion trap.…….32

2.6. ETD reaction showing formation of ions in the nCI source and product ion formation in the ion trap. …….34

2.7. ESI and nCI source setup in Bruker HCTultra PTM Discovery System mass spectrometer showing positive and negative ions trapped in the QIT (used with permission from reference 19).……...36

2.8. The Cornell mechanism for N-Cα bond cleavage in ETD of peptides and proteins……37

2.9. The Utah-Washington mechanism for N-Cα bond cleavage in ETD of peptides and proteins.……38

2.10. Peptide sequence nomenclature for MS/MS.……..41

2.11. Fmoc protective group attached to a generic amino acid residue.……..43

2.12. Outline of steps involved in SPSS peptide synthesis.…….45

2.13. Amino acids with acidic side chains.……..46

2.14. Amino acids with aliphatic side chains.……..47

2.15. Amino acids with basic side chains. ……...48

2.16. Amino acids with aromatic side chains. (Histidine also contains an aromatic side chain but was already included in Figure 2.15…….... 48

2.17. Amino acids with amine side chains…….....49

2.18. Amino acids with hydroxyl side chains. (Tyrosine also contains a hydroxyl amino acid side chain but was already included with the amino acids with aromatic side chains in Figure 2.16.)……..49

2.19. Amino acids with side chains containing sulfur…….50

2.20. Amino acids with phosphorylated side chains.…….....50

3.1. ESI mass spectra generated from 10:1 molar ratio mixtures of $Pr^{3+}$ with (a) l fibrinopeptide B, (b) [$Glu^1$]-fibrinopeptide B, and (c) des-$Arg^{14}$-[$Glu^1$]-fibrinopeptide B……..……61

3.2. ETD mass spectra of (a) $[M + Pr – H]^{2+}$, (b) $[M + Pr]^{3+}$, and (c) $[M + Pr + H]^{4+}$ for fibrinopeptide B produced by addition of $Pr^{3+}$……..64

3.3. ETD mass spectrum of $[M + Pr – H]^{2+}$ for [$Glu^1$]-fibrinopeptide B……..…….65

3.4. ETD mass spectrum of $[M + Pr – H]^{2+}$ for des-$Arg^{14}$- [$Glu^1$]-fibrinopeptide B…….67

3.5. ETD mass spectra of (a) $[M + Eu – H]^{2+}$, (b) $[M + Eu]^{3+}$, and (c) $[M + Eu + H]^{4+}$ for fibrinopeptide B produced by addition of $Eu^{3+}$…….68

3.6. ETD mass spectrum of $[M + Eu – H]^{2+}$ for [$Glu^1$]-fibrinopeptide B……...……...69

3.7. ETD mass spectrum of $[M + Eu – H]^{2+}$ for des-$Arg^{14}$-[$Glu^1$]-fibrinopeptide B..……...70

3.8. ETD mass spectrum of $[M + Pr]^{3+}$ for [$Glu^1$]-fibrinopeptide B……..72

3.9. ETD mass spectrum of $[M + Pr]^{3+}$ for des-$Arg^{14}$-[$Glu^1$]-fibrinopeptide B…….73

3.10. ETD mass spectrum of $[M + Eu]^{3+}$ for [$Glu^1$]-fibrinopeptide B…….74

3.11. ETD mass spectrum of $[M + Eu]^{3+}$ for des-$Arg^{14}$-[$Glu^1$]-fibrinopeptide B……...75

3.12. ETD mass spectra of $[M + Pr + H]^{4+}$ for (a) [$Glu^1$]-fibrinopeptide B, and (b) des-$Arg^{14}$-[$Glu^1$]-fibrinopeptide B……76

3.13. ETD mass spectra of $[M + Met + H]^{4+}$ for fibrinopeptide B produced by adduction to (a) $La^{3+}$, (b) $Sm^{3+}$, (c) $Ho^{3+}$, and (d) $Lu^{3+}$……..79

3.14. ETD mass spectrum of $[M + Cr]^{3+}$ for fibrinopeptide B……....80

3.15. ETD mass spectrum of $[M + Yb]^{3+}$ for fibrinopeptide B……84

3.16. ETD mass spectra of $[M + 2H]^{2+}$ for (a) fibrinopeptide B, (b) $[Glu^1]$-fibrinopeptide B, and **(c)** des-$Arg^{14}$-$[Glu^1]$-fibrinopeptide B……..……88

4.1. ETD mass spectra of $[M + Pr + H]^{4+}$ for (a) EGF(985-996), (b) hirudin(54-65), and (c) casein kinase II substrate……...……...……110

4.2. ETD mass spectrum of $[M + Pr + H]^{4+}$ for ACTH(22-39)……...……111

4.3. ETD mass spectra of $[M + Pr]^{3+}$ for (a) EGF(985-996), (b) hirudin(54-65), and (c) gastrin I(1-14)……..……112

4.4. ETD mass spectrum of $[M + Pr]^{3+}$ for ACTH(22-39)……..113

4.5. ETD mass spectrum of $[M + Pr]^{3+}$ for casein kinase II substrate…..…..……...119

4.6. ETD mass spectra of $[M + Pr - H]^{2+}$ for (a) LMWCr peptide, (b) EGF(985-996), (c) hirudin(54-65), and (d) human gastrinI(1-14)……..120

4.7. CID mass spectrum of $[M + Pr + H]^{4+}$ for fibrinopeptide B…….……121

4.8. CID mass spectrum of $[M + Pr]^{3+}$ for fibrinopeptide B……....122

4.9. ETD mass spectra of $[M + Pr - H]^{2+}$ for (a) E6, (b) E7, (c) D7, (d) E8, and (e) D10……...125

4.10. ETD mass spectra of $[M + Pr]^{3+}$ for (a) DAAAAAA, (b) EAAAAAA, (c) AAADAAA, (d) AAAEAAA, and (e) $[M + Pr - H]^{2+}$ for AAAAAAE……127

4.11. ETD mass spectra of $[M + Pr]^{3+}$ for (a) DAADAAD and (b) EAAEAAE…….....…….....128

4.12. CID mass spectrum of $[M + Pr]^{3+}$ for EAAAAAA…….……...……...129

5.1**.** ETD mass spectrum of $[M + Pr + H]^{4+}$ for heat shock protein fragment (hsp)……153

5.2. ETD mass spectrum of $[M + Pr]^{3+}$ for EGF (988-998)…….154

5.3. ETD mass spectrum of $[M + Pr]^{3+}$ for heat shock protein fragment (hsp)……...155

5.4. ETD mass spectrum of $[M + Pr]^{3+}$ for EDDpSDEEN……...……...156

5.5. ETD mass spectrum of $[M + Pr]^{3+}$ for EDDpTDEEN……...……...157

5.6. ETD mass spectrum of $[M + Pr]^{3+}$ for EDDpYDEEN…….....158

5.7. ETD mass spectrum of $[M + Pr]^{3+}$ for PDGF (pTyr Y-8P)……..160

5.8. ETD mass spectrum of $[M + Pr - H]^{2+}$ for PDGF (pTyrL-5P)……161

5.9. ETD mass spectrum of $[M + Pr - H]^{2+}$ for EGF (DL-6)……..162

5.10. ETD mass spectrum of $[M + Pr - H]^{2+}$ for PDGF(pTyr Y-8P……..……163

5.11. ETD mass spectrum of $[M + Pr - H]^{2+}$ for EGF(988-998)……..…….164

5.12. ETD mass spectrum of $[M + Pr - H]^{2+}$ for hsp…….165

5.13. ETD mass spectrum of $[M + Pr - H]^{2+}$ for EDDpSDEEN.……166

5.14. ETD mass spectrum of $[M + Pr - H]^{2+}$ for EDDpTDEEN……..167

5.15. ETD mass spectrum of $[M + Pr - H]^{2+}$ for EDDpYDEEN……..168

5.16. ETD mass spectrum of $[M + Pr - H]^{2+}$ for pSAAAAA (pSA5)……..…….176

5.17. ETD mass spectrum of $[M + Pr - H]^{2+}$ for pTAAAAA (pTA5)……..177

5.18. ETD mass spectrum of $[M + Pr - H]^{2+}$ for pYAAAAA (pYA5)……..178

5.19. ETD mass spectrum of $[M + Pr - H]^{2+}$ for pSAAAAAAA (pSA7)…….179

5.20. ETD mass spectrum of $[M + Pr - H]^{2+}$ for pTAAAAAAA (pTA7)…….180

5.21. ETD mass spectrum of $[M + Pr - H]^{2+}$ for pYAAAAAAA (pYA7)…….……...181

5.22. ETD mass spectrum of $[M + Pr - H]^{2+}$ for AApSAAA (A2pSA3)……..182

5.23. ETD mass spectrum of $[M + Pr - H]^{2+}$ for AApTAAA (A2pTA3)……..……183

5.24. ETD mass spectrum of $[M + Pr - H]^{2+}$ for AApYAAA (A2pYA3)…….184

5.25. ETD mass spectrum of $[M + Pr - H]^{2+}$ for AAApSAAAA (A3pSA4) ……185

5.26. ETD mass spectrum of $[M + Pr - H]^{2+}$ for AAApTAAAA (A3pTA4)……186

5.27. ETD mass spectrum of $[M + Pr - H]^{2+}$ for AAApYAAAA (A3pYA4).....187

5.28. ETD mass spectrum of $[M + Pr - H]^{2+}$ for AAAApSA (A4pSA)……188

5.29. ETD mass spectrum of $[M + Pr - H]^{2+}$ for AAAApTA (A4pTA)……189

5.30. ETD mass spectrum of $[M + Pr - H]^{2+}$ for AAAApYA (A4pYA)……...190

5.31. ETD mass spectrum of $[M + Pr – H]^{2+}$ for AAAAAApSA (A6pSA).....191

5.32. ETD mass spectrum of $[M + Pr – H]^{2+}$ for AAAAAApTA (A6pTA)……..192

5.33. ETD mass spectrum of $[M + Pr – H]^{2+}$ for AAAAAApYA (A6pYA)…….193

6.1. ESI mass spectrum of A7 (a) without $Cr^{3+}$ and (b) with $Cr^{3+}$ at a 1:10 molar ratio of A7:Cr……209

6.2. Relative intensity of ions formed as a function of nebulizer gas pressure in psi for (a) A7 and (b) A3KA3……..211

6.3. Relative intensity of ions formed as a function of drying gas flow rate in L/min for (a) A7 and (b) A3KA3……..213

6.4. Relative intensity of ions formed as a function of drying gas temperature in °C for (a) A7 and (b) A3KA3…….....215

6.5. Tandem mass spectra of A7 showing (a) CID of $[M + Cr – H + 2H_2O]^{2+}$ and (b) CID $MS^3$ of $[M + Cr – H + H_2O]^{2+}$….....216

6.6. Relative intensity of ions formed as a function of the absolute value of the capillary entrance potential in V for (a) A7 and (b) A3KA3……218

6.7. Relative intensity of ions formed as a function of the absolute value of the capillary exit potential in V for (a) A7 and (b) A3KA3……...219

6.8. Relative intensity of ions formed as a function of skimmer potential in V for (a) A7 and (b) A3KA3……..221

6.9. Relative intensity of ions formed as a function of capillary exit to skimmer potential ratio for (a) A7 and (b) A3KA3.……...222

6.10. Relative intensity of ions formed for A7 with (a) unrinsed and (b) rinsed microcentrifuge tubes with varying vendors and colors……...224

6.11. Relative intensity of ions formed for A3KA3 with (a) unrinsed and (b) rinsed microcentrifuge tubes with varying vendors and colors….....225

6.12. ESI mass spectra of the solvent system (ACN:$H_2O$ at 50:50 v:v) with erucimide contaminant in colorless safe-lock microcentrifuge tubes after (a) no rinse, (b) 2 rinses, and (c) 4 rinses with IPA solvent.....229

6.13. ESI mass spectrum of A7 in the presence of $Cr^{3+}$ using optimized parameters. The ratio of $[M + 2H]^{2+}$ intensity to $[M + H]^{+}$ intensity is 4:1.....230

6.14. CID mass spectrum of $[M + 2H]^{2+}$ for A7.....232

6.15. CID mass spectrum of $[M + H]^{+}$ for A7……...233

6.16. ETD mass spectrum of $[M + 2H]^{2+}$ for A7…….....234

## CHAPTER 1: AN OVERVIEW OF THE DISSERTATION

The successful completion of the Human Genome Project in 2003 led to the development of the "omics" movement.[1,2] In 2011, the Human Proteome Organization (HUPO) launched the Human Proteome Project (HPP) comprised of the Chromosome-based Human Proteome Project (C-HPP) and the Biology/Disease Human Proteome Project (B/D HPP). One of the goals of the HPP is to identify and characterize at least one protein product from each of the 20,300 protein-coding genes.[3] HUPO intends to eventually generate a map of the protein architecture of the human body to become a tool for deciphering biological function and advance diagnosis and treatment of diseases.[4] Mass spectrometry serves as an important tool in the HPP for deciphering polypeptide coding and sequence information.[3,5-13] The development of electrospray ionization (ESI) and matrix-assisted laser desorption ionization (MALDI) in the 1990s allowed large molecules to be successfully analyzed.[14-16] These two ionization methods, ESI and MALDI, ushered in even more widespread utilization of mass spectrometry (MS) in the analysis of biopolymers. The HPP is well underway with around 87% of target proteins in Phase I of C-HPP confidently identified.[17]

Proteins have four levels of structure.[18] The primary structure contains the coding for the amino acid residues that make up the polypeptide sequence. Understanding the structure, function and energetic properties of functional groups on side chains of amino acid residues requires knowledge about the primary structure of the protein.[19-22] A generic polypeptide contains an amine group at the N-terminus and a C-terminal carboxylic acid. Secondary

structures contain beta-sheets, helices, and other distorted regions formed due to hydrogen bonding between amino acid residues along a polypeptide sequence. Tertiary levels involve non-covalent interactions between secondary forms to facilitate folding of polypeptides into their lowest energy structures. Tertiary structures can be referred to as protein subunits that interact to form the final level called quaternary structures that make up the entire protein. The information elucidated from protein structure and sequence can be utilized for designing drugs targeting specific protein function in medicinal chemistry.[23-26]

Two major methods for the sequencing of peptides are Edman degradation and mass spectrometry.[27] Edman degradation involves a series of chemical reactions that cleave and identify amino acid residues at the N-terminus of a peptide.[27-29] The process is repeated once the next residue is made available to eventually reveal the sequence of the peptide under analysis. A free α-amino group must be available for the process to occur. However, as much as 80-90% of mammalian proteins are blocked at the N-terminus with acetyl, formyl, or pyroglutamyl groups either in nature or by trace contaminants in commercial or laboratory preparations of the peptide.[29,30] In some instances, a peptide may completely lack an N-terminus, such as in the case of cyclosporine, which is cyclic.[31] Another major drawback is that the process is labor-intensive and time-consuming and some cycles can last 40 minutes per residue.[32] In addition, the use of acid for hydrolysis can cause cleavage within the peptide chain creating new N-terminal sites, which are subject to sequencing and adds background noise to the subsequent analysis.[28] Edman degradation is unidirectional, and interpretation of results becomes more ambiguous as analysis progresses further into the peptide sequence.[27]

Mass spectrometry has emerged as the preferred method for in-depth characterization and analysis of protein structure and function in biological systems providing high through-put and

sensitivity.[33,34] Unlike Edman degradation, analysis is not limited to the N-terminus. Several studies discuss protonation of samples and subsequent analysis by tandem mass spectrometry (MS/MS) methods, such as collision-induced dissociation (CID),[35,36] surface-induced dissociation (SID),[37-39] post-source decay (PSD),[40-42] photodissociation (PD),[43,44] electron capture dissociation (ECD),[9,45-48] and electron transfer dissociation (ETD).[49-52] Advancements in ion sources, mass analyzers, and computer algorithms for data analysis assist in generating sequence information from protonated ions, $[M + nH]^{n+}$, $n \geq 1$.[6,33,53] Automated mass spectrometers exist in several configurations and improve identification of peptide precursor and product ions.[27,34] In addition, positive ion mode studies focusing on gas-phase acid and base properties,[54-60] fragmentation mechanisms,[61-67] and product and precursor ion structures[68-73] aid in the development of data libraries and repositories for de novo sequencing. Mass spectrometry provides crucial structural information about peptide and protein post-translational modifications (PTMs) such as acetylation of N-terminal sites and location of phosphorylation and sulfonation anywhere within the sequence.[34]

Over the past 25 to 30 years, mass spectrometry has become a key tool for sequencing peptides and proteins from protonated molecular ions. The more common of the two methods, "bottom-up" or "shotgun" proteomics, involves isolation of proteins from their biological systems followed by digestion using enzymes.[33,74,75] The enzymes, such as trypsin and chymotrypsin, cleave the peptide backbone adjacent to or incorporate specific amino acid residues.[18,75] Small peptides are produced that can be analyzed by single stage MS methods or undergo fragmentation by MS/MS techniques such as CID and electron-based dissociation including ECD or ETD.[33,74,76-78] In bottom-up proteomics, peptides are easier to fractionate, ionize and fragment by MS/MS methods than whole proteins, and experimental and theoretical

analysis of peptides is simpler than for entire proteins.[33] Bottom-up proteomics involves working backwards after mass spectra have been analyzed to decode original protein sequences. Automated methods can decipher some protein sequences. In other instances, researchers work with mass spectral data to elucidate the initial peptide sequence, similar to solving a puzzle. The combination of mass spectrometers and separation techniques such as liquid chromatography (LC) helps to provide information for all the peptides present in a protein digest in a timely manner and helps to further automate the process.[33] While bottom-up protein analysis is the more conventional method, the process contains disadvantages. Enzymatic digestion tends to cleave post-translational modifications, making identification of modified sites difficult. In addition, repeat sequences are often missed and MS methods will not be able to differentiate between multiple identical peptides with the same sequence.[33,79] Despite some drawbacks, the bottom-up approach is commonly employed in literature and real-world applications.

The "top-down" approach is the less common of the two methods. Ionization of proteins occur in their native state and the complexes undergo dissociation (CID, ETD, or ETD).[80-83] The method is advantageous because ionization of the entire protein allows for easy determination of the exact mass. In addition, the lack of protein digests, such as peptides, eliminates the need for piecing together of information from fragments. Top-down can be useful for small proteins since cleavage sites may not be available for digest enzymes.[80,82] Protein structure characterization is possible by combining top-down methods with techniques such as ion mobility mass spectrometry (IMS). However, several disadvantages are associated with the top-down proteomics approach. Entire proteins can be more difficult to ionize because of inaccessibility of protonation sites. Lags in processing exist due to limited data interpretation software available for the intense amounts of data associated with a single whole protein. In

addition, the processes are so time intensive that analysis of a single protein in its native form can take several years to complete. The determination of mass for entire protein complexes in top down analysis requires high resolution instrumentation.[77] In addition, complex mixtures of proteins are more difficult to study [80,84-86]

While most routine automated analysis for peptide and protein sequence information is performed in positive ion mode, analysis of some peptides and proteins can be challenging. Such peptides lack basic sites and or contain highly acidic sites that preferentially deprotonate and lend themselves to negative ion mode studies.[41,87-90] Without formation of an ion from the intact molecule (i.e., the precursor ion), the peptide cannot be detected by positive mode MS. However, analysis of peptides and proteins containing acidic groups is important. Acidic peptides and proteins are involved in neurological processes and disorders;[91-94] for example, increases in acidic glial fibrillary proteins are implicated in neurological disorders such as dementia.[95] Blood coagulation and clotting process proteins also contain long sequences of highly acidic amino acid residues.[96,97] Highly acidic species serve as possible potential candidates for vaccines for malaria, as well as HIV inhibitor proteins.[98-100] Digestion and other metabolic processes are facilitated by peptides containing many acidic residues.[93,101,102] Acidic peptides are not limited to those only containing aspartic and glutamic acid residues. Phosphorylation and sulfonation of amino acid residues adds acidic character to peptides modified post translationally. Many of these modified peptides and proteins are involved in cellular processes[97,103] as well and may not readily form protonated ions.[104-108] A better understanding of MS/MS product ion formation for acidic peptides is necessary to improve the development of automated sequencing routines.

Metal ions can be complexed to peptides to facilitate the formation of positive ions for MS/MS. Complexation of metal ions to biological proteins and peptides is ubiquitous in nature. One example is the blood protein hemoglobin that naturally binds to $Fe^{3+}$ to perform its function of shuttling gases in and out of the body via the blood.[109] Metal-peptide complexes provide abundant sequence information by MS/MS techniques such as ECD and ETD. Metal cations investigated involve alkali,[110,111] divalent alkaline earth,[112-115] transition,[116-126] and trivalent lanthanides.[127,128] Factors such as metal ion identity and chemical properties can affect the type of product ions formed by ECD or ETD.[113,123] Metal adduction can facilitate the formation of multiply positively charged ions that are necessary for ECD and ETD. As discussed in Chapter 2, ECD and ETD require ions with a charge state of at least 2+ because the process involves transfer of an electron as demonstrated in equation 1.1 below. Addition of an electron to a singly charged ion results in neutral species that cannot be analyzed by MS.

$$[M + Met]^{n+} + e^- \rightarrow [M + Met]^{(n-1)+} \rightarrow \text{Product Ions}, \quad \text{where Met = metal} \qquad (1.1)$$

The studies in this dissertation focus on trivalent metal cationization of peptides, such as acidic peptides and a few neutral peptides, that are typically challenging to study in the positive ion mode. Emphasis is placed on sequence coverage and useful fragmentation information by ETD. Goals of this research involve an increase in the understanding of how trivalent lanthanide metal cations affect the dissociation of acidic peptides and an investigation into the potential use of trivalent metals as cationizing agents in peptide sequencing.

Chapter 2 lays the experimental foundation for all subsequent chapters of this dissertation. Instrumentation and experimental procedures and conditions utilized are described. Electrospray ionization was employed in all experiments, and analysis was performed on the Bruker HCTultra PTM Discovery System quadrupole ion trap (QIT) mass analyzer.

Dissociation methods on the QIT include CID and ETD. Many of the model peptides discussed in Chapters 3, 4, 5, and 6 were synthesized by me in the Cassady laboratory; therefore, the solid phase peptide synthesis protocol is also discussed. The end of the chapter contains information about peptide sequencing nomenclature and structures of amino acids used in this dissertation.

Chapters 3-5 focus on ETD studies of acidic peptide cations formed by adduction of trivalent lanthanide metal ions. Chapter 3 deals with the test peptide fibrinopeptide B and its analogs. The suitability of lanthanide cationization for ETD analysis of acidic peptides is established.[128] Chapter 4 is a more expansive report of several biological and model acidic peptides. Results for trivalent praseodymium, $Pr^{3+}$, are presented, but it is inferred that all other trivalent lanthanide metal cations (except promethium and europium) would produce similar results. Chapter 5 focuses on phosphorylated acidic peptides. The presence of the phosphate group imparts additional acidic character and increased chances for deprotonation. To date, trivalent lanthanide cationization presented in this dissertation is the only method available for consistently obtaining MS/MS spectra of these highly acidic peptides.

Chapter 3 discusses the ability of trivalent lanthanide metal cationization to provide extensive sequence coverage for acidic fibrinopeptide B and its analogs by ETD. The experiments include an ETD investigation on the metal-adducted ions formed by ESI and the product ions formed. All lanthanide metal ions, except radioactive promethium (Pm), were investigated. Acidic peptides preferentially form negative ions, but many routine MS analysis techniques are performed in the positive ion mode. Addition of a multiply charged metal ion facilitates formation of charged positive ions by ESI. In addition, ETD is limited by the requirement of multiply charged positive ions (for example, $[M + 2H]^{2+}$ or $[M + 3H]^{3+}$). Electron transfer dissociation of all ions formed by ESI, ($[M + Met - H]^{2+}$, $[M + Met]^{3+}$, and

$[M + Met + H]^{4+}$) provide useful sequence information. The 3+ and 4+ ions both generate extensive fragmentation for two of the three fibrinopeptide B analogs, which were used as test peptides to identify the lanthanide ions that generate the most useful structural information. The $[M + Met + H]^{4+}$ provides the most sequence coverage with almost a complete set of complimentary c- and z-ions involving cleavage between the amino acid residues. Only europium (Eu) provides minimal backbone cleavage. Electron transfer dissociation of $[M + Eu - H]^{2+}$ simply yields the charge reduced ion $[M + Eu - H]^{+}$ and a water loss ion, $[M + Eu - H_2O]^{+}$. While ETD of $[M + Eu]^{3+}$ of fibrinopeptide B and analogs provided more sequence information than for $[M + Eu - H]^{2+}$, significantly less cleavage results than what was provided by the other lanthanide metal ions. Any of the non-radioactive trivalent lanthanide metal cations is suitable for MS of the acidic peptides employed in the study except $Eu^{3+}$.

Chapter 4 expands upon the work of Chapter 3 by probing the effect of trivalent metal cationization on ETD of a variety of biological and model acidic peptides. The $Pr^{3+}$ is utilized as the representative trivalent lanthanide metal ion because the work of Chapter 3 found that trivalent lanthanide metal ions with one major isotope produce mass spectra that are easier to interpret and have fewer overlapping of peaks. As previously discussed, many of the biological peptides are acidic and undergo facile deprotonation. Effects of peptide size as well as ionic charge on ETD of these metal-peptide complexes is discussed. Peptides containing only two types of amino acid residues (neutral alanine and aspartic or glutamic acid residues) served as model peptides for elucidating the general patterns of fragmentation by ETD when cationized by $Pr^{3+}$. Increasing peptide chain length leads to more useful peptide backbone cleavage information for peptides with the lowest possible charge state (2+). For peptides containing seven amino acid residues, increasing the charge state promotes peptide backbone fragmentation.

Peptide ions with a charge of 3+, $[M + Met]^{3+}$, with seven amino acid residues provide more sequence information than those with the same chain length and a charge state of 2+, $[M + Met – H]^{2+}$. Model peptides with two acidic residues also produce more backbone dissociation. Biological peptides all show abundant backbone cleavage by ETD. Higher charge states (4+ and 3+) provide more useful sequence information than the lower charge state (2+). For both model and biological acidic peptides, metal-adducted product ions only occur after at least half of the peptide chain in incorporated in that sequence. In addition, metallated product ions contain at least two acidic sites, which suggests that metal adduction involves coordination of the metal ion between at least two acidic groups.

Chapter 5 investigates ETD of biological and model acidic phosphorylated peptides, containing one site of phosphorylation, cationized by the lanthanide cation $Pr^{3+}$. The most highly acidic biological peptides contain phosphate groups, which form by post-translational modification. In serine, threonine, and tyrosine, the most commonly phosphorylated amino acid residues, phosphate groups replace the hydroxyl side chains. This phosphate group impart additional acidic character onto the peptide. One of the most common positive ion mode automated MS methods for peptide sequencing, CID, suffers from loss or migration of the phosphate group,[129-131] which hinders unambiguous identification of the site of phosphorylation. Electron based techniques such as ECD and ETD have emerged as preferential methods for phosphopeptide analysis due to the reduced probability of phosphate group loss or migration.[129,132-135] Trivalent lanthanide metal ions facilitate formation of multiply positively charged ions required for ECD or ETD. The trivalent lanthanide metal cation, $Pr^{3+}$, adducts with acidic phosphorylated peptides to form $[M + Pr + H]^{4+}$, $[M + Pr]^{3+}$, and $[M + Pr – H]^{2+}$ by ESI. The same type of ions occurs in work presented in Chapters 3 and 4 with non-phosphorylated

acidic peptides. Model acidic phosphorylated peptides formed only $[M + Pr - H]^{2+}$. Facile deprotonation at the phosphate group essentially canceled one positive charge provided by the metal ion resulting in the abundant formation of $[M + Pr - H]^{2+}$. Unambiguous location of phosphorylation site occurs with complete sequence information from ETD of $[M + Pr + H]^{4+}$ and $[M + Pr]^{3+}$, which is a major factor for consideration in analysis of phosphorylated peptides. Limited peptide sequence coverage with fewer backbone cleavage sites result from ETD of $[M + Pr - H]^{2+}$ than for the 4+ and 3+ species. For model peptides, the most backbone cleavage occurs when the phosphorylated residue is located in the middle of the chain. At both the N- and C-termini, limited sequence coverage results. Electron transfer dissociation of $[M + Pr - H]^{2+}$ did not generate enough backbone cleavage information to conclusively determine the site of phosphorylation.

Chapter 6 discusses the optimization of ESI conditions for formation of maximum intensity of $[M + 2H]^{2+}$ by enhanced protonation of small peptides with trivalent chromium, $Cr^{3+}$. Enhanced protonation by $Cr^{3+}$ was first observed by Dr. Heather Watson of the Cassady group in her CID study of transition metal-adducted peptides.[126] The goal of this work was peptide sequencing using metalation; enhanced protonation was an unexpected discovery. Another Cassady group member, Dr. Changgeng Feng, later investigated $Cr^{3+}$ and ten other transition and main group trivalent metals for their ability to facilitate the formation of $[M + 2H]^{2+}$ in small neutral and acidic peptides.[124] The resulting precursor ions can then be subjected to MS/MS techniques such as CID and ETD, allowing sequencing with the same methods normally used for basic peptides. Chapter 6 outlines the effect of instrument parameters and experimental conditions (including sample solution container choice) on the intensity of $[M + 2H]^{2+}$ formed. The ratio of capillary exit to skimmer potential proves to be an important parameter for

maximizing enhanced protonation. The most intense formation of $[M + 2H]^{2+}$ occurs within a narrow range of voltage ratios. Nebulizer gas pressure also affects formation of $[M + 2H]^{2+}$ since lower pressures form ions with higher intensities. When solutions are prepared and stored in glass vials, the peptides degrade and all enhanced protonation is lost within four hours of sample preparation. Plastic vials preserved the solution and enhanced protonation still occurs weeks after sample preparation. Rinsing of vials is also critical to forming the most intense ions. Rinsing plastic vials with isopropanol eliminates a contaminant from the manufactural process and leads to overall higher intensities of $[M + 2H]^{2+}$. This investigation provides information that is beneficial to sample preparation methods in general and not specific to enhanced protonation.

Chapter 7 is a summarization of the most important aspects in this dissertation and its impact on the field of MS and proteomics on a grand scale. Potential future investigations are also proposed that can expand this work for researchers.

## References


1. International Human Genome Sequencing Consortium. Finishing the Euchromatic Sequence of the Human Genome. *Nature* **2004**, *431*, 931-945.

2. Auerbach, D.; Thaminy, S.; Hottiger, M. O.; Stagljar, I. The Post-Genomic Era of Interactive Proteomics: Facts and Perspectives. *Proteomics* **2002**, *2*, 611-623.

3. Omenn, G. S.; Lane, L.; Lundberg, E. K.; Beavis, R. C.; Overall, C. M.; Deutsch, E. W. Metrics for the Human Proteome Project 2016: Progress on Identifying and Characterizing the Human Proteome, Including Post-Translational Modifications. *J. Proteome Res.* **2016**, *15*, 3951-3960.

4. Human Proteome Organization: The Human Proteome Project Mission. *https://hupo.org/human-proteome-project* (accessed Feb 19, 2018).

5. Cantor, D. I.; Nice, E. C.; Baker, M. S. Recent Findings from the Human Proteome Project: Opening the Mass Spectrometry Toolbox to Advance Cancer Diagnosis, Surveillance and Treatment. *Expert Rev. Proteomics* **2015**, *12*, 279-293.

6. Kollipara, S.; Agarwal, N.; Varshney, B.; Paliwal, J. Technological Advancements in Mass Spectrometry and Its Impact on Proteomics. *Anal. Lett.* **2011**, *44*, 1498-1520.

7. Michalski, A.; Cox, J.; Mann, M. More than 100,000 Detectable Peptide Species Elute in Single Shotgun Proteomics Runs but the Majority is Inaccessible to Data-Dependent LC-MS/MS. *J. Proteome Res.* **2011**, *10*, 1785-1793.

8. Nilsson, T.; Mann, M.; Aebersold, R.; Yates, J. R.; Bairoch, A.; Bergeron, J. J. M. Mass Spectrometry in High-throughput Proteomics: Ready for the Big Time. *Nat. Methods* **2010**, *7*, 681-685.

9. Yang, H.; Fung, Y. M. E.; Zubarev, A. R.; Zubarev, R. A. The Use of ECD for Proteomics-wide Identification and Quantification of iso-Asp Residues. *Mol. Cell. Proteomics* **2009**, S13-S13.

10. Omenn, G. S.; Lane, L.; Lundberg, E. K.; Beavis, R. C.; Nesvizhskii, A. I.; Deutsch, E. W. Metrics for the Human Proteome Project 2015: Progress on the Human Proteome and Guidelines for High-Confidence Protein Identification. *J. Proteome Res.* **2015**, *14*, 3452-3460.

11. Wilhelm, M.; Schlegl, J.; Hahne, H.; Gholami, A. M.; Lieberenz, M.; Savitski, M. M.; Ziegler, E.; Butzmann, L.; Gessulat, S.; Marx, H.; Mathieson, T.; Lemeer, S.; Schnatbaum, K.; Reimer, U.; Wenschuh, H.; Mollenhauer, M.; Slotta-Huspenina, J.; Boese, J.; Bantscheff, M.; Gerstmair, A.; Faerber, F.; Kuster, B. Mass-Spectrometry-based Draft of the Human Proteome. *Nature* **2014**, *509*, 582-587.

12. Wiese, H.; Kuhlmann, K.; Wiese, S.; Stoepel, N. S.; Pawlas, M.; Meyer, H. E.; Stephan, C.; Eisenacher, M.; Drepper, F.; Warscheid, B. Comparison of Alternative MS/MS and Bioinformatics Approaches for Confident Phosphorylation Site Localization. *J. Proteome Res.* **2014**, *13*, 1128-1137.

13. McAlister, G. C.; Russell, J. D.; Rumachik, N. G.; Hebert, A. S.; Syka, J. E. P.; Geer, L. Y.; Westphall, M. S.; Pagliarini, D. J.; Coon, J. J. Analysis of the Acidic Proteome with Negative Electron-Transfer Dissociation Mass Spectrometry. *Anal. Chem.* **2012**, *84*, 2875-2882.

14. Fenn, J. B.; Mann, M.; Meng, C. K.; Wong, S. F.; Whitehouse, C. M. Electrospray Ionization for Mass Spectrometry of Large Biomolecules. *Science* **1989**, *246*, 64-71.

15. Fenn, J. B.; Mann, M.; Meng, C. K.; Wong, S. F. Electrospray Ionization--Principles and Practice. *Mass Spectrom. Rev.* **1990**, *9*, 37-70.

16. Hillenkamp, F.; Karas, M.; Beavis, R. C.; Chait, B. T. Matrix-Assisted Laser Desorption/Ionization Mass Spectrometry of Biopolymers. *Anal. Chem.* **1991**, *63*, 1193A-1203A.

17. Human Proteome Organization: Chromosome-based Human Proteome Project (C-HPP). *https://hupo.org/C-HPP* (accessed Feb 19, 2018).

18. Nelson, D. L.; Cox, M. M. *Lehninger Principles of Biochemistry;* W. H. Freeman: New York, 2004.

19. Eyles, S. J.; Speir, J. P.; Kruppa, G. H.; Gierasch, L. M.; Kaltashov, I. A. Protein Conformational Stability Probed by Fourier Transform Ion Cyclotron Resonance Mass Spectrometry. *J. Am. Chem. Soc.* **2000**, *122*, 495-500.

20. Kaltashov, I. A.; Eyles, S. J. Studies of Biomolecular Conformations and Conformational Dynamics by Mass Spectrometry. *Mass Spectrom. Rev.* **2002**, *21*, 37-71.

21. Aebersold, R.; Mann, M. Mass Spectrometry-based Proteomics. *Nature* **2003**, *422*, 198-207.

22. Aebersold, R.; Goodlett, D. R. Mass Spectrometry in Proteomics. *Chem. Rev.* **2001**, *101*, 269-296.

23. Xu, F.; Yang, T.; Fang, D.; Xu, Q.; Chen, Y. An Investigation of Heat Shock Protein 27 and P-glycoprotein Mediated Multi-drug Resistance in Breast Cancer Using Liquid Chromatography-Tandem Mass Spectrometry-based Targeted Proteomics. *J. Proteomics* **2014**, *108*, 188-197.

24. Cunningham, R.; Ma, D.; Li, L. Mass Spectrometry-based Proteomics and Peptidomics for Systems Biology and Biomarker Discovery. *Front. Biol.* **2012**, *7*, 313-335.

25. Cass, S. M. F.; Tepe, J. J. Identification of Phosphoproteins and Their Impact as Biomarkers in Cancer Therapeutics. *Curr. Signal Transd. T.* **2011**, *6*, 113-140.

26. Williams, J. P.; Brown, J. M.; Campuzano, I.; Sadler, P. J. Identifying Drug Metallation Sites on Peptides Using Electron Transfer Dissociation (ETD), Collision Induced Dissociation (CID) and Ion Mobility-Mass Spectrometry (IM-MS). *Chem. Commun.* **2010**, *46*, 5458-5460.

27. Biemann, K. Contributions of Mass Spectrometry to Peptide and Protein-Structure. *Biomed. Environ. Mass Spectrom.* **1988**, *16*, 99-111.

28. Smith, J. B. Peptide Sequencing by Edman Degradation. *eLS* **2001**.

29. Hall, S. C.; Smith, D. M.; Masiarz, F. R.; Soo, V. W.; Tran, H. M.; Epstein, L. B.; Burlingame, A. L. Mass Spectrometric and Edman Sequencing of Lipocortin I Isolated by Two-Dimensional SDS/PAGE of Human Melanoma Lysates. *Proc. Natl. Acad. Sci. USA* **1993**, *90*, 1927-1931.

30. Driessen, H.; De Jong, W.; Tesser, G.; Bloemendal, H. The Mechanism of N-terminal Acetylation of Protein. *Crit. Rev. Biochem* **1985**, *18*, 281-325.

31. Sowden, J. M.; Allen, B. R. Cyclosporine in Dermatology: A Historical Overview. *Int. J. Dermatol.* **1992**, *31*, 520-523.

32. Mortz, E.; Nguyen, T.; Kofoed, T. Applications of N-terminal Edman Sequencing for Proteins and Peptides. *Alphalyse Application Note* **2013**, *0916*.

33. Zhang, Y.; Fonslow, B. R.; Shan, B.; Baek, M.; Yates, J. R. Protein Analysis by Shotgun/Bottom-up Proteomics. *Chem. Rev.* **2013**, *113*, 2343-2394.

34. Cravatt, B. F.; Simon, G. M.; Yates Iii, J. R. The Biological Impact of Mass-Spectrometry-based Proteomics. *Nature* **2007**, *450*, 991.

35. Biemann, K.; Martin, S. A. Mass Spectrometric Determination of the Amino Acid Sequence of Peptides and Proteins. *Mass Spectrom. Rev.* **1987**, *6*, 1-76.

36. Papayannopoulos, I. A. The Interpretation of Collision-induced Dissociation Tandem Mass Spectra of Peptides. *Mass Spectrom. Rev.* **1995**, *14*, 49-73.

37. Johns, J. L.; Dongre, A. K.; Somogyi, A.; Wysocki, V. H. Sequence Dependence of Peptide Fragmentation Efficiency Curves Determined by Electrospray Ionization/Surface-induced Dissociation Mass Spectrometry. *J. Am. Chem. Soc.* **1994**, *116*, 8368-8369.

38. Bailey, T. H.; Laskin, J.; Futrell, J. H. Energetics of Selective Cleavage at Acidic Residues Studied by Time- and Energy-Resolved Surface-Induced Dissociation in FT-ICR MS. *Int. J. Mass Spectrom.* **2003**, *222*, 313-327.

39. Dongre, A.; Somogyi, A.; Wysocki, V. H. Surface-induced Dissociation: An Effective Tool to Probe Structure, Energetics and Fragmentation Mechanisms of Protonated Peptides. *J. Mass Spectrom.* **1996**, *31*, 339-350.

40. Spengler, B. Special Feature Tutorial: Post-source Decay Analysis in MALDI-TOF MS of Biomolecules. *J. Mass Spectrom.* **1997**, *32*, 1019-1036.

41. Jai-nhuknan, J.; Cassady, C. J. Negative Ion Postsource Decay Time-of-Flight Mass Spectrometry of Peptides Containing Acidic Amino Acid Residues. *Anal. Chem.* **1998**, *70*, 5122-5128.

42. Keough, T.; Lacey, M. P.; Youngquist, R. S. Derivatization Proceedures to Facilitate de novo Sequencing of Lysine-terminated Tryptic Peptides Using Postsource Decay Matrix-assisted Laser Desorption/Ionization Mass Spectrometry. *Rapid Commun. Mass Spectrom.* **2000**, *14*, 2348-2356.

43. Madsen, J. A.; Kaoud, T. S.; Dalby, K. N.; Brodbelt, J. S. 193-nm Photodissociation of Singly and Multiply Charged Peptide Anions for Acidic Proteome Characterization. *Proteomics* **2011**, *11*, 1329-1334.

44. Little, D. P.; Speir, J. P.; Senko, M. W.; O'Connor, P. B.; McLafferty, F. W. Infrared Multiphoton Dissociation of Large Multiply Charged Ions for Biomolecule Sequencing. *Anal. Chem.* **1994**, *66*, 2809-2815.

45. Zubarev, R. A.; Horn, D. M.; Fridriksson, E. K.; Kelleher, N. L.; Kruger, N. A.; Lewis, M. A.; Carpenter, B. K.; McLafferty, F. W. Electron Capture Dissociation for Structural Characterization of Multiply Charged Protein Cations. *Anal. Chem.* **2000**, *72*, 563-573.

46. McLafferty, F. W.; Horn, D. M.; Breuker, K.; Ge, Y.; Lewis, M. A.; Cerda, B. A.; Zubarev, R. A.; Carpenter, B. K. Electron Capture Dissociation of Gaseous Multiply Charged Ions by Fourier Transform ion Cyclotron Resonance. *J. Am. Soc. Mass Spectrom.* **2001**, *12*, 245-249.

47. Zubarev, R. A.; Kruger, N. A.; Fridriksson, E. K.; Lewis, M. A.; Horn, D. M.; Carpenter, B. K.; McLafferty, F. W. Electron Capture Dissociation of Gaseous Multiply-charged Proteins is Favored at Disulfide Bonds and Other Sites of High Hydrogen Atom Affinity. *J. Am. Chem. Soc.* **1999**, *121*, 2857-2862.

48. Zubarev, R. A.; Haselmann, K. F.; Budnik, B.; Kjeldsen, F.; Jensen, F. Towards an Understanding of the Mechanism of Electron-capture Dissociation: A Historical Perspective and Modern Ideas. *Eur. J. Mass Spectrom.* **2002**, *8*, 337-349.

49. Syka, J. E. P.; Coon, J. J.; Schroeder, M. J.; Shabanowitz, J.; Hunt, D. F. Peptide and Protein Sequence Analysis by Electron Transfer Dissociation Mass Spectrometry. *Proc. Natl. Acad. Sci. USA* **2004**, *101*, 9528-9533.

50. Coon, J. J. Collisions or Electrons? Protein Sequence Analysis in the 21st Century. *Anal. Chem.* **2009**, *81*, 3208-3215.

51. Good, D. M.; Wirtala, M.; McAlister, G. C.; Coon, J. J. Performance Characteristics of Electron Transfer Dissociation Mass Spectrometry. *Mol. Cell. Proteomics* **2007**, *6*, 1942-1951.

52. Gunawardena, H. P.; Gorenstein, L.; Erickson, D. E.; Xia, Y.; McLuckey, S. A. Electron Transfer Dissociation of Multiply Protonated and Fixed Charge Disulfide Linked Polypeptides. *Int. J. Mass Spectrom.* **2007**, *265*, 130-138.

53. Yates, J. R.; Osterman, A. L. Introduction: Advances in Genomics and Proteomics. *Chem. Rev.* **2007**, *108*, 3363-3366.

54. Harrison, A. G. The Gas-Phase Basicities and Proton Affinities of Amino Acids and Peptides. *Mass Spectrom. Rev.* **1997**, *16*, 201-217.

55. Ewing, N. P.; Pallante, G. A.; Zhang, X.; Cassady, C. J. Gas-phase Basicities for Ions from Bradykinin and Its des-Arginine Analogues. *J. Mass Spectrom.* **2001**, *36*, 875-881.

56. Kaltashov, I. A.; Fabris, D.; Fenselau, C. C. Assessment of Gas Phase Basicities of Protonated Peptides by the Kinetic Method. *J. Phys. Chem.* **1995**, *99314*, 10046-10051.

57. Cassady, C. J.; Carr, S. R.; Zhang, K.; Chung-Phillips, A. Experimental and Ab-Initio Studies on Protonations of Alanine and Small Peptides of Alanine and Glycine. *J. Org. Chem.* **1995**, *60*, 1704-1712.

58. Bokatzian, S. S.; Stover, M. L.; Plummer, C. E.; Dixon, D. A.; Cassady, C. J. An Experimental and Computational Investigation into the Gas-Phase Acidities of Tyrosine and Phenylalanine: Three Structures for Deprotonated Tyrosine. *J. Phys. Chem. B* **2014**, *118*, 12630-12643.

59. Plummer, C. E.; Stover, M. L.; Bokatzian, S. S.; Davis, J. T. M.; Dixon, D. A.; Cassady, C. J. An Experimental and Computational Study of the Gas-Phase Acidities of the Common Amino Acid Amides. *J. Phys. Chem. B* **2015**, *119*, 9661-9669.

60. Stover, M. L.; Plummer, C. E.; Miller, S. R.; Cassady, C. J.; Dixon, D. A. Gas-Phase Acidities of Phosphorylated Amino Acids. *J. Phys. Chem. B* **2015**, *119 (46)*, 14604-14621.

61. Wysocki, V. H.; Tsaprailis, G.; Smith, L. L.; Breci, L. A. Mobile and Localized Protons: A Framework for Understanding Peptide Dissociation. *J. Mass Spectrom.* **2000**, *35*, 1399-1406.

62. Paizs, B.; Suhai, S. Fragmentation Pathways of Protonated Peptides. *Mass Spectrom. Rev.* **2005**, *24*, 508-548.

63. Tang, X.; Thibault, P.; Boyd, R. K. Fragmentation Reactions of Multiply-Protonated Peptides and Implications for Sequencing by Tandem Mass Spectrometry with Low-Energy Collision-Induced Dissociation. *Anal. Chem.* **1993**, *65*, 2824-2834.

64. Sullivan, A. G.; Brancia, F. L.; Tyldesley, R.; Bateman, R.; Sidhu, K.; Hubbard, S. J.; Oliver, S. G.; Gaskell, S. J. The Exploitation of Selective Cleavage of Singly Protonated Peptide Ions Adjacent to Aspartic Acid Residues Using a Quadrupole Orthogonal Time-of-Flight Mass Spectrometer Equipped with a Matrix-assisted Laser Desorption/Ionization Source. *Int. J. Mass Spectrom.* **2001**, *210/211*, 665-676.

65. Polce, M. J.; Ren, D.; Wesdemiotis, C. Dissociation of the Peptide Bond in Protonated Peptides. *J. Mass Spectrom.* **2000**, *35*, 1391-1398.

66. Chawner, R.; Eyers, C. E.; Gaskell, S. J. The Influence of a C-terminal Basic Residue on Peptide Fragmentation Pathways. *Int. J. Mass Spectrom.* **2012**, *316–318*, 284-291.

67. Boyd, R.; Somogyi, Á The Mobile Proton Hypothesis in Fragmentation of Protonated Peptides: A Perspective. *J. Am. Soc. Mass Spectrom.* **2010**, *21*, 1275-1278.

68. van Dongen, W. D.; de Koster, C. G.; Heerma, W.; Haverkamp, J. Sequence-Ion Studies in Peptides: The Generation of C" Ions. *Rapid Commun. Mass Spectrom.* **1993**, *7*, 241-244.

69. Cordero, M. M.; Houser, J. J.; Wesdemiotis, C. The Neutral Products Formed During Backbone Fragmentations of Protonated Peptides in Tandem Mass Spectrometry. *Anal. Chem.* **1993**, *65*, 1594-1601.

70. Molesworth, S.; Osburn, S.; Van Stipdonk, M. Influence of Size on Apparent Scrambling of Sequence During CID of b-Type Ions. *J. Am. Soc. Mass Spectrom.* **2009**, *20*, 2174-2181.

71. Harrison, A. G.; Csizmadia, I. G.; Tang, T. H. Structure and Fragmentation of $b_2$ Ions in Peptide Mass Spectra. *J. Am. Soc. Mass Spectrom.* **2000**, *11*, 427-436.

72. Bythell, B. J.; Somogyi, A.; Paizs, B. What is the Structure of $b_2$ Ions Generated from Doubly Protonated Tryptic Peptides? *J. Am. Soc. Mass Spectrom.* **2009**, *20*, 618-624.

73. Oomens, J.; Young, S.; Molesworth, S.; van Stipdonk, M. Spectroscopic Evidence for an Oxazolone Structure of the $b_2$ Fragment Ion from Protonated Tri-alanine. *J. Am. Soc. Mass Spectrom.* **2009**, *20*, 334-339.

74. Wysocki, V. H.; Resing, K. A.; Zhang, Q.; Cheng, G. Mass Spectrometry of Peptides and Proteins. *Methods* **2005**, *35*, 211-222.

75. Switzar, L.; Giera, M.; Niessen, W. M. A. Protein Digestion: An Overview of the Available Techniques and Recent Developments. *J. Proteome Res.* **2013**, *12*, 1067-1077.

76. Liu, C.; Lai, C. Effects of Electron-Transfer Coupled with Collision-Induced Dissociation (ET/CID) on Doubly Charged Peptides and Phosphopeptides. *J. Am. Soc. Mass Spectrom.* **2011**, *22*, 57-66.

77. Bogdanov, B.; Smith, R. D. Proteomics by FTICR Mass Spectrometry: Top Down and Bottom Up. *Mass Spectrom. Rev.* **2005**, *24*, 168-200.

78. Hardouin, J. Protein Sequence Information by Matrix-assisted Laser Desorption/ionization In-source Decay Mass Spectrometry. *Mass Spectrom. Rev.* **2007**, *26*, 672-682.

79. Yates, J. R.; Ruse, C. I.; Nakorchevsky, A. Proteomics by Mass Spectrometry: Approaches, Advances, and Applications. *Annu. Rev. Biomed. Eng.* **2009**, *11*, 49-79.

80. Kelleher, N. L. Top-down Proteomics. *Anal. Chem.* **2004**, *76*, 196-203.

81. Zabrouskov, V.; Senko, M. W.; Du, Y.; Leduc, R. D.; Kelleher, N. L. New and Automated MSn Approaches for Top-Down Identification of Modified Proteins. *J. Am. Soc. Mass Spectrom.* **2005**, *16*, 2027-2038.

82. Savaryn, J. P.; Catherman, A. D.; Thomas, P. M.; Abecassis, M. M.; Kelleher, N. L. The Emergence of Top-down Proteomics in Clinical Research. *Genome Med.* **2013**, *5*, 53-61.

83. Catherman, A. D.; Skinner, O. S.; Kelleher, N. L. Top Down Proteomics: Facts and Perspectives. *Biochem. Biophys. Res. Commun.* **2014**, *445*, 683-693.

84. Zhang, H.; Cui, W.; Wen, J.; Blankenship, R. E.; Gross, M. L. Native Electrospray and Electron-Capture Dissociation in FTICR Mass Spectrometry Provide Top-Down Sequencing of a Protein Component in an Intact Protein Assembly. *J. Am. Soc. Mass Spectrom.* **2010**, *21*, 1966-1968.

85. Reid, G. E.; McLuckey, S. A. 'Top down' Protein Characterization via Tandem Mass Spectrometry. *J. Mass Spectrom.* **2002**, *37*, 663-675.

86. Durbin, K. R.; Fornelli, L.; Fellers, R. T.; Doubleday, P. F.; Narita, M.; Kelleher, N. L. Quantitation and Identification of Thousands of Human Proteoforms Below 30 kDa. *J. Proteome Res.* **2016**, *15*, 976-982.

87. Ewing, N. P.; Cassady, C. J. Dissociation of Multiply-charged Negative Ions for Hirudin (54-65), Fibrinopeptide B, and Insulin A (Oxidized). *J. Am. Soc. Mass Spectrom.* **2001**, *12*, 105-116.

88. Gao, J.; Cassady, C. J. Negative Ion Production from Peptides and Proteins by Matrix-assisted Laser Desorption/ionization Time-of-flight Mass Spectrometry. *Rapid Commun. Mass Spectrom.* **2008**, *22*, 4066-4072.

89. Crizer, D. M.; Xia, Y.; McLuckey, S. A. Transition Metal Complex Cations as Reagents for Gas-Phase Transformation of Multiply Deprotonated Polypeptides. *J. Am. Soc. Mass Spectrom.* **2009**, *20*, 1718-1722.

90. Huzarska, M.; Ugalde, I.; Kaplan, D. A.; Hartmer, R.; Easterling, M. L.; Polfer, N. C. Negative Electron Transfer Dissociation of Deprotonated Phosphopeptide Anions: Choice of Radical Cation Reagent and Competition between Electron and Proton Transfer. *Anal. Chem.* **2010**, *82*, 2873-2878.

91. Pierotti, A. R.; Prat, A.; Chesneau, V.; Gaudoux, F.; Leseney, A. M.; Foulon, T.; Cohen, P. N-Arginine Dibasic Convertase, a Metalloendopeptidase as a Prototype of a Class of Processing Enzymes. *Proc. Natl. Acad. Sci. USA* **1994**, *91*, 6078-6082.

92. Foulon, T.; Cadel, S.; Chesneau, V.; Draoui, M.; Prat, A.; Cohen, P. Two Novel Metallopeptides with a Specificity for Basic Residues: Functional Properties, Structure, and Cellular Distribution. In *Neuropeptides: Basic and Clinical Advances*; Crawley, J. N., McLean, S., Eds.; New York Academy of Sciences: New York, 1996; Vol. 780, 106-120.

93. Lemaire, S.; Yamashiro, D.; Rao, A. J.; Li, C. H. Synthesis and Biological Activity of Beta-Melanotropins and Analogs. *J. Med. Chem.* **1977**, *20*, 155-158.

94. Tatemoto, K. Neuropeptide Y: Complete Amino Acid Sequence of the Brain Peptide. *Proc. Natl. Acad. Sci. USA* **1982**, *79*, 5485-5489.

95. Lamers, K. J. B.; Vos, P.; Verbeek, M. M.; Rosmalen, F.; van Geel, W. J. A.; van Engelen, B. G. M. Protein S-100B, Neuron-Specific Enolase (NSE), Myelin Basic Protein (MBP) and Glial Fibrillary Acidic Protein (GFAP) in Cerebrospinal Fluid (CSF) and Blood of Neurological Patients. *Brain Res. Bull.* **2003**, *61*, 261-264.

96. Ebert, R. F.; Bell, W. R. Assay of Human Fibrinopeptides by High-Performance Liquid Chromatography. *Anal. Biochem.* **1985**, *148*, 70-78.

97. Voet, D.; Voet, J. G. *Biochemistry;* John Wiley & Sons: New York, 1995.

98. Chougnet, C.; Troye-Blomberg, M.; Deloron, P.; Kabilan, L.; Lepers, J. P.; Savel, J.; Perlmann, P. Human Immune Response in Plasmodium falciparum Malaria. Synthetic Peptides Corresponding to Known Epitopes of the Pf155/RESA Antigen Induce Production of Parasite-Specific Antibodies in Vitro. *J. Immunol.* **1991**, *147*, 2295-2301.

99. Nara, P. L.; Hwang, K. M.; Rausch, D. M.; Lifso, J. D.; Eiden, L. E. CD4 Antigen-based Antireceptor Peptides Inhibit Infectivity of Human Immunodeficiency Virus In Vitro at Multiple Stages of the Viral Life Cycle. *Proc. Natl. Acad. Sci. USA* **1989**, *86*, 7139-7143.

100. Lifson, J. D.; Hwang, K. M.; Nara, P. L.; Fraser, B.; Padgett, M.; Dunlop, N. M.; Eiden, L. E. Synthetic CD4 Peptide Derivatives that Inhibit HIV Infection and Cytopathicity. *Science* **1988**, *241*, 712-716.

101. Morley, J. S. Structure-Function Relationships in Gastrin-like Peptides. *Proc. R. Soc. London, B* **1968**, *170*, 97-111.

102. Luis Moroder, J.-P.B., Yuji Kobayashi, Synthetic Immunogens. Part IV: Conformational Studies on Gastrin Conjugates with the Human Immunoglobulin G1 Hinge Peptide 225-232/225'-232'. *Biopolymers* **1991**, *31*, 595-604.

103. Manning, G.; Whyte, D. B.; Martinez, R.; Hunter, T.; Sudarsanam, S. The Protein Kinase Complement of the Human Genome. *Science* **2002**, *298*, 1912-1916, 1933-1934.

104. Vinh, J.; Loyaux, D.; Redeker, V.; Rossier, J. Sequencing Branched Peptides with CID/PSD MALDI-TOF in the Low-picomole Range: Application to the Structural Study of the Posttranslatinal Polyglycylation of Tubulin. *Anal. Chem.* **1997**, *69*, 3979-3985.

105. Lapko, V. N.; Jiang, X. Y.; Smith, D. L.; Song, P. S. Posttranslational Modification of Oat Phytochrome A: Phosphorylation of a Specific Serine in a Multiple Serine Cluster. *Biochemistry* **1997**, *36*, 10595-10599.

106. Yagami, T.; Kitagawa, K.; Futaki, S. Liquid Secondary-ion Mass Spectrometry of Peptides Containing Multiple Tyrosine-O-sulfates. *Rapid Commun. Mass Spectrom.* **1995**, *9*, 1335-1341.

107. Gibson, B. W.; Cohen, P. Liquid Secondary-Ion Mass-Spectrometry of Phosphorylated and Sulfated Peptides and Proteins. In *Methods in Enzymology*; McCloskey, J. A., Ed.; Academic Press: San Diego, CA, 1990; Vol. 193; 193, pp 480-501.

108. Ishihama, Y.; Wei, F. Y.; Aoshima, K.; Sato, T.; Kuromitsu, J.; Oda, Y. Enhancement of the Efficiency of Phosphoproteomic Identification by Removing Phosphates after Phosphopeptide Enrichment. *J. Proteome Res.* **2007**, *6*, 1139-1144.

109. Finch, C. A. In *In The Role of Iron in Hemoglobin Synthesis;* Conference on Hemoglobin, 2-3 May 1957; National Academy of Sciences-National Research Council: 1958; pp 95.

110. Iavarone, A. T.; Paech, K.; Williams, E. R. Effects of Charge State and Cationizing Agent on the Electron Capture Dissociation of a Peptide. *Anal. Chem.* **2004**, *76*, 2231-2238.

111. Voinov, V. G.; Hoffman, P. D.; Bennett, S. E.; Beckman, J. S.; Barofsky, D. F. Electron Capture Dissociation of Sodium-Adducted Peptides on a Modified Quadrupole/Time-of-Flight Mass Spectrometer. *J. Am. Soc. Mass Spectrom.* **2015**, *26*, 2096-2104.

112. Fung, Y. M. E.; Liu, H.; Chan, T. W. D. Electron Capture Dissociation of Peptides Metalated with Alkaline-Earth Metal Ions. *J. Am. Soc. Mass Spectrom.* **2006**, *17*, 757-771.

113. Liu, H.; Håkansson, K. Divalent Metal Ion-Peptide Interactions Probed by Electron Capture Dissociation of Trications. *J. Am. Soc. Mass Spectrom.* **2006**, *17*, 1731-1741.

114. Liu, H.; Håkansson, K. Electron Capture Dissociation of Tyrosine O-Sulfated Peptides Complexed with Divalent Metal Cations. *Anal. Chem.* **2006**, *78*, 7570-7576.

115. Asakawa, D.; Takeuchi, T.; Yamashita, A.; Wada, Y. Influence of Metal–Peptide Complexation on Fragmentation and Inter-Fragment Hydrogen Migration in Electron Transfer Dissociation. *J. Am. Soc. Mass Spectrom.* **2014**, *25*, 1029-1039.

116. Chen, X.; Chan, W. Y. K.; Wong, P. S.; Yeung, H. S.; Chan, T. W. D. Formation of Peptide Radical Cations ($M^{+\cdot}$) in Electron Capture Dissociation of Peptides Adducted With Group IIB Metal Ions. *J. Am. Soc. Mass Spectrom.* **2011**, *22*, 233-244.

117. Chen, X.; Fung, Y. M. E.; Chan, W. Y. K.; Wong, P. S.; Yeung, H. S.; Chan, T. W. D. Transition Metal Ions: Charge Carriers That Mediate the Electron Capture Dissociation Pathways of Peptides. *J. Am. Soc. Mass Spectrom.* **2011**, *22*, 2232-2245.

118. Chen, X.; Wang, Z.; Li, W.; Wong, Y. L. E.; Chan, T. W. D. Effect of Structural Parameters on the Electron Capture Dissociation and Collision-induced Dissociation Pathways of Copper(II)-peptide Complexes. *Eur. J. Mass Spectrom.* **2015**, *21*, 649-657.

119. Chen, X.; Liu, G.; Wong, Y. L. E.; Deng, L.; Wang, Z.; Li, W.; Chan, T. W. D. Dissociation of Trivalent Metal Ion ($Al^{3+}$, $Ga^{3+}$, $In^{3+}$ and $Rh^{3+}$)–peptide Complexes Under Electron Capture Dissociation Conditions. *Rapid Commun. Mass Spectrom.* **2016**, *30*, 705-710.

120. Kleinnijenhuis, A. J.; Mihalca, R.; Heeren, R. M. A.; Heck, A. J. R. Atypical Behavior in the Electron Capture Induced Dissociation of Biologically Relevant Transition Metal Ion Complexes of the Peptide Hormone Oxytocin. *Int. J. Mass Spectrom.* **2006**, *253*, 217-224.

121. van der Burgt, Y. E. M.; Palmblad, M.; Dalebout, H.; Heeren, R. M. A.; Deelder, A. M. Electron Capture Dissociation of Peptide Hormone Changes Upon Opening of the Tocin Ring and Complexation with Transition Metal Cations. *Rapid Commun. Mass Spectrom.* **2009**, *23*, 31-38.

122. Dong, J.; Vachet, R. W. Coordination Sphere Tuning of the Electron Transfer Dissociation Behavior of Cu(II)-peptide Complexes. *J. Am. Soc. Mass Spectrom.* **2012**, *23*, 321-329.

123. Asakawa, D.; Wada, Y. Electron Transfer Dissociation Mass Spectrometry of Peptides Containing Free Cysteine Using Group XII Metals as a Charge Carrier. *J Phys Chem B* **2014**, *118*, 12318-12325.

124. Feng, C.; Commodore, J. J.; Cassady, C. J. The Use of Chromium(III) to Supercharge Peptides by Protonation at Low Basicity Sites. *J. Am. Soc. Mass Spectrom.* **2015**, *26*, 347-358.

125. Pu, D.; Vincent, J. B.; Cassady, C. J. The Effects of Chromium(III) Coordination on the Dissociation of Acidic Peptides. *J. Mass Spectrom.* **2008**, *43*, 773-781.

126. Watson, H. M.; Vincent, J. B.; Cassady, C. J. Effects of Transition Metal Ion Coordination on the Collision-induced Dissociation of Polyalanines. *J. Mass Spectrom.* **2011**, *46*, 1099-1107.

127. Flick, T. G.; Donald, W. A.; Williams, E. R. Electron Capture Dissociation of Trivalent Metal Ion-Peptide Complexes. *J. Am. Soc. Mass Spectrom.* **2013**, *24*, 193-201.

128. Commodore, J. J.; Cassady, C. J. The Effects of Trivalent Lanthanide Cationization on the Electron Transfer Dissociation of Acidic Fibrinopeptide B and its Analogs. *J. Am. Soc. Mass Spectrom.* **2016**, *27*, 1499-1509.

129. Stensballe, A.; Jensen, O. N.; Olsen, J. V.; Haselmann, K. F.; Zubarev, R. A. Electron Capture Dissociation of Singly and Multiply Phosphorylated Peptides. *Rapid Commun. Mass Spectrom.* **2000**, *14*, 1793-2000.

130. Palumbo, A. M.; Reid, G. E. Evaluation of Gas-Phase Rearrangement and Competing Fragmentation Reactions on Protein Phosphorylation Site Assignment Using Collision Induced Dissociation-MS/MS and $MS^3$. *Anal. Chem.* **2008**, *80*, 9735-9747.

131. Edelson-Averbukh, M.; Shevchenko, A.; Pipkorn, R.; Lehmann, W. D. Gas-Phase Intramolecular Phosphate Shift in Phosphotyrosine-Containing Peptide Monoanions. *Anal. Chem.* **2009**, *81*, 4369-4381.

132. Molina, H.; Horn, D. M.; Tang, N.; Mathivanan, S.; Pandey, A. Global Proteomic Profiling of Phosphopeptides Using Electron Transfer Dissociation Tandem Mass Spectrometry. *Proc. Natl. Acad. Sci. USA.* **2007**.

133. Lopez-Clavijo, A. F.; Duque-Daza, C. A.; Creese, A. J.; Cooper, H. J. Electron Capture Dissociation Mass Spectrometry of Phosphopeptides: Arginine and Phosphoserine. *Int. J. Mass Spectrom.* **2015**, *390*, 63-70.

134. Creese, A. J.; Cooper, H. J. The Effect of Phosphorylation on the Electron Capture Dissociation of Peptide Ions. *J. Am. Soc. Mass Spectrom.* **2008**, *19*, 1263-1274.

135. Hayakawa, S.; Hashimoto, M.; Nagao, H.; Awazu, K.; Toyoda, M.; Ichihara, T.; Shigeri, Y. Study of the Dissociation of a Charge-reduced Phosphopeptide Formed by Electron Transfer From an Alkali Metal Target. *Rapid Commun. Mass Spectrom.* **2008**, *22*, 567-572.

# CHAPTER 2: INSTRUMENTATION, EXPERIMENTAL PROCEDURES AND THEORY

## 2.1 Overview

This chapter includes a discussion of the theory and experimental procedures for all the research in this dissertation. All research was performed on a Bruker (Billerica, MA, USA) HCTultra PTM Discovery System high capacity quadrupole ion trap (QIT) mass spectrometer with electrospray ionization (ESI). Electrospray ionization will be discussed first followed by the theory and description of the mass analyzer employed. Peptide sequence was elucidated with the tandem mass spectrometry (MS/MS) methods of collision-induced dissociation (CID) and electron transfer dissociation (ETD). These will be discussed after instrumentation. Some of the peptides investigated were synthesized in the Cassady lab, so peptide synthesis procedures along with fragmentation nomenclature and amino acid structures will be discussed towards the end of the chapter.

## 2.2 Electrospray ionization

Formation of molecular ions is important for analysis of biological molecules by mass spectrometry because mass-to-charge (*m/z*) analysis can only be performed on charged particles. Using the concepts first introduced by Dole,[1] Yamashita and Fenn[2-4] developed electrospray ionization (ESI) in the 1980s. Fenn was awarded the Nobel Prize in Chemistry in 2002 for the ESI technique due its ability to ionize large molecules and biomolecules.[5] ESI is widely utilized in routine mass spectrometry analysis because it can be paired with common separation processes such as liquid chromatography.[6,7] ESI is a "soft" ionization method where quasi-

molecular ions with little to no fragments are formed. Production of multiply charged ions, $[M + nH]^{n+}$ or $[M – nH]^{n-}$, from large molecules is of particular importance in ESI. Certain electron-based tandem mass spectrometry methods (MS/MS or $MS^n$), such as electron transfer dissociation (ETD) and electron capture dissociation (ECD), are only possibly due to the formation of multiply charged ions.

During ESI, a sample in the solution-phase is introduced into a strong electric field and undergoes desolvation to produce gas-phase ions.[4] The two most accepted mechanisms to explain ion formation by ESI are the charge residue and the ion evaporation models.[1,4,5,8-13] Generally, ionization by ESI occurs in three steps referred to as droplet formation, droplet shrinkage, and desorption of gaseous ions.[14] A Taylor cone forms at the tip of the needle due to the partial separation of charges created by the electrostatic forces acting on the analyte solution. The electrostatic force causes a fine mist of droplets to emerge from the Taylor cone along with the assistance of the nebulizing gas (nitrogen in the QIT). Nitrogen also serves as the drying gas and assists in the rapid evaporation of solvent from the mist droplets. This causes the size of the droplets to shrink. Decreasing size leads to increased charge density on the surface of the droplets. At the Rayleigh limit, the droplet breaks apart due to Coulombic explosion as shown in Figure 2.1. The Rayleigh limit is used to refer to a critical value reached when the Coulombic force experienced by the charges within the drop is equal to the surface tension. The charged droplets are ripped apart into smaller more highly charged droplets. The shrinkage and explosion processes occur repeatedly until quasi-molecular ions form.

In this research, the sample was introduced through a syringe and transfer line using a KD scientific (Holliston, MA, USA) syringe pump set to a flow rate of ~ 80 µL/hr. Formation of multiply charged ions by ESI was facilitated by the addition of metal ions to the infused

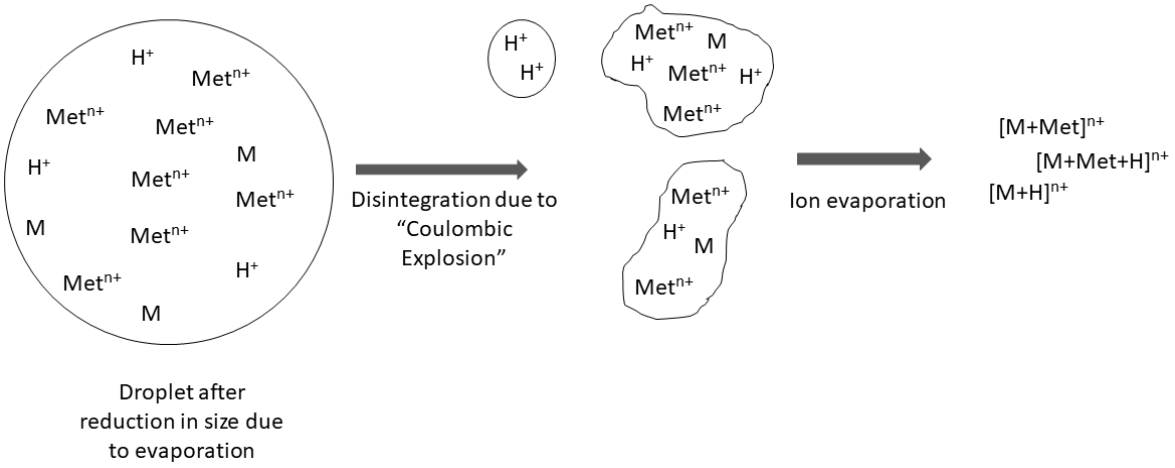


Figure 2.1. *S*chematic of desolvation of ions in ESI source.

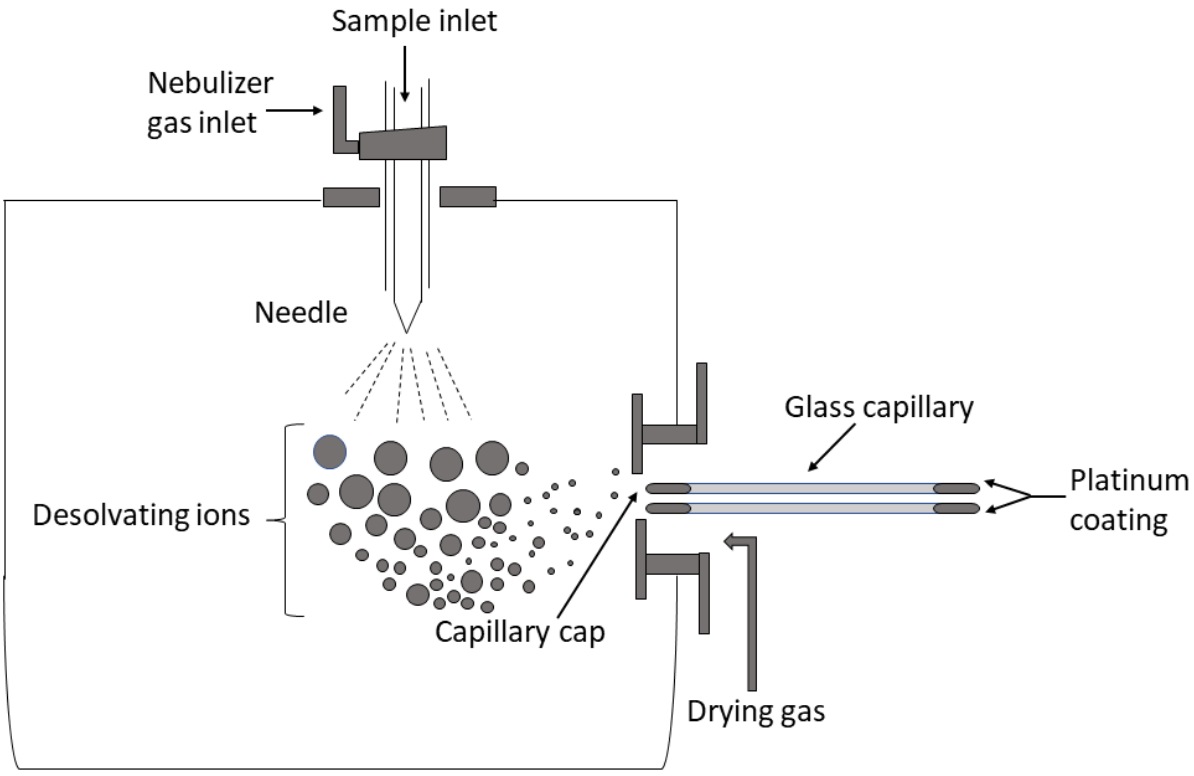


Figure 2.2. Schematic of ESI source for the Bruker HCTultra PTM Discovery System.

solutions. The sample is introduced perpendicular to the ion extraction capillary to minimize entry of neutrals into the mass analyzer as shown in Figure 2.2. In the Bruker HCTultra, the needle is kept at ground and a high voltage (-3 to -4 kV) is placed on the capillary entrance, stainless steel end plate, and capillary cap. In other ESI source designs, the capillary is kept at ground and the high voltage is placed on the needle. The high potential difference created between the capillary and the needle regions creates an electrostatic field that helps to disperse the infused solution into charged droplets. Drying gas and nebulizing gas, both nitrogen, flow opposite and with the sample solution, respectively, to assist in evaporation of the charged droplet. The nebulizer gas pressure was optimized between 5 and 10 psi. Drying gas was heated between 250° and 300°C and had a flow rate of 5-10 L/min.

Samples were dissolved in solvent systems containing a mixture of water:acetonitrile at 50:50 v/v. Acetic acid, or formic acid were sometimes added at 0.1-2% (v/v) to assist with ion formation. Acids assist with formation of positive protonated ions. All the work in this dissertation was carried out in the positive ion mode. In addition, metal ions facilitate the formation of multiply positively charged ions of peptides that do not favorably protonate. Sample concentrations infused were 5-10 µM, and metal ion concentrations were 50-100 µM; therefore, peptide:metal molar concentrations were typically 1:10.

### 2.3 Quadrupole ion trap

The quadrupole ion trap (QIT) was introduced as the Paul trap by Wolfgang Paul in 1958. He won the Nobel Prize in Physics for its development in 1989.[15] The QIT can store ions for milliseconds to seconds in three dimensions (3D) using a quadrupolar oscillating electric field. Both positive and negative ions can be trapped simultaneously in the QIT, which is necessary for ETD experiments.

The QIT, which is made of stainless steel, consists of two identical dome-shaped end cap electrodes and a central hyperbolic ring electrode. Each end cap has a small opening to allow ions to enter the trap and another spherical hole to allow ions to be ejected to the detector. Ions are guided from the ESI region into the trap by a combination of two octopole ion guides and electrostatic lenses as shown in Figure 2.3. Ions are confined to the center of the trap by applying a radiofrequency (RF) potential to the ring electrode while the end caps are maintained at ground. A quadrupolar field results, trapping the ions. Helium gas at pressures of ~$10^{-3}$ Torr serves as a buffer to dampen the motion of the trapped ions. The buffer gas is present at all times in the trap to prevent unwanted energetic collisions and to allow the ions to be concentrated in the center of the trap.

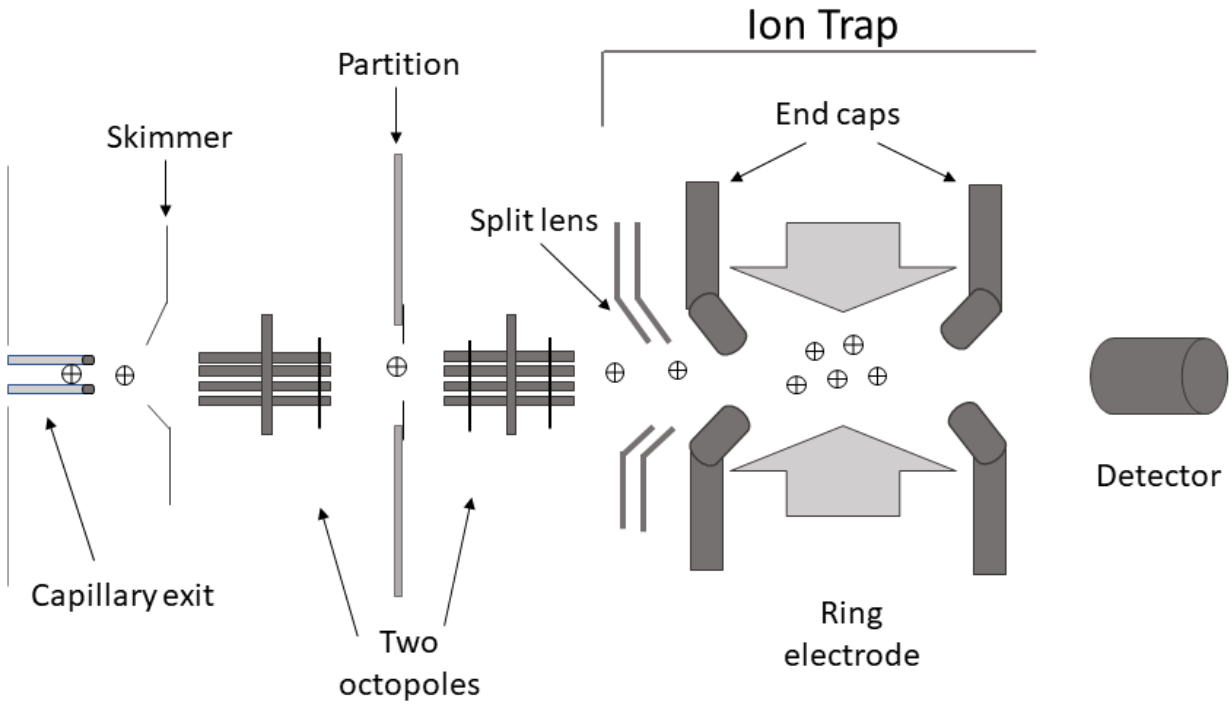


Figure 2.3. Schematic showing transfer of ions from ion source to ion trap.

Solutions of Mathieu's second-order linear differential equation[16] can be used to best describe the ion motion in a QIT. The ion motion form of the Mathieu equation is shown in Equation 2.1 with *u* representing the motion along the x, y, and z axes and ξ being a dimensionless parameter ($\xi = \Omega t/2$ where Ω is frequency of the RF potential and *t* is time). The $a_u$ and $q_u$ are dimensionless trapping parameters.

$$\frac{d^2u}{d\xi^2} + (a_u - 2q_u cos2\xi)\, u = 0 \qquad (2.1)$$

If Ωt/2 is substituted for $\xi$ in Equation 2.1, the new expression becomes

$$\frac{d^2u}{dt^2} = \frac{\Omega^2}{4}\frac{d^2u}{d\xi^2} \qquad (2.2)$$

After substituting Equation 2.2 back into Equation 2.1 and then multiplying by mass of the ion (m), a new expression is obtained.

$$m\frac{d^2u}{dt^2} = m\frac{\Omega^2}{4}\,(a_u - 2q_u \cos\Omega t)u \qquad (2.3)$$

The left side of Equation 2.3 can represent the force of an ion (F) times the acceleration (a) in each of the x-, y-, and z-directions (*u*); i.e. F = ma. The forces in the three coordinate directions (x, y, and z) can be resolved individually since the field in the quadrupole ion trap is not coupled. Therefore, considering the force in the x-direction, $F_x$, experienced by an ion of mass *m* with acceleration *a* and charge *e* at any point within the quadrupolar field, then $F_x$ (Equation 2.4) is:

$$F_x = ma = m\frac{d^2x}{dt^2} = -e\frac{\partial}{\partial x} \qquad (2.4)$$

Considering Equation 2.5, the radiofrequency (RF) potential can be applied to the ring electrode alone (VcosΩt) or in combination with a direct current (DC) potential, U.

$$\emptyset_0 = (U + V\cos\Omega t) \qquad (2.5)$$

In the above equation, the field of the alternating current (AC) is described by the angular frequency (Ω) in rads$^{-1}$ with angular frequency being equal to 2Π$f$ (where $f$ is measured in Hertz). U is the amplitude of the DC voltage and V is that of the AC voltage.

The cylindrical coordinates of the inner cavity of the QIT can be represented as r, z. The radius of the ring electrode, r, has a perpendicular z component representing the shortest distance from the end caps to the center of the ion trap. Differentiating the electric potential (Equation 2.5) with respect to x gives the potential gradient, (Equation 2.6).

$$\frac{\partial \emptyset}{\partial x} = \frac{2x}{r_0^2}\,(U + V\cos\Omega t) \qquad (2.6)$$

The force on an ion can then be obtained by substituting equation 2.6 into 2.4 to give Equation 2.7.

$$m\frac{d^2x}{dt^2} = \frac{-2e}{r_0^2}(U + V\cos\Omega t)x \qquad (2.7)$$

By recalling that $u$ represents $x$, the movement of the ion cloud in the radial direction can be obtained by directly comparing the right-hand sides of Equations 2.3 and 2.7. This allows the force to be expressed in terms of the dimensionless trapping parameters, $a$ and $q$ as shown in the equations 2.8 and 2.9. The expression $ze$ refers to the charge of the ion in Coulombs, where $z$ is the ion's nominal charge and $e$ is the charge of an electron.

$$a_x = \frac{8zeU}{mr_0^2\Omega^2} \qquad (2.8)$$

$$q_x = -\frac{4zeV}{mr_0^2\Omega^2} \qquad (2.9)$$

The $a_z$ and $q_z$ trapping parameters corresponding to the movement of the ion cloud in the axial direction are frequently used in discussions of the stability diagram of the QIT. These parameters are defined in Equations 2.10 and 2.11 and illustrated in the Mathieu stability diagram[15] shown in Figure 2.4.

$$a_z = -\frac{8zeU}{mr_0^2\Omega^2} \quad (2.10)$$

$$q_z = \frac{4zeV}{mr_0^2\Omega^2} \quad (2.11)$$

The Mathieu stability diagram[15] illustrates the voltage ranges in the QIT where ions of a particular m/z can be stored. At a particular V, all ions above a specific m/z value remain trapped in the QIT according to the following equation with $q_{max}$ being the maximum value where $q_z$ intersects with the boundary created by $\beta_z$=1. For most QIT instruments, the maximum value of $q_z$ is 0.908. The relationship of ionic *m/z* and $q_{max}$ is as shown in Equation 2.12.

$$\frac{m}{z} = \frac{4eV}{q_{max}\Omega^2 r_0^2} \quad (2.12)$$

During excitation for MS/MS or ion detections, trapped ions are excited by placing an auxiliary voltage on the end caps causing the orbital radius and frequency of the ions to increase. Each ion with a specific *m/z* has a specific oscillating frequency referred to as the secular frequency. As a result of the applied voltage, the ion cloud moves away from the center of the trap. Increasing the RF voltage (V) causes the ions to sequentially come into resonance (based of their *m/z*), expanding their radius of motion and eventually expelling the ions from the trap to the detector.

The detector is the Daly system, named after the inventor Norman Richard Daly.[17] This is the most commonly used detector[18] in mass spectrometers because of its increased lifetime. The long lifetime is achieved because the ions and neutrals do not come into direct contact with the actual electron multiplication dynodes. Ions exciting the trap are focused onto a conversion

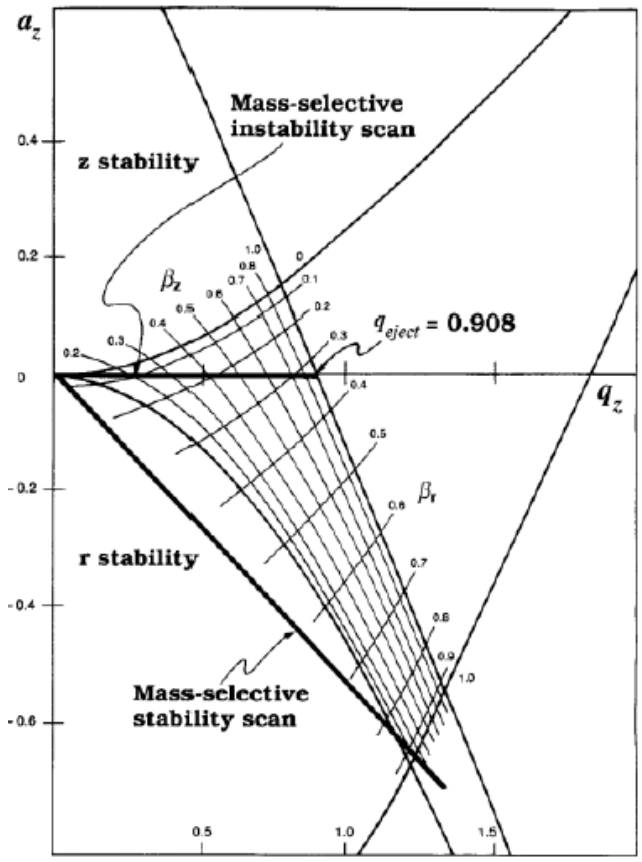


Figure 2.4. Mathieu stability diagram (used with permission from reference 15).

dynode which emits a photon beam. These photons pass through a quartz or glass window and strike a photomultiplier tube (PMT) that operates similarly to an electron multiplier (EM). The detector consists of dynode surfaces of usually a copper-beryllium alloy that readily expels electrons upon bombardment with any particles including electrons. A series of stages allows for multiplying of electrons with a gain of as much as $10^6$ to $10^7$. Emitted electrons strike the opposite surface and an electrical current is measured at the anode.

The QIT employed in this work is a high capacity spherical ion trap (HCT).[19] The HCT is not bigger than a regular QIT. However, the trap has an RF voltage applied to all three

electrodes to create a field that more closely mimics that of a hexapole. Therefore, ions are forced closer together in the center of the trap resulting in better ion motion control, increased interactions and overlap of clouds of ions for MS/MS (especially important for ETD), increased sensitivity, and increased storage capacity of the trap compared to a linear trap (Figure 2.5).

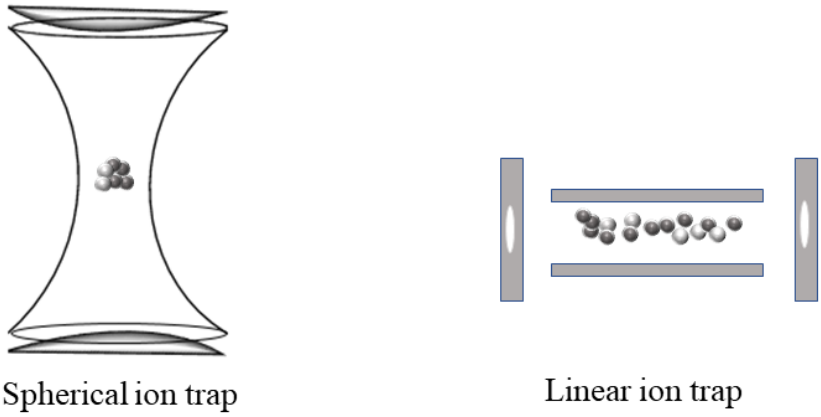


Figure 2.5. Diagram showing overlap of ions in a spherical vs. a linear ion trap.

## 2.4 Dissociation methods

### 2.4.1 Collision-induced dissociation

The most common method of tandem mass spectrometry is collision-induced dissociation (CID), also known as collision-activated dissociation (CAD). The technique was first introduced in the late 1960s and has grown to be the widely employed in $MS^n$ experiments. In CID, ions are excited with extra kinetic energy and allowed to collide with a neutral bath gas to bring about dissociation. Peptide ions of interest, referred to as precursor ions, are isolated by resonance frequency ejection techniques. A broadband range of frequencies (for the AC voltage) is applied

to the ions in the trap. The ions with these applied frequencies increase their kinetic energy and are ejected from the trap. The resonant frequency of the ion of interest is excluded; thus, the precursor ions remain in the trap. These precursor ions are accelerated and collide with the inert bath gas (helium in the QIT). Collision processes lead to conversion of some translational energy into internal energy that is distributed along the backbone of the peptide. Unimolecular dissociation of the precursor ion follows. Lowest energy processes generally dominate in CID with backbone cleavage occurring between the C-N amide bond forming b-, and y-ions. Also common is cleavage of side chains of amino acids residues in the peptide sequence. CID occurs in two processes as shown in equations 2.13 and 2.14:

$$\text{Collision activation:} \quad m_1^+ + He \rightarrow [m_1^+]^* + He^{/} \tag{2.13}$$

$$\text{Unimolecular dissociation:} \quad [m_1^+]^* \rightarrow m_2^+ + m_3 \tag{2.14}$$

In the above equations, $m_1^+$ represents the precursor ion, He is helium (inert gas), $He^{/}$ is helium after the collision with the precursor ion, and $m_2^+$ and $m_3$ are product ions.

Low energy CID (1-100 eV), the most common form of MS/MS,[20] was performed in the Bruker HCTultra PTM QIT for experiments in this dissertation. Ions are excited to the upper vibrational states. High energy CID imparts keV of energy (3-10 keV)[14] resulting in excitation to both electronic and vibrational states. More fragmentation occurs with high energy CID that can be performed in magnetic sectors and time-of-flight mass analyzers (TOF), but QIT and linear quadrupoles employ low energy CID.

### 2.4.2 Electron transfer dissociation

Electron transfer dissociation, one of the newer MS/MS techniques used in peptide sequencing,[21-23] was introduced by Hunt and coworkers in 2004.[24] Unlike in CID, sites of

posttranslation modification (PTMs), such as phosphorylation, glycosylation, and sulfonation, are preserved in ETD allowing for easier identification of the site of modification.[25-27] The ETD process involves transfer of a low energy electron from a radical anion to a positive, multiply charged ($[M + nH]^{n+}$, $n \geq 2$) precursor ion to initiate dissociation as shown in Figure 2.6. In this

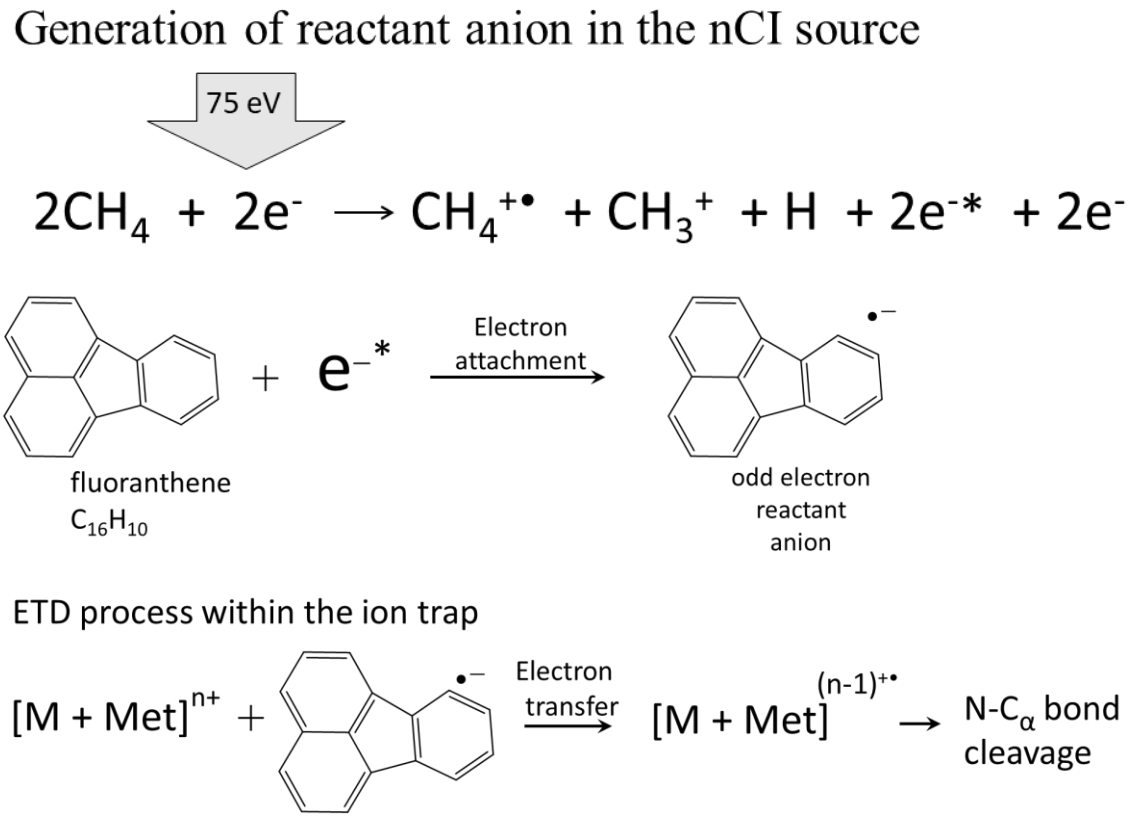


Figure 2.6. ETD reaction showing formation of ions in the nCI source and product ion formation in the ion trap.

study, the positive, multiply charged precursor ions are metallated, $([M + Met])^{n+}$, $n \geq 2$). If an electron is transferred to a singly charged species, the neutral molecule resulting cannot be detected during mass spectrometry.

The ETD process involves several steps as illustrated in Figure 2.6. The low energy electrons are generated in a multi-step process. In the first step, high energy electrons are generated by an electron ionization (EI) filament at 75 eV. In the next step, these high energy electrons interact with methane gas in a negative chemical ionization chamber (nCI) to produce low energy electrons ($e^{-}$*, 1 eV) from the resulting plasma. These low energy electrons are transferred to an ETD reagent gas with a low electron affinity, such as fluoranthene as was used in this work. Fluoranthene radical anions are moved to the QIT by electrostatic focusing. The position of the nCI and ESI sources in relation to the ion trap is shown in Figure 2.7. During an ETD reaction, the reagent (fluoranthene) anion and an *m/z*-selected multiply positively charged precursor ion undergo an ion/ion reaction as shown in the last reaction of Figure 2.6. The fluoranthene anion transfers a low energy electron to a multiply charged precursor cation. The resulting reduced ion, $[M + nH]^{(n-1)+\bullet}$ undergoes dissociation with N-Cα backbone cleavage generating c- and z-ions. (The c- and z-ions will be discussed in Section 2.5). Immediately after the anion/cation reaction, the "smart decomposition" function is used to further dissociate any charge reduced product ions; for example, analysis of $[M + Met]^{3+}$ may yield an electron transfer no dissociation (ETnoD) product $[M + Met]^{2+}$ that is subjected to smart decomposition. Smart decomposition enhances ETD product ion formation by using resonant excitation (very low energy CID) to overcome attractive forces (e.g., hydrogen or noncovalent bonding) that may hold peptide fragments together following the electron transfer process. In the studies in this dissertation, the low energy electron may be captured by the metal ion, but in most instances, it is

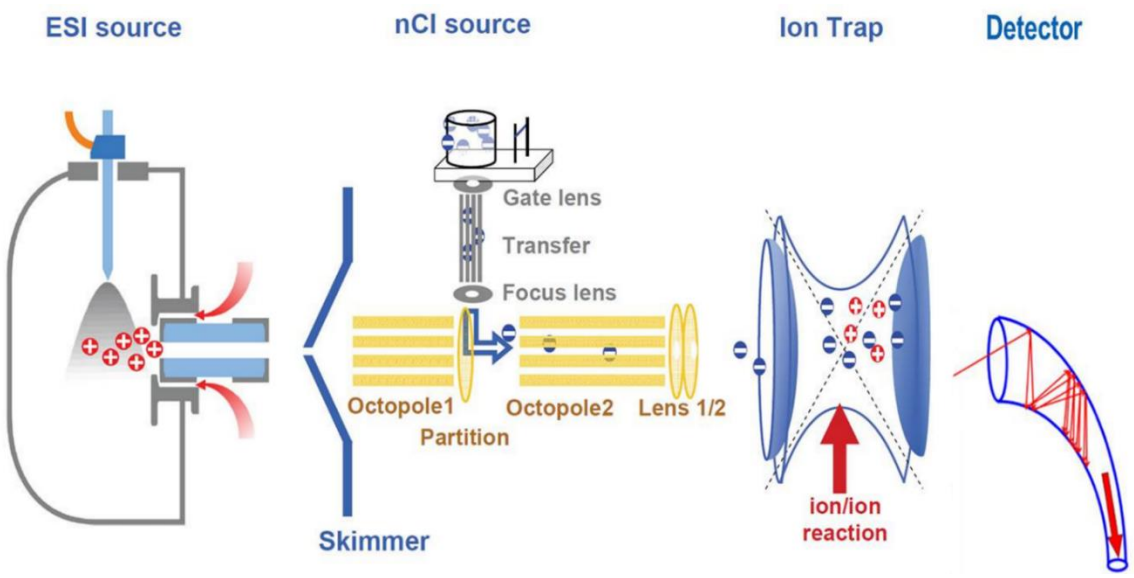


Figure 2.7. ESI and nCI source setup in Bruker HCTultra PTM Discovery System mass spectrometer showing positive and negative ions trapped in the QIT (used with permission from reference 19).

believed to be directed to another charged site and the metal ions retain their trivalent charge. Electron transfer dissociation is similar to electron capture dissociation (ECD), which is another tandem mass spectrometry technique. However, ECD uses electrons generated from an electron filament in a Fourier transform ion cyclotron resonance (FT-ICR) cell to initiate dissociation.[27] The electrons are captured by a multiply charged peptide ion in the ECD process. Both ECD and ETD produce primarily c- and z-ions resulting from backbone cleavage of the N-Cα bond of peptides.

Two mechanisms exist to explain the formation of c- and z-ions by ECD and ETD of protonated peptides. In the Cornell mechanism proposed by McLafferty and coworkers,[28] the captured or transferred electron is localized at a positive site (such as ammonium or guanidium groups) and forms a radical center on the hydrogen. This hydrogen then attacks an oxygen atom of the backbone carbonyl to form a fragile odd-electron radical species.[29,30] This odd-electron

intermediate was verified by O'Connor and coworkers.[31] The radical species then undergoes homolytic cleavage of the N-Cα bond to form c- and z- ions,[32] as shown in Figure 2.8. The Cornell mechanism relies on the presence of a highly basic amino acid residue in a peptide sequence. However, some peptides lack this highly basic site yet still undergo ETD and ECD.

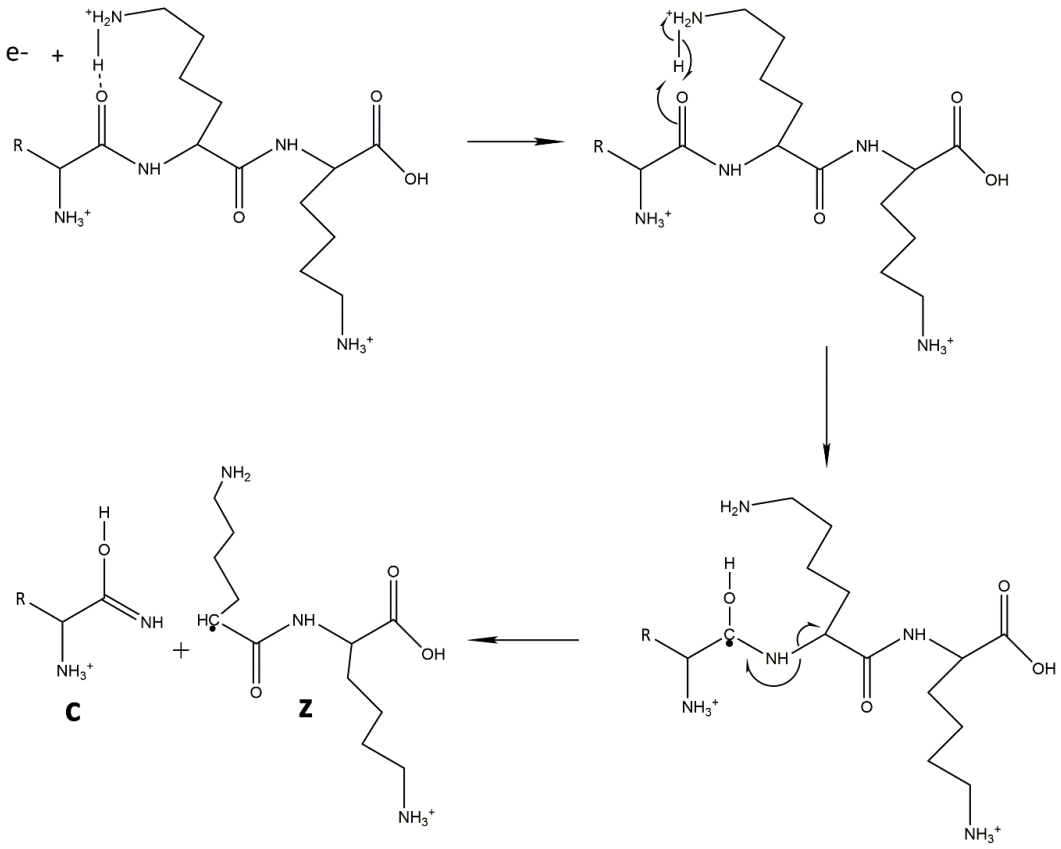


Figure 2.8. The Cornell mechanism for N-Cα bond cleavage in ETD of peptides and proteins.

Therefore, the Utah-Washington (UW) mechanism was developed to explain N-Cα bond cleavage of such molecules. Tureček and Syrstad[33] and Simons and coworkers[34] independently

presented the UW mechanism shown in Figure 2.9. An electron attaches directly to an amide II* orbital. The intermediate, which can be refered to as an aminoketyl radical-anion, undergoes proton transfer resulting in an aminoketyl radical that dissociates to form c- and z- fragments. Alternatively, the aminoketyl radical-anion can undergo N-Cα bond cleavage forming an enole-imidate intermediate that subsequently undergoes proton transfer to form c- and z- product ions.[35] The Cornell and UW mechanisms differ in the fact that the UW mechanism occurs in the absence of amino acid residues with highly basic side chains.

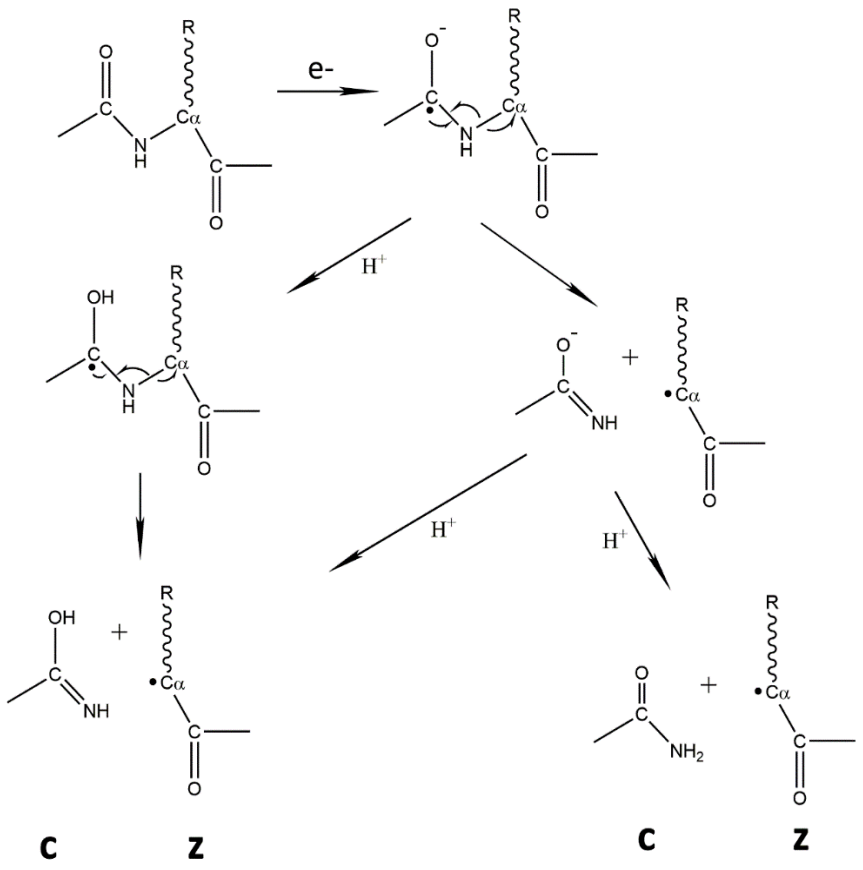


Figure 2.9. The Utah-Washington mechanism for N-Cα bond cleavage in ETD of peptides and proteins.

The mechanism involved in ETD of metal-peptide complexes is not as fully explored as that of protonated peptides. The capture or transfer of an electron in a metal-peptide complex can lead to either N-Cα bond cleavage or reduction of the metal center: $[M + Met]^{3+} + e^- \rightarrow [M+ Met]^{2+}$. Dissociation or reduction are often competing processes in the ECD or ETD of these metal-peptide complexes. In some ECD studies,[36-39] the fragmentation of metal-peptide complexes has been discussed on the basis of the Cornell mechanism. This is justified by the presumption that the N-Cα bond cleavage in ETD of protonated peptides and metal-peptide complexes are similar. With the metal ion bound to a deprotonated carboxylic acid functionality, electron attachment occurs at a proton site remote from the metal cation. The resultant radical center on the metal-adducted intermediate dissociates to form the characteristic c- and z- product ions. Exceptions exist such as divalent copper, $Cu^{2+}$, which will favorably sequester that electron to be reduced to $Cu^+$.[38,40,41] Here, the reduction is driven by the stability of the formation of $Cu^+$, which has filled d-orbitals. Therefore, $Cu^+$ metal-peptide complexes exhibit different fragmentation patterns than other metals in its series. A similar different fragmentation is observed for trivalent europium, $Eu^{3+}$, as discussed in Chapter 3. The stability of the half-filled f-orbital of the $Eu^{2+}$ drives the sequestration of the transferred electron. Metal cations that will not be favorably reduced, such as $Zn^{2+}$, $Mn^{2+}$ or the other trivalent lanthanide metal ions, may facilitate abundant N-Cα bond cleavage via the formation of the radical ion remote from the metal-adducted site. In addition to the metal properties, the ability of the non-reduced metal ion to facilitate N-Cα bond cleavage by the Cornell mechanism is dependent on the presence of excess protons in the system. Therefore, in this mechanism removal of these remote protons should limit the fragmentation efficiency observed by ECD/ETD.

In two separate studies involving metal-peptide complexes, Asakawa and coworkers[42,43]

observed that the number of excess protons had no influence on the yield of ETD product ions. In a further study, Asakawa and coworkers[44] performed ETD on Zn(II)-polyhistidine complexes in the absence of remote protons and observed the formation of c- and z-ions similar to systems containing excess protons. Excess protons were removed by amidation of the C-terminal carboxylic acid group. In a series of ETD experiments and density functional theory (DFT) calculations, the researchers postulated that N-Cα bond cleavage of metal-peptide complexes are dominated by the mechanism as outlined by the UW model instead of the Cornell mechanism. Electron transfer dissociation of doubly protonated polyhistidine complexes and Zn(II)-polyhistidine produced the same type of fragment ions in the absence of the remote protons. The N-Cα bond cleavage occurred via the aminoketyl radical as formed in the UW mechanism to produce the c- and z-fragment ions observed. In this dissertation, metal-peptide complexes of biological and model acidic peptides yielded abundant N-Cα bond cleavage. In many cases, full sequence coverage occurred. Therefore, the results in this dissertation are more consistent with the UW mechanism.

## 2.5 Peptide sequencing nomenclature

The standard peptide fragmentation nomenclature throughout this dissertation for labelling ions in the CID and ETD spectra was developed by Roepstorff and Fohlman[45] and modified by Biemann.[46] Cleavage along the backbone of a protonated or deprotonated peptide forms product ions as shown in Figure 2.10. After cleavage, the charge remains with one side of the peptide dissociation products while the other portion is neutral and not detected by the mass spectrometer. If the charge is retained on the N-terminal portion of the peptide, the products are described as a, b, or c-ions, and on the C-terminal portion, products are labeled as x, y, or z-ions. Subscripts denote the site of cleavage along the peptide backbone. For example, in Figure 2.10,

cleavage between the N-Cα bond of the first amino acid residues from the C-terminus forms $z_1$ and $c_3$. Prime symbols provide information about mobile hydrogens relative to the structure obtained from cleavage at a site. Addition of hydrogens is denoted by prime symbols to the right of the fragment letter. For example, $c_n^{//+}$ means $[c_n + 2H]^+$. On the left, prime symbols mean loss or subtraction of hydrogens. For example, $^{/}z_n$ means $[z_n - H]^+$. In addition, product ion nomenclature will also indicate the presence of a metal ion. For example, $[c_8^{/} + Pr]^+$ is a singly charged product ion formed after cleavage of the N-Cα bond after the eight amino acid residue

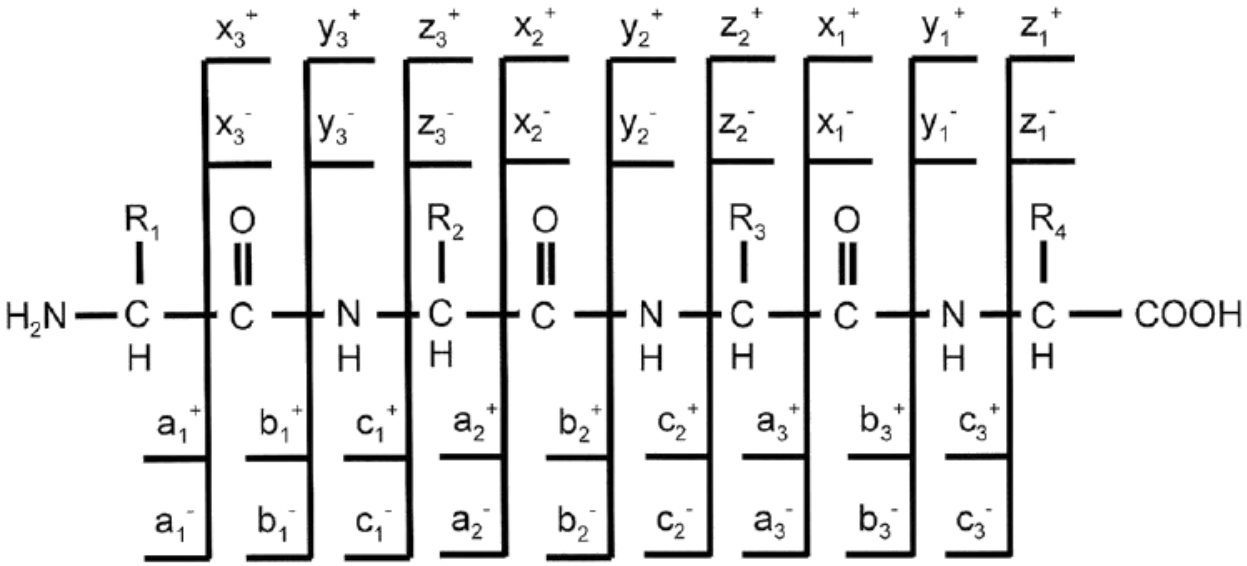


Figure 2.10. Peptide sequence nomenclature for MS/MS.

from the N-terminus and contains a $Pr^{3+}$. As mentioned previously in Section 2.4.2, the ions commonly generated during ETD are $c_n$ and $z_n$ resulting from the cleavage between N-Cα

peptide backbone bonds. Unlike CID (which forms $b_n$ and $y_n$), ETD and ECD are nonergodic with faster processes occurring as opposed to lower energy processes.[28]

## 2.6 Peptide synthesis

Some of the peptides studied were synthesized using Fmoc solid phase peptide synthesis procedures (SPPS) developed by Merrifield.[47] An Advanced ChemTech Model 90 peptide synthesizer (Louisville, KY, USA) was employed.

Solid phase peptide synthesis requires that the peptide be assembled from the C-terminus and lengthened in a step-wise manner by adding amino acid residues to complete the sequence at the N-terminus. The process starts with an amino acid residue attached to a Wang resin, which is an insoluble polystyrene bead. Each additional residue is attached to a labile 9-fluoroenylmethyloxycarbonyl (Fmoc) group as shown in Figure 2.11. The Fmoc group helps to prevent unwanted reactions of the side chain on the amino acid residue. The Fmoc-amino acid residues and Fmoc-amino acid Wang resins were purchased commercially. For the model peptides, the lack of a commercially available phosphorylated amino acid Wang resin meant that the phosphorylated residue could not be placed as the C-terminal residue in the phosphorylated peptides.

The peptide synthesis process occurs in a set of repeated cycles of coupling and deprotection as outlined in Figure 2.12. An amino acid unit with a protected N-terminus is coupled onto a solid phase peptide (bound to the resin support) with a free N-terminal amine. Once the new peptide bond is created (coupled), the N-terminal site of the newly added amino acid unit is deprotected to reveal an active site for coupling of another amino acid unit. Repeated coupling and deprotecting steps adds the desired number and types of amino acid residues

required. Cleavage of the newly synthesized peptide from the resin support occurred followed by deprotection of all side chains yielding a crude free peptide.

In the work presented in this dissertation, many of the model peptides were synthesized in the Cassady laboratory. The processes involve many chemicals purchased from various sources. Apart from the amino acid residues and Wang resins, the other chemicals included 1-hydroxybenzotriazole hydrate (HOBt), N,N-dimethylformamide (DMF), 1,3-diisopropylcarbodiimide (DIC), N-methyl-2-pyrrolidinone (NMP), trifluoroacetic acid (TFA), triisopropylsilane (TIS), methanol (MeOH), and ethyl ether. The C-terminal amino acid residues in a peptide sequence contain the Fmoc protecting groups and Wang resins.

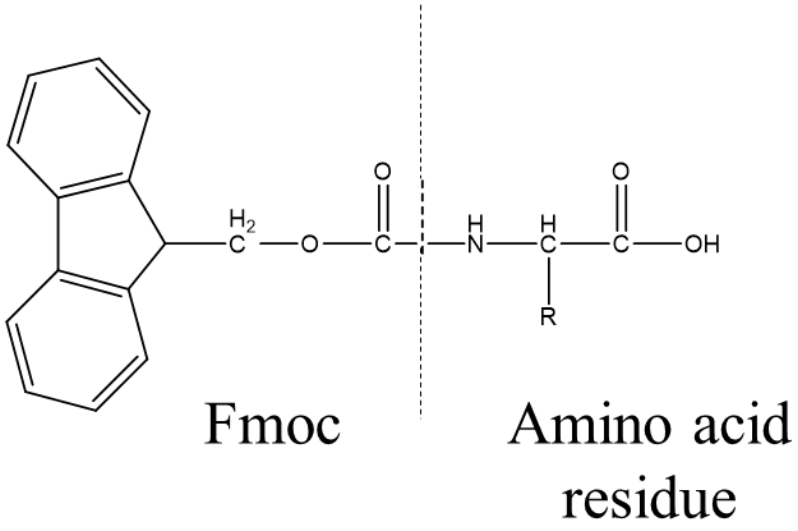


Figure 2.11. Fmoc protective group attached to a generic amino acid residue.

The desired resin was placed in a reaction vessel that was attached to the peptide synthesizer. Amino acid residue solutions were prepared at 0.5 M as solutions of 0.5 M 1-HOBt (prepared as 0.5M in NMP). These were placed in separate amino acid vessels and attached to the instrument in designated positions. The resin in the reaction vessel is first washed withDMF, MeOH, and then DMF again. A solution of PIP containing 20% piperidine in DMF (v/v) was used to remove the Fmoc protecting group. The coupling was carried out by the HOBt that served to reduce racemization along with DIC (prepared as 0.5 M in NMP) to activate the carboxyl group. Coupling was allowed to occur by mechanical shaking of the reaction vessel for 60-75 minutes per amino acid residue. Each coupling step was followed by the same wash steps as described above. The series of repeated wash/deprotect/couple/wash steps were customized by writing a program that met the needs of the synthesis.

Once all the residues were added, the side chain protecting groups and the C-terminal resin were cleaved to release the free peptide. Cleavage was achieved by adding a mixture containing 9.5 mL TFA, 0.3 mL TIS, and 0.5 mL ultrapure Milli-Q (MQ) 18 MΩ water to the reaction vessel and allowed to mix for three hours. The resulting mixture was filtered to remove the resin and protecting groups. Diethyl ether cooled to -78° C on a dry ice/acetone slurry was added to the filtrate to precipitate the peptide. The precipitating peptide solution was left for three hours in the freezer. After three hours, a gel-like mixture was centrifuged at 3000 rpm for 20 minutes to separate the gel from the solution. Another three-hour precipitation step was repeated with diethyl ether followed by centrifugation. The resulting gel containing the peptide of interest was dried in a desiccator overnight. The crude synthesized peptide was used directly for mass analysis. In some instances, peptide modification such as methyl esterification was performed as described in Section 2.6.1.

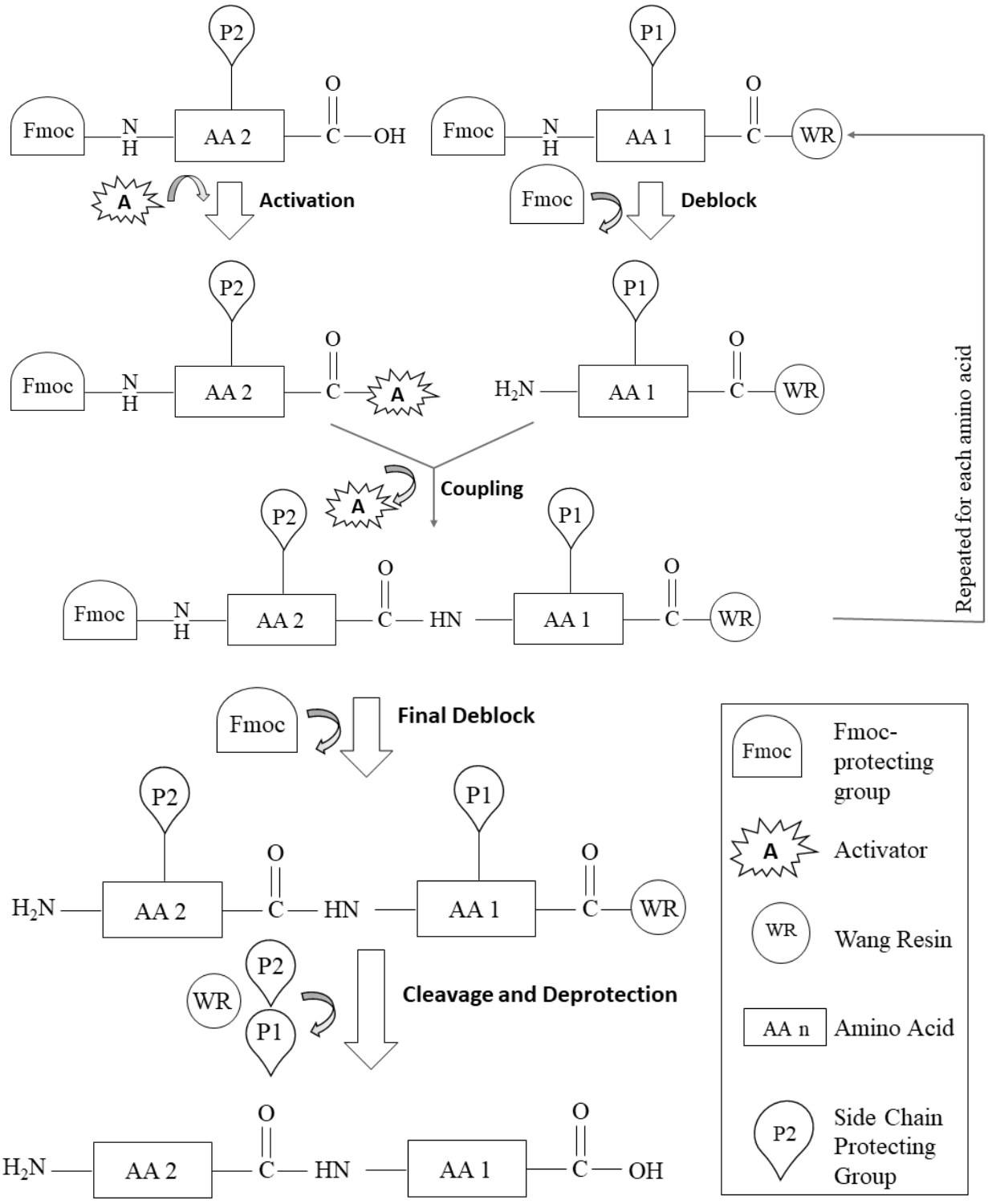


Figure 2.12. Outline of steps involved in SPSS peptide synthesis.

## 2.7 Amino acid structure

The peptides employed in the experiments are composed of different amino acid residues with varying sequences and chain length. The structures of the common 20 amino acids are shown in Figures 2.13 to 2.19. In addition, the structures of the phosphorylated amino acid residues used are shown in Figure 2.20.

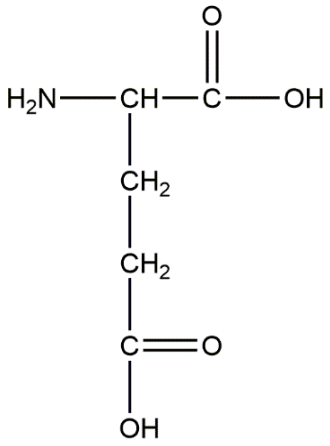


Glutamic acid (Glu, E)

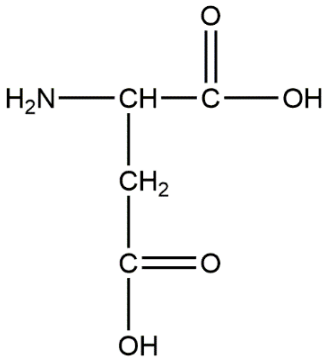


Aspartic acid (Asp, D)

Figure 2.13. Amino acids with acidic side chains.

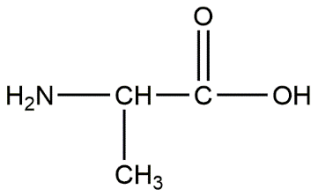


Alanine, (Ala, A)

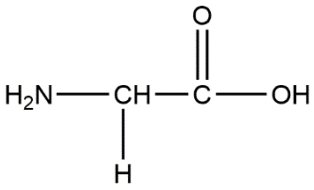


Glycine (Gly, G)

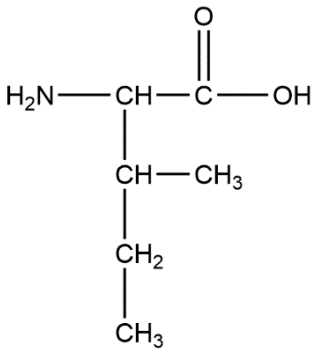


Isoleucine (Ile, I)

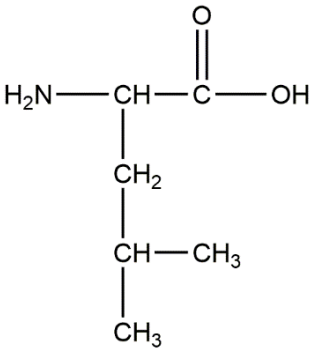


Leucine (Leu, L)

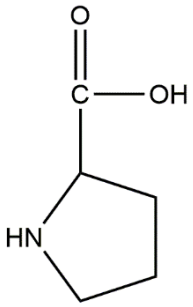


Proline (Pro, P)

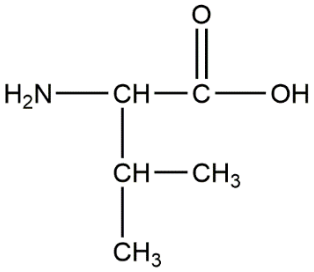


Valine (Val, V)

Figure 2.14. Amino acids with aliphatic side chains.

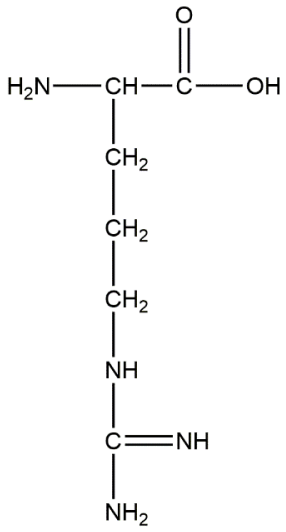


Arginine (Arg, R)

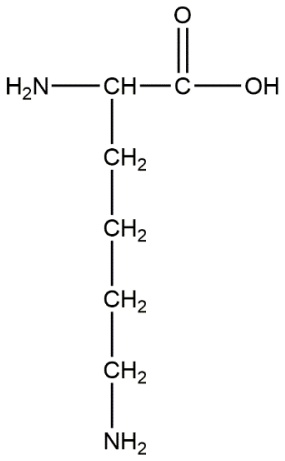


Lysine (Lys, K)

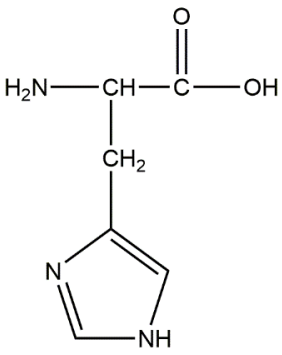


Histidine (His, H)

Figure 2.15. Amino acids with basic side chains.

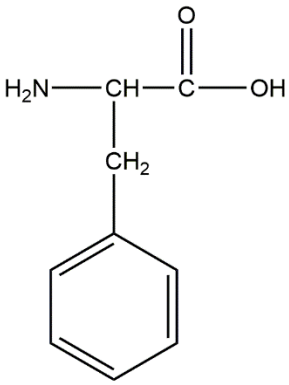


Phenylalanine (Phe, F)

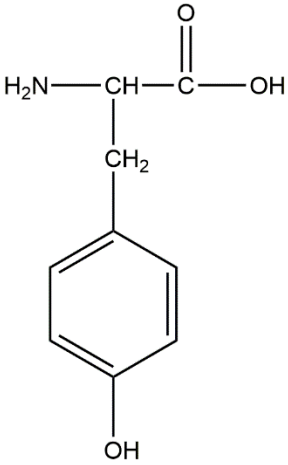


Tyrosine (Tyr, Y)

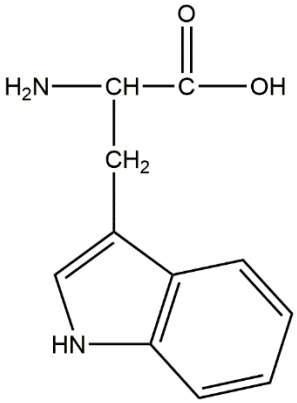


Tryptophan (Trp, W)

Figure 2.16. Amino acids with aromatic side chains. (Histidine also contains an aromatic side chain but was already included in Figure 2.15.)

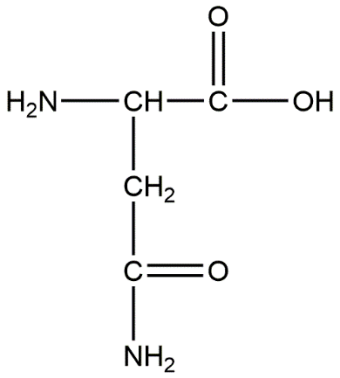


Asparagine (Asn, N)

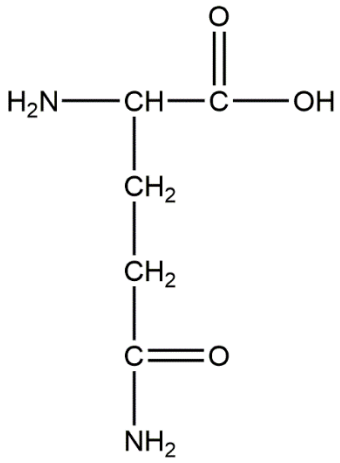


Glutamine (Gln, Q)

Figure 2.17. Amino acids with amine side chains.

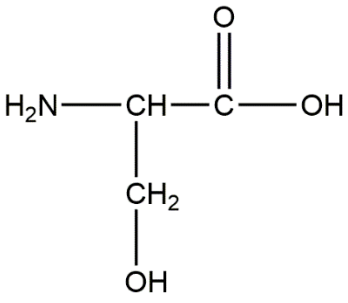


Serine (Ser, S)

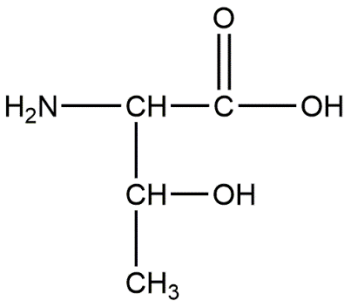


Threonine (Thr, T)

Figure 2.18. Amino acids with hydroxyl side chains. (Tyrosine also contains a hydroxyl amino acid side chain but was already included with the amino acids with aromatic side chains in Figure 2.16.).

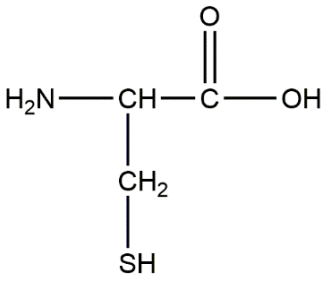


Cysteine (Cys, C)

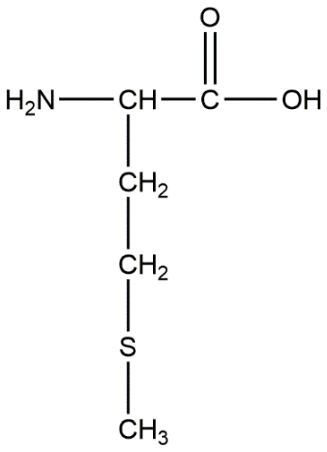


Methionine (Met, M)

Figure 2.19. Amino acids with side chains containing sulfur.

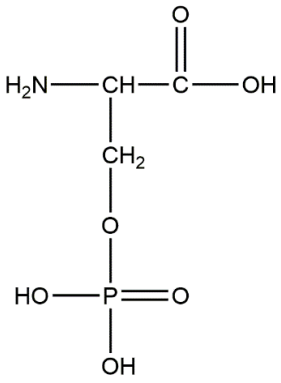


Phosphoserine (pS)

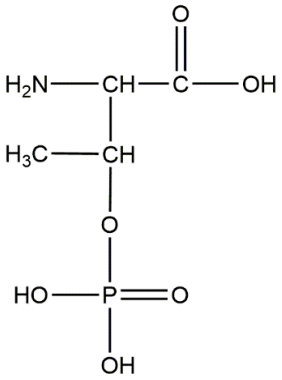


Phosphothreonine (pT)

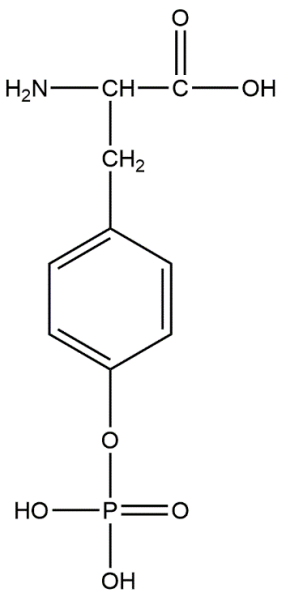


Phosphotyrosine (pY)

Figure 2.20. Amino acids with phosphorylated side chains.

## References


1. Dole, M.; Mack, L. L.; Hines, R. L. Molecular Beams of Macroions. *J. Chem. Phys.* **1968**, *49*, 2240-&.

2. Yamashita, M.; Fenn, J. B. Electrospray Ion-Source - Another Variation on the Free-Jet Theme. *J. Phys. Chem.* **1984**, *88*, 4451-4459.

3. Fenn, J. B.; Mann, M.; Meng, C. K.; Wong, S. F.; Whitehouse, C. M. Electrospray Ionization for Mass Spectrometry of Large Biomolecules. *Science* **1989**, *246*, 64-71.

4. Fenn, J. B.; Mann, M.; Meng, C. K.; Wong, S. F. Electrospray Ionization--Principles and Practice. *Mass Spectrom. Rev.* **1990**, *9*, 37-70.

5. Smith, R. D.; Loo, J. A.; Loo, R. R. O.; Busman, M.; Udseth, H. R. Principles and Practice of Electrospray Ionization - Mass-Spectrometry for Large Polypeptides and Proteins. *Mass Spectrom. Rev.* **1991**, *10*, 359-451.

6. Whitehouse, C. M.; Dreyer, R. N.; Yamashita, M.; Fenn, J. B. Electrospray Ionization for Liquid Chromatographs and Mass Spectrometers. *Anal. Chem.* **1985**, *57*, 675-679.

7. Ikonomou, M. G.; Blades, A. T.; Kebarle, P. Investigations of the Electrospray Interface for Liquid-Chromatography Mass-Spectrometry. *Anal. Chem.* **1990**, *62*, 957-967.

8. Kebarle, P. A Brief Overview of the Present Status of the Mechanisms Involved in Electrospray Mass Spectrometry. *J. Mass Spectrom.* **2000**, *35*, 804-817.

9. Kebarle, P.; Peschke, M. On the Mechanisms by Which the Charged Droplets Produced by Electrospray Lead to Gas Phase Ions. *Anal. Chim. Acta* **2000**, *406*, 11-35.

10. Ikonomou, M. G.; Blades, A. T.; Kebarle, P. Electrospray-Ion Spray: A Comparison of Mechanisms and Performance. *Anal. Chem.* **1991**, *63*, 1989-1998.

11. Wilm, M. S.; Mann, M. Electrospray and Taylor-Cone Theory, Doles Beam of Macromolecules at Last. *Int. J. Mass Spectrom.* **1994**, *136*, 167-180.

12. Gomez, A.; Tang, K. Q. Charge and Fission of Droplets in Electrostatic Sprays. *Phys. Fluids* **1994**, *6*, 404-414.

13. Tang, K.; Gomez, A. On the Structure of an Electrostatic Spray of Monodisperse Droplets. *Phys. Fluids* **1994**, *6*, 2317-2332.

14. Chhabil, D. *Fundamentals of contemporary mass spectrometry;* John Wiley & Sons, Inc.: New Jersey, 2007.

15. Paul, W. Electromagnetic Traps for Charged and Neutral Particles. *Rev. Mod. Phys.* **1990**, *62*, 531-540.

16. March, R. E. An Introduction to Quadrupole Ion Trap Mass Spectrometry. *J. Mass Spectrom.* **1997**, *32*, 351-369.

17. Daly, N. R. Scintillation Type Mass Spectrometer Ion Detector. *Rev. Sci. Instrum.* **1960**, *31*, 264-267.

18. Pramann, A.; Rademann, K. A New Scintillation-type Time-of-flight Anion Detector. *Rev. Sci. Instrum.* **2001**, *72*, 3475-3476.

19. Bruker Daltonics *HCTultra PTM Discovery System User Manual;* Billerica, MA, 2006.

20. Wells, J. M.; McLuckey, S. A. Collision-induced Dissociation (CID) of Peptides and Proteins. *Biol. Mass Spectrom.* **2005**, *402*, 148-185.

21. Coon, J. J. Collisions or Electrons? Protein Sequence Analysis in the 21st Century. *Anal. Chem.* **2009**, *81*, 3208-3215.

22. Good, D. M.; Wirtala, M.; McAlister, G. C.; Coon, J. J. Performance Characteristics of Electron Transfer Dissociation Mass Spectrometry. *Mol. Cell. Proteomics* **2007**, *6*, 1942-1951.

23. Gunawardena, H. P.; Gorenstein, L.; Erickson, D. E.; Xia, Y.; McLuckey, S. A. Electron Transfer Dissociation of Multiply Protonated and Fixed Charge Disulfide Linked Polypeptides. *Int. J. Mass Spectrom.* **2007**, *265*, 130-138.

24. Syka, J. E. P.; Coon, J. J.; Schroeder, M. J.; Shabanowitz, J.; Hunt, D. F. Peptide and Protein Sequence Analysis by Electron Transfer Dissociation Mass Spectrometry. *Proc. Natl. Acad. Sci. USA* **2004**, *101*, 9528-9533.

25. Cooper, H. J.; Håkansson, K.; Marshall, A. G. The Role of Electron Capture Dissociation in Biomolecular Analysis. *Mass Spectrom. Rev.* **2005**, *24*, 201-222.

26. Zubarev, R. A. Reactions of Polypeptide Ions with Electrons in the Gas Phase. *Mass Spectrom. Rev.* **2003**, *22*, 57-77.

27. Zubarev, R. A. Electron-capture Dissociation Tandem Mass Spectrometry. *Curr. Opin. Biotechnol.* **2004**, *15*, 12-16.

28. Zubarev, R. A.; Kelleher, N. L.; McLafferty, F. W. Electron Capture Dissociation of Multiply Charged Protein Cations. A Nonergodic Process. *J. Am. Chem. Soc.* **1998**, *120*, 3265-3266.

29. Savitski, M. M.; Kjeldsen, F.; Nielsen, M. L.; Zubarev, R. A. Hydrogen Rearrangement to and from Radical z Fragments in Electron Capture Dissociation of Peptides. *J. Am. Soc. Mass Spectrom.* **2007**, *18*, 113-120.

30. McLafferty, F. W.; Horn, D. M.; Breuker, K.; Ge, Y.; Lewis, M. A.; Cerda, B. A.; Zubarev, R. A.; Carpenter, B. K. Electron Capture Dissociation of Gaseous Multiply Charged Ions by Fourier Transform ion Cyclotron Resonance. *J. Am. Soc. Mass Spectrom.* **2001**, *12*, 245-249.

31. Lin, C.; Cournoyer, J. J.; O'Connor, P. B. Use of a Double Resonance Electron Capture Dissociation Experiment to Probe Fragment Intermediate Lifetimes. *J. Am. Soc. Mass Spectrom.* **2006**, *17*, 1605-1615.

32. Axelsson, J.; Palmblad, M.; Håkansson, K.; Håkansson, P. Electron Capture Dissociation of Substance P Using a Commercially Available Fourier Transform Ion Cyclotron Resonance Mass Spectrometer. *Rapid Commun. Mass Spectrom.* **1999**, *13*, 474-477.

33. Syrstad, E. A.; Tureček, F. Toward a General Mechanism of Electron Capture Dissociation. *J. Am. Soc. Mass Spectrom.* **2005**, *16*, 208-224.

34. Sobczyk, M.; Anusiewicz, I.; Berdys-Kochanska, J.; Sawicka, A.; Skurski, P.; Simons, J. Coulomb-assisted Dissociative Electron Attachment: Application to a Model Peptide. *J. Phys. Chem. A* **2005**, *109*, 250-258.

35. Chen, X.; Tureček, F. The Arginine Anomaly: Arginine Radicals are Poor Hydrogen Atom Donors in Electron Transfer Induced Dissociations. *J. Am. Chem. Soc.* **2006**, *128*, 12520-12530.

36. Fung, Y. M. E.; Liu, H.; Chan, T. W. D. Electron Capture Dissociation of Peptides Metalated with Alkaline-Earth Metal Ions. *J. Am. Soc. Mass Spectrom.* **2006**, *17*, 757-771.

37. Chen, X.; Chan, W. Y. K.; Wong, P. S.; Yeung, H. S.; Chan, T. W. D. Formation of Peptide Radical Cations ($M^{+\cdot}$) in Electron Capture Dissociation of Peptides Adducted with Group IIB Metal Ions. *J. Am. Soc. Mass Spectrom.* **2011**, *22*, 233-244.

38. Chen, X.; Fung, Y. M. E.; Chan, W. Y. K.; Wong, P. S.; Yeung, H. S.; Chan, T. W. D. Transition Metal Ions: Charge Carriers that Mediate the Electron Capture Dissociation Pathways of Peptides. *J. Am. Soc. Mass Spectrom.* **2011**, *22*, 2232-2245.

39. Flick, T. G.; Donald, W. A.; Williams, E. R. Electron Capture Dissociation of Trivalent Metal Ion-Peptide Complexes. *J. Am. Soc. Mass Spectrom.* **2013**, *24*, 193-201.

40. Liu, H.; Håkansson, K. Divalent Metal Ion-Peptide Interactions Probed by Electron Capture Dissociation of Trications. *J. Am. Soc. Mass Spectrom.* **2006**, *17*, 1731-1741.

41. Dong, J.; Vachet, R. W. Coordination Sphere Tuning of the Electron Transfer Dissociation Behavior of Cu(II)-peptide Complexes. *J. Am. Soc. Mass Spectrom.* **2012**, *23*, 321-329.

42. Asakawa, D.; Takeuchi, T.; Yamashita, A.; Wada, Y. Influence of Metal–Peptide Complexation on Fragmentation and Inter-Fragment Hydrogen Migration in Electron Transfer Dissociation. *J. Am. Soc. Mass Spectrom.* **2014**, *25*, 1029-1039.

43. Asakawa, D.; Wada, Y. Electron Transfer Dissociation Mass Spectrometry of Peptides Containing Free Cysteine Using Group XII Metals as a Charge Carrier. *J Phys Chem B* **2014**, *118*, 12318-12325.

44. Asakawa, D.; Yamashita, A.; Kawai, S.; Takeuchi, T.; Wada, Y. N–Cα Bond Cleavage of Zinc-Polyhistidine Complexes in Electron Transfer Dissociation Mediated by Zwitterion Formation: Experimental Evidence and Theoretical Analysis of the Utah–Washington Model. *J Phys Chem B* **2016**, *120*, 891-901.

45. Roepstorff, P.; Fohlman, J. Proposal for a Common Nomenclature for Sequence Ions in Mass Spectra of Peptides. *Biomed. Mass Spectrom.* **1984**, *11*, 601.

46. Biemann, K. Contributions of Mass Spectrometry to Peptide and Protein-Structure. *Biomed. Environ. Mass Spectrom.* **1988**, *16*, 99-111.

47. Merrifield, R. B. Solid Phase Peptide Synthesis. I. The Synthesis of a Tetrapeptide. *J. Am. Chem. Soc.* **1963**, *85*, 2149-2154.

48. Greene, T. W.; Wuts, P. G. M., Eds.; In *Protective Groups in Organic Synthesis;* John Wiley & Sons, Inc.: New York, 1991.

# CHAPTER 3: THE EFFECTS OF TRIVALENT LANTHANIDE CATIONIZATION ON THE ELECTRON TRANSFER DISSOCIATION OF ACIDIC FIBRINOPEPTIDE B AND ITS ANALOGS

## 3.1 Overview

Electrospray ionization (ESI) on mixtures of acidic fibrinopeptide B and two peptide analogs with trivalent lanthanide salts generates $[M + Met + H]^{4+}$, $[M + Met]^{3+}$, and $[M + Met - H]^{2+}$, where M = peptide and Met = metal (except radioactive promethium). These ions undergo extensive and highly efficient electron transfer dissociation (ETD) to form metallated and non-metallated c- and z-ions. All metal-adducted product ions contain at least two acidic sites, which suggests attachment of the lanthanide cation at the side chains of one or more acidic residues. The three peptides undergo similar fragmentation. ETD on $[M + Met + H]^{4+}$ leads to cleavage at every residue; the presence of both metal ion and extra proton is very effective in promoting sequence-informative fragmentation. Backbone dissociation of $[M + Met]^{3+}$ is also extensive, although cleavage does not always occur between adjacent glutamic acid residues. For $[M + Met - H]^{2+}$, a more limited range of product ions form. All lanthanide metal peptide complexes display similar fragmentation except for europium (Eu). ETD on $[M + Eu - H]^{2+}$ and $[M + Eu]^{3+}$ yields a limited amount of peptide backbone cleavage; however, $[M + Eu + H]^{4+}$ dissociates with cleavage at every residue. Except for the results for $Eu^{3+}$, metallated-peptide ion formation by ESI, ETD fragmentation efficiencies, and product ion formation are unaffected by the identity of the lanthanide cation. Adduction with trivalent lanthanide metal ions is a promising tool for ETD sequence analysis of acidic peptides.

## 3.2 Introduction

Many naturally occurring acidic peptides and proteins are involved in biological processes. For example, fibrinopeptide B is part of the blood coagulation process,[1] gastrin I is utilized in digestion in the stomach,[2,3] N-arginine dibasic convertase is important to neurological functions[4], and low-molecular-weight chromium binding peptide (LMWCr) may be involved in carbohydrate metabolism.[5-7] These peptides often contain a series of adjacent acidic residues and, consequently, may be difficult to protonate. Some highly acidic peptides will not form doubly or even singly protonated ions by electrospray ionization (ESI) or matrix-assisted laser desorption/ionization (MALDI).[8-11]

The tendency of acidic peptides to deprotonate can cause problems for tandem mass spectrometry (MS/MS) analysis in the positive ion mode by electron transfer dissociation (ETD) and electron capture dissociation (ECD). In ETD and ECD, addition of an electron to a multiply charged ion creates a charge reduced radical species that undergoes non-ergodic processes; the result is N-Cα cleavage along the peptide backbone to produce c- and z-ions.[12-18] Electron-based techniques usually lead to more uniform cleavage along the peptide backbone[12,13,19-21] than collisionally activated dissociation methods (CAD/CID), and labile post-translational modification sites such as phosphorylation are generally conserved. [22-27] A drawback of both ECD and ETD is that a multiply charged precursor ion is necessary[12,17,19,28-30] because addition of an electron to a singly charged ion generates a neutral molecule that cannot be detected by mass spectrometry.[31] Also, multiple charging is advantageous because fragmentation by MS/MS generally increases with higher charge states on the precursor ion.[13,30,32-37]

Studies using a variety of metal ions have demonstrated the ability of metallated peptides to provide sequence-informative fragmentation by ECD. Lui and Håkansson[38] complexed

divalent and alkaline earth metals with the neuropeptide substance P to produce $[M + Met + H]^{3+}$, where M = peptide and Met = metal. The ECD spectra were dominated by a-, b-, c-, y-, and z-ions, and the identity of the metal ion affected fragmentation. In another study by these same researchers,[39] extensive sequence coverage resulted from ECD of metallated ions produced by mixing divalent alkaline earth metal salts with peptides containing O-sulfated tyrosine residues; these spectra were dominated by c- and z-ions. Members of the c- and z-series were also found when Chan and coworkers[40] performed ECD on complexes of divalent alkaline earth metal ions with two nonapeptides. A wider variety of backbone cleavage ions, a-, b-, c-, y- and z-, were seen when Chan and coworkers[41-43] performed ECD on several small peptides adducted to divalent transition metal cations. In one study,[42] these researchers observed low fragmentation efficiencies, and the metal-adducted precursor ion was over 30 times greater in intensity than product ions in the ECD spectra. In an ECD study involving Cu(II)-peptide complexes by the Chan group,[43] only metal-adducted a-, b-, and y-ions form; the researchers determined that the type of basic residue, length of peptide sequence and the presence of amide hydrogen(s) affected the series of metallated product ions generated. More recently, Chan and coworkers[44] performed ECD on model peptides metallated with three main group metal trivalent cations and one transition metal cation. A variety of metallated and non-metallated a-, b-, c-, and z-ions were observed, and the identity of the trivalent cation affected product ion formation. Voinov et al.[45] also found a range of product ions in ECD experiments on singly and doubly sodiated substance P analogs and on an amidated phosphorylated tyrosine kinase peptide. Heeren and coworkers[46,47] observed differences in the ECD spectra of $[M + Met]^{2+}$ for a nine-residue oxytocin peptide by varying the divalent transition metal. Williams and coworkers[48] found abundant formation of c- and z-ions for ECD on metal-peptide complexes of cesium and

lithium ions adducted to synthetic peptides containing alanine and lysine residues. Later work by the Williams group[49] showed that lanthanide metal adduction to a series of peptides yielded $[M + Met - H]^{2+}$ and $[M + Met]^{3+}$, which underwent ECD to yield almost complete sequence coverage.

A few metallated peptide studies have also involved ETD. Dong and Vachet[50] performed ETD on small copper-cationized peptides and observed c- and z-ions. For several acidic peptides, Asakawa and coworkers[51] demonstrated that metallated peptide ions with 2+ or 3+ charges produced by cationization with potassium or calcium ions underwent more sequence-informative ETD compared with dissociation of the analogous protonated ions. In another study, Asakawa and Wada[52] complexed peptides containing cysteine residues with three divalent metal ions. The nature of the metal affected the production of c- and z-ions by ETD. To date, little is known about the type of metal ion that might be most suitable for sequencing peptides.

Lanthanide ions can be favorable for multiple charging because attachment of a single metal ion delivers a 3+ charge onto a peptide. Several studies demonstrate the ability of trivalent metal cation adduction to create quasi-molecular ions with increased charge states for small peptides in ESI.[49,53-57] In the current work, the effects of lanthanide cationization on ETD of the model acidic peptide fibrinopeptide B and two of its analogs were studied. Trivalent metal ions were used because ideally the added 3+ charge will compensate for any deprotonation at acidic residues and leave a charge of 2+ or greater on the peptide precursor ions to be subjected to ETD. Also, trivalent metal ion adduction can result in more highly charged peptide ions (3+ and 4+) that can enhance ETD/ECD fragmentation. A goal of the current study is to determine the lanthanide metal ion most suitable for promoting acidic peptide fragmentation by ETD.

## 3.3 Experimental

### 3.3.1 Mass spectrometry

All experiments were performed on the Bruker (Billerica, MA, USA) HCTultra PTM Discovery System high capacity quadrupole ion trap (QIT) mass spectrometer, which was discussed in Chapter 2. Ions were produced by ESI on mixtures of metal salts and peptides. The needle at the ESI source (see Figure 2.2) was grounded, and the ESI capillary was glass with platinum coating at the entrance and exit. A high voltage of -3.5 kV was placed on the capillary entrance, as well as the stainless steel endplate and capillary entrance cap. Nitrogen drying gas was heated to 260°C and flowed at 5-10 L/min. Nitrogen also served as nebulizer gas, and the pressure was optimized between 5 and 10 psi. A KD Scientific (Holliston, MA, USA) syringe pump was used to infuse sample solutions with a 10:1 metal ion:peptide molar ratio mixture at a flow rate of 3 µL/min. Final peptide concentrations were 5 µM in acetonitrile:water at a 50:50 volume ratio. All spectra shown are the result of signal averaging of 200 scans.

Fluoranthene served as the reagent anion for ETD experiments and was generated in a negative chemical ionization source (nCI) employing methane reagent gas. Accumulation time for the reagent anion was 8-12 ms. The lower end mass-to-charge (*m/z*) cutoff was set to 120 with the anion/cation reaction times in the range of 180-250 ms. The ion charge control (ICC) value was set to 300,000-400,000 to maximize electron transfer. Immediately after the anion/cation reaction, the "smart decomposition" function is enabled to overcome attractive forces, such as hydrogen or other noncovalent bonds, that may prevent ions from separating after the electron transfer process. Smart decomposition is discussed in greater detail in Section 2.4.2.

### 3.3.2 Peptides

The peptide fibrinopeptide B was purchased from Fisher Scientific (Pittsburg, PA, USA)

and American Peptide Company Inc (Vista, CA, USA). Des-Arg$^{14}$-[Glu$^{1}$]-fibrinopeptide B was custom synthesized by Biomatik USA (Wilmington, Delaware, USA). [Glu$^{1}$]-fibrinopeptide B was purchased from Anaspec EGT (Freemont, California, USA). Lanthanide series metal nitrate salts were purchased from Alfa Aesar (Ward Hill, MA, USA). Ultrapure Milli-Q 18 MΩ water was produced with a Barnstead (Dubuque, IA, USA) E-pure system.

## 3.4 Results

### 3.4.1 Adduction of trivalent metal cations to peptides

Fibrinopeptide B (pEGVNDNEEGFFSAR) was employed to investigate the ability of trivalent lanthanide cations to promote multiple positive charging in acidic peptides that routinely favor deprotonation in ESI. Two analogs were also studied. [Glu$^{1}$]-fibrinopeptide B (EGVNDNEEGFFSAR) lacks the cyclic glutamic acid residue at the N-terminus, resulting in an extra acidic site at the side chain of the N-terminal glutamic acid residue and a basic amino group at the N-terminus. In des-Arg$^{14}$-[Glu$^{1}$]-fibrinopeptide B (EGVNDNEEGFFSA), the highly basic C-terminal arginine residue (gas-phase basicity of arginine = 1006.6 kJ/mol[58]) is absent and the N-terminal residue is not cyclized.

Fibrinopeptide B and its analogs were combined with every trivalent lanthanide cation except promethium (Pm), atomic number 61, because of its highly radioactive nature. Mass spectra in Figure 3 show praseodymium ions, $Pr^{3+}$, adducted to fibrinopeptide B, [Glu$^{1}$]-fibrinopeptide B, and des-Arg$^{14}$-[Glu$^{1}$]-fibrinopeptide B. Throughout this report, Pr(III) is used as a representative lanthanide ion because it consistently yielded high quality spectra and has one major stable isotope, thus providing straightforward spectra for interpretation. The most abundant metallated ions were $[M + Met + H]^{4+}$ and $[M + Met]^{3+}$. Doubly charged ions, $[M + Met – H]^{2+}$ and $[M + 2H]^{2+}$, formed in lower abundances for all three peptides. In a recent

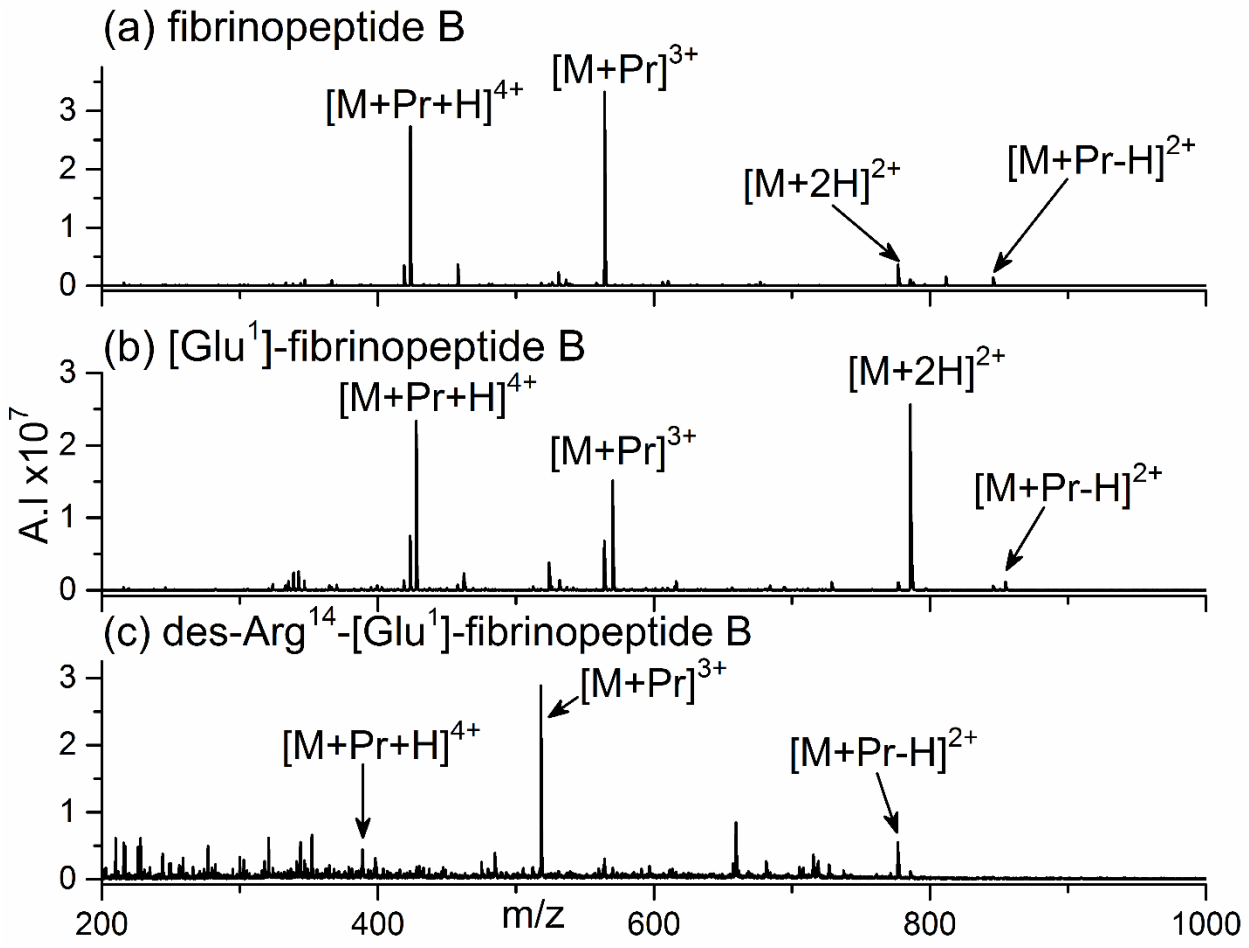


Figure 3.1. ESI mass spectra generated from 10:1 molar ratio mixtures of $Pr^{3+}$ with (a) fibrinopeptide B, (b) [$Glu^{1}$]-fibrinopeptide B, and (c) des-$Arg^{14}$-[$Glu^{1}$]-fibrinopeptide B. The reduced signal-to-noise ratio (S/N) of Figure 3.1c is due to the lower purity of this peptide, which was custom synthesized. The spectra have no expansion of the intensity axis; all peaks are shown to scale.

study of lanthanide ion-peptide complexes by Williams and coworkers,[49] $[M + Met - H]^{2+}$ formed for peptides of less than 1000 Da in molecular mass while $[M + Met]^{3+}$ dominated for larger peptides. The $[M + Met + H]^{4+}$ found here has not been reported in any ETD/ECD work to date. [Glu[1]]-fibrinopeptide B shows a similar pattern of metallated ion formation; removal of cyclization at the N-terminal glutamic acid residue has minimal effect on metal adduction. All lanthanide ions generated abundant multiply charged precursor ions in positive ion mode ESI with each peptide.

Removal of the C-terminal arginine to form des-Arg[14]-[Glu[1]]-fibrinopeptide B caused a shift in the intensity of the metal-adducted ions. Figure 3.1(c) shows the ESI spectrum of this peptide with $Pr^{3+}$ and is representative of species observed with the other lanthanide cations. Most abundant is $[M + Met]^{3+}$, while $[M + Met + H]^{4+}$ is significantly reduced. The lack of the arginine residue seemingly limits this peptide's ability to obtain a proton for formation of $[M + Met + H]^{4+}$.

### 3.4.2 Electron transfer dissociation on $[M + Met - H]^{2+}$

For the three peptides, the metallated ions were isolated and subjected to ETD. The established nomenclature from Roepstorff and Fohlman[59] as modified by Biemann[60] is used in labelling of spectra to keep track of the number of hydrogens incorporated into the ETD product ions. A prime symbol to the left indicates loss of a hydrogen (i.e., $^{/}c_n = [c_n - H]^+$) and to the right indicates the addition of a hydrogen at the cleavage site (i.e., $c_n^{//} = [c_n + 2H]^+$). For easier product ion identification in the figures, non-metallated z- ions are labeled in red, non-metallated c-ions in blue, metal-adducted z-ions in bright pink, and metal-adducted c-ions in green. Precursor ion that did not dissociate is indicated in purple with a large purple diamond arrow head. ETnoD product ions are labeled in black, as are neutral loss ions. The c- and z-ions

correspond to N-Cα bond cleavage, which is the typical peptide backbone cleavage observed by ECD[13] and ETD.[17]

Figure 3.2(a) shows the ETD spectrum of $[M + Pr - H]^{2+}$ for fibrinopeptide B. All product ions are singly charged. The most prominent ions are of the z-series: $z_n^{//+}$ and $[z_n^{/} + Pr]^+$. Some larger metallated c-ions form and lack additional hydrogens, $[^{/}c_n + Pr]^+$, n = 9 and 11-13, which is consistent with the precursor ion being hydrogen deficient. Cleavage occurs at every residue except for between the glutamic acid residues (E) at positions 7 and 8. Only 60%-70% of the precursor ion dissociates, with a substantial amount being observed as the ETnoD product, $[M + Pr - H]^+$, even in the presence of a smart decomposition pulse. The ETD fragmentation efficiency for $[M + Met - H]^{2+}$ is lower than for the 3+ and 4+ precursor ions. The spectra contain neutral losses involving $CO_2$, $CO_2H$, $C_2H_3O_2$, and OH. The loss of 59 Da has been observed elsewhere[61-63] and may correspond to elimination of $C_2H_3O_2$ from the side chains of glutamic and aspartic acid residues. Although $CH_2O_2$ is a common side chain loss from glutamic and aspartic acid residues in electron-based techniques,[64] this was not observed in the current study.

All trivalent lanthanide cations except europium (Eu) produce similar ETD fragmentation for $[M + Met - H]^{2+}$ with the three peptides. Figure 3.3 shows ETD of $[M + Pr - H]^{2+}$ for [$Glu^1$]-fibrinopeptide B. Despite a slightly lower efficiency, the type and intensity of product ions match those of fibrinopeptide B as shown in Figure 3.2(a). For [$Glu^1$]-fibrinopeptide B, $z_7^{/+}$ forms from cleavage between the two adjacent glutamic acids residues, E7 and E8.

A different fragmentation pattern results from ETD on $[M + Met - H]^{2+}$ for des-$Arg^{14}$-[$Glu^1$]-fibrinopeptide B. Non-metallated product ions are absent, as illustrated in Figure 3.4 with $Pr^{3+}$. Metallated c- and z-ions form, similar to the fragmentation of the other two

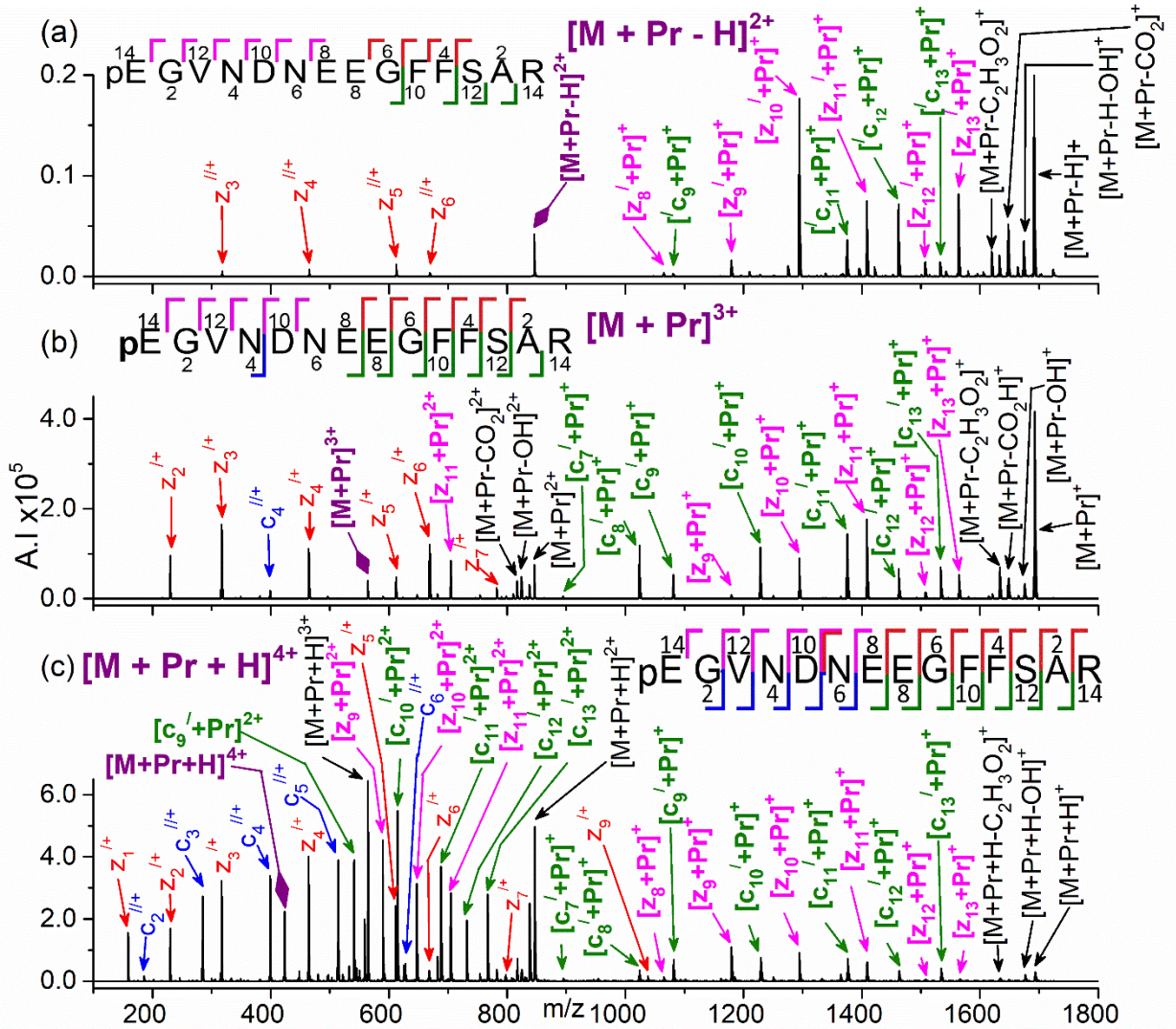


Figure 3.2. ETD mass spectra of (a) $[M + Pr - H]^{2+}$, (b) $[M + Pr]^{3+}$, and (c) $[M + Pr + H]^{4+}$ for fibrinopeptide B produced by addition of $Pr^{3+}$. In the figures, the following colors are used to label the ions: non-metallated z-ions = red, non-metallated c-ions = blue, metal-adducted z-ions = bright pink, and metal-adducted c-ions = green. Undissociated precursor ion is labeled in purple with a large purple diamond arrow head. Neutral loss products and electron transfer without dissociation (ETnoD) ions are labeled in black. A prime symbol to the left indicates loss of a hydrogen (i.e., $^{/}c_n = [c_n - H]^+$) and to the right indicates the addition of a hydrogen at the cleavage site (i.e., $c_n^{//} = [c_n + 2H]^+$). The spectra have no expansion of the intensity axis; all peaks are shown to scale.

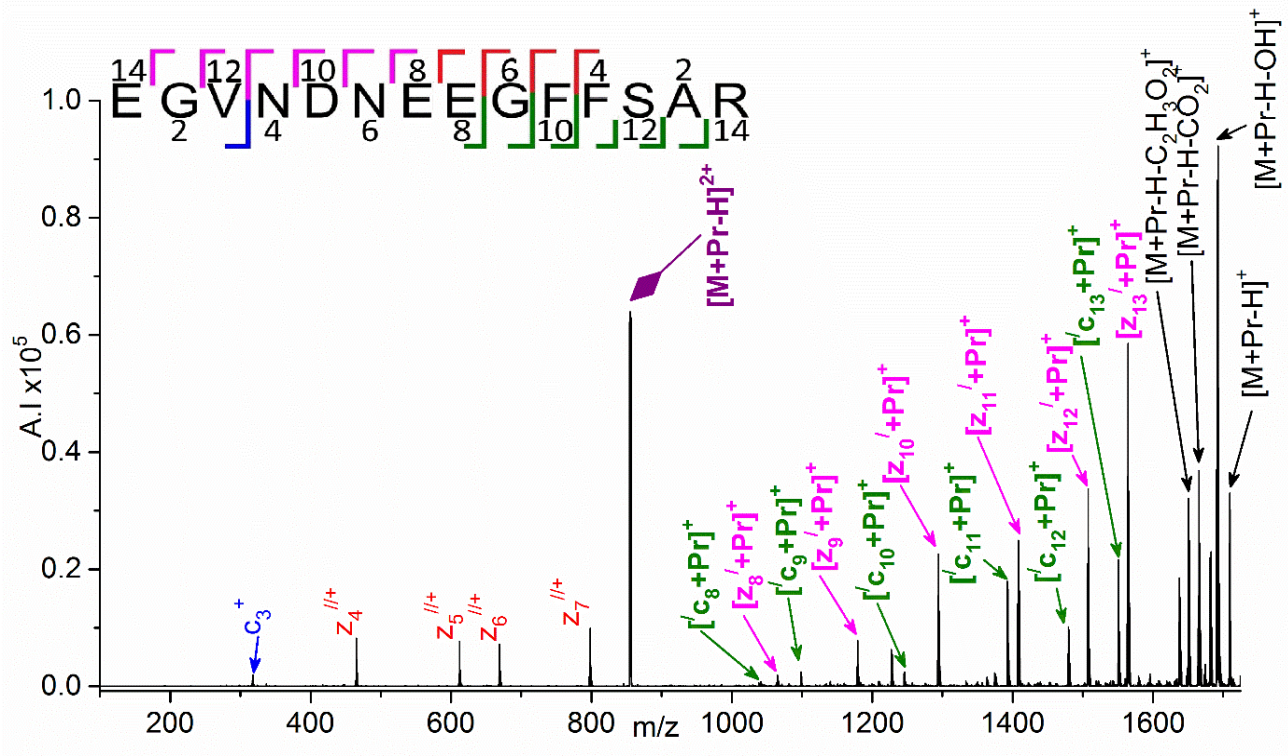


Figure 3.3. ETD mass spectrum of $[M + Pr - H]^{2+}$ for [Glu$^1$]-fibrinopeptide B. In the figure, the following colors are used to label the ions: non-metallated z-ions = red, non-metallated c-ions = blue, metal-adducted z-ions = bright pink, and metal-adducted c-ions = green. Undissociated precursor ion is labeled in purple with a large purple diamond arrow head. Neutral loss products and electron transfer without dissociation (ETnoD) ions are labeled in black. A prime symbol to the left indicates loss of a hydrogen (i.e., $^{/}c_n = [c_n - H]^+$) and to the right indicates the addition of a hydrogen at the cleavage site (i.e., $c_n^{//} = [c_n + 2H]^+$). The spectrum has no expansion of the intensity axis; all peaks are shown to scale.

peptides (Figure 3.2(a) and Figure 3.3). In addition, like fibrinopeptide B, cleavage between E7 and E8 is not observed.

The only unique behavior is for $Eu^{3+}$, where $[M + Eu - H]^{2+}$ has low dissociation efficiency and almost no backbone cleavage. As shown in Figure 3.5(a) for fibrinopeptide B, the only significant products are the charge reduced ion, $[M + Eu - H]^{+}$, from ETnoD and a water loss species. A similar effect is seen in Figures 3.6 and 3.7 for the two peptide analogs.

### 3.4.3 Electron transfer dissociation on $[M + Met]^{3+}$

Figure 3.2(b) shows that ETD on $[M + Pr]^{3+}$ for fibrinopeptide B yields a mix of metallated and non-metallated c- and z-ions. Most have a charge of 1+, although a few 2+ ions form. The z-series are $z_n^{/+}$ and $[z_n + Pr]^{+}$. The only non-metallated c-ion is $c_4^{//+}$. All other c-ions are $[c_n^{/} + Pr]^{+}$, n = 7-13. Cleavage occurs at every residue except on the N-terminal side of the glutamic acid residue at position 7 (E7). Cleavage between the glutamic acid residues at positions 7 and 8 is minimal. The neutral losses are similar to those observed for $[M + Met - H]^{2+}$.

With the exception of $Eu^{3+}$, the identity of the lanthanide ion does not affect the ETD spectra of $[M + Met]^{3+}$. Similar dissociation patterns and relative ion intensities are observed for fibrinopeptide B and its two analogs (Figures 3.2(b), 3.8, and 3.9). ETD fragmentation efficiency is highest for fibrinopeptide B and des-$Arg^{14}$-[$Glu^{1}$]-fibrinopeptide B; typically > 90% of the selected precursor ion dissociates. [$Glu^{1}$]-fibrinopeptide B has a slightly lower ETD efficiency of $[M + Met]^{3+}$ but still has cleavage at every residue. Intense product ions and high signal-to-noise ratios (S/N) allow for easy identification of ETD product ions in all spectra.

In contrast to the extensive sequence coverage from the other lanthanide ions, $[M + Eu]^{3+}$ yields an intense ETnoD ion and a decreased amount of backbone cleavage for all three peptides,

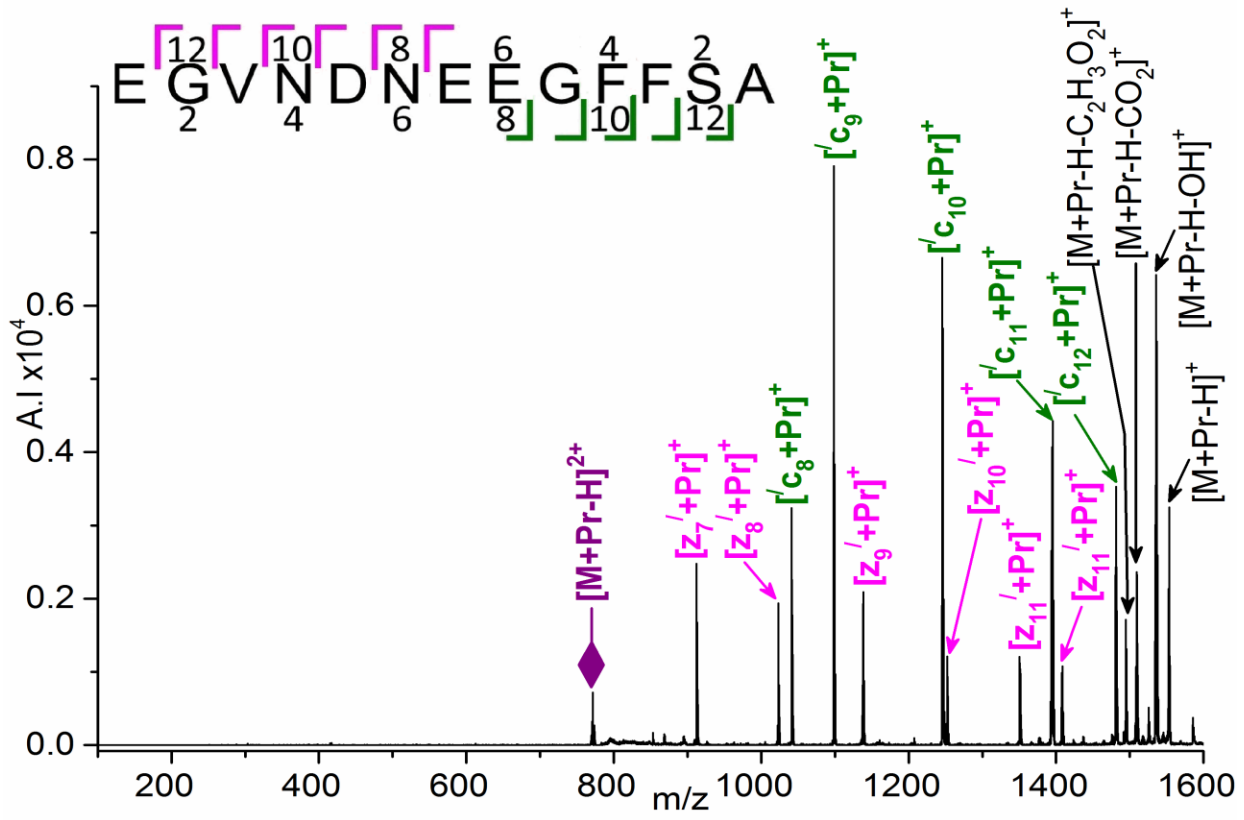


Figure 3.4. ETD mass spectrum of $[M + Pr - H]^{2+}$ for des-Arg$^{14}$- [Glu$^{1}$]-fibrinopeptide B. In the figure, the following colors are used to label the ions: metal-adducted z-ions = bright pink, and metal-adducted c-ions = green. Undissociated precursor ion is labeled in purple with a large purple diamond arrow head. Neutral loss products and electron transfer without dissociation (ETnoD) ions are labeled in black. A prime symbol to the left indicates loss of a hydrogen (i.e., $^{/}c_n = [c_n - H]^+$) and to the right indicates the addition of a hydrogen at the cleavage site (i.e., $c_n^{//} = [c_n + 2H]^+$). The spectrum has no expansion of the intensity axis; all peaks are shown to scale.

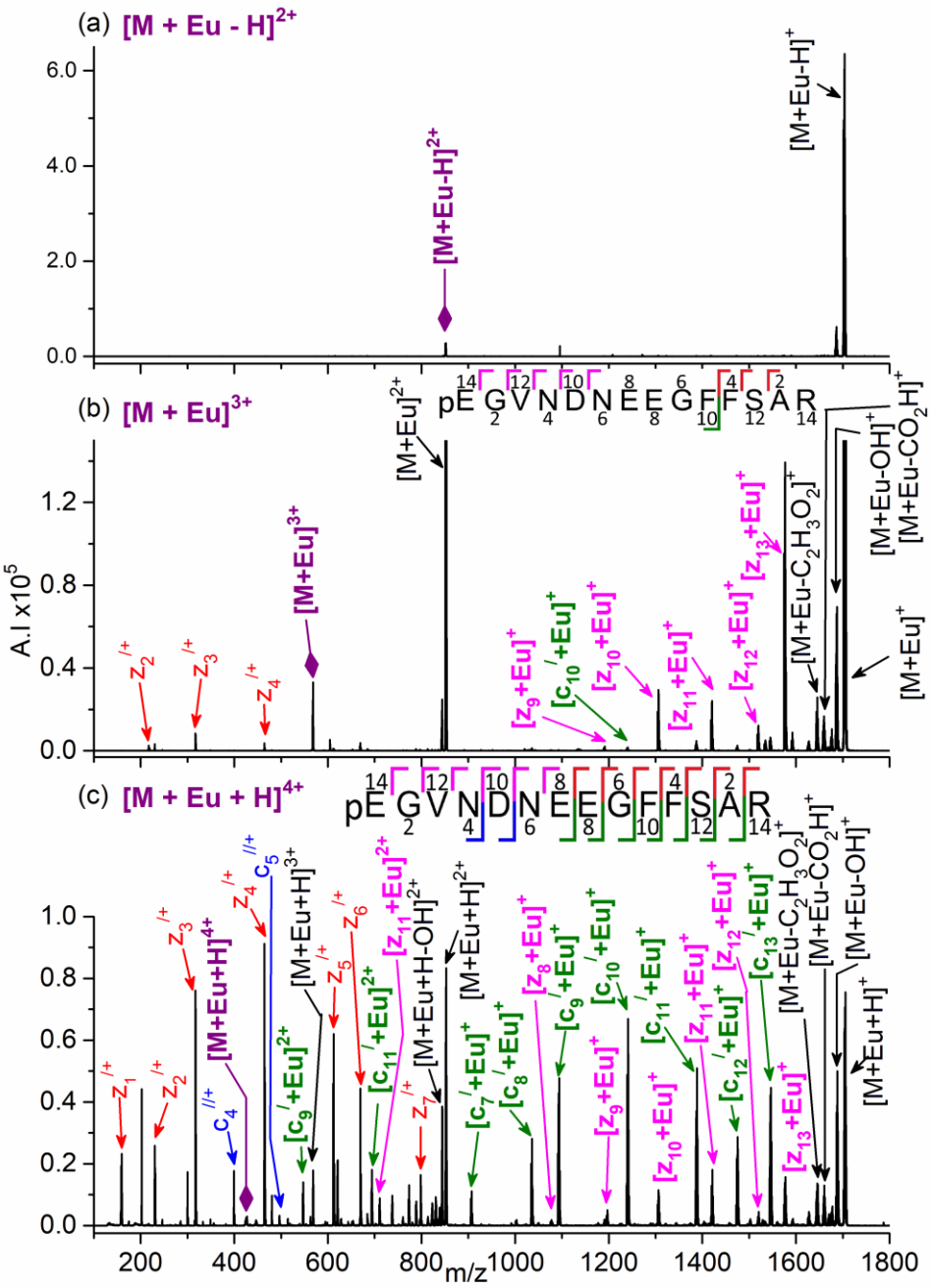


Figure 3.5. ETD mass spectra of (a) $[M + Eu - H]^{2+}$, (b) $[M + Eu]^{3+}$, and (c) $[M + Eu + H]^{4+}$ for fibrinopeptide B produced by addition of Eu(III). In the figures, the following colors are used to label the ions: non-metallated z-ions = red, non-metallated c-ions = blue, metal-adducted z-ions = bright pink, and metal-adducted c-ions = green. Undissociated precursor ion is labeled in purple with a large purple diamond arrow head. Neutral loss products and electron transfer without dissociation (ETnoD) ions are labeled in black. A prime symbol to the left indicates loss of a hydrogen (i.e., $^{/}c_n = [c_n - H]^+$) and to the right indicates the addition of a hydrogen at the cleavage site (i.e., $c_n^{//} = [c_n + 2H]^+$). The spectra have no expansion of the intensity axis; all peaks are shown to scale.

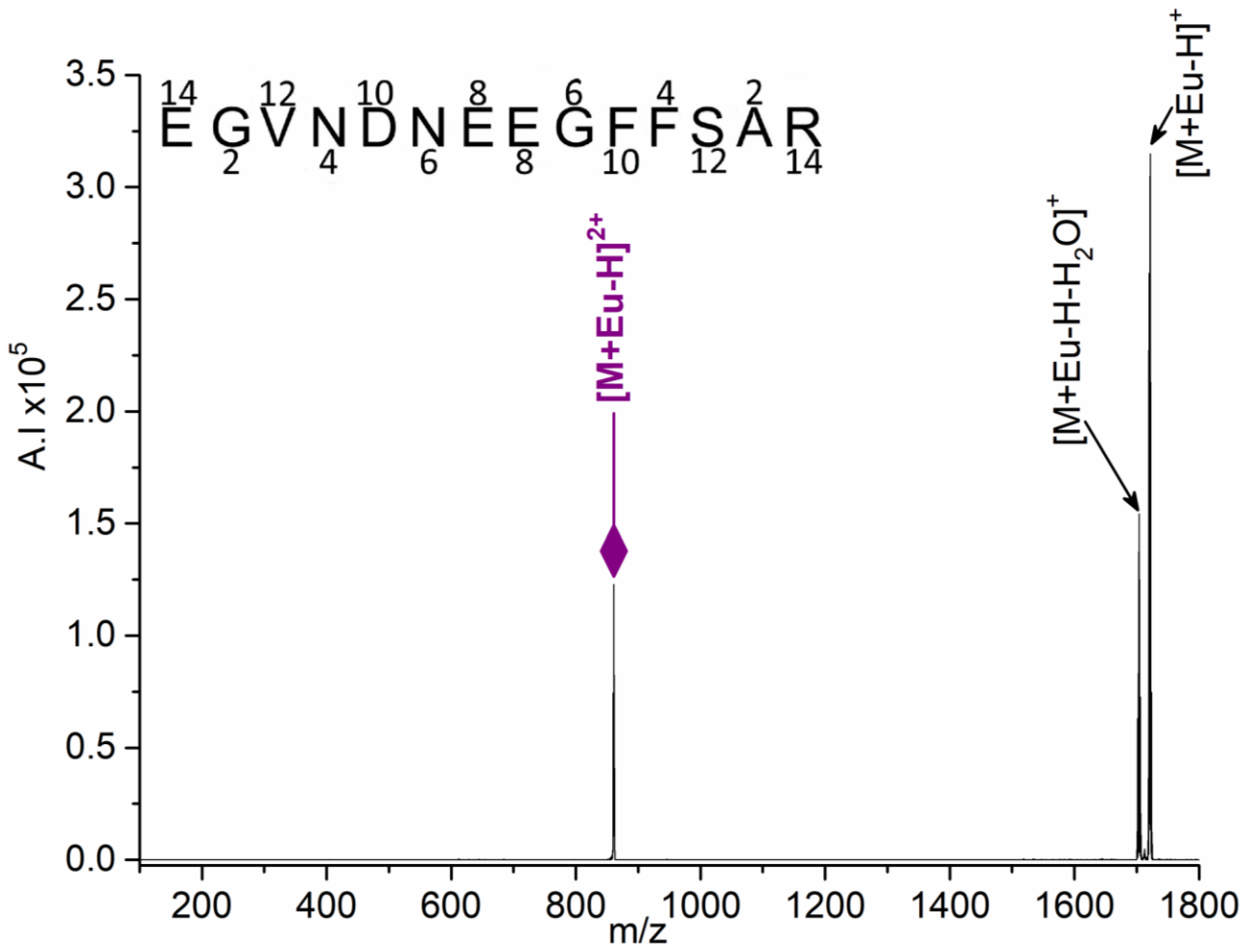


Figure 3.6. ETD mass spectrum of $[M + Eu - H]^{2+}$ for [Glu[1]]-fibrinopeptide B. In the figure, undissociated precursor ion is labeled in purple with a large purple diamond arrow head. Neutral loss products and electron transfer without dissociation (ETnoD) ions are labeled in black. The spectrum has no expansion of the intensity axis; all peaks are shown to scale.

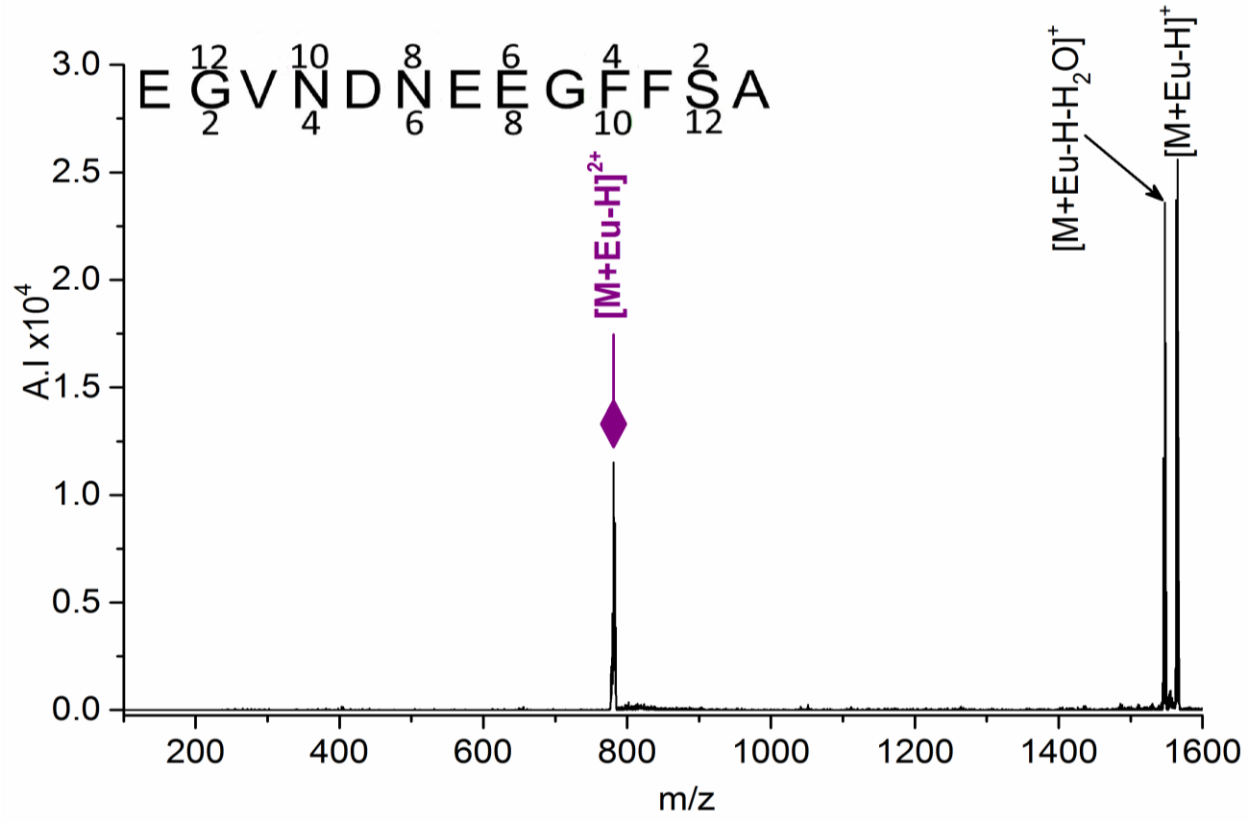


Figure 3.7. ETD mass spectrum of $[M + Eu - H]^{2+}$ for des-$Arg^{14}$-[$Glu^{1}$]-fibrinopeptide B. In the figure, undissociated precursor ion is labeled in purple with a large purple diamond arrow head. Neutral loss products and electron transfer without dissociation (ETnoD) ions are labeled in black. The spectrum has no expansion of the intensity axis; all peaks are shown to scale.

as shown in Figure 3.5(b) for fibrinopeptide B and Figures 3.10 and 3.11 for the two analogs.

### 3.4.4 Electron transfer dissociation on $[M + Met + H]^{4+}$

The most structurally informative ETD spectra were found for $[M + Met + H]^{4+}$. A mix of non-metallated and metallated c- and z- ions form for fibrinopeptide B, as shown in Figure 3.2(c). Product ions have 1+ and 2+ charges. Backbone cleavages occur between all residues and a high S/N allows for easy identification of ETD products. Non-metallated and metallated c- and z-series, as well as neutral losses, are the same as for $[M + Met]^{3+}$.

Little variation is evident among the lanthanide cations for ETD of $[M + Met + H]^{4+}$. A few non-metallated c-ions are absent for $[M + Eu + H]^{4+}$ from fibrinopeptide B, but surprisingly full sequence coverage occurs, as is evident in Figure 3.5(c). More than 90% of $[M + Met + H]^{4+}$ dissociates for fibrinopeptide B (Figure 3.5(c)) and [Glu$^1$]-fibrinopeptide B (Figure 3.12(a)). As for des-Arg$^{14}$-[Glu$^1$]-fibrinopeptide B, no measurable precursor was left after ETD on $[M + Met + H]^{4+}$, as shown in Figure 3.12(b). Similar extensive fragmentation and product ion formation is observed for ETD on $[M + Met – H]^{4+}$ for all three peptides.

In Figures 3.12(a) and 3.12(b) for ETD on $[M + Met + H]^{4+}$ for [Glu$^1$]-fibrinopeptide B and des-Arg$^{14}$-[Glu$^1$]-fibrinopeptide B, an intense $c_7^{//+}$ forms, which corresponds to cleavage between E7 and E8. In contrast, no $c_7^{//+}$ but only low intensity $z_7^{/+}$ and $[c_7^{/} + Pr]^+$ results from ETD on $[M + Pr + H]^{4+}$ for fibrinopeptide B in Figure 3.2(c). Thus, removal of cyclization on the N-terminal glutamic acid facilitates increased cleavage between the two glutamic acid residues.

## 3.5 Discussion

### 3.5.1 Impact of metal ion properties

When discussing ETD on metal-cationized peptides, electronic properties are of

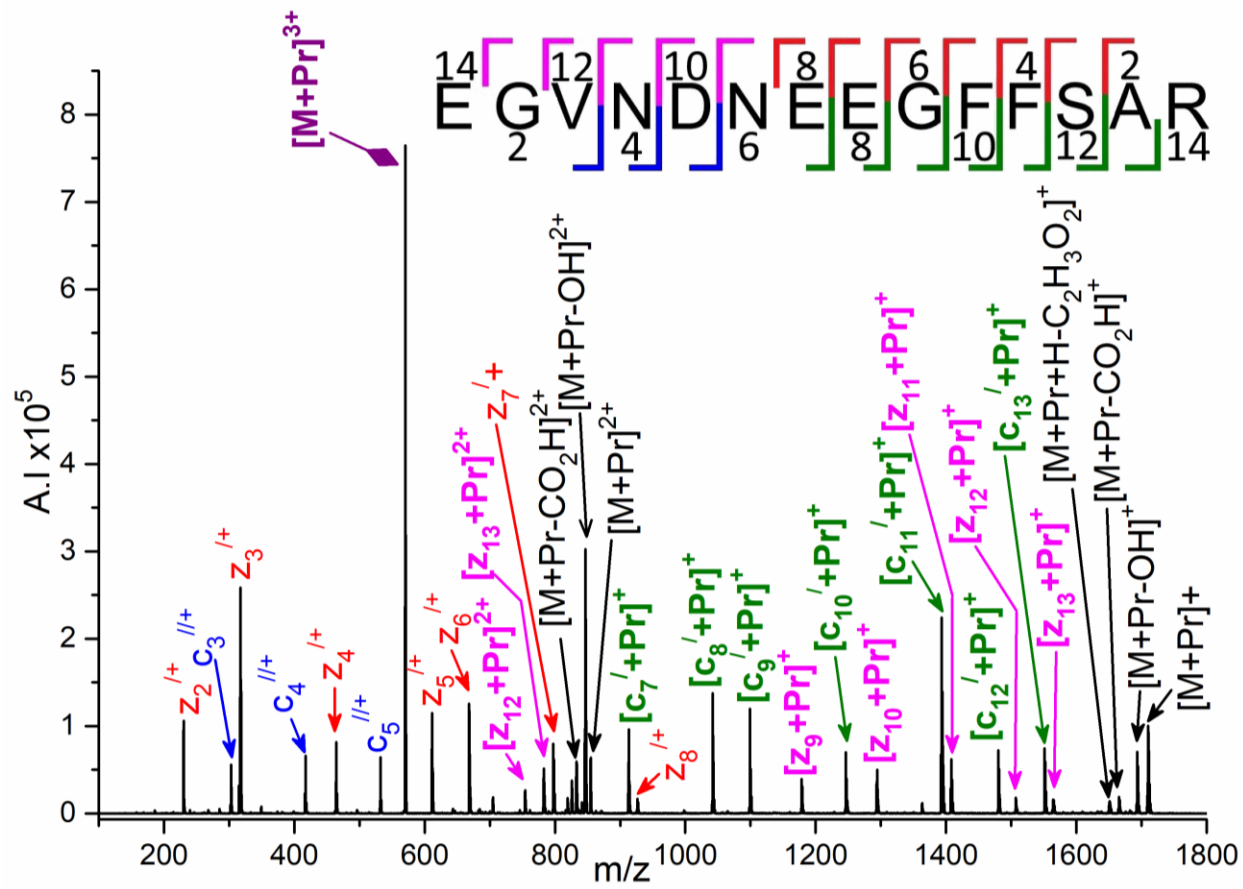


Figure 3.8. ETD mass spectrum of $[M + Pr]^{3+}$ for [Glu[1]]-fibrinopeptide B. In the figure, the following colors are used to label the ions: non-metallated z-ions = red, non-metallated c-ions = blue, metal-adducted z-ions = bright pink, and metal-adducted c-ions = green. Undissociated precursor ion is labeled in purple with a large purple diamond arrow head. Neutral loss products and electron transfer without dissociation (ETnoD) ions are labeled in black. A prime symbol to the left indicates loss of a hydrogen (i.e., $^{/}c_n = [c_n - H]^+$) and to the right indicates the addition of a hydrogen at the cleavage site (i.e., $c_n^{//} = [c_n + 2H]^+$). The spectrum has no expansion of the intensity axis; all peaks are shown to scale.

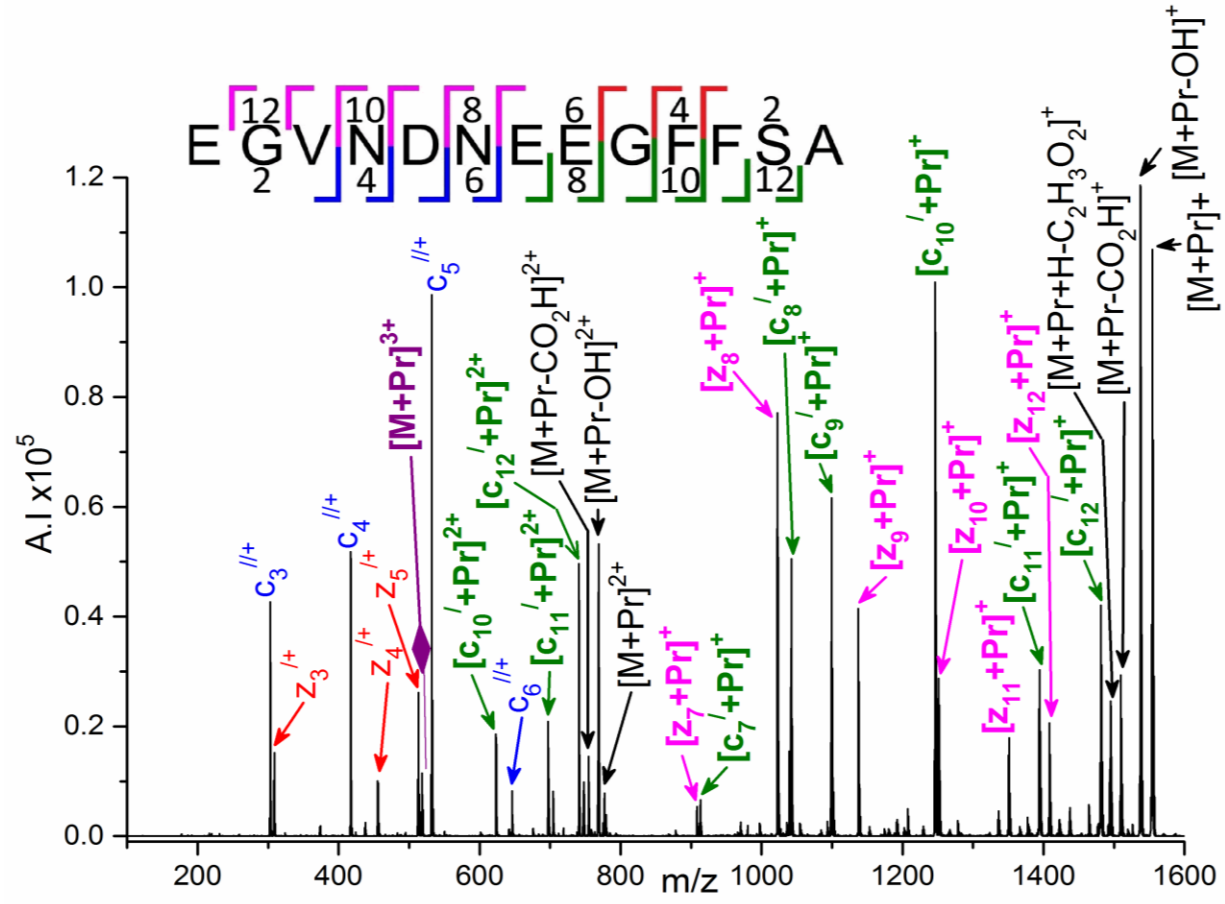


Figure 3.9. ETD mass spectrum of $[M + Pr]^{3+}$ for des-Arg$^{14}$-[Glu$^{1}$]-fibrinopeptide B. In the figure, the following colors are used to label the ions: non-metallated z-ions = red, non-metallated c-ions = blue, metal-adducted z-ions = bright pink, and metal-adducted c-ions = green. Undissociated precursor ion is labeled in purple with a large purple diamond arrow head. Neutral loss products and electron transfer without dissociation (ETnoD) ions are labeled in black. A prime symbol to the left indicates loss of a hydrogen (i.e., $^{/}c_n = [c_n - H]^+$) and to the right indicates the addition of a hydrogen at the cleavage site (i.e., $c_n^{//} = [c_n + 2H]^+$). The spectrum has no expansion of the intensity axis; all peaks are shown to scale.

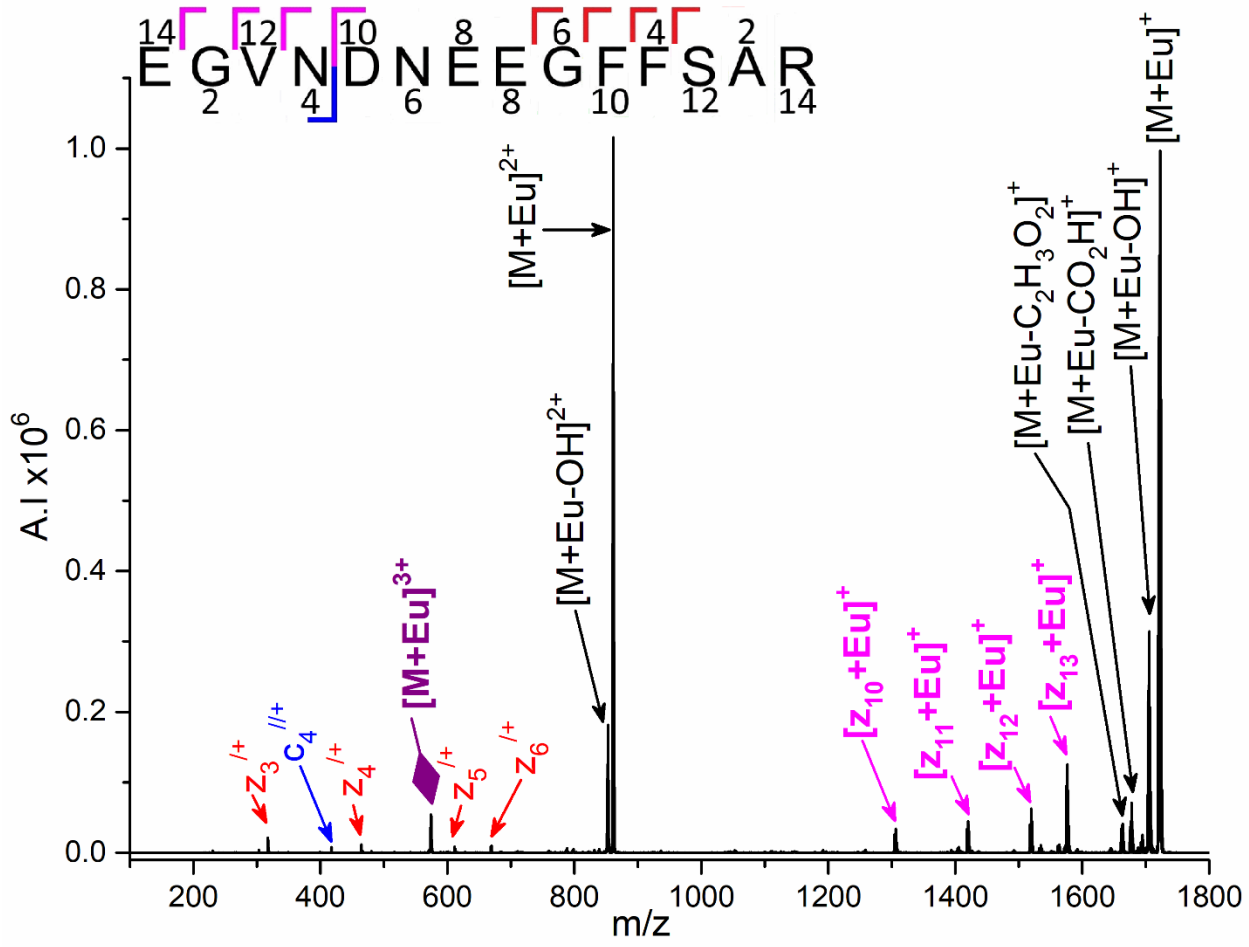


Figure 3.10. ETD mass spectrum of $[M + Eu]^{3+}$ for [Glu[1]]-fibrinopeptide B. In the figure, the following colors are used to label the ions: non-metallated z-ions = red, non-metallated c-ions = blue, and metal-adducted z-ions = bright pink. Undissociated precursor ion is labeled in purple with a large purple diamond arrow head. Neutral loss products and electron transfer without dissociation (ETnoD) ions are labeled in black. A prime symbol to the left indicates loss of a hydrogen (i.e., $^{/}c_n = [c_n - H]^+$) and to the right indicates the addition of a hydrogen at the cleavage site (i.e., $c_n^{//} = [c_n + 2H]^+$). The spectrum has no expansion of the intensity axis; all peaks are shown to scale.

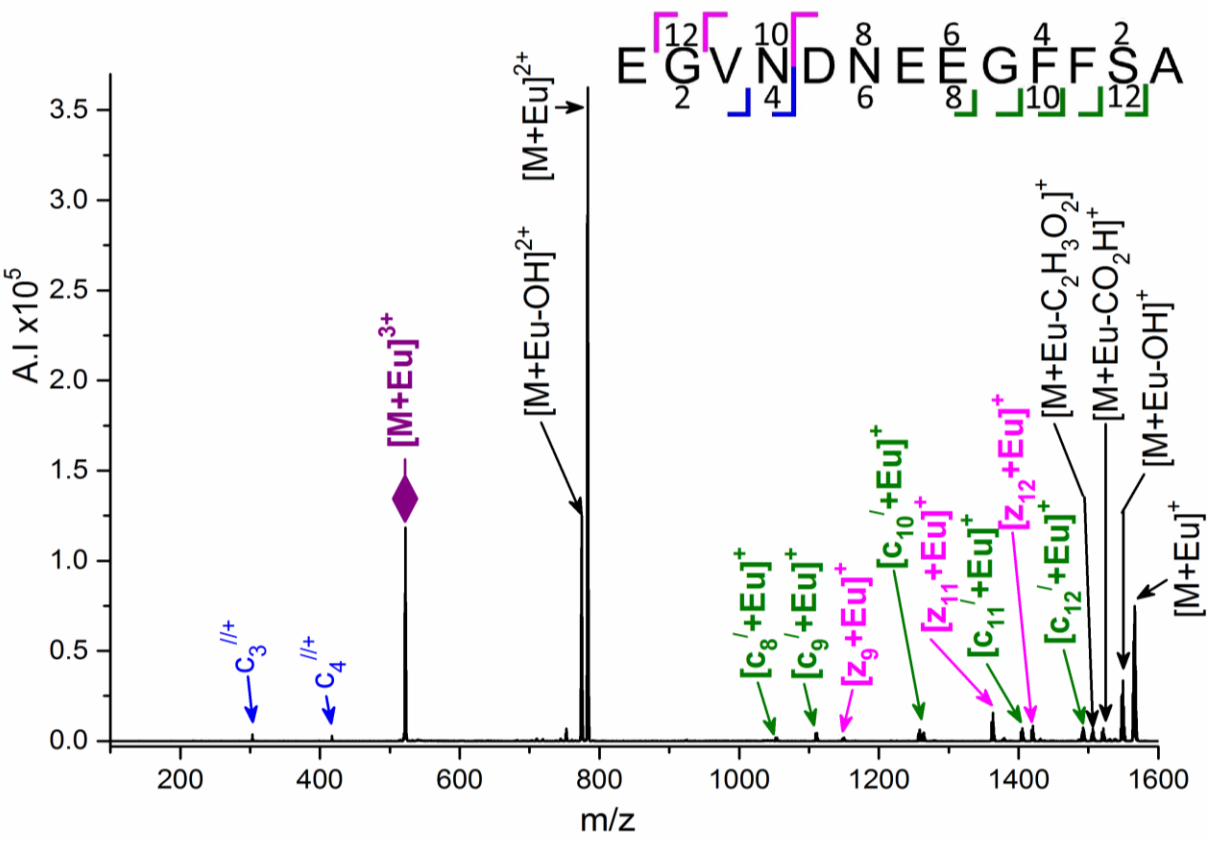


Figure 3.11. ETD mass spectrum of $[M + Eu]^{3+}$ for des-Arg$^{14}$-[Glu$^{1}$]-fibrinopeptide B. In the figure, the following colors are used to label the ions: non-metallated c-ions = blue, metal-adducted z-ions = bright pink, and metal-adducted c-ions = green. Undissociated precursor ion is labeled in purple with a large purple diamond arrow head. Neutral loss products and electron transfer without dissociation (ETnoD) ions are labeled in black. A prime symbol to the left indicates loss of a hydrogen (i.e., $^{/}c_n = [c_n - H]^+$) and to the right indicates the addition of a hydrogen at the cleavage site (i.e., $c_n^{//} = [c_n + 2H]^+$). The spectrum has no expansion of the intensity axis; all peaks are shown to scale.

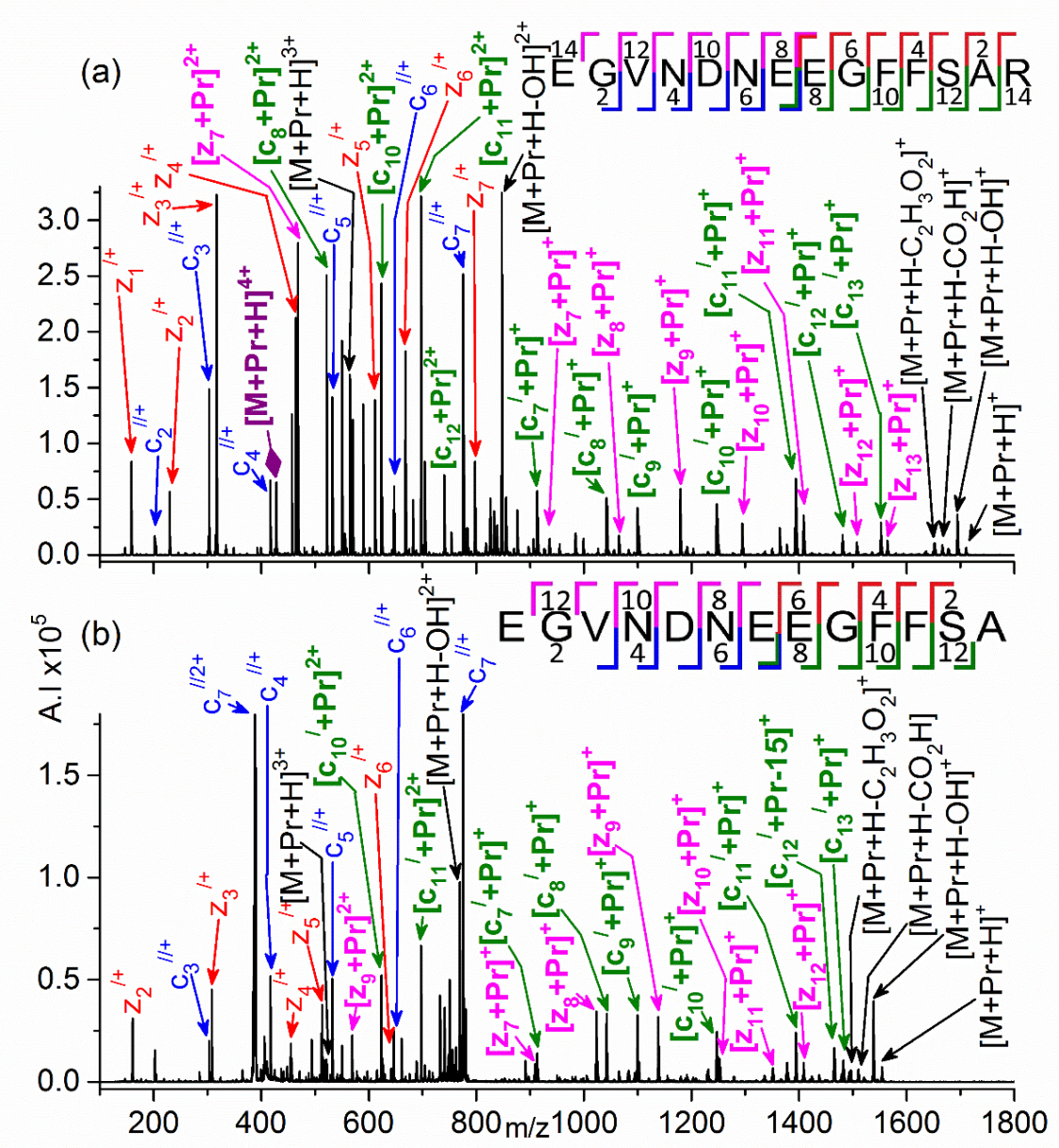


Figure 3.12. ETD mass spectra of $[M + Pr + H]^{4+}$ for (a) [Glu$^1$]-fibrinopeptide B, and (b) des-Arg$^{14}$-[Glu$^1$]-fibrinopeptide B. In the figures, the following colors are used to label the ions: non-metallated z-ions = red, non-metallated c-ions = blue, metal-adducted z-ions = bright pink, and metal-adducted c-ions = green. Undissociated precursor ion is labeled in purple with a large purple diamond arrow head. Neutral loss products and electron transfer without dissociation (ETnoD) ions are labeled in black. A prime symbol to the left indicates loss of a hydrogen (i.e., $^{/}c_n = [c_n - H]^+$) and to the right indicates the addition of a hydrogen at the cleavage site (i.e., $c_n^{//} = [c_n + 2H]^+$). The spectra have no expansion of the intensity axis; all peaks are shown to scale.

importance. The trivalent lanthanide ions have an electronic configuration of $[Xe]4f^m\ 6s^0$, where m steadily increases from zero for the first element in the series (lanthanum, La) to 14 for the final element in the series (lutetium, Lu).[65] Changing electron configuration affects the solid-and solution-phase chemistries of the lanthanide series, although to a lesser extent than electronic configuration affects the transition metal series.[65] In several previous studies of ECD/ETD on metallated peptides, properties related to electronic configuration, such as ionization energy (IE), have been shown to affect fragmentation.[38-40,46] For peptide complexes with divalent transition and alkaline earth metal ions, Liu and Håkansson[38] postulated that a lower second ionization energy (IE2) indicates that there can be more facile electron transfer from the metal ion to the peptide backbone following the initial electron capture by the metal ion. In support of this, they found that adduction of divalent metal ions with lower IE2 values (965-1563 kJ/mol) yielded more extensive backbone cleavage by ECD than metals with higher IE2 values (1649-1756 kJ/mol).

For trivalent metal ions, addition of an electron directly to the metal ion during ETD can result in the gas-phase metal ion being reduced from the 3+ state to 2+. This process relates to the third ionization energy (IE3). Across the lanthanide series, IE3 values increase in the range of 1850 to 2415 kJ/mol.[65] With IEs of this magnitude, a divalent metal ion would be unlikely to cause peptide backbone dissociation based on the work of Liu and Håkansson;[38] however, trivalent metal ions have the advantage of ETD/ECD fragmentation increasing as the charge on the precursor ion increases.[30,36,37,66] For the lanthanide series, outliers from a smooth upward IE3 trend are Eu (IE3 = 2404 kJ/mol[65]) and ytterbium, Yb (IE3 = 2415 kJ/mol[65]), where higher values occur because their divalent ions have the stability of half-filled and completely filled f-

shells, respectively. (Disregarding Eu and Yu, the highest IE3 for a lanthanide is 2285 kJ/mol[65].) Therefore in ETD experiments, $Eu^{3+}$ and $Yb^{3+}$ may have a greater tendency to retain the electron and be reduced to 2+ ions. Several reports have found that direct metal reduction in ETD/ECD can compete with electron transfer to the peptide and restrict backbone dissociation.[43,50] In the current work, the ETD spectra of metallated peptides vary little as the lanthanide metal ion is changed. (For example, see Figure 3.13 for ETD on $[M + Met + H]^{4+}$ involving four trivalent lanthanide ions.) The only exception is for $Eu^{3+}$, as shown in Figure 3.5, which is discussed below. The fact that the IE3 values vary over a relatively small range in the lanthanide series may contribute to their general consistency in promoting ETD fragmentation.

The ability of other common trivalent metal ions to induce ETD fragmentation was considered. The Cassady group has previously found that trivalent chromium, $Cr^{3+}$, readily cationizes acidic and neutral peptides[57,67,68] and that during CID these Cr(III)-peptide ions undergo extensive sequence-informative fragmentation.[67] Also, Cr(III) readily binds to acidic peptides in solution.[10,69,70] However, $Cr^{3+}$ proved to be a poor choice for sequencing fibrinopeptide B by ETD (Figure 3.14). Cleavage was inefficient and backbone fragmentation was restricted to a few sites near the C-terminus; instead, an intense ETnoD product, $[M + Cr]^{2+}$, formed. This sequestered fragmentation is analogous to what Liu and Håkansson[38] observed for divalent metal ion-peptide complexes when IE2 was relatively high. The $Cr^{3+}$ result probably relates to the very high IE3 of 2987 kJ/mol[71] for Cr, which can lead to energetically favorable gas-phase retention of an electron to generate $Cr^{2+}$ and to limited cleavage along the peptide backbone. Although fibrinopeptide B was not involved, the Cassady group has also found that main group trivalent aluminum, $Al^{3+}$, is a poor promoter of ETD fragmentation.[72] This is consistent with the high IE3 of 2745 kJ/mol for Al.[71] In addition, the Cassady group attempted

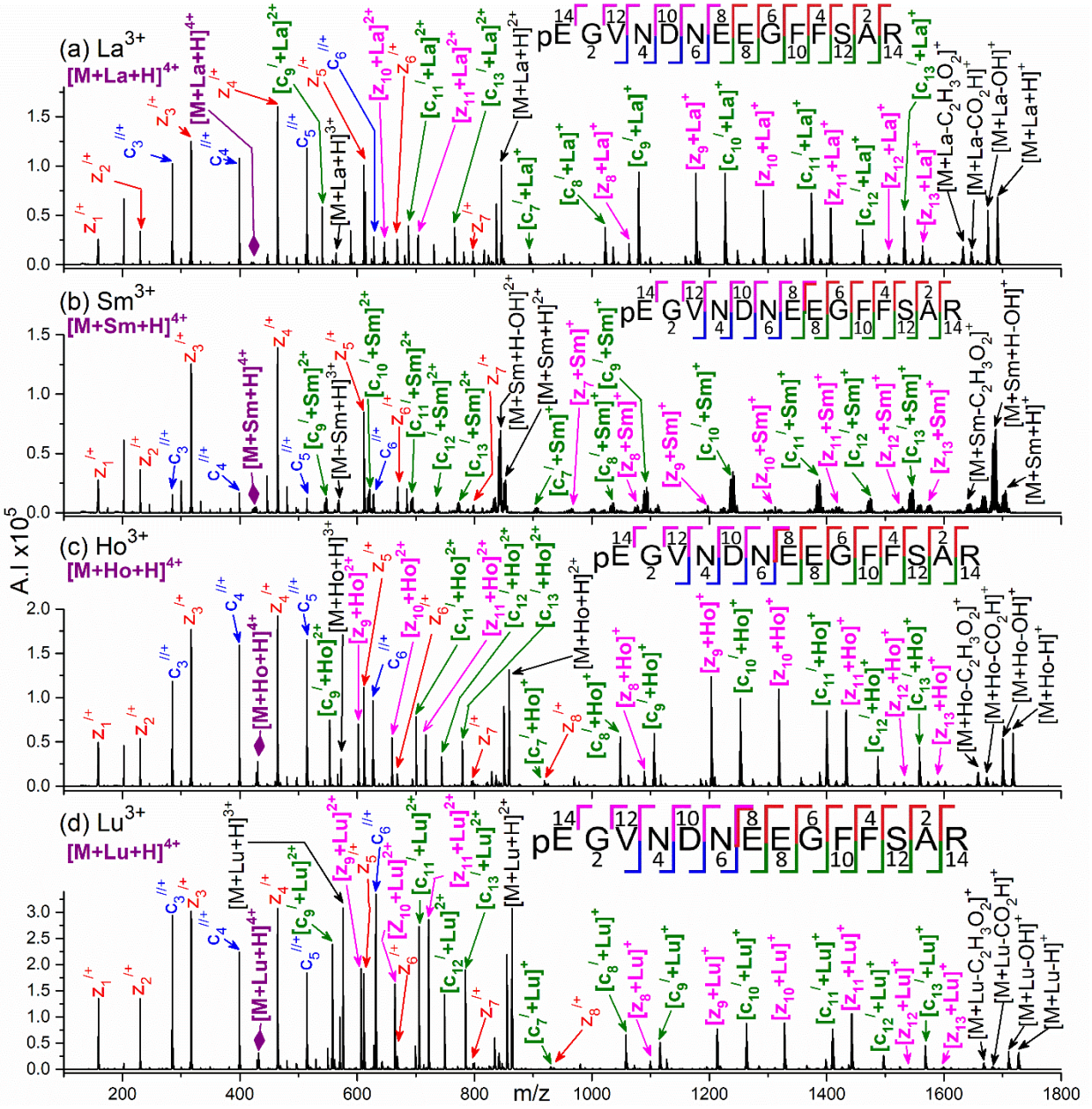


Figure 3.13. ETD mass spectra of $[M + Met + H]^{4+}$ for fibrinopeptide B produced by adduction to (a) La(III), (b) Sm(III), (c) Ho(III), and (d) Lu(III). In the figures, the following colors are used to label the ions: non-metallated z-ions = red, non-metallated c-ions = blue, metal-adducted z-ions = bright pink, and metal-adducted c-ions = green. Undissociated precursor ion is labeled in purple with a large purple diamond arrow head. Neutral loss products and electron transfer without dissociation (ETnoD) ions are labeled in black. A prime symbol to the left indicates loss of a hydrogen (i.e., $^{/}c_n = [c_n - H]^+$) and to the right indicates the addition of a hydrogen at the cleavage site (i.e., $c_n^{//} = [c_n + 2H]^+$). The spectra have no expansion of the intensity axis; all peaks are shown to scale.

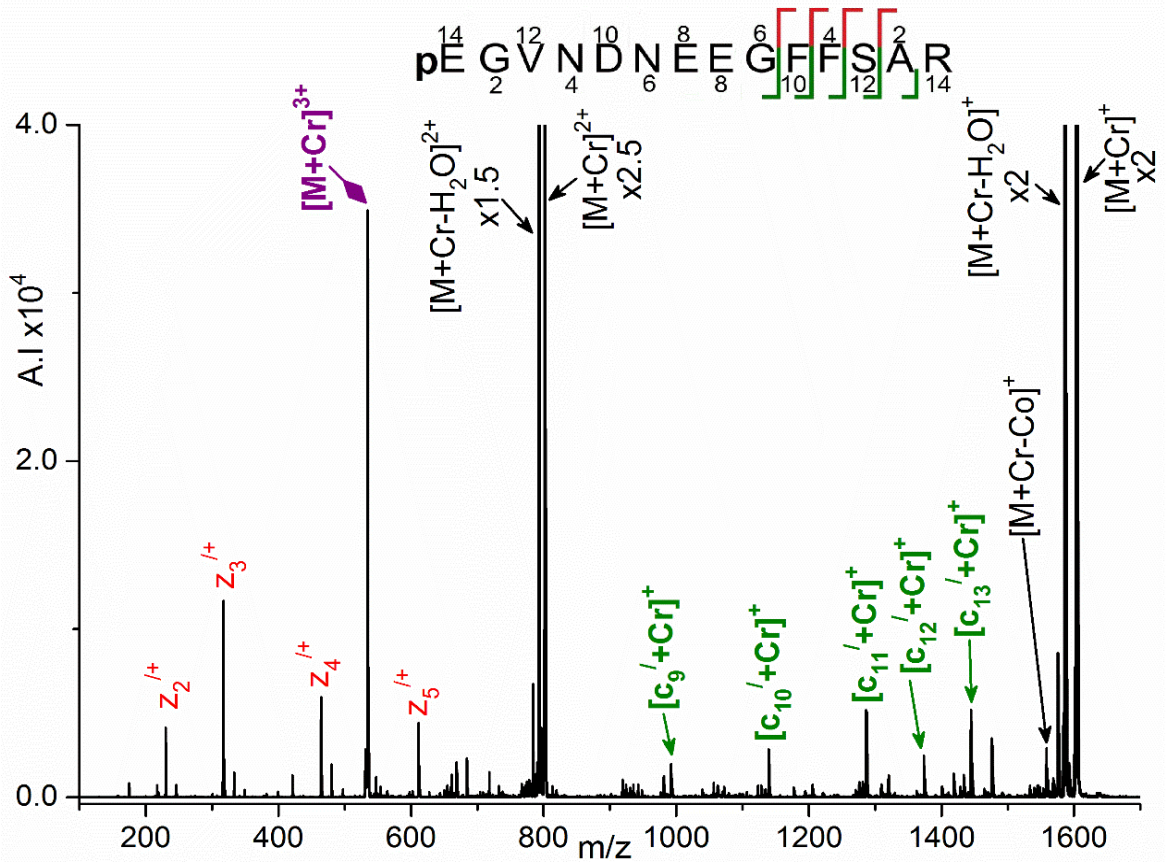


Figure 3.14. ETD mass spectrum of $[M + Cr]^{3+}$ for fibrinopeptide B. In the figure, the following colors are used to label the ions: non-metallated z-ions = red, and metal-adducted c-ions = green. Undissociated precursor ion is labeled in purple with a large purple diamond arrow head. Neutral loss products and electron transfer without dissociation (ETnoD) ions are labeled in black. A prime symbol to the left indicates loss of a hydrogen (i.e., $^{/}c_n = [c_n - H]^+$) and to the right indicates the addition of a hydrogen at the cleavage site (i.e., $c_n^{//} = [c_n + 2H]^+$). This spectrum has an expansion of the y-axis with four product ions that do not involve backbone cleavage being significantly off-scale.

to study trivalent iron, $Fe^{3+}$, with fibrinopeptide B. These experiments were unsuccessful because the ESI signal of iron(III)-cationized peptide was unstable and irreproducible. The Cassady group has encountered this problem previously[57,68] and attribute it to $Fe^{3+}$ reduction to $Fe^{2+}$ in solution (reduction potential, $E^0 = +0.771$ V [73]) during ESI. With an ESI source of similar design to our source (i.e., grounded needle with cations spraying into an electric field of negative polarity), Hoppilliard and coworkers[74] have also reported reduction of easily reduced metal cations.

Decreased ETD fragmentation efficiency and limited backbone cleavage is a recurring trend for $[M + Eu - H]^{2+}$ and $[M + Eu]^{3+}$ from the three peptides throughout this study. Williams and coworkers[49] also observed a lack of ECD product ion formation for peptides adducted to $Eu^{3+}$. $Eu^{3+}$ has an electronic configuration of $[Xe]4f^6$ that becomes a highly stable $[Xe]4f^7$ upon addition of one electron. This is indicated by the relatively high IE3 of Eu and the fact that it commonly forms divalent compounds.[65] However, Yb also acquires a stable electronic configuration, $[Xe]4f^{14}$, upon single electron recombination, but as shown in Figure 3.15, ETD of $[M + Yb]^{3+}$ for fibrinopeptide B yields extensive sequence-informative fragmentation despite a relatively intense charge reduced ETnoD ion. The backbone cleavage ions are similar in type and intensity to those obtained with other lanthanide ions. Therefore, an additional factor needs to be considered to account for the differences in ETD fragmentation observed between Eu(III) and Yb(III) peptide-complexes. Inside the mass analyzer, the metal cations exist in the metal-peptide complexes formed during ESI and not in a free state. Thus, the chemistry of metal-peptide complexes will affect their ETD fragmentation. Several studies show that in aqueous and ammoniated complexes, the standard electrode reduction potential ($E^0$) of $Yb^{3+}$ is considerably lower than for $Eu^{3+}$.[75-77] Reduction of $Eu^{3+}$ to $Eu^{2+}$ has $E^0$ of -0.36 V,[73] whereas for

$Yb^{3+}$ this $E^0$ is -1.05 V.[73] That is, in solution $Eu^{3+}$ reduces more readily than $Yb^{3+}$. Williams and coworkers referred to $Eu^{3+}$ as an "electron trap"[49] because of its propensity to favorably undergo a one electron reduction in a "solvated" complex such as in aqueous media or, in this case, a peptide. During the ETD and ECD processes, in some instances, $Eu^{3+}$ may be preferentially undergoing direct reduction instead of allowing the electron to be directed at the peptide backbone to facilitate normal ECD/ ETD N-Cα bond cleavage.

Similar to $Eu^{3+}$, the divalent ion of copper, $Cu^{2+}$, is easily reduced ($E^0$ = +0.153V[73]) and exhibits different fragmentation patterns in peptide complexes than other members of its series. Chan[43] and coworkers and Dong and Vachet[50] have postulated that metal ion reduction leads to changes in the coordination sphere of $Cu^{2+}$, which contribute significantly to the fragmentation patterns observed by ETD/ECD. However, unlike $Cu^{2+}$ and other transition metal ions with interactive outer d-orbitals, the f-orbitals of the lanthanides have weak overlap with binding ligands.[65] Therefore, lanthanide metal center reduction has minimal to no effect on orbital geometries.[65] As a consequence, we speculate that coordination sphere changes may have a less significant role in dissociation of peptide complexes for $Eu^{3+}$ than for $Cu^{2+}$.

For $Eu^{3+}$, the extent of structurally-informative ETD fragmentation is dependent on the nature of the peptide-metal ion complex. Proton deficient $[M + Eu - H]^{2+}$, as seen in Figure 3.5(a), generates no backbone cleavage ions and the peptide cannot be sequenced. In contrast, in Figure 3.5(c), $[M + Eu + H]^{4+}$ generates abundant product ions involving cleavage at every residue. Here, the extra proton is allowing backbone cleavage pathways to dominate the spectra and the impact of electron sequestration by $Eu^{3+}$ is minimized. In an ETD study, Vachet and coworkers[50] found that the presence of an extra proton in conjunction with acidic residues to bind $Cu^{2+}$ allowed increased peptide backbone cleavage; that is, the transfer of an electron to

protonated peptide sites competed favorably with reduction of $Cu^{2+}$. Likewise, in the current study, less metal reduction occurs during ETD of $[M + Eu + H]^{4+}$ and instead c- and z-ion formation increases. In contrast, $[M + Eu - H]^{2+}$ and $[M + Eu]^{3+}$ lack an extra proton and undergo minimal, if any, backbone dissociation. In addition, the higher ionic charge on $[M + Eu + H]^{4+}$ may play a role in its enhanced dissociation. Peptide fragmentation by ETD generally increases as the precursor ion charge increases, although this effect is complex and also relates to the types of amino acid residues present and the length of the peptide sequence.[30,36,37]

While $[M + Eu]^{3+}$ provides less sequence coverage by ETD (Figure 3.5(b)) than the other lanthanide ions, more product ions form in the current study than Williams and coworkers[49] observed by ECD for several other peptides. This difference may relate to fragmentation efficiency. In ECD on a Fourier transform ion cyclotron resonance (FT-ICR) mass spectrometer, the percentage of the precursor ion that dissociates is limited by the ability of the electron beam, focused by a high magnetic field, to overlap with the analyte cations.[78] No such limitation exists in ETD (where a cation/anion reaction occurs), generally making the process more efficient. In addition, our Bruker HCTultra has a high capacity QIT that allows ions to cluster together and interact in a spherical cloud-like formation in the center of the mass analyzer.[79] This promotes a high degree of overlap between the peptide cations and the ETD reagent anions, which results in effective electron transfer and high fragmentation efficiencies.

From lanthanum (La) to lutetium (Lu), the ionic radius of the 3+ ion decreases from 103.2 pm for La to 86.1 pm for Lu.[65] This larger than normal decrease in the ionic radii is known as the "lanthanide contraction." The 4f orbital acts as a poor shield against the nuclear charge exhibited on the 6s shells by the nucleus. This decrease in ionic radii can affect the chemistry of the trivalent lanthanide ions.[65] Surprisingly, the size of the trivalent metal cation

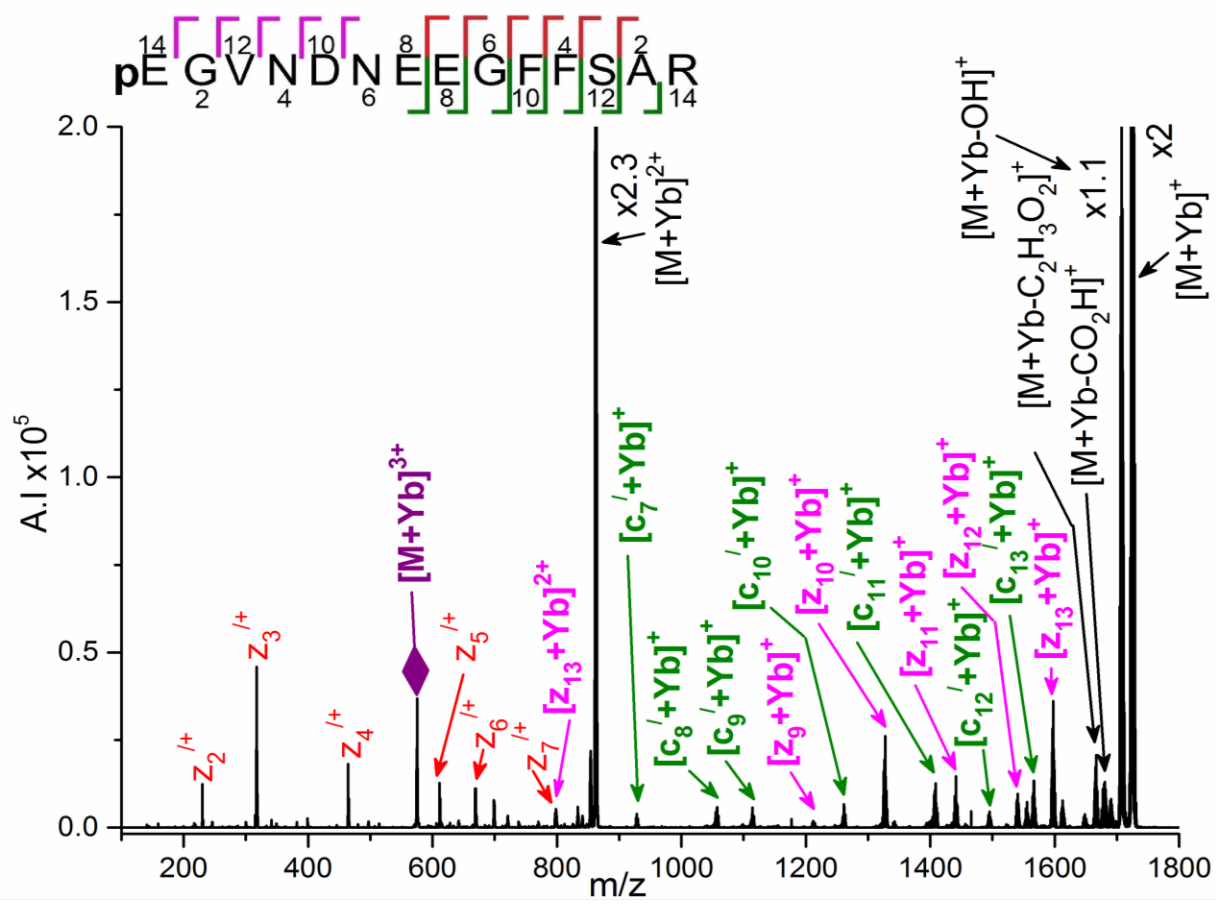


Figure 3.15. ETD mass spectrum of $[M + Yb]^{3+}$ for fibrinopeptide B. In the figure, the following colors are used to label the ions: non-metallated z-ions = red, non-metallated c-ions = blue, metal-adducted z-ions = bright pink, and metal-adducted c-ions = green. Undissociated precursor ion is labeled in purple with a large purple diamond arrow head. Neutral loss products and electron transfer without dissociation (ETnoD) ions are labeled in black. A prime symbol to the left indicates loss of a hydrogen (i.e., $^{/}c_n = [c_n - H]^+$) and to the right indicates the addition of a hydrogen at the cleavage site (i.e., $c_n^{//} = [c_n + 2H]^+$). This spectrum has an expansion of the y-axis with three product ions that do not involve backbone cleavage being significantly off-scale.

causes no variation in the ETD fragmentation in the current study.

### 3.5.2 Dissociation trends and sequence information

For the lanthanide ions other than $Eu^{3+}$, all three precursor ions provide sequence-informative fragmentation. The trends, which are illustrated in Figure 3.2 with $Pr^{3+}$, are that $[M + Met + H]^{4+}$ yields ETD cleavage at every residue, $[M + Met]^{3+}$ cleaves at almost every residue (with one or two exceptions), and $[M + Met - H]^{2+}$ cleaves at almost every residue but with lower product ion intensities. Generally, ETD spectra of $[M + Met]^{3+}$ are sufficient for sequencing. This precursor ion has the advantage of forming in abundance even in the absence of a basic arginine, lysine, or histidine residue on the peptide; for example, $[M + Pr]^{3+}$ is the base peak in Figure 3.1(c) for ESI involving des-Arg$^{14}$-[Glu$^{1}$]-fibrinopeptide B. However, even better conditions for sequencing occur with $[M + Met + H]^{4+}$, where proton adduction leads to more intense and wide-ranging fragmentation. In ESI on peptides, protons are postulated to initially bind to basic residues, with a preference for arginine.[80-83] Although the ESI process may have preferentially deposited the extra proton on the N-terminal arginine residue, that is not always its location in the ETD product ions. As seen in Figure 3.2 for fibrinopeptide B, $c_n^{//+}$, n = 2-6, occur in much greater intensity for the 4+ precursor than the 3+ and 2+ precursors; these ions contain no residues with basic side chains. Note that for the 3+ and 4+ precursors the additional proton does not change the product ion series; for example, the non-metallated c-series is $c_n^{//+}$ for both $[M + Met]^{3+}$ and $[M + Met + H]^{4+}$. Instead, the added proton increases the intensity of product ions from these series and causes more members of the series to be observed.

Variation in the ETD product ion series is a noteworthy aspect of this work. $[M + Met]^{3+}$ and $[M + Met + H]^{4+}$ yield the same product ion series, while $[M + Met - H]^{2+}$ is unique. The metallated c-series is $[c_n^{/} + Met]^{+}$ for the 3+ and 4+ precursors, but $[^{/}c_n + Met]^{+}$ for the 2+

precursor. This difference of two hydrogens may be explained by the proton deficiency of the precursor ion, $[M + Met - H]^{2+}$.

The ETD z-series products are particularly interesting. While the 3+ and 4+ precursors generate $z_n^{/+}$, $[z_n + Met]^+$, and $[z_n + Met]^{2+}$, the proton deficient 2+ precursor yields z-ions with one *more* hydrogen, $z_n^{//+}$ and $[z_n^{/} + Met]^+$. The z-series routinely found in ETD and ECD is $z_n^{/+}$, which is a radical of the type $[z + H]^{+\cdot}$.[31,84] In a high resolution FT-ICR ECD study on 15,000 mass spectra of tryptic peptides, Zubarev and coworkers[85] also occasionally observed $z_n^{//+}$ formation. We found that ETD on $[M + 2H]^{2+}$ from fibrinopeptide B and [Glu$^1$]-fibrinopeptide B generates an extensive z-series that is almost exclusively $z_n^{//+}$. (A minor amount of $z^{/+}$ forms but is ~10% the intensity of $z^{//+}$.) With no arginine residue, $[M + 2H]^{2+}$ from des-Arg$^{14}$-[Glu$^1$]-fibrinopeptide B produces only two z-ions, both of which are the normal $z_n^{/+}$. (ETD spectra for $[M + 2H]^{2+}$ are in Figure 3.16). Thus, ETD on both $[M + Met - H]^{2+}$ and $[M + 2H]^{2+}$ form the unusual $z_n^{//+}$ series for fibrinopeptide B and [Glu$^1$]-fibrinopeptide B, but not for des-Arg$^{14}$-[Glu$^1$]-fibrinopeptide B. The additional hydrogen in $z_n^{//+}$ may be residing at the C-terminal arginine residue of fibrinopeptide B and of [Glu$^1$]-fibrinopeptide B. This unique fragmentation, which was also observed during ETD of $[M + 2H]^{2+}$ for other acidic peptides discussed in Chapter 4,[86] appears to relate to the presence of several acidic residues in conjunction with a nearby basic residue. We are currently conducting additional studies on this effect with custom synthesized peptides. Salt bridge intermediates involving acidic and basic sites are known to affect peptide fragmentation.[53-55,87,88] The sequences of fibrinopeptide B and its [Glu$^1$] analog possibly allow a salt bridge formation that impacts their electron-induced fragmentation pathways.

Throughout this study, all metallated product ions contain an acidic amino acid residue, which suggests attachment of the lanthanide cation at the acidic side chains. This is consistent

with several studies suggesting that trivalent metal ions preferentially bind to acidic sites on peptides.[49,53-55,57] For example, in Figure 3.2 showing the ETD spectra of 2+, 3+, and 4+ precursors from fibrinopeptide B, only peptide fragments containing at least two acidic sites (i. e., glutamic acid or aspartic acid side chains and the C-terminal carboxylic acid group) are metallated. In their ECD study on several peptides, Williams and coworkers[49] also observed metal-adducted ions from peptide fragments containing at least one acidic amino acid residue.

The sequences of the peptides result in minor variations in the ETD spectra that relate to cleavages near acidic residues. For fibrinopeptide B with a cyclized N-terminal glutamic acid residue, ETD on $[M + Met + H]^{4+}$ generates low intensity product ions, $z_7^{\cdot/+}$ and $[c_7^{\cdot/} + Pr]^+$, corresponding to cleavage between the two glutamic acid residues at E7 and E8, as shown in Figure 3.2(c). In contrast, more intense peaks, $c_7^{\cdot//+}$ and $z_7^{\cdot/+}$, corresponding to the cleavage between E7 and E8 occur for ETD on $[M + Met + H]^{4+}$ for [Glu[1]]-fibrinopeptide B and des-Arg[14]-[Glu[1]]-fibrinopeptide B (Figure 3.12). The two analogs have a non-cyclized glutamic acid residue at the N-terminus, which provides acidic sites at E1, D4, E7, and E8, as well as at the C-terminus. With fibrinopeptide B, there are acidic sites at only D4, E7, E8, and the C-terminus. The metallated product ions always contain two acidic sites, suggesting simultaneous coordination of the lanthanide ion to both locations. Because fibrinopeptide B has only four acidic sites, there is a greater probability of coordination involving both E7 and E8, which might hinder cleavage between these residues. The presence of an additional acidic site at E1 in [Glu[1]]-fibrinopeptide B and des-Arg[14]-[Glu[1]]-fibrinopeptide may yield more possibilities for metal ion coordination, thus minimizing E7 and E8 simultaneous coordination and enhancing E7-E8 cleavage. The work of Williams and coworkers[49] also suggested simultaneous coordination of trivalent lanthanide cations to two acidic sites.

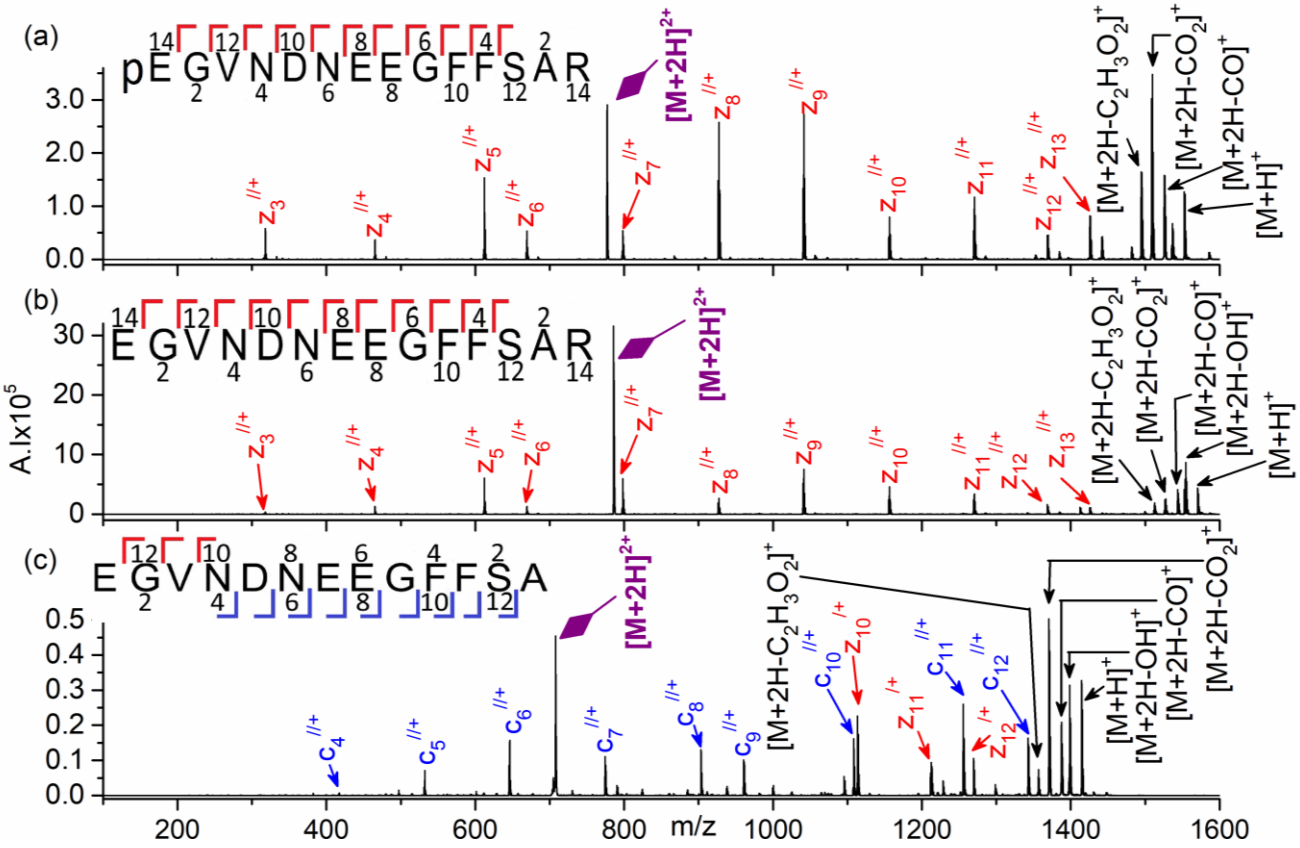


Figure 3.16. ETD mass spectra of $[M + 2H]^{2+}$ for (a) fibrinopeptide B, (b) $[Glu^1]$-fibrinopeptide B, and (c) des-$Arg^{14}$-$[Glu^1]$-fibrinopeptide B. In the figures, the following colors are used to label the ions: non-metallated z-ions = red, and non-metallated c-ions = blue. Undissociated precursor ion is labeled in purple with a large purple diamond arrow head. Neutral loss products and electron transfer without dissociation (ETnoD) ions are labeled in black. A prime symbol to the left indicates loss of a hydrogen (i.e., $'c_n = [c_n - H]^+$) and to the right indicates the addition of a hydrogen at the cleavage site (i.e., $c_n^{//} = [c_n + 2H]^+$). The spectra have no expansion of the intensity axis; all peaks are shown to scale.

Isotopic composition of the metal ion influences the appearance of the ETD spectra. Six lanthanide metals have one major stable isotope in an abundance greater than 95%, Eu has two stable isotopes in near equal abundances, and the remaining lanthanide metals have multiple staple isotopes of significant intensities. Spectra from lanthanide metal ions with one major isotope have easily resolved peaks, which simplify interpretation; for example, see Figures 3.2, 3.13(a), 3.13(c), and 3.13(d). In contrast, Figure 3.13(b) is the ETD spectrum for $[M + Sm + H]^{4+}$ from fibrinopeptide B. $Sm^{3+}$ has seven major isotopes with the most abundant at 26.7%.[73] Ionic peak broadening and overlapping occurs when the lanthanide metal has several stable isotopes, which can reduce resolution and make interpretation more difficult. The only benefit to using a lanthanide metal with many isotopes is that the elucidation of metallated product ions is easier because the metal creates a characteristic isotopic distribution that is evident in the spectra.

### 3.6 Conclusions

Trivalent lanthanide cations readily adduct to the acidic fibrinopeptide B and its analogs to form $[M + Met + H]^{4+}$, $[M + Met]^{3+}$, and $[M + Met - H]^{2+}$. These ions undergo ETD to generate abundant sequence-informative product ions and extensive peptide backbone cleavage. The intense signals of the multiply charged precursor ions and the high fragmentation efficiency of ETD yield spectra with high S/N, which is beneficial for automated techniques. For peptides lacking a highly basic amino acid residue, trivalent lanthanide ion adduction may be particularly useful because it provides ready formation of multiply charged peptide ions that can be subjected to ETD. In the current study, $Pr^{3+}$ consistently produced intense metallated peptide ions and allowed for easy interpretation of ETD spectra, but any lanthanide metal ion with one major

isotope is adequate for peptide analysis. In addition, metallated product ions can be easily confirmed using a companion metal such as $Sm^{3+}$ that has multiple stable isotopes. The ability of multiply charged trivalent lanthanide-peptide complexes to undergo extensive ETD fragmentation could prove to be very useful in the sequencing of acidic peptides. Because peptide analysis in proteomics studies commonly involves liquid chromatographic (LC) separation of mixtures, we are currently exploring the addition of metal ions to LC eluents. This appears to be a feasible method for producing metallated peptide ions for study by tandem mass spectrometry.

## References


1. Ebert, R. F.; Bell, W. R. Assay of Human Fibrinopeptides by High-Performance Liquid Chromatography. *Anal. Biochem.* **1985**, *148*, 70-78.

2. Edkins, J. S. The Chemical Mechanism of Gastric Secretion 1. *J. Physiol. Lond.* **1906**, *34*, 133-144.

3. Dimaline, R.; Lee, C. M. Chicken Gastrin - A Member of the Gastrin Cck Family with Novel Structure-Activity-Relationships. *Am. J. Physiol.* **1990**, *259*, G882-G888.

4. Pierotti, A. R.; Prat, A.; Chesneau, V.; Gaudoux, F.; Leseney, A. M.; Foulon, T.; Cohen, P. N-Arginine Dibasic Convertase, a Metalloendopeptidase as a Prototype of a Class of Processing Enzymes. *Proc. Natl. Acad. Sci. USA* **1994**, *91*, 6078-6082.

5. Speetjens, J. K.; Parand, A.; Crowder, M. W.; Vincent, J. B.; Woski, S. A. Low-molecular Weight Chromium-binding Substance and Biomimetic $[Cr_3O(O_2CH_2CH_3)_6(H_2O)_3]^+$ Do Not Cleave DNA Under Physiologically-relevant Conditions. *Polyhedron* **1999**, *18*, 2617-2624.

6. Vincent, J. B. Elucidating a Biological Role for Chromium at a Molecular Level. *Acc. Chem. Res.* **2000**, *33*, 503-510.

7. Davis, C. M.; Vincent, J. B. Isolation and Characterization of a Biologically Active Chromium Oligopeptide from Bovine Liver. *Arch. Biochem. Biophys.* **1997**, *339*, 335-343.

8. Lapko, V. N.; Jiang, X. Y.; Smith, D. L.; Song, P. S. Posttranslational Modification of Oat Phytochrome A: Phosphorylation of a Specific Serine in a Multiple Serine Cluster. *Biochemistry* **1997**, *36*, 10595-10599.

9. Yagami, T.; Kitagawa, K.; Futaki, S. Liquid Secondary-ion Mass Spectrometry of Peptides Containing Multiple Tyrosine-O-sulfates. *Rapid Commun. Mass Spectrom.* **1995**, *9*, 1335-1341.

10. Chen, Y.; Watson, H. M.; Gao, J.; Sinha, S. H.; Cassady, C. J.; Vincent, J. B. Characterization of the Organic Component of Low-Molecular-Weight Chromium-Binding Substance and Its Binding of Chromium. *J. Nutr.* **2011**, *141*, 1225-1232.

11. Jai-nhuknan, J.; Cassady, C. J. Negative Ion Postsource Decay Time-of-Flight Mass Spectrometry of Peptides Containing Acidic Amino Acid Residues. *Anal. Chem.* **1998**, *70*, 5122-5128.

12. Zubarev, R. A.; Kelleher, N. L.; McLafferty, F. W. Electron Capture Dissociation of Multiply Charged Protein Cations. A Nonergodic Process. *J. Am. Chem. Soc.* **1998**, *120*, 3265-3266.

13. Zubarev, R. A.; Horn, D. M.; Fridriksson, E. K.; Kelleher, N. L.; Kruger, N. A.; Lewis, M. A.; Carpenter, B. K.; McLafferty, F. W. Electron Capture Dissociation for Structural Characterization of Multiply Charged Protein Cations. *Anal. Chem.* **2000**, *72*, 563-573.

14. Zubarev, R. A.; Kruger, N. A.; Fridriksson, E. K.; Lewis, M. A.; Horn, D. M.; Carpenter, B. K.; McLafferty, F. W. Electron Capture Dissociation of Gaseous Multiply-charged Proteins is Favored at Disulfide Bonds and Other Sites of High Hydrogen Atom Affinity. *J. Am. Chem. Soc.* **1999**, *121*, 2857-2862.

15. Chen, X.; Tureček, F. The Arginine Anomaly: Arginine Radicals are Poor Hydrogen Atom Donors in Electron Transfer Induced Dissociations. *J. Am. Chem. Soc.* **2006**, *128*, 12520-12530.

16. Zubarev, R. A.; Haselmann, K. F.; Budnik, B.; Kjeldsen, F.; Jensen, F. Towards an Understanding of the Mechanism of Electron-capture Dissociation: A Historical Perspective and Modern Ideas. *Eur. J. Mass Spectrom.* **2002**, *8*, 337-349.

17. Syka, J. E. P.; Coon, J. J.; Schroeder, M. J.; Shabanowitz, J.; Hunt, D. F. Peptide and Protein Sequence Analysis by Electron Transfer Dissociation Mass Spectrometry. *Proc. Natl. Acad. Sci. USA* **2004**, *101*, 9528-9533.

18. Syrstad, E. A.; Tureček, F. Toward a General Mechanism of Electron Capture Dissociation. *J. Am. Soc. Mass Spectrom.* **2005**, *16*, 208-224.

19. McLafferty, F. W.; Horn, D. M.; Breuker, K.; Ge, Y.; Lewis, M. A.; Cerda, B. A.; Zubarev, R. A.; Carpenter, B. K. Electron Capture Dissociation of Gaseous Multiply Charged Ions by Fourier Transform ion Cyclotron Resonance. *J. Am. Soc. Mass Spectrom.* **2001**, *12*, 245-249.

20. Cooper, H. J.; Håkansson, K.; Marshall, A. G. The Role of Electron Capture Dissociation in Biomolecular Analysis. *Mass Spectrom. Rev.* **2005**, *24*, 201-222.

21. Leymarie, N.; Costello, C. E.; O'Connor, P. B. Electron Capture Dissociation Initiates a Free Radical Reaction Cascade. *J. Am. Chem. Soc.* **2003**, *125*, 8949-8958.

22. Mirgorodskaya, E.; Roepstorff, P.; Zubarev, R. A. Localization of O-glycosylation Sites in Peptides by Electron Capture Dissociation in a Fourier Transform Mass Spectrometer. *Anal. Chem.* **1999**, *71*, 4431-4436.

23. Shi, S. D. H.; Hemling, M. E.; Carr, S. A.; Horn, D. M.; Lindh, I.; McLafferty, F. W. Phosphopeptide/Phosphoprotein Mapping by Electron Capture Dissociation Mass Spectrometry. *Anal. Chem.* **2001**, *73*, 19-22.

24. Kelleher, N. L.; Zubarev, R. A.; Bush, K.; Furie, B.; Furie, B. C.; McLafferty, F. W.; Walsh, W. T. Localization of Labile Posttranslational Modifications by Electron Capture Dissociation: The Case of y-Carboxyglutamic Acid. *Anal. Chem.* **1999**, *71*, 4250-4253.

25. Mann, M.; Jensen, O. N. Proteomic Analysis of Post-translational Modifications. *Nat. Biotechnol.* **2003**, *21*, 255-261.

26. Stensballe, A.; Jensen, O. N.; Olsen, J. V.; Haselmann, K. F.; Zubarev, R. A. Electron Capture Dissociation of Singly and Multiply Phosphorylated Peptides. *Rapid Commun. Mass Spectrom.* **2000**, *14*, 1793-2000.

27. Zhao, C.; Sethuraman, M.; Clavreul, N.; Kaur, P.; Cohen, R. A.; O'Connor, P. B. Detailed Map of Oxidative Post-translational Modifications of human P21Ras Using Fourier Transform Mass Spectrometry. *Anal. Chem.* **2006**, *78*, 5134-5142.

28. Zubarev, R. A. Electron Capture Dissociation LC/MS/MS for Bottom-Up Proteomics. *Methods Mol. Biol.* **2009**, *492*, 413-416.

29. Coon, J. J. Collisions or Electrons? Protein Sequence Analysis in the 21st Century. *Anal. Chem.* **2009**, *81*, 3208-3215.

30. Good, D. M.; Wirtala, M.; McAlister, G. C.; Coon, J. J. Performance Characteristics of Electron Transfer Dissociation Mass Spectrometry. *Mol. Cell. Proteomics* **2007**, *6*, 1942-1951.

31. Turecek, F.; Julian, R. R. Peptide Radicals and Cation Radicals in the Gas Phase. *Chem. Rev.* **2013**, *113*, 6691-6733.

32. Dongre, A. R.; Jones, J. L.; Somogyi, A.; Wysocki, V. H. Influence of Peptide Composition, Gas-Phase Basicity, and Chemical Modification on Fragmentation Efficiency: Evidence for the Mobile Proton Model. *J. Am. Chem. Soc.* **1996**, *118*, 8365-8374.

33. Kjeldsen, F.; Giessing, A. M. B.; Ingrell, C. R.; Jensen, O. N. Peptide Sequencing and Characterization of Post-Translational Modifications by Enhanced Ion-Charging and Liquid Chromatography Electron-Transfer Dissociation Tandem Mass Spectrometry. *Anal. Chem.* **2007**, *79*, 9243-9252.

34. Wells, J. M.; Stephenson Jr., J. L.; McLuckey, S. A. Charge dependence of protonated insulin decompositions. *Int. J. Mass Spectrom.* **2000**, *203*, A1-A9.

35. Madsen, J. A.; Brodbelt, J. S. Comparison of Infrared Multiphoton Dissociation and Collision-Induced Dissociation of Supercharged Peptides in Ion Traps. *J. Am. Soc. Mass Spectrom.* **2009**, *20*, 349-358.

36. Chalkley, R. J.; Medzihradszky, K. F.; Lynn, A. J.; Baker, P. R.; Burlingame, A. L. Statistical Analysis of Peptide Electron Transfer Dissociation Fragmentation Mass Spectrometry. *Anal. Chem.* **2010**, *82*, 579-584.

37. Sharma, V.; Eng, J. K.; Feldman, S.; von Haller, P. D.; MacCoss, M. J.; Noble, W. S. Precursor Charge State Prediction for Electron Transfer Dissociation Tandem Mass Spectra. *J. Proteome Res.* **2010**, *9*, 5438-5444.

38. Liu, H.; Håkansson, K. Divalent Metal Ion-Peptide Interactions Probed by Electron Capture Dissociation of Trications. *J. Am. Soc. Mass Spectrom.* **2006**, *17*, 1731-1741.

39. Liu, H.; Håkansson, K. Electron Capture Dissociation of Tyrosine O-Sulfated Peptides Complexed with Divalent Metal Cations. *Anal. Chem.* **2006**, *78*, 7570-7576.

40. Fung, Y. M. E.; Liu, H.; Chan, T. W. D. Electron Capture Dissociation of Peptides Metalated with Alkaline-Earth Metal Ions. *J. Am. Soc. Mass Spectrom.* **2006**, *17*, 757-771.

41. Chen, X.; Chan, W. Y. K.; Wong, P. S.; Yeung, H. S.; Chan, T. W. D. Formation of Peptide Radical Cations ($M^{+\cdot}$) in Electron Capture Dissociation of Peptides Adducted with Group IIB Metal Ions. *J. Am. Soc. Mass Spectrom.* **2011**, *22*, 233-244.

42. Chen, X.; Fung, Y. M. E.; Chan, W. Y. K.; Wong, P. S.; Yeung, H. S.; Chan, T. W. D. Transition Metal Ions: Charge Carriers that Mediate the Electron Capture Dissociation Pathways of Peptides. *J. Am. Soc. Mass Spectrom.* **2011**, *22*, 2232-2245.

43. Chen, X.; Wang, Z.; Li, W.; Wong, Y. L. E.; Chan, T. W. D. Effect of Structural Parameters on the Electron Capture Dissociation and Collision-induced Dissociation Pathways of Copper(II)-peptide Complexes. *Eur. J. Mass Spectrom.* **2015**, *21*, 649-657.

44. Chen, X.; Liu, G.; Wong, Y. L. E.; Deng, L.; Wang, Z.; Li, W.; Chan, T. W. D. Dissociation of Trivalent Metal Ion ($Al^{3+}$, $Ga^{3+}$, $In^{3+}$ and $Rh^{3+}$)–peptide Complexes Under Electron Capture Dissociation Conditions. *Rapid Commun. Mass Spectrom.* **2016**, *30*, 705-710.

45. Voinov, V. G.; Hoffman, P. D.; Bennett, S. E.; Beckman, J. S.; Barofsky, D. F. Electron Capture Dissociation of Sodium-Adducted Peptides on a Modified Quadrupole/Time-of-Flight Mass Spectrometer. *J. Am. Soc. Mass Spectrom.* **2015**, *26*, 2096-2104.

46. Kleinnijenhuis, A. J.; Mihalca, R.; Heeren, R. M. A.; Heck, A. J. R. Atypical Behavior in the Electron Capture Induced Dissociation of Biologically Relevant Transition Metal Ion Complexes of the Peptide Hormone Oxytocin. *Int. J. Mass Spectrom.* **2006**, *253*, 217-224.

47. van der Burgt, Y. E. M.; Palmblad, M.; Dalebout, H.; Heeren, R. M. A.; Deelder, A. M. Electron Capture Dissociation of Peptide Hormone Changes Upon Opening of the Tocin Ring and Complexation with Transition Metal Cations. *Rapid Commun. Mass Spectrom.* **2009**, *23*, 31-38.

48. Iavarone, A. T.; Paech, K.; Williams, E. R. Effects of Charge State and Cationizing Agent on the Electron Capture Dissociation of a Peptide. *Anal. Chem.* **2004**, *76*, 2231-2238.

49. Flick, T. G.; Donald, W. A.; Williams, E. R. Electron Capture Dissociation of Trivalent Metal Ion-Peptide Complexes. *J. Am. Soc. Mass Spectrom.* **2013**, *24*, 193-201.

50. Dong, J.; Vachet, R. W. Coordination Sphere Tuning of the Electron Transfer Dissociation Behavior of Cu(II)-peptide Complexes. *J. Am. Soc. Mass Spectrom.* **2012**, *23*, 321-329.

51. Asakawa, D.; Takeuchi, T.; Yamashita, A.; Wada, Y. Influence of Metal–Peptide Complexation on Fragmentation and Inter-Fragment Hydrogen Migration in Electron Transfer Dissociation. *J. Am. Soc. Mass Spectrom.* **2014**, *25*, 1029-1039.

52. Asakawa, D.; Wada, Y. Electron Transfer Dissociation Mass Spectrometry of Peptides Containing Free Cysteine Using Group XII Metals as a Charge Carrier. *J Phys Chem B* **2014**, *118*, 12318-12325.

53. Prell, J. S.; Flick, T. G.; Oomens, J.; Berden, G.; Williams, E. R. Coordination of Trivalent Metal Cations to Peptides: Results from IRMPD Spectroscopy and Theory. *J. Phys. Chem. A* **2009**, *114*, 854-860.

54. Shi, T.; Hopkinson, A. C.; Siu, K. W. M. Coordination of Triply Charged Lanthanum in the Gas Phase: Theory and Experiment. *Chem. Eur. J.* **2007**, *13*, 1142-1151.

55. Shi, T.; Siu, K. W. M.; Hopkinson, A. C. Generation of $[La(peptide)]^{3+}$ Complexes in the Gas Phase: Determination of the Number of Binding Sites Provided by Dipeptide, Tripeptide, and Tetrapeptide Ligands. *J. Phys. Chem. A* **2007**, *111*, 11562-11571.

56. Shvartsburg, A. A.; Jones, R. C. Attachment of metal trications to peptides. *J. Am. Soc. Mass Spectrom.* **2004**, *15*, 406-408.

57. Feng, C.; Commodore, J. J.; Cassady, C. J. The Use of Chromium(III) to Supercharge Peptides by Protonation at Low Basicity Sites. *J. Am. Soc. Mass Spectrom.* **2015**, *26*, 347-358.

58. Hunter, E.P., Lias, S.G. Proton Affinity Evaluation. In *NIST Chemistry WebBook, NIST Standard Reference Database Number 69*; Linstrom, P.J., Mallard, W.G., Ed.; NIST: National Institute of Standards and Technology, Gaithersburg MD, 20899, (accessed February 5, 2016).

59. Roepstorff, P.; Fohlman, J. Proposal for a Common Nomenclature for Sequence Ions in Mass Spectra of Peptides. *Biomed. Mass Spectrom.* **1984**, *11*, 601.

60. Biemann, K. Contributions of Mass Spectrometry to Peptide and Protein-Structure. *Biomed. Environ. Mass Spectrom.* **1988**, *16*, 99-111.

61. Chung, T. W.; Hui, R.; Ledvina, A.; Coon, J. J.; Turecek, F. Cascade Dissociations of Peptide Cation-Radicals. Part 1. Scope and Effects of Amino Acid Residues in Penta-, Nona-, and Decapeptides. *J. Am. Soc. Mass Spectrom.* **2012**, *23*, 1336-1350.

62. Han, H.; Xia, Y.; McLuckey, S. A. Ion Trap Collisional Activation of c and z˙ Ions Formed via Gas-phase Ion/Ion Electron-transfer Dissociation. *J. Proteome Res.* **2007**, *6*, 3062-3069.

63. Fung, Y. M. E.; Chan, T. W. D. Experimental and Theoretical Investigations of the Loss of Amino Acid Side Chains in Electron Capture Dissociation of Model Peptides. *J. Am. Soc. Mass Spectrom.* **2005**, *16*, 1523-1535.

64. Xia, Q.; Lee, M.; Rose, C.; Marsh, A.; Hubler, S.; Wenger, C.; Coon, J. Characterization and Diagnostic Value of Amino Acid Side Chain Neutral Losses Following Electron-Transfer Dissociation. *J. Am. Soc. Mass Spectrom.* **2011**, *22*, 255-264.

65. Cotton, S. *Lanthanide and Actinide Chemistry;* John Wiley and Sons, Ltd.: West Sussex, England, 2006.

66. Frese, C. K.; Altelaar, A. F. M.; Hennrich, M. L.; Nolting, D.; Zeller, M.; Griep-Raming, J.; Heck, A. J. R.; Mohammed, S. Improved Peptide Identification by Targeted Fragmentation Using CID, HCD and ETD on an LTQ-Orbitrap Velos. *J. Proteome Res.* **2011**, *10*, 2377-2388.

67. Pu, D.; Vincent, J. B.; Cassady, C. J. The Effects of Chromium(III) Coordination on the Dissociation of Acidic Peptides. *J. Mass Spectrom.* **2008**, *43*, 773-781.

68. Watson, H. M.; Vincent, J. B.; Cassady, C. J. Effects of Transition Metal Ion Coordination on the Collision-induced Dissociation of Polyalanines. *J. Mass Spectrom.* **2011**, *46*, 1099-1107.

69. Davis, C. M.; Vincent, J. B. Chromium Oligopeptide Activates Insulin Receptor Tyrosine Kinase Activity. *Biochemistry* **1997**, *36*, 4382-4385.

70. Sun, Y.; Ramirez, J.; Woski, S. A.; Vincent, J. B. The Binding of Trivalent Chromium to Low-molecular-weight Chromium-binding Substance (LMWCr) and the Transfer of Chromium from Transferrin and $Cr(pic)_3$ to LMWCr. *J. Biol. Inorg. Chem.* **2000**, *5*, 129-136.

71. Kramida, A., Ralchenko, Y., Reader, J. Atomic Spectra Database. In *NIST Atomic Spectra Database (ver. 5.2)*; NIST ASD Team, Ed.; NIST: National Institute of Standards and Technology, Gaithersburg MD, 20899, (accessed May 17, 2016), 2015.

72. Schaller-Duke, R. M.; Bogala, M. R.; Cassady, C. J. Collision-Induced Dissociation and Electron Transfer Dissocation of Metal Adducted Oligosaccharides. *J. Am. Soc Mass Spectrom*. **2018**, in press.

73. Lide, D. R., Ed.; In *CRC Handbook of Chemistry and Physics;* CRC Press: Cleveland, OH, 1992-1993.

74. Lavanant, H.; Virelizier, H.; Hoppilliard, Y. Reduction of Copper(II) Complexes by Electron Capture in an Electrospray Ionization Source. *J. Am. Soc. Mass Spectrom.* **1998**, *9*, 1217-1221.

75. Amorello, D.; Romano, V.; Zingales, R. The Formal Redox Potential of the Yb(III, II) Couple at 0 Degrees C in 3.22 Molal NaCl Medium. *Ann. Chim.* **2004**, *94*, 113-121.

76. Laitinen, H.; Taebel, W. Europium and Ytterbium in Rare Earth Mixtures: Polarographic Determination. *Ind. Eng. Chem. Anal. Ed.* **1941**, *13*, 825-829.

77. Walters, G. C.; Pearce, D. The Potential of the $Yb^{+++}$ -$Yb^{++}$ Electrode. *J. Am. Chem. Soc.* **1940**, *62*, 3330-3332.

78. Tsybin, Y. O.; Håkansson, P.; Budnik, B. A.; Haselmann, K. F.; Kjeldsen, F.; Gorschkov, M.; Zubarev, R. A. Improved Low-energy Electron Injection Systems for High Rate Electron Capture Dissociation in Fourier Transform Ion Cyclotron Resonance Mass Spectrometry. *Rapid Commun. Mass Spectrom.* **2001**, *15*, 1849-1854.

79. Kaplan, D., Brekenfeld, A., Hartmer, R., Ledertheil, T., Gebhardt, C., Schubert, M. Technical Note #24 Extending the Capacity in Modern Spherical High Capacity Ion Traps (HCT). In *Bruker Daltonics Technical Notes* Bruker Daltonics: (accessed February 19, 2016).

80. Suckau, D.; Shi, Y.; Beu, S. C.; Senko, M. W.; Quinn, J. P.; Wampler, F. M.; McLafferty, F. W. Coexisting Stable Conformations of Gaseous Protein Ions. *Proc. Natl. Acad. Sci. USA* **1993**, *90*, 790-793.

81. Loo, J. A.; Edmonds, C. G.; Udseth, H. R.; Smith, R. D. Effect of Reducing Disulfide-Containing Proteins on Electrospray Ionization Mass Spectra. *Anal. Chem.* **1990**, *62*, 693-698.

82. Chowdhury, S. K.; Katta, V.; Chait, B. T. Probing Conformation Changes in Proteins by Mass Spectrometry. *J. Am. Chem. Soc.* **1990**, *112*, 9012-9013.

83. Guevremont, R.; Siu, K. W. M.; Le Blanc, J. C. Y.; Berman, S. S. Are the Electrospray Mass Spectra of Proteins Related to Their Aqueous Solution Chemistry? *J. Am. Soc. Mass Spectrom.* **1992**, *3*, 216-224.

84. Zhurov, K. O.; Fornelli, L.; Wodrich, M. D.; Laskay, U. A.; Tsybin, Y. O. Principles of Electron Capture and Transfer Dissociation Mass Spectrometry Applied to Peptide and Protein Structure Analysis. *Chem. Soc. Rev.* **2013**, *42*, 5014-5030.

85. Savitski, M. M.; Kjeldsen, F.; Nielsen, M. L.; Zubarev, R. A. Hydrogen Rearrangement to and from Radical z Fragments in Electron Capture Dissociation of Peptides. *J. Am. Soc. Mass Spectrom.* **2007**, *18*, 113-120.

86. Commodore, J. J.; Cassady, C. J. Effects of Acidic Peptide Size and Sequence on Trivalent Praseodymium Adduction and Electron Transfer Dissociation Mass Spectrometry. *J. Mass Spectrom.* **2017**, *52*, 218-229.

87. Oh, H.; Breuker, K.; Sze, S. K.; Ge, Y.; Carpenter, B. K.; McLafferty, F. W. Secondary and Tertiary Structures of Gaseous Protein Ions Characterized by Electron Capture Dissociation Mass Spectrometry and Photofragment Spectroscopy. *Proc. Natl. Acad. Sci. USA* **2002**, *99*, 15863-15868.

88. Lee, S. W.; Kim, H. S.; Beauchamp, J. L. Salt Bridge Chemistry Applied to Gas-phase Peptide Sequencing: Selective Fragmentation of Sodiated Gas-Phase Peptide Ions Adjacent to Aspartic Acid Residues. *J. Am. Chem. Soc.* **1998**, *120*, 3188-3195.

# CHAPTER 4: EFFECTS OF ACIDIC PEPTIDE SIZE AND SEQUENCE ON TRIVALENT PRASEODYMIUM ADDUCTION AND ELECTRON TRANSFER DISSOCIATION MASS SPECTROMETRY

## 4.1 Overview

Using the lanthanide praseodymium, $Pr^{3+}$, metallated ion formation by electrospray ionization (ESI) and electron transfer dissociation (ETD) were studied for 25 biological and model acidic peptides. For chain lengths of seven or more residues, even highly acidic peptides that can be difficult to protonate by ESI form metallated ions and undergo abundant ETD fragmentation. Peptides with predominantly acidic residues form only the deprotonated ion, $[M + Pr – H]^{2+}$, which yields near complete ETD sequence coverage for larger peptides. Peptides that generate $[M + Pr]^{3+}$ cleaves between every residue. Acidic peptides that contain at least one residue with a basic side chain also produce the protonated ion, $[M + Pr + H]^{4+}$; this ion undergoes the most extensive sequence coverage by ETD. Primarily metallated and non-metallated c- and z-ions form for all peptides investigated. Metal-adducted product ions are only present when at least half of the peptide sequence can be incorporated into the ion; this suggests that the metal ion simultaneously attaches to more than one acidic site. The only site consistently lacking dissociation is at the N-terminal side of a proline residue. Increasing peptide chain length generates more backbone cleavage for metal-peptide complexes with the same charge state. For acidic peptides with the same length, increasing the precursor ion charge state from 2+ to 3+ also leads to more cleavage. The results of this study indicate that highly acidic peptides can be sequenced by ETD of complexes formed with $Pr^{3+}$.

## 4.2 Introduction

Electron transfer dissociation (ETD) and electron capture dissociation (ECD) are important tandem mass spectrometry (MS/MS) techniques for the analysis of peptides and proteins.[1-5] These processes result in cleavage along the peptide backbone that is usually more uniform than collision-induced dissociation (CID)[6,7] and infrared multi-photon dissociation (IRMPD),[8] which favor lower energy pathways. In addition, post-translational modifications such as phosphorylation are preserved during ETD and ECD.[9-14] In both processes, an electron is added to a multiply charged cation creating a charge reduced radical species that undergoes a non-ergodic process to form c- and z-ions by N-Cα bond cleavage along the peptide backbone.[1-5,15-17] A major drawback to both methods, however, is that they generally require multiply positively charged precursor ions.[1,4,18-21] Upon electron capture, an ion with a single positive charge would be reduced to a neutral molecule that cannot be analyzed by mass spectrometry.[22] Formation of multiply charged ions is also advantageous because MS/MS fragmentation efficiency and sequence information often increase with increasing precursor ion charge state.[2,21,23-28] In addition, higher charges on peptides and proteins generally require less energy to initiate fragmentation.[23-26] Multiple charging can shift the mass-to-charge ratios (*m/z*) of the ions to a range of the spectrum with optimal resolution[29] and can increase signal intensity in mass spectrometers that use image current detection.[30,31] However, certain peptides, such as acidic peptides, may not form doubly or even singly positively charged ions by electrospray ionization (ESI) or matrix-assisted laser desorption/ionization (MALDI),[32-35] making analysis by ECD or ETD challenging. While deprotonated peptides (i.e., negative ions) can be analyzed by dissociation techniques such as electron detachment (EDD),[36] electron-induced (EID),[37] and negative electron transfer dissociation (NETD),[38] these processes generally suffer from low

product ion intensities that are most notable when an electron interacts with a peptide anion (i.e., EDD and EID).

Peptides containing acidic amino acid residues are important in many biological processes. For example, acidic peptides are involved in bone growth,[39-42] stimulation of hormone releasing factor secretion,[43] blood coagulation[44,45] and the circulatory system,[46] development of the brain,[47] carbohydrate metabolism,[48-50] and differentiation of cells involved in immune response.[51,52] Potential vaccines for malaria[53] and HIV[54-56] have utilized acidic peptides.

One method of ionizing peptides that do not readily protonate is to form positively charged ions by addition of a metal ion. Sequence information from the resulting metallated peptide cations has been obtained in studies employing ECD[57-68] and ETD.[69-72] Flick and Williams[68] demonstrated the ability of trivalent lanthanide metal ions to produce multiply positively charged ions with peptides. During a recent ETD study discussed in Chapter 3 involving the addition of trivalent lanthanide metal cations to acidic peptides,[72] the Cassady group also noted that multiply charged metallated ions form by ESI even in the absence of a highly basic arginine amino acid residue (gas-phase basicity of arginine = 1006.6 kJ/mol[73]). In the work in Chapter 3, metal-peptide complexes form with as much as a 4+ charge, $[M + Pr + H]^{4+}$, simultaneously incorporating a trivalent metal cation and an extra hydrogen. Extensive peptide backbone cleavage and sequence information were obtained from ETD of these 4+ ions. However, the initial study discussed in Chapter 3 focused primarily on one peptide and its analogs, so limited observations were made regarding effects of peptide size and sequence on ETD of these metallated peptide complexes.

Structural parameters including amino acid composition and chain length have been shown to affect electron-based dissociation of protonated peptides and metal-adducted peptide

complexes.[62,69,74-76] In an ECD study involving model peptides containing two arginine residues, Chan and coworkers[74] found that $[M + 2H]^{2+}$ produced less backbone cleavage for peptides with increasing numbers of glutamic acid and asparagine residues. These researchers also noted that while a greater number of glutamic acid residues led to suppressed cleavage for $[M + 2H]^{2+}$, $[M + 3H]^{3+}$ underwent more dissociation and provided more sequence coverage. In two separate studies,[62,75] Chan and coworkers noted that increasing peptide chain length suppressed backbone cleavage for ECD of $[M + 2H]^{2+}$ and $[M + Cu]^{2+}$. In contrast, ECD of $[M + 3H]^{3+}$ and $[M + Cu + H]^{3+}$ produced abundant backbone cleavage for the same peptides. Vachet and Dong[69] investigated Cu(II)-peptide complexes and determined that an increase in the number of copper binding motifs such as histidine, aspartic acid, glutamic acid and methionine promoted cleavage by ETD. Wysocki, Coon, and coworkers[76] performed ETD on thousands of multiply protonated peptides; they observed that the intensities of the c-series changed as the lysine, arginine, and glutamic acid residues were positioned further away from the C-terminus. These researchers also noted that the effect of the position of the basic or acidic amino acid residue on ETD becomes less significant with a more highly charged precursor ion.

The current study explores the effects of chain length, as well as amino acid position and composition, on ETD of lanthanide metal-adducted acidic peptide ions without highly basic amino acid residues. Both biological and model peptides were employed. In our previous study discussed in Chapter 3,[72] the entire lanthanide series (except radioactive promethium) was investigated. Praseodymium, $Pr^{3+}$, was found to give high quality and reproducible ETD spectra that are not complicated by the presence of multiple metal isotopes. Thus, $Pr^{3+}$ was selected to represent the lanthanide series in the present work.

## 4.3 Experimental

### 4.3.1 Mass spectrometry

All experiments were performed on a Bruker (Billerica, MA, USA) HCTultra PTM Discovery System high capacity quadrupole ion trap (QIT) mass spectrometer, which was discussed in Chapter 2. At the ESI source, the needle was held at ground. The capillary entrance, the stainless steel endplate, and the capillary entrance cap, shown in Figure 2.2, were set at a high voltage of -3.5 kV. Nitrogen drying gas was heated to 260°C and flowed at 5-10 L/min. Nitrogen was also the nebulizer gas, and the pressure was optimized between 5 and 10 psi. All spectra shown are the result of signal averaging 200 scans. Mixtures of metal salt and acidic peptide in a 10:1 $Pr^{3+}$:peptide molar ratio were infused into the ESI source at a flow rate of 3 µL/min using a KD scientific (Holliston, MA, USA) syringe pump. Final peptide concentrations were 5 µM in acetonitrile:water at a 50:50 volume ratio.

The reagent anion for ETD experiments, fluoranthene, was generated in a negative chemical ionization source (nCI) with methane serving as the nCI reagent gas. The reagent anion was accumulated for 8-12 ms. The ion charge control (ICC) value was 300, 000-400, 000 to maximize electron transfer. The lower end *m/z* cutoff was set to 120 with anion/cation reaction times in the range of 180-250 ms. The "smart decomposition" function was enabled to facilitate further dissociation of any charge reduced (ETnoD) ions. Smart decomposition uses very low energy CID (resonant excitation) to overcome attractive forces (e.g., hydrogen or noncovalent bonding) that may hold peptide fragments together after the electron transfer process. Smart decomposition enhances observed ETD product ion formation. Section 2.4.2 provides a more detailed explanation of smart decomposition.[72]

In positive mode low-energy CID experiments, the optimum number of ions (approximately 200 000) were accumulated in the ion trap for up to 200 ms. Precursor ions were mass selected using ejection pulses. Isolation widths were typically set 4 *m/z* wide for maximum intensity but occasionally lowered to 1 *m/z* to remove interfering peaks. Helium served as the collision gas. Collision sweep energies of 30 to 200% and amplitude of 0.8 to 1.2 V were utilized.

### 4.3.2 Peptides

The acidic peptides were purchased from various vendors. Gastrin 1(1-14), hirudin(54-65) (desulfated), and adrenocorticotrophic hormone (ACTH(22-39)) were obtained from Bachem Americas (Torrance, CA, USA); human epidermal growth factor receptor peptide ((EGF)985-996) from Alfa Aesar (Ward Hill, MA, USA); casein kinase II peptide substrate from Sigma-Aldrich (St. Louis, MO, USA); and low molecular weight chromium binding (LMWCr) peptide from Gen Script (Piscataway, NJ, USA). Model peptides were synthesized in our laboratory with an Advanced ChemTech Model 90 peptide synthesizer (Louisville, KY, USA) using standard Fmoc protocol.[77] Praseodymium(III) nitrate salt was purchased from Alfa Aesar. A Barnstead (Dubuque, IA, USA) E-pure system was used to produce ultrapure Milli-Q 18 MΩ water.

## 4.4 Results and discussion

The established peptide cleavage nomenclature of Roepstorff and Fohlman[78] as modified by Biemann[79] is used in labeling of spectra to help identify the number of hydrogens incorporated into product ions formed by ETD and CID. A prime symbol to the right indicates addition of hydrogen (i.e., $z_n^{/} = [z_n + H]^+$) and to the left indicates loss of hydrogen (i.e., ${}^{//}z_n = [z_n - 2H]^+$). In the figures, the following colors are used to label the ions: non-metallated

z-ions = red, non-metallated c-ions = blue, non-metallated a-ions = orange, non-metallated b-ions = olive green, non-metallated y-ions = burgundy, metal-adducted z-ions = bright pink, metal-adducted c-ions = green, metal-adducted b-ions = blue-green, and metal-adducted y-ions = brown. Undissociate is labeled in purple with a large purple diamond arrow head. Neutral loss products and electron transfer without dissociation (ETnoD) ions are labeled in black. ECD[1,2,5,15,17] and ETD[4,16] typically yield c- and z-ions that correspond to N-Cα peptide bond cleavage.

### 4.4.1 Biological peptides

Several biological acidic peptides were employed to investigate the effects of size and sequence on $Pr^{3+}$ cationization by ESI and on ETD product ion formation. The peptides and their sequences are shown in Table 4.1, along with their metallated ions formed by ESI. They contain a variety of amino acid residues with chain lengths ranging from seven to eighteen residues.

As the data in Table 4.1 indicates, two of the biological peptides, hirudin(54-65) and EGF(985-996) produced all three metallated ions by ESI: $[M + Pr - H]^{2+}$, $[M + Pr]^{3+}$, and $[M + Pr + H]^{4+}$. These ions were also observed in our prior work with fibrinopeptide B discussed in Chapter 3.[72] The most acidic species studied, LMWCr peptide, generates no 3+ and 4+ ions but only $[M + Pr - H]^{2+}$. The facile deprotonation is consistent with the fact that six of the residues of this heptapeptide are acidic. In contrast, casein kinase II substrate and ACTH(22-39) do not produce the deprotonated ion, but only the 3+ and 4+ ions, with $[M + Pr + H]^{4+}$ occurring in greatest abundance for both peptides. Although casein kinase II substrate contains seven aspartic acid residues and an acidic C-terminus, there are three highly basic arginine residues at its N-terminus that can accept a proton. Hirudin(54-65),

Table 4.1. ESI ion formation and corresponding ETD product ions for acidic biological peptides cationized by $Pr^{3+}$.

| Peptide name | Number of residues | Number of acidic residues[a] | Sequence[b] | Metallated ion formed by ESI | $c_n$-ions | $z_n$- ions |
|---|---|---|---|---|---|---|
| **Low molecular weight chromium binding (LMWCr) peptide** | 7 | 6 | **E$^1$E$^2$E$^3$E$^4$**G**D$^6$D$^7$** | $[M + Pr - H]^{2+}$ | $[^{/}c_n + Pr]^+$, n = 4-6 | $[^{/}z_n + Pr]^+$, n = 5-6 |
| **Casein kinase II peptide substrate** | 12 | 7 | RRRA**D$^5$D$^6$**S**D$^8$D$^9$D$^{10}$D$^{11}$D$^{12}$** | $[M + Pr]^{3+}$ | $c_n^{//+}$, n = 2<br>$[c_n + Pr]^+$, n = 10, 11<br>$[c_n + Pr]^{2+}$, n = 10, 11 | -[c] |
| | | | | $[M + Pr + H]^{4+}$ | $c_n^{//+}$, n = 2-9<br>$[c_n + Pr]^+$, n = 9-11<br>$[c_n + Pr]^{2+}$, n = 9, 10 | - |
| **Human epidermal growth factor receptor peptide (985-996), EGF(985-996)** | 12 | 5 | **D$^1$**VV**D$^4$**A**D$^6$E$^7$**YLIP**Q$^{12}$** | $[M + Pr - H]^{2+}$ | $[^{/}c_n + Pr]^+$, n = 7-9, 11 | $[^{/}z_n + Pr]^+$, n = 7-11 |
| | | | | $[M + Pr]^{3+}$ | $c_n^{//+}$, n = 2-7<br>$[^{/}c_n + Pr]^+$, n = 8-9, 11 | $z_n^{/+}$, n = 3-5<br>$[^{/}z_n + Pr]^+$, n = 11<br>$[^{/}z_n + Pr]^{2+}$, n = 6-11 |
| | | | | $[M + Pr + H]^{4+}$ | $c_n^{//+}$, n = 2-6<br>$[^{/}c_n + Pr]^+$, n = 6-9, 11<br>$[^{/}c_n + Pr]^{2+}$, n = 9 | $z_n^{/+}$, n = 1, 3-5<br>$[^{/}z_n + Pr]^+$, n = 6-11<br>$[^{/}z_n + Pr]^{2+}$, n = 11 |
| **Hirudin(54-65)** | 12 | 6 | G**D$^2$F**E$^4$E$^5$**IP**E$^8$E$^9$**YL**Q$^{12}$** | $[M + Pr - H]^{2+}$ | $[^{/}c_n + Pr]^+$, n = 7-11 | $[^{/}z_n{}^{+} Pr]^+$, n = 7-11 |
| | | | | $[M + Pr]^{3+}$ | $c_n^{//+}$, n = 3,4<br>$[^{/}c_n + Pr]^+$, n = 7-11<br>$[^{/}c_n + Pr]^{2+}$, n = 11 | $z_n^{/+}$, n = 2-5 |

Table 4.1, continued.

| Peptide name | Number of residues | Number of acidic residues[a] | Sequence[b] | Metallated ion formed by ESI | $c_n$-ions | $z_n$- ions |
|---|---|---|---|---|---|---|
| | | | | | | $[^{/}z_n + Pr]^+$, n = 7-11 |
| | | | | $[M + Pr + H]^{4+}$ | $c_n^{//+}$, n = 2-5<br>$[^{/}c_n + Pr]^+$, n = 7-11 | $z_n^{/+}$, n = 2-5<br>$[^{/}z_n + Pr]^+$, n = 7-11 |
| **Human gastrin I (1-14)** | 14 | 6 | pEGPWL**E**$^{6}$**E**$^{7}$**E**$^{8}$**E**$^{9}$**E**$^{10}$AYG**W**$^{14}$ | $[M + Pr - H]^{2+}$ | $[^{/}c_n + Pr]^+$, n = 8-13 | $[^{/}z_n + Pr]^+$, n = 8-11, 13 |
| | | | | $[M + Pr]^{3+}$ | $c_n^{//+}$, n = 4-6<br>$[^{/}c_n + Pr]^+$, n = 8-13<br>$[^{/}c_n + Pr]^{2+}$, n = 11-13 | $z_n^{/+}$, n = 1-6<br>$[^{/}z_n + Pr]^+$, n = 7-11, 13 |
| **Adrenocorticotropic hormone, ACTH (22-39)** | 18 | 6 | VYPNGA**E**$^{7}$**D**$^{8}$**E**$^{9}$SA**E**$^{12}$AFPL**E**$^{17}$**F**$^{18}$ | $[M + Pr]^{3+}$ | $c_n^{//+}$, n = 3-11<br>$[^{/}c_n + Pr]^+$, n = 9, 12, 13, 15-17<br>$[^{/}c_n + Pr]^{2+}$, n = 15-17 | $[^{/}z_n + Pr]^+$, n = 9-15, 17 |
| | | | | $[M + Pr + H]^{4+}$ | $c_n^{//+}$, n = 3-11<br>$[^{/}c_n + Pr]^+$, n = 9-13, 15-17<br>$[^{/}c_n + Pr]^{2+}$, n = 9, 15, 16 | $z_n^{/+}$, n = 2, 3, 5-8<br>$[^{/}z_n + Pr]^+$, n = 9-15, 17 |

[a] Acidic residues refers to the number of aspartic acid (D), glutamic acid (E), and C-terminal residues in the peptide sequence. If an aspartic acid or glutamic acid residue is located on the C-terminus, then it is counted as only one acidic residue.

[b] Bold font is used to indicate acidic residues. A number immediately following an acidic residue indicates its position in the peptide sequence.

[c] - means that no ions were observed.

EGF(985-996), and ACTH(22-39) are still able to form $[M + Pr + H]^{4+}$ in the absence of a highly basic arginine, lysine, or histidine residue. This may be attributed to the fact that these peptides contain proline (gas-phase basicity of proline = 886.0 kJ/mol[73,80]) that is the fifth most basic amino acid[81] and can sometimes accept a proton.[82]

The most extensive sequence coverage is obtained for ETD of $[M + Pr + H]^{4+}$. Figure 4.1 shows ETD spectra of $[M + Pr + H]^{4+}$ for EGF(985-996), hirudin(54-65), and casein kinase II substrate, while Figure 4.2 gives the spectrum from ACTH(22-39). Efficient fragmentation with a high signal-to-noise ratio (S/N) allows for easy identification of product ions. A mixture of complementary non-metallated and metallated c- and z-ions form, except for casein kinase II substrate that yields only c-ions, as seen in Figure 4.1(c). Most ions are singly charged although there are a few doubly charged ions. The c-series are $c_n^{//+}$ and $[^{/}c_n + Pr]^+$, while the z-series are $z_n^{/+}$ and $[^{/}z_n + Pr]^+$. All non-metallated c-ions have two extra hydrogens, while non-metallated z-ions contain one. Metallated c- and z-ions lose one hydrogen relative to the direct backbone cleavage product ion. For some peptides, both metallated and non-metallated ions can form at the same cleavage site. For example, in Figure 4.1(a), product ions with and without $Pr^{3+}$ form between $D^6$ and $E^7$ for EGF(985-996). Cleavage occurs at almost every residue for the 4+ ions, except between $R^1$ and $R^2$ for casein kinase II substrate and except N-terminal to proline residues for hirudin(54-65), EGF(985-996), and ACTH(22-39). The side chain of proline forms a ring that incorporates the backbone, which prevents dissociation of the peptide into two pieces following cleavage of the N-Cα bond. Lack of cleavage N-terminal to proline has previously been observed in ECD and ETD studies of protonated peptides.[76,83-85]

For all the biological peptides, ETD on $[M + Pr]^{3+}$ yields a mix of metallated and non-metallated c- and z-ions. Most are singly charged, but some doubly charged ETD product ions

form as well. The c- and z-series are the same as those observed for $[M + Pr + H]^{4+}$. Figure 4.3. shows the ETD spectra of $[M + Pr]^{3+}$ for EGF(985-996), hirudin(54-65), and gastrin I(1-14), while the spectra for ACTH(22-39) and casein kinase II substrate appear in Figures 4.4 and 4.5, respectively. For 3+ ions from five of the biological peptides, cleavage occurs at every residue (except N-terminal to proline) and the peptides can be sequenced. Interestingly, ETD of $[M + Pr]^{3+}$ for casein kinase produces cleavages at only three sites (see Figure 4.5.), although $[M + Pr+ H]^{4+}$ shown in Figure 4.1(c) cleaves at almost every residue. This may indicate that the three highly basic N-terminal arginine residues are sequestering the metal ion.

The least amount of sequence informative fragmentation is obtained from $[M + Pr – H]^{2+}$. As shown in Figure 4.6., only metal-adducted c- and z-ions form. All product ions are singly charged and lack a hydrogen, which can be explained by the fact that the precursor ion is already deprotonated. The previous study with fibrinopeptide B discussed in Chapter 3 found similar decreased product ion formation for ETD of $[M + Pr – H]^{2+}$ compared to $[M + Pr]^{3+}$ and $[M + Pr + H]^{4+}$.[72] Cleavage between $E^3$ and $E^4$ is missing from LMWCr peptide and between $E^7$ and $E^8$ for human gastrin I(1-14). A similar lack of cleavage between adjacent glutamic acid residues was observed in the lower charged state ion (2+) in an ECD study involving trivalent lanthanide ions[68] and in our fibrinopeptide B study.[72] This effect appears to be most pronounced for central residues in a series of acidic residues and may relate to the metal ion bridging between two or more acidic sites.

The types of amino acid residues present in a peptide sequence can affect the ions formed by ETD. While casein kinase II substrate has a twelve residue sequence like EGF(985-996) and hirudin(54-65), the presence of the three highly basic arginine residues at its N-terminus leads to the formation of only c-ions by ETD for $[M + Pr]^{3+}$ and $[M + Pr + H]^{4+}$. This is interesting

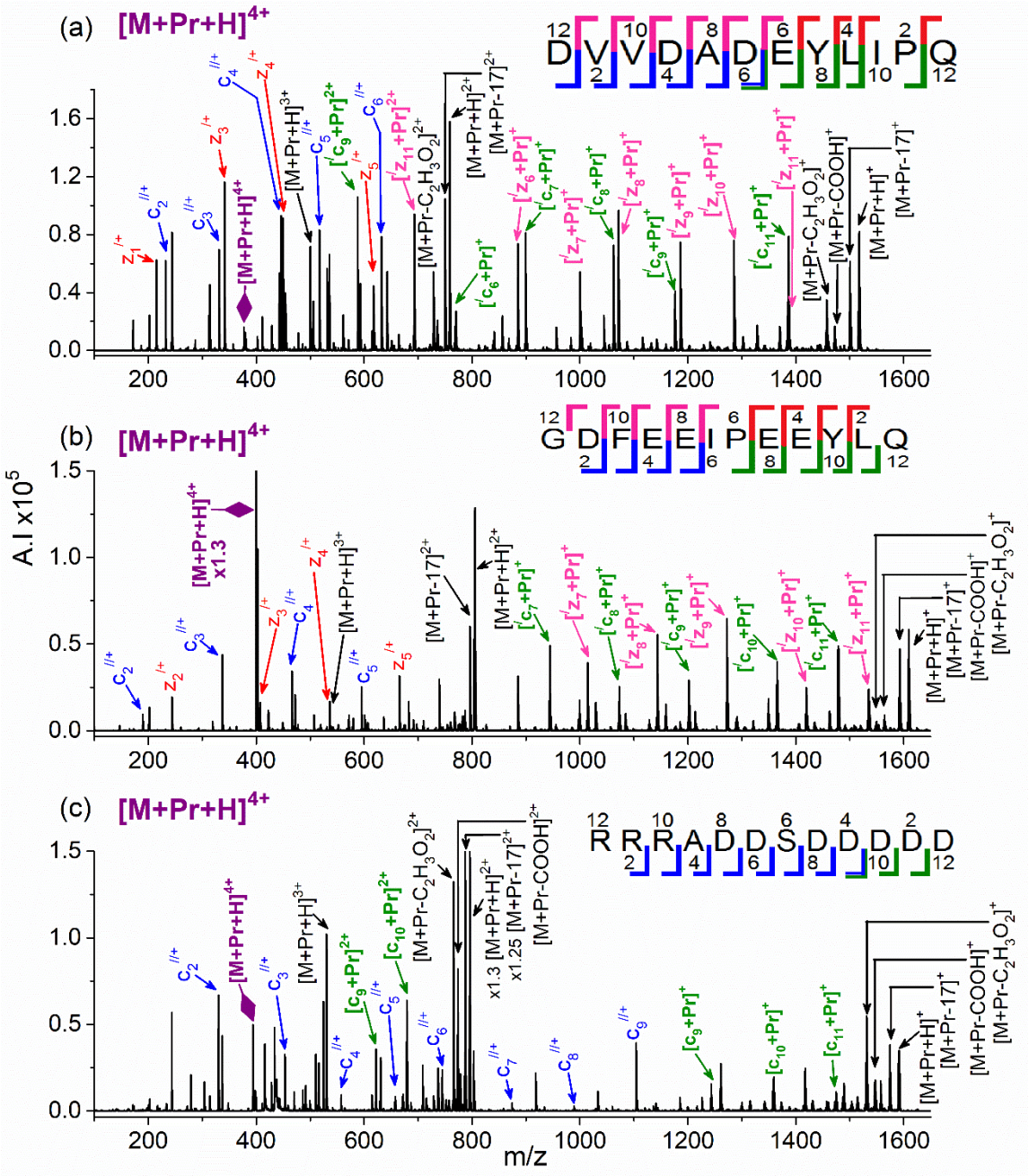


Figure 4.1. ETD mass spectra of $[M + Pr + H]^{4+}$ for (a) EGF(985-996), (b) hirudin(54-65), and (c) casein kinase II substrate. In the figures, the following colors are used to label the ions: non-metallated z-ions = red, non-metallated c-ions = blue, metal-adducted z-ions = bright pink, and metal-adducted c-ions = green. Undissociated precursor ion is labeled in purple with a large purple diamond arrow head. Neutral loss products and electron transfer without dissociation (ETnoD) ions are labeled in black. A prime symbol to the left indicates loss of a hydrogen (i.e., $^{/}c_n = [c_n - H]^+$) and to the right indicates the addition of a hydrogen at the cleavage site (i.e., $cn^{//} = [c_n + 2H]^+$).

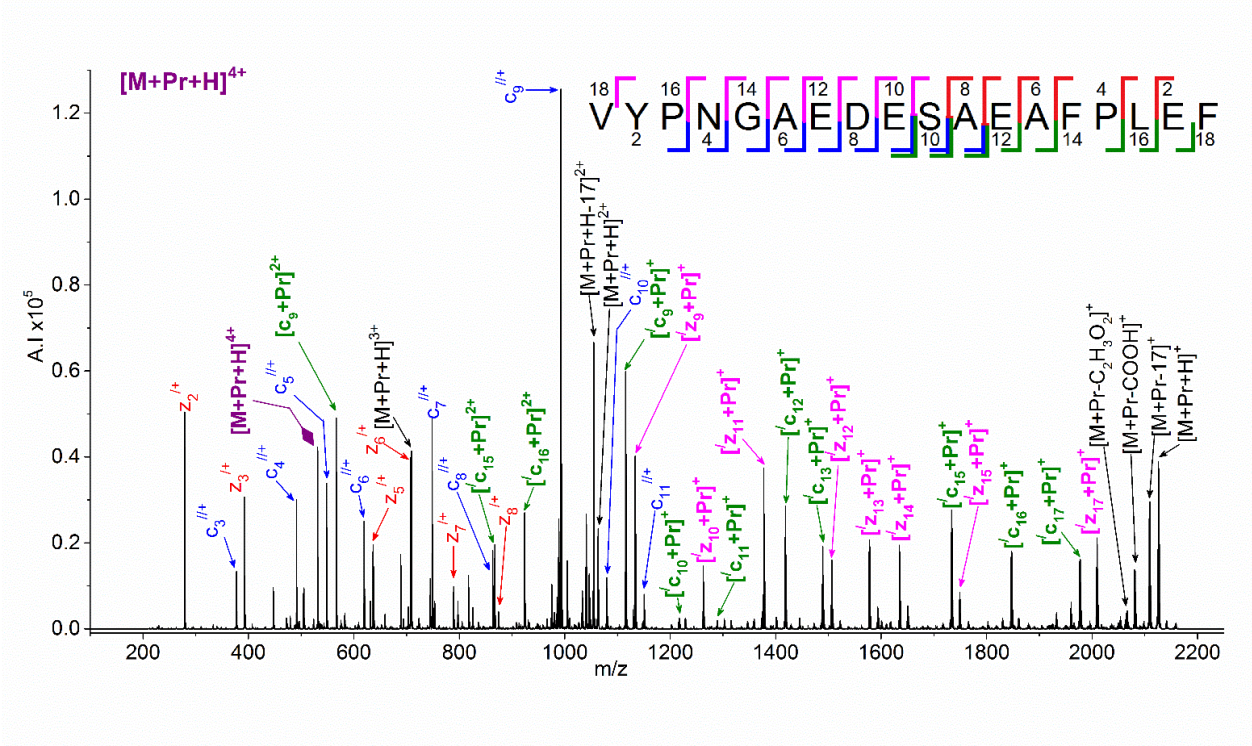


Figure 4.2. ETD mass spectrum of $[M + Pr + H]^{4+}$ for ACTH(22-39). In the figure, the following colors are used to label the ions: non-metallated z-ions = red, non-metallated c-ions = blue, metal-adducted z-ions = bright pink, and metal-adducted c-ions = green. Undissociated precursor ion is labeled in purple with a large purple diamond arrow head. Neutral loss products and electron transfer without dissociation (ETnoD) ions are labeled in black. A prime symbol to the left indicates loss of a hydrogen (i.e., $^{/}c_n = [c_n - H]^+$) and to the right indicates the addition of a hydrogen at the cleavage site (i.e., $c_n^{//} = [c_n + 2H]^+$). The spectrum has no expansion of the intensity axis; all peaks are shown to scale.

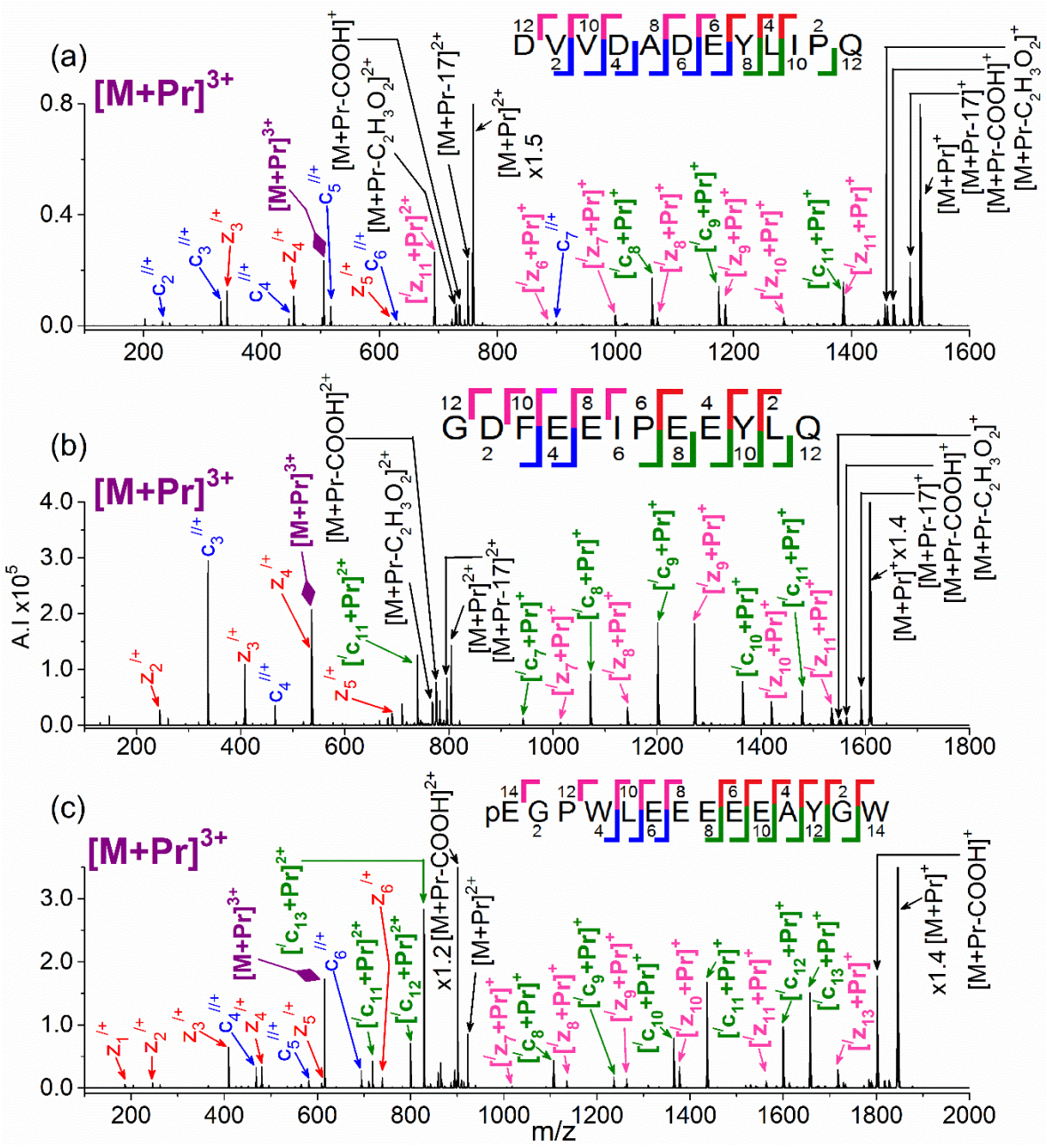


Figure 4.3. ETD mass spectra of $[M + Pr]^{3+}$ for (a) EGF(985-996), (b) hirudin(54-65), and (c) gastrin I(1-14). In the figures, the following colors are used to label the ions: non-metallated z-ions = red, non-metallated c-ions = blue, metal-adducted z-ions = bright pink, and metal-adducted c-ions = green. Undissociated precursor ion is labeled in purple with a large purple diamond arrow head. Neutral loss products and electron transfer without dissociation (ETnoD) ions are labeled in black. A prime symbol to the left indicates loss of a hydrogen (i.e., $^{/}c_n = [c_n - H]^+$) and to the right indicates the addition of a hydrogen at the cleavage site (i.e., $c_n^{//} = [c_n + 2H]^+$).

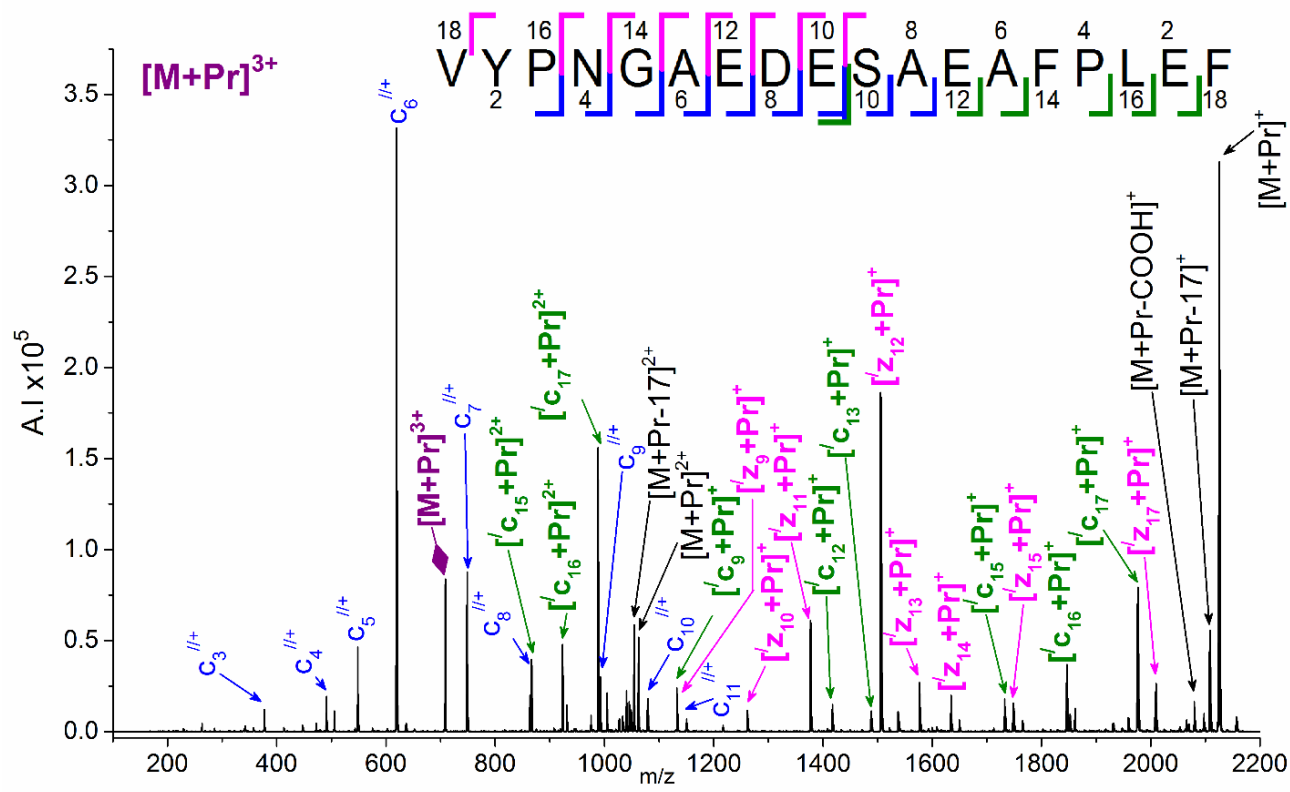


Figure 4.4. ETD mass spectrum of $[M + Pr]^{3+}$ for ACTH(22-39). In the figure, the following colors are used to label the ions: non-metallated z-ions = red, non-metallated c-ions = blue, metal-adducted z-ions = bright pink, and metal-adducted c-ions = green. Undissociated precursor ion is labeled in purple with a large purple diamond arrow head. Neutral loss products and electron transfer without dissociation (ETnoD) ions are labeled in black. A prime symbol to the left indicates loss of a hydrogen (i.e., $^{/}c_n = [c_n - H]^+$) and to the right indicates the addition of a hydrogen at the cleavage site (i.e., $c_n^{//} = [c_n + 2H]^+$). The spectrum has no expansion of the intensity axis; all peaks are shown to scale.

because the one highly basic arginine residue located at the C-terminus in fibrinopeptide B did not lead to its formation of only C-terminal product ions.[72] Instead, for fibrinopeptide B, members of both the c- and the z-series form for ETD of $[M + Pr - H]^{2+}$, $[M + Pr]^{3+}$, and $[M + Pr + H]^{4+}$ (refer to Chapter 3).

The ETD spectra of $[M + Pr + H]^{4+}$, $[M + Pr]^{3+}$, and $[M + Pr - H]^{2+}$ are much more sequence informative than CID spectra of these ions. Example CID spectra for fibrinopeptide B are shown in Figures 4.7 and 4.8. Typically, b- and y- ions form by CID, but the spectra contain more neutral losses that complicate interpretation. The CID spectra also generally have lower product ion intensities and S/N ratios.

### 4.4.2 Model peptides

Several model peptides were employed to investigate the effects of peptide structural features on ETD of acidic peptides adducted with $Pr^{3+}$. Factors under consideration include chain length, type and number of acidic amino acid residues, and the location of acidic residues. The heptapeptides investigated were XAAAAAA, AAAXAAA, AAAAAAX, XAAXAAX, and XXXXXXX (X7), where A is alanine and X is aspartic acid (D) or glutamic acid (E) residues. In addition, EEEEEE (E6), EEEEEEEE (E8), and DDDDDDDDDD (D10) were studied. For the model peptides, metallated precursor ion production by ESI and ETD product ion information is given in Table 4.2.

Six of the heptapeptides (DAAAAAA, EAAAAAA, AAADAAA, AAAEAAA, DAADAAD, and EAAEAAE) produce predominantly $[M + Pr]^{3+}$ by ESI. In addition, $[M + Pr - H]^{2+}$ forms in low abundances but could not be isolated for further analysis by ETD. The other peptides yield predominantly $[M + Pr - H]^{2+}$. The formation of only $[M + Pr - H]^{2+}$ for peptides E6, D7, E7, E8, and D10 can be attributed to the fact that the

Table 4.2. ESI ion and corresponding ETD product ions for acidic model peptides cationized by $Pr^{3+}$.

| **Peptide sequence**[a] | **Number of residues** | **Number of acidic residues**[b] | **Metallated ion formed by ESI** | **$c_n$-ions** | **$z_n$-ions** | **$y_n$-ions** |
|---|---|---|---|---|---|---|
| **D**[1]AAAAAA**A**[7] | 7 | 2 | $[M + Pr]^{3+}$ | $[^{/}c_n + Pr]^{+}$, n = 4-6<br>$[^{/}c_n + Pr]^{2+}$, n = 6 | $z_n^{/+}$, n = 2<br>$[^{/}z_n + Pr]^{+}$, n = 5, 6<br>$[^{/}z_n + Pr]^{+}$, n = 6 | $[y_n + Pr]^{+}$, n = 4-6<br>$[y_n + Pr]^{2+}$, n = 6 |
| **E**[1]AAAAAA**A**[7] | 7 | 2 | $[M + Pr]^{3+}$ | $[^{/}c_n + Pr]^{+}$, n = 4-6<br>$[^{/}c_n + Pr]^{2+}$, n = 5, 6 | $[^{/}z_n + Pr]^{+}$, n = 5, 6<br>$[^{/}z_n + Pr]^{2+}$, n = 6 | $[y_n + Pr]^{+}$, n = 4-6<br>$[y_n + Pr]^{2+}$, n = 6 |
| AAA**D**[4]AA**A**[7] | 7 | 2 | $[M + Pr]^{3+}$ | $[^{/}c_n + Pr]^{+}$, n = 4-6<br>$[^{/}c_n + Pr]^{2+}$, n = 6 | $z_n^{/+}$, n = 2<br>$[^{/}z_n + Pr]^{+}$, n = 4-6 | - |
| AAA**E**[4]AA**A**[7] | 7 | 2 | $[M + Pr]^{3+}$ | $[^{/}c_n + Pr]^{+}$, n = 4-6<br>$[^{/}c_n + Pr]^{2+}$, n = 5, 6 | $z_n^{/+}$, n = 2<br>$[^{/}z_n + Pr]^{+}$, n = 4-6<br>$[^{/}z_n + Pr]^{2+}$, n = 6 | - |
| AAAAAA**D**[7] | 7 | 1 | -[c] | | | |
| AAAAAA**E**[7] | 7 | 1 | $[M + Pr - H]^{2+}$ | - | $[^{/}z_n + Pr]^{+}$, n = 5-6 | - |
| **D**[1]AA**D**[4]AA**D**[7] | 7 | 3 | $[M + Pr]^{3+}$ | $c_n^{//+}$, n = 1-3<br>$[^{/}c_n + Pr]^{+}$, n = 4-6<br>$[^{/}c_n + Pr]^{2+}$, n = 6 | $[^{/}z_n + Pr]^{+}$, n = 5, 6<br>$[^{/}z_n + Pr - CO]^{+}$, n = 4 | - |
| **E**[1]AA**E**[4]AA**E**[7] | 7 | 3 | $[M + Pr]^{3+}$ | $c_n^{//+}$, n = 1-3<br>$[^{/}c_n + Pr]^{+}$, n = 4-6<br>$[^{/}c_n + Pr]^{2+}$, n = 6 | $[^{/}z_n + Pr]^{+}$, n = 4-6 | - |
| **E**[1]**E**[2]**E**[3]**E**[4]**E**[5]**E**[6] (E6) | 6 | 6 | $[M + Pr - H]^{2+}$ | $[^{/}c_n + Pr]^{+}$, n = 4, 5 | $[^{/}z_n + Pr]^{+}$, n = 5 | - |
| **D**[1]**D**[2]**D**[3]**D**[4]**D**[5]**D**[6]**D**[7] (D7) | 7 | 7 | $[M + Pr - H]^{2+}$ | $c_n^{//+}$, n = 6<br>$[^{/}c_n + Pr]^{+}$, n = 5, 6 | $[^{/}z_n + Pr]^{+}$, n = 6<br>$[^{/}z_n + Pr - C_2H_3O_2]+$, n = 6 | - |

Table 4.2, continued.

| Peptide sequence[a] | Number of residues | Number of acidic residues[b] | Metallated ion formed by ESI | $c_n$-ions | $z_n$-ions | $y_n$-ions |
|---|---|---|---|---|---|---|
| **$E^1E^2E^3E^4E^5E^6E^7$** (E7) | 7 | 7 | $[M + Pr - H]^{2+}$ | $[^{/}c_n + Pr]^+$, n = 5, 6 | $[^{/}z_n + Pr]^+$, n = 5, 6 | - |
| **$E^1E^2E^3E^4E^5E^6E^7E^8$** (E8) | 8 | 8 | $[M + Pr - H]^{2+}$ | $[^{/}c_n + Pr]^+$, n = 5-7 | $[^{/}z_n + Pr]^+$, n = 5-7 | - |
| **$D^1D^2D^3D^4D^5D^6D^7D^8D^9D^{10}$** (D10) | 10 | 10 | $[M + Pr - H]^{2+}$ | $[^{/}c_n + Pr]^+$, n = 6-9 | $[^{/}z_n + Pr]^+$, n = 6-9 | - |

[a] Bold font is used to indicate acidic residues. A number immediately following an acidic residue indicates its position in the peptide sequence.
[b] Acidic residues refers to the number of aspartic acid (D), glutamic acid (E), and C-terminal residues in the peptide sequence. If an aspartic acid or glutamic acid residue is located on the C-terminus, then it is counted as only one acidic residue.
[c] - means that no ETD ions were observed.

sequence consists of only acidic side chains that preferentially deprotonate. Likewise, LMWCr peptide is also highly acidic and only forms $[M + Pr - H]^{2+}$. A peptide sequence containing mostly aspartic or glutamic acid residues would undergo abundant deprotonation and generate $[M + Pr - H]^{2+}$ despite the addition of a trivalent metal cation. None of the model peptides produce $[M + Pr + H]^{4+}$, suggesting that the N-terminus as the only basic site is not sufficient to sequester a proton.

The heptapeptide AAAAAAD did not adduct $Pr^{3+}$ despite multiple attempts involving several lots of peptide synthesized in our laboratory. (The peptide did protonate and deprotonate by ESI indicating that it had been correctly synthesized.) In contrast, AAAAAAE metallated readily by ESI to form $[M + Pr - H]^{2+}$. Previous studies suggest the possibility of the lanthanide metal ion simultaneously coordinating to more than one acidic site.[68,72] Since the aspartic or glutamic acid residues are at the C-terminus of these two peptides, their side chain and C-terminal carboxylic acid sites are in close proximity but have different directional orientations.[86] The shorter side chain of the aspartic acid may limit its ability to achieve a conformation that will allow $Pr^{3+}$ to coordinate to both carboxylic acid groups. Glutamic acid, however, has an extra methylene group on the side chain that may allow for greater flexibility in achieving a di-coordinated Pr(III)-AAAAAAE complex.

Several peptides with less than seven amino acid residues were investigated: DDD, EEE, AAAAEE, AAAADD, AAAEAA, and DAAADA. The tripeptides EEE and DDD did not adduct $Pr^{3+}$. The hexapeptides formed predominantly $[M + Pr - H]^{2+}$, but ETD only generates one or two cleavage products, which is not useful for sequencing the peptides. Table 4.3 lists the ions formed by ESI and ETD product ions for these tri- and hexapeptides.

Table 4.3. ESI ion formation and corresponding ETD product ions for model tri- and hexapeptides cationized by $Pr^{3+}$.

| **Peptide sequence**[a] | **Number of residues**[b] | **Number of acidic residues**[a] | **Metallated ion formed by ESI** | **$c_n$-ions** | **$z_n$-ions** |
|---|---|---|---|---|---|
| **DDD** | 3 | 3 | -[c] | | |
| **EEE** | 3 | 3 | - | | |
| AAAA**DD** | 6 | 2 | $[M + Pr - H]^{2+}$ | $[^{/}c_n + Pr]^{+}$, n = 4, 5 | - |
| AAAA**EE** | 6 | 2 | $[M + Pr - H]^{2+}$ | - | $[^{/}z + Pr]^{+}$, n = 5 |
| AAA**E**A**A** | 6 | 2 | $[M + Pr - H]^{2+}$ | $[^{/}c_n + Pr]^{+}$, n = 5 | $[^{/}z + Pr]^{+}$, n = 5 |
| **D**AAA**DA** | 6 | 3 | $[M + Pr - H]^{2+}$ | $[^{/}c_n + Pr]^{+}$, n = 4, 5 | - |

[a] Bold font is used to indicate acidic residues.
[b] Acidic residues refers to the number of aspartic acid (D), glutamic acid (E), and C-terminal residues in the peptide sequence. If an aspartic acid or glutamic acid residue is located on the C-terminus, then it is counted as only one acidic residue.
-[c] – indicates that no ion was observed.

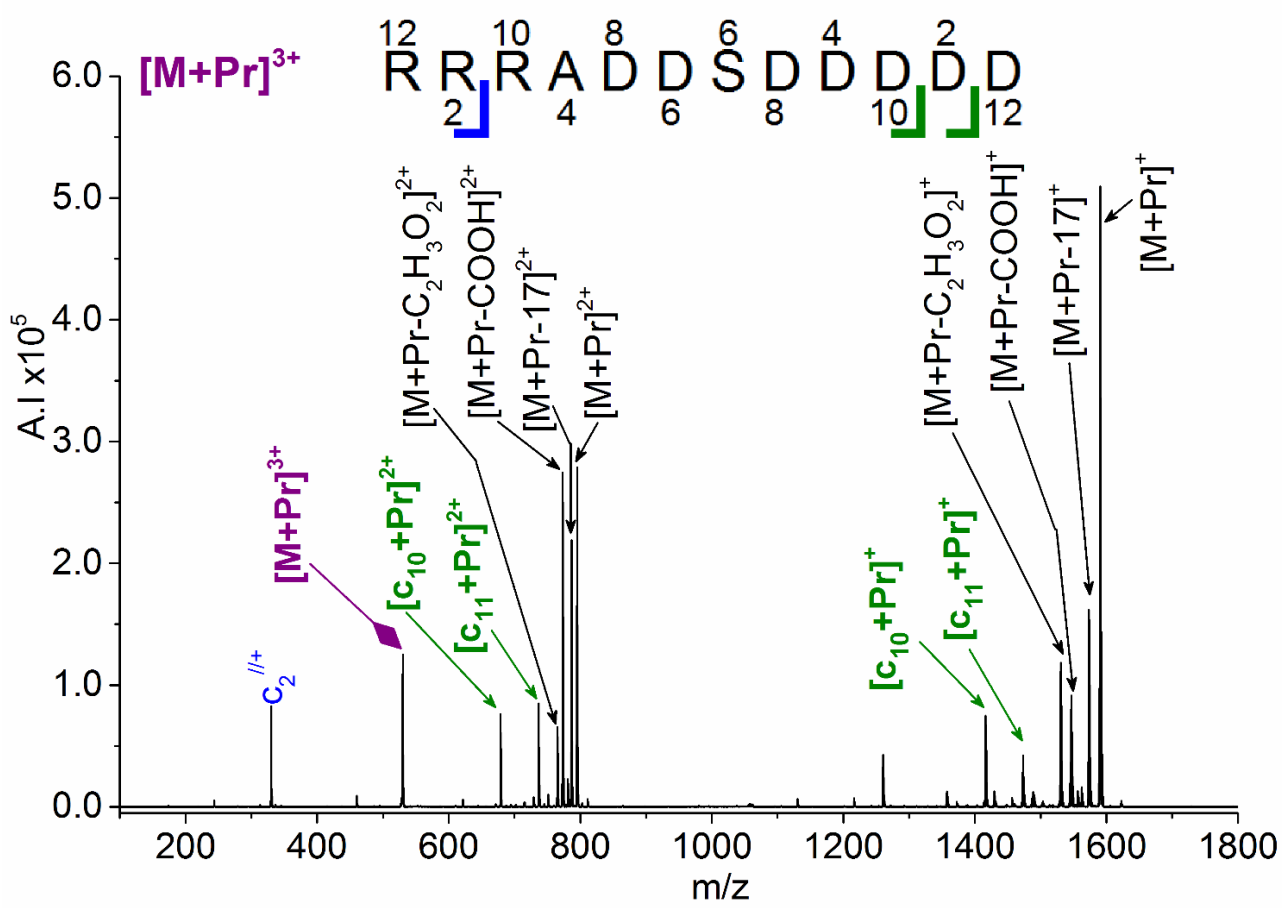


Figure 4.5. ETD mass spectrum of $[M + Pr]^{3+}$ for casein kinase II substrate. In the figure, the following colors are used to label the ions: non-metallated c-ions = blue, and metal-adducted c-ions = green. Undissociated precursor ion is labeled in purple with a large purple diamond arrow head. Neutral loss products and electron transfer without dissociation (ETnoD) ions are labeled in black. A prime symbol to the left indicates loss of a hydrogen (i.e., $^{/}c_n = [c_n - H]^+$) and to the right indicates the addition of a hydrogen at the cleavage site (i.e., $c_n^{//} = [c_n + 2H]^+$). The spectrum has no expansion of the intensity axis; all peaks are shown to scale.

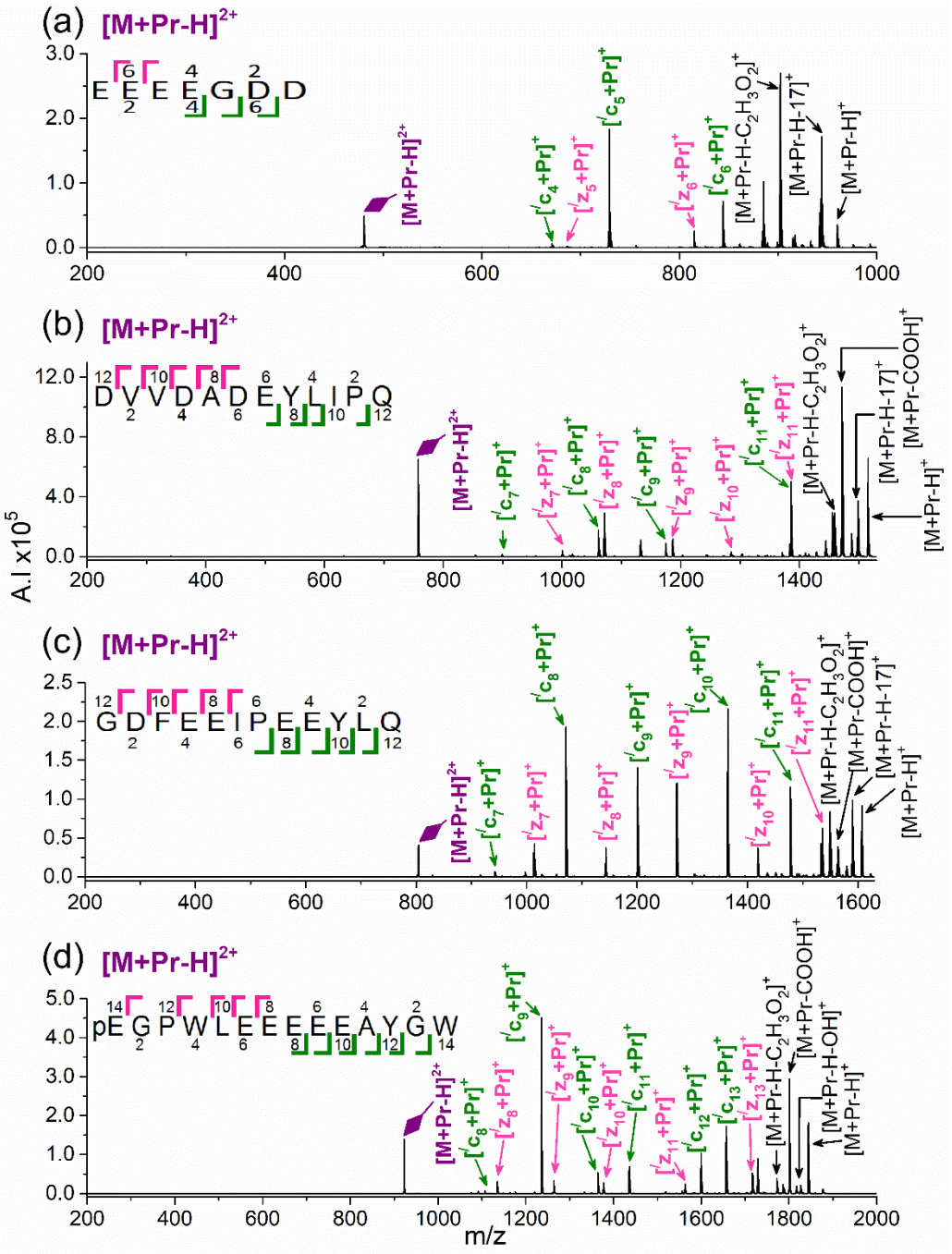


Figure 4.6. ETD mass spectra of $[M + Pr - H]^{2+}$ for (a) LMWCr peptide, (b) EGF(985-996), (c) hirudin(54-65), and (d) human gastrinI(1-14). In the figures, the following colors are used to label the ions: metal-adducted z-ions = bright pink, and metal-adducted c-ions = green. Undissociated precursor ion is labeled in purple with a large purple diamond arrow head. Neutral loss products and electron transfer without dissociation (ETnoD) ions are labeled in black. A prime symbol to the left indicates loss of a hydrogen (i.e., $^{/}c_n = [c_n - H]^+$) and to the right indicates the addition of a hydrogen at the cleavage site (i.e., $c_n^{//} = [c_n + 2H]^+$). The spectrum has no expansion of the intensity axis; all peaks are shown to scale.

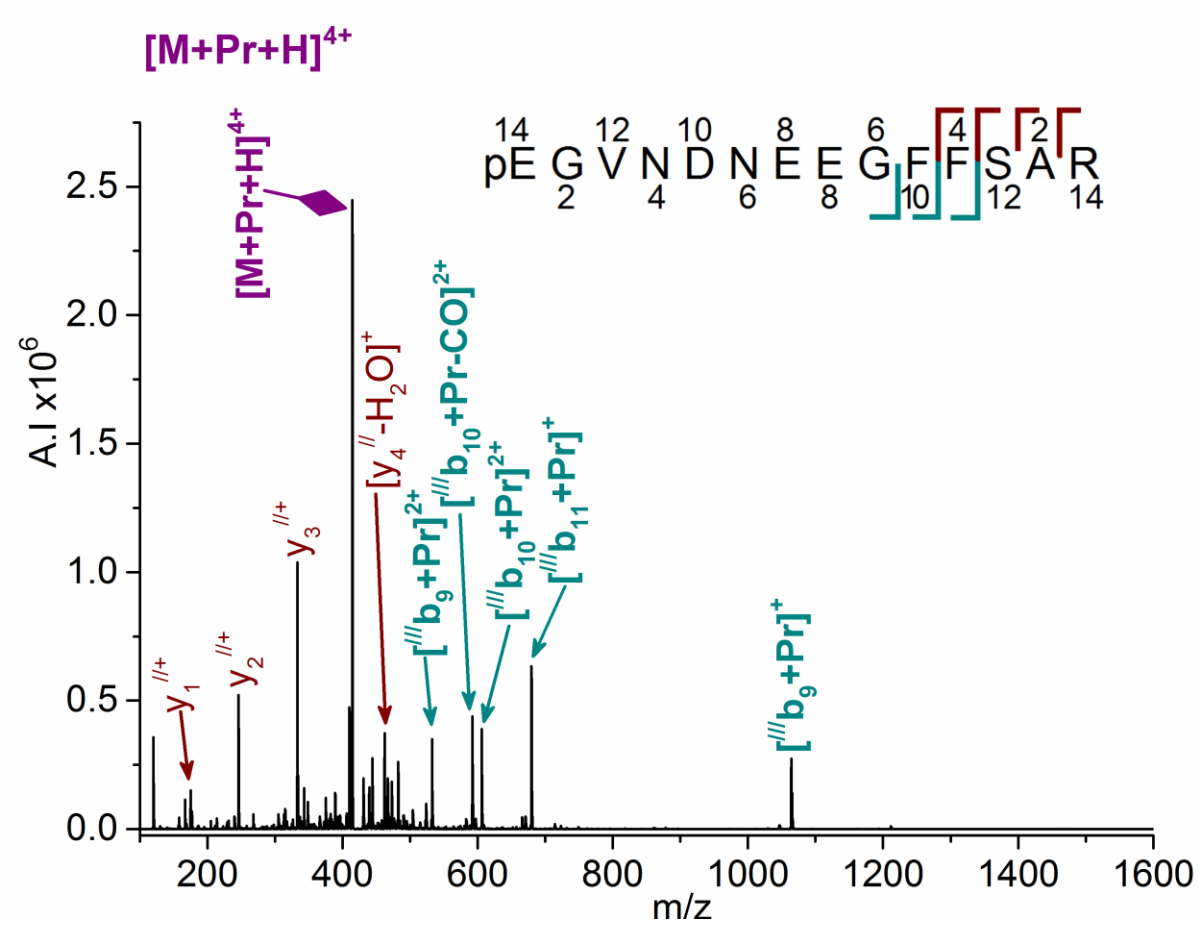


Figure 4.7. CID mass spectrum of $[M + Pr + H]^{4+}$ for fibrinopeptide B. In the figure, the following colors are used to label the ions: non-metallated y-ions = burgundy, and metal-adducted b-ions = blue-green. Undissociated precursor ion is labeled in purple with a large purple diamond arrow head. Neutral loss products and electron transfer without dissociation (ETnoD) ions are labeled in black. A prime symbol to the left indicates loss of a hydrogen (i.e., $^{/}c_n = [c_n - H]^+$) and to the right indicates the addition of a hydrogen at the cleavage site (i.e., $c_n^{//} = [c_n + 2H]^+$). The spectrum has no expansion of the intensity axis; all peaks are shown to scale.

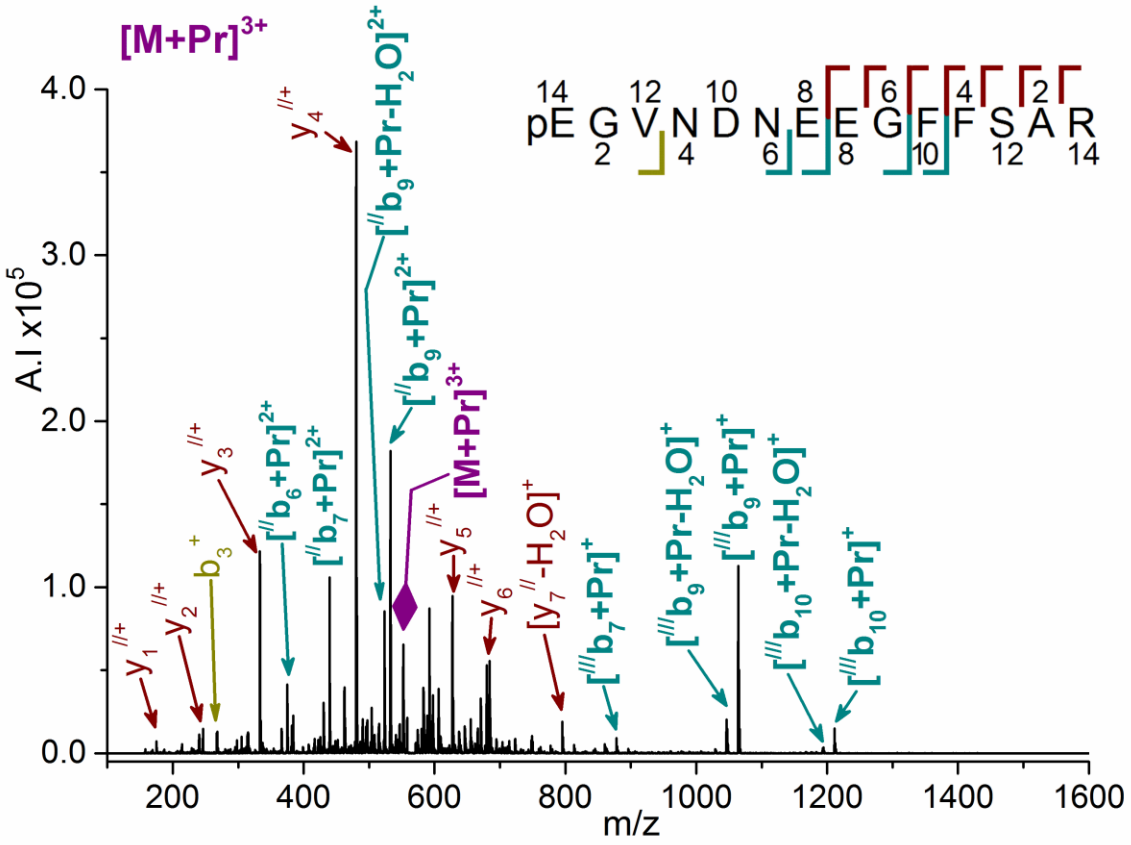


Figure 4.8. CID mass spectrum of $[M + Pr]^{3+}$ for fibrinopeptide B. In the figure, the following colors are used to label the ions: non-metallated b-ions = olive green, non-metallated y-ions = burgundy, metal-adducted b-ions = blue-green. Undissociated precursor ion is labeled in purple with a large purple diamond arrow head. Neutral loss products and electron transfer without dissociation (ETnoD) ions are labeled in black. A prime symbol to the left indicates loss of a hydrogen (i.e., $^{/}c_n = [c_n - H]^+$) and to the right indicates the addition of a hydrogen at the cleavage site (i.e., $c_n^{//} = [c_n + 2H]^+$). The spectrum has no expansion of the intensity axis; all peaks are shown to scale.

The peptides E6, E7, D7, E8, and D10 were chosen both to investigate ETD fragmentation of highly acidic metallated peptides and to explore the effect of chain length on ETD. Figure 4.9 shows the ETD spectra of $[M + Pr - H]^{2+}$ for these peptides. Members of the c- and z-series dominate and all product ions are metal-adducted. For E6, only $[^{/}c_n + Pr]^+$, n = 4 and 5, and $[^{/}z_5 + Pr]^+$ form, as shown in Figure 4.9(a). Cleavage at only three sites on the peptide backbone limits sequence information. In Figure 4.9(c), D7 produces the same number of ETD product ions as E6. However, in Figure 4.9(b), E7 forms one additional ion than E6, $[^{/}z_5 + Pr]^+$, thus giving slightly more sequence information. Increasing the peptide chain length from seven to eight residues leads to much more peptide backbone cleavage with only cleavage between the fourth and fifth residues being absent in E8, as seen in Figure 4.9(d). For the polyglutamic acid peptides, the trend is that sequence informative fragmentation increases in the order E6 < E7 < E8. In Figure 4.9(e), ETD of $[M + Pr - H]^{2+}$ for D10 yields cleavage at every residue except between the central acidic residues $D^5$ and $D^6$.

Our results indicate that increasing the peptide chain length increases ETD fragmentation for Pr(III)-peptide ions lacking residues with highly basic side chains. However, peptide sequence must also play a role because Chan and coworkers[75] reported an opposite effect. In an ECD study of protonated ions from peptides containing glutamic acid residues and two highly basic arginine residues, they observed that peptides with longer sequences (15 to 23 residues) underwent less backbone cleavage than peptides with shorter chain lengths of eight residues. This group postulated that an extensive network of hydrogen bonding involving the arginine residues helped to suppress the normal ECD mechanism for N-Cα bond cleavage. In another study involving Cu(II)-peptide complexes of basic peptides by Chan and coworkers,[62][62] the researchers also observed decreased backbone cleavage for larger peptides.

The heptapeptides DAAAAAA, EAAAAAA, AAADAAA, and AAAEAAA undergo efficient and informative ETD fragmentation. As show in Figure 4.10(a) and 4.10(b) for $[M + Pr]^{3+}$, when the acidic residue is at the N-terminus, a mixture of metallated c-, z-, and y-ions form. Backbone cleavage occurs at every residue. When the acidic residue is in the middle of the sequence, only metal-adducted c- and z-ions form with cleavage at every residue, as seen in Figure 4.10(c) and 4.10(d). For the heptapeptide with the acidic residue at the C-terminus, ETD of $[AAAAAAE + Pr - H]^{2+}$ generates only metal-adducted C-terminal ions; i.e., $[^{/}z_n + Pr]^{+}$, n = 5-6. Only two sites on the peptide backbone cleave and neither is adjacent to the acidic residue.

As was the case with the biological peptides, $[M + Pr]^{3+}$ generates more extensive ETD cleavage than $[M + Pr - H]^{2+}$. For example, ETD of $[M + Pr - H]^{2+}$ cleaves at a maximum of four sites for the heptapeptide E7, three for D7, and two for AAAAAAE, as shown in Figures 4.9 and 4.10. However, ETD of $[M + Pr]^{3+}$ for the other heptapeptides, DAAAAAA, EAAAAAA, AAADAAA, AAAEAAA, DAADAAD, and EAAEAAE yields cleavage at every residue, as shown in Figures 4.10 and 4.11. Significantly less sequence coverage occurs for CID of $[M + Pr]^{3+}$ for the model peptides. As shown in Figure 4.12 for CID of $[M +Pr]^{3+}$ for EAAAAAA, cleavage occurs at only three sites along the peptide backbone.

Heptapeptides DAADAAD and EAAEAAE were chosen to investigate the effect of multiple scattered acidic residues on ETD. As shown in Figure 4.11, ETD on $[M + Pr]^{3+}$ produces a mixture of metal-adducted c- and z-ions as well as non-metallated c-ions for both peptides. Full sequence coverage occurs, with the c-series being complete for both peptides. Thus, the presence of scattered acidic residues appears particularly effective at promoting fragmentation.

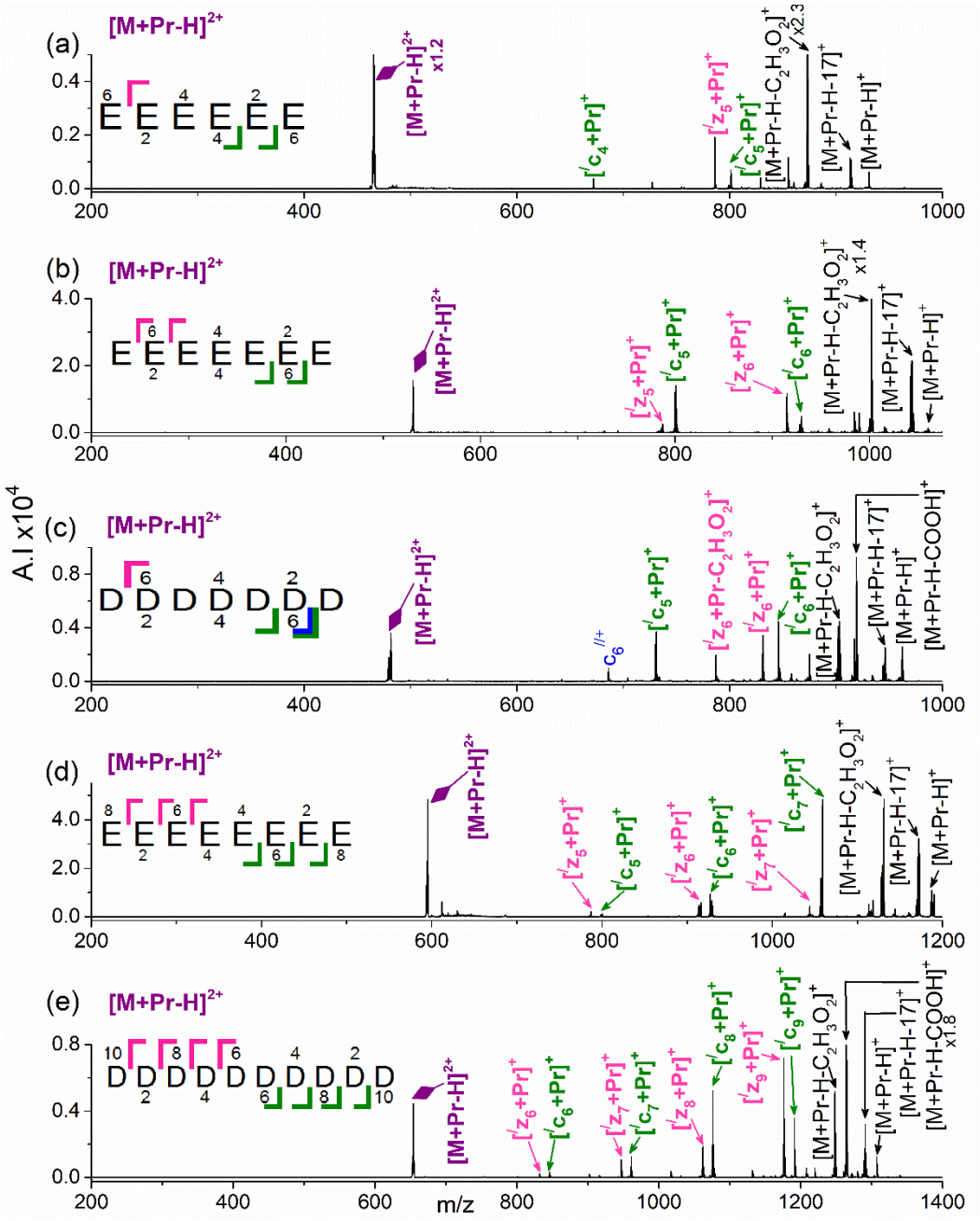


Figure 4.9. ETD mass spectra of $[M + Pr - H]^{2+}$ for (a) E6, (b) E7, (c) D7, (d) E8, and (e) D10. In the figures, the following colors are used to label the ions: non-metallated z-ions = red, non-metallated c-ions = blue, non-metallated a-ions = orange, non-metallated b-ions = olive green, non-metallated y-ions = burgundy, metal-adducted z-ions = bright pink, metal-adducted c-ions = green, metal-adducted b-ions = blue-green, and metal-adducted y-ions = brown. Undissociated precursor ion is labeled in purple with a large purple diamond arrow head. Neutral loss products and electron transfer without dissociation (ETnoD) ions are labeled in black. A prime symbol to the left indicates loss of a hydrogen (i.e., $^{/}c_n = [c_n - H]^+$) and to the right indicates the addition of a hydrogen at the cleavage site (i.e., $c_n^{//} = [c_n + 2H]^+$).

For the model peptides, the presence of aspartic acid versus glutamic acid had no noticeable effect on the ETD spectra of $[M + Pr]^{3+}$. The Cassady group has also found that the identity and position of acidic residues has negligible impact on ETD of doubly protonated acidic model peptides.[87] In addition, the spectra here show no evidence of increased cleavage abundance adjacent to the acidic residues. Chan and coworkers[88] also reported no enhanced cleavage C-terminal to aspartic or glutamic acid residues in their ECD work on protonated nonapeptides. However, their spectra suggest that there may be moderately enhanced cleavage on the N-terminal side of both residues. In addition, in an ETD study on thousands of protonated peptides, Wysocki, Coon, and coworkers[76] found that the probability of cleavage N-terminal to glutamic acid increases as the peptide chain length increases; peptide ions with an average length of 17 residues and an average charge of 3.5 showed enhanced cleavage N-terminal to glutamic acid when compared to peptides with an average of 15 residues and a charge of 3.8.

Metal-adducted ions only appear after half of the sequence has been incorporated into the ETD product ion irregardless of the size of the peptide chain. For all peptides in this study, no metallated product ion contains less than half of the number of residues in its peptide. For example, for the heptapeptides, $[^{/}c_4 + Pr]^+$, $[^{/}z_4 + Pr]^+$, or $[y_4 + Pr]^+$ are the smallest metallated ETD product ions. This trend can also be observed for all the model heptapeptide spectra of Figure 4.10. This effect even occurs for longer peptides, including the biological peptides. As an example, in Figure 4.1(a) showing ETD of $[M + Pr + H]^{4+}$ for the dodecapeptide EGF(985-996), the smallest metal-adducted product ions are $[^{/}c_6 + Pr]^+$ and $[^{/}z_6 + Pr]^+$. Spectra from the Cassady group's previous CID study involving $Cr^{3+}$ adduction to acidic peptides also exhibit this trend.[89] Trivalent metal adduction may involve simultaneous coordination of more than one amino acid residue with the metal cation. Peptide chains may need to contain at least

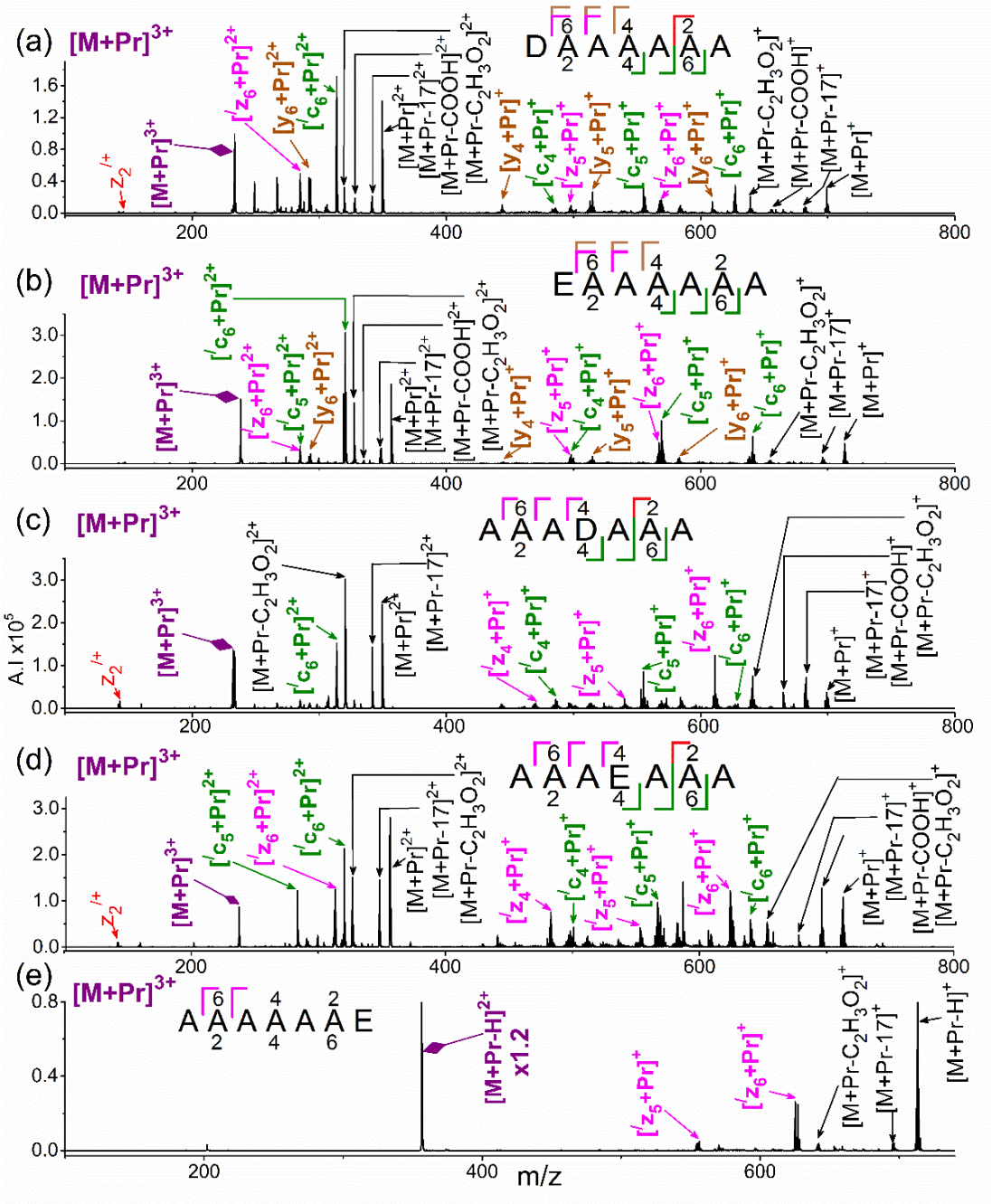


Figure 4.10. ETD mass spectra of $[M + Pr]^{3+}$ for (a) DAAAAAA, (b) EAAAAAA, (c) AAADAAA, (d) AAAEAAA, and (e) $[M + Pr - H]^{2+}$ for AAAAAAE. In the figures, the following colors are used to label the ions: non-metallated z-ions = red, non-metallated c-ions = blue, metal-adducted z-ions = bright pink, metal-adducted c-ions = green, and metal-adducted y-ions = brown. Undissociated precursor ion is labeled in purple with a large purple diamond arrow head. Neutral loss products and electron transfer without dissociation (ETnoD) ions are labeled in black. A prime symbol to the left indicates loss of a hydrogen (i.e., $^{/}c_n = [c_n - H]^+$) and to the right indicates the addition of a hydrogen at the cleavage site (i.e., $c_n^{//} = [c_n + 2H]^+$).

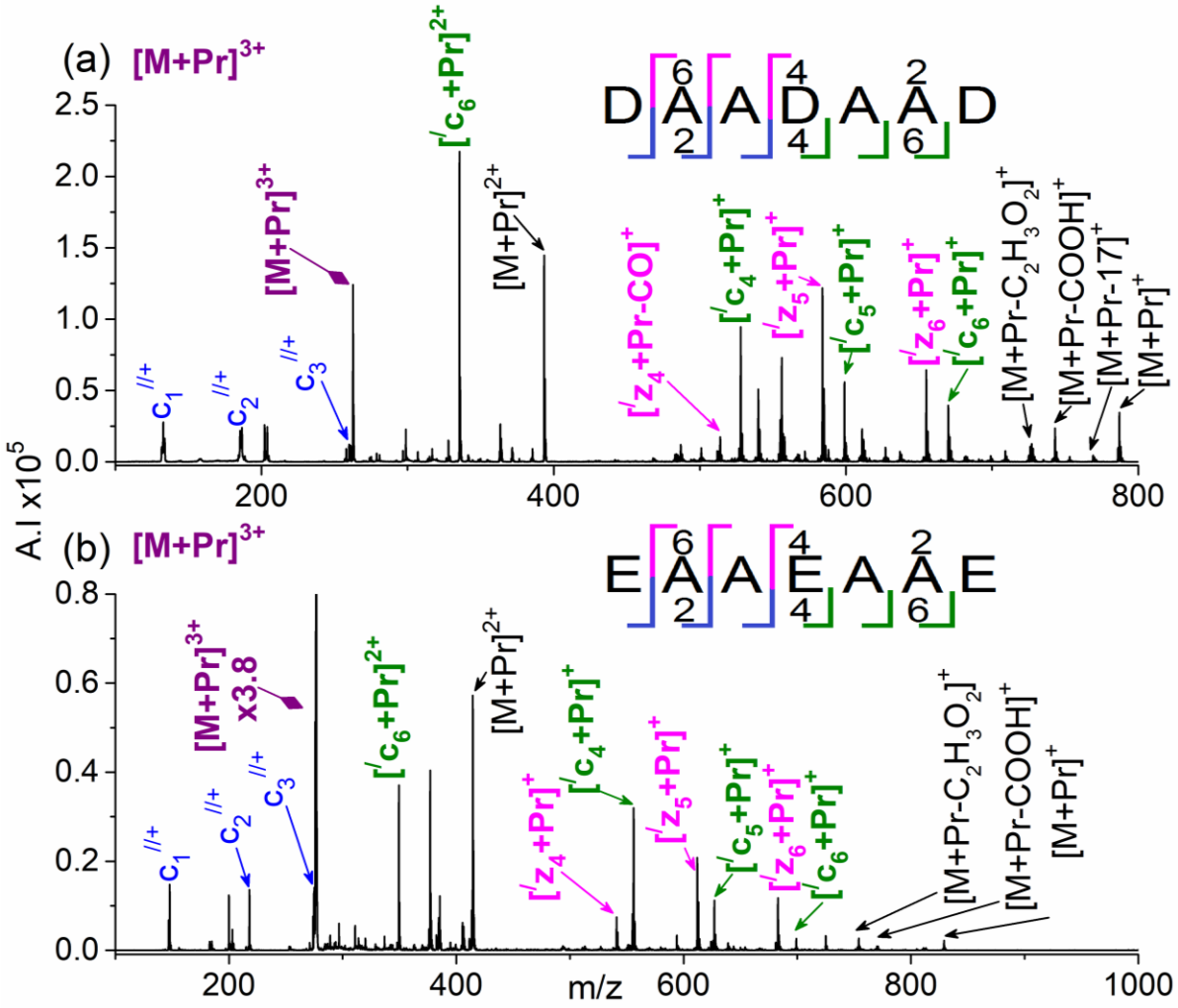


Figure 4.11. ETD mass spectra of $[M + Pr]^{3+}$ for (a) DAADAAD and (b) EAAEAAE. In the figures, the following colors are used to label the ions: non-metallated c-ions = blue, metal-adducted z-ions = bright pink, and metal-adducted c-ions = green. Undissociated precursor ion is labeled in purple with a large purple diamond arrow head. Neutral loss products and electron transfer without dissociation (ETnoD) ions are labeled in black. A prime symbol to the left indicates loss of a hydrogen (i.e., $^{/}c_n = [c_n - H]^+$) and to the right indicates the addition of a hydrogen at the cleavage site (i.e., $c_n^{//} = [c_n + 2H]^+$).

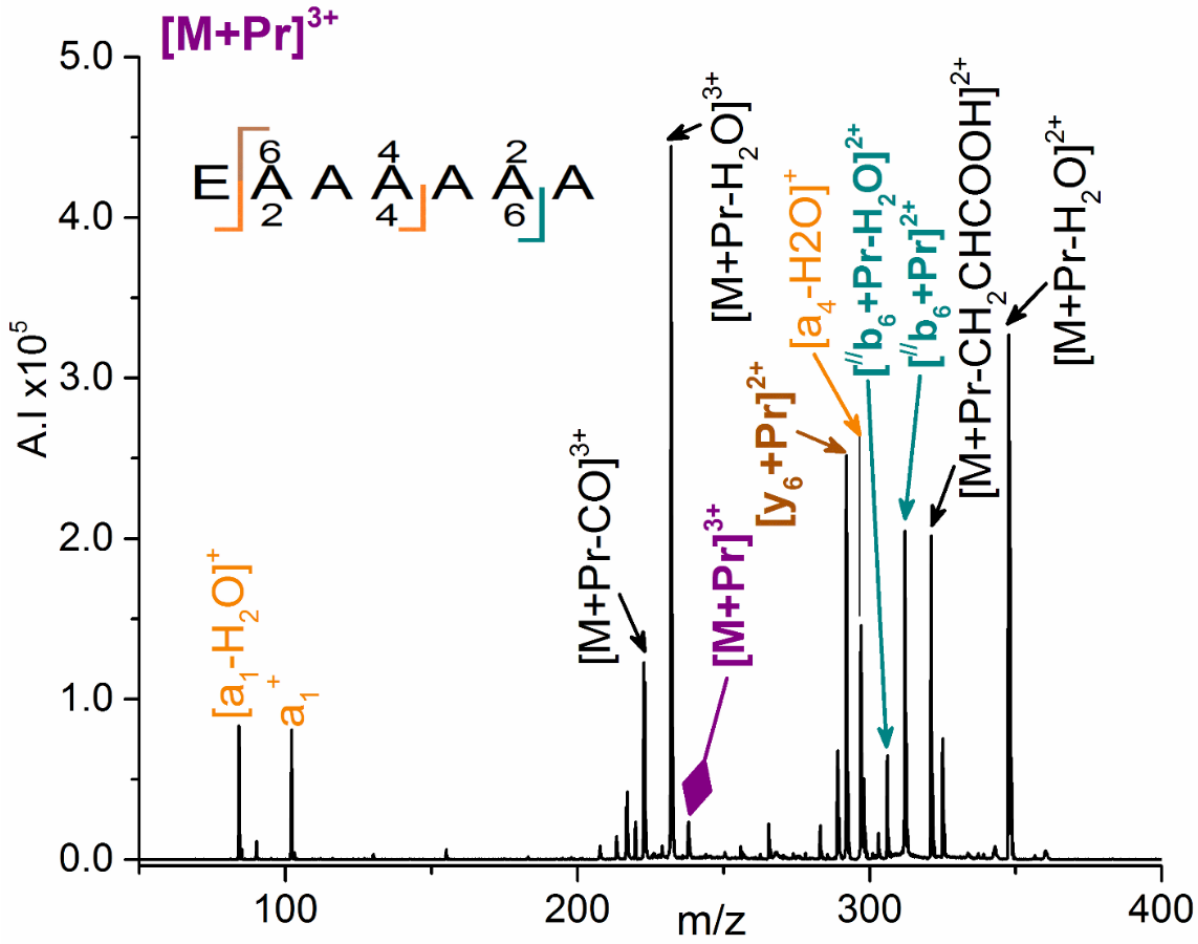


Figure 4.12. CID mass spectrum of $[M + Pr]^{3+}$ for EAAAAAA. In the figure, the following colors are used to label the ions: non-metallated a-ions = orange, non-metallated b-ions = olive green, non-metallated y-ions = burgundy, metal-adducted b-ions = blue-green, and metal-adducted y-ions = brown. Undissociated precursor ion is labeled in purple with a large purple diamond arrow head. Neutral loss products and electron transfer without dissociation (ETnoD) ions are labeled in black. A prime symbol to the left indicates loss of a hydrogen (i.e., $^{/}c_n = [c_n - H]^+$) and to the right indicates the addition of a hydrogen at the cleavage site (i.e., $c_n^{//} = [c_n + 2H]^+$). The spectrum has no expansion of the intensity axis; all peaks are shown to scale.

four amino acid residues to properly interact with the metal ions. This is supported by the fact that neither of the tripeptides (D3 and E3) were able to form metal-adducted ions by ESI.

The neutrals eliminated from ETD product ions include $NH_3$ (17 Da), OH (17 Da), COOH (45 Da), and $C_2H_3O_2$ (59 Da). Our quadrupole ion trap (QIT) mass analyzer does not have sufficient resolution to distinguish between $NH_3$ and OH elimination. For ECD and ETD on protonated peptides, 17 Da typically corresponds to the loss of $NH_3$ from the amino group of the N-terminus.[22,90,91] However, Coon and coworkers[91] reported 17 Da loss as OH elimination from a serine side chain in an N-acetylated peptide; modification of the N-terminus suppressed $NH_3$ loss. The absence or minimal elimination of 17 Da could be indicative of a peptide with a modified N-terminus. Gastrin I(1-14) from the current study and fibrinopeptide B from our previous study in Chapter 3[72] both have a cyclized N-terminus with no amino group; these two peptides showed less 17 Da loss in comparison to the other acidic peptides studied. However, these peptides did exhibit some 17 Da elimination, which suggests that loss of OH can occur at aspartic acid and glutamic acid side chains. In addition, for ECD and ETD on protonated peptides, aspartic acid normally yields a side chain loss of COOH (45 Da) and glutamic acid has a loss of $C_2H_3O_2$ (59 Da).[90-92] These neutral losses were also found in our ETD spectra of Pr(III)-adducted peptides. In general, the presence of the metal ion has negligible impact on the appearance of product ions involving neutral loss.

### 4.5 Conclusions

The current study illustrates the effects of peptide chain length and amino acid composition and position on ETD of acidic biological and model peptides without highly basic amino acid residues. Peptides with greater than six amino acid residues form multiply charged ions by $Pr^{3+}$. ETD of $[M + Pr - H]^{2+}$ generally provides more sequence informative

fragmentation for longer peptides such as model peptide D10 or human gastrin I(1-14) than shorter peptides such as D7. ETD of $[M + Pr]^{3+}$ can provide full sequence coverage for peptides containing as little as seven amino acid residues. For the acidic peptides in the current study as well as previous work discussed in Chapter 3 involving acidic fibrinopeptide B and analogs,[72] ETD of $[M + Pr + H]^{4+}$ provides the most sequence informative fragmentation and leads to cleavage at every residue. However, production of this protonated and metallated 4+ precursor ion generally requires that the peptide contain at least one residue with a basic side chain. While only $Pr^{3+}$ was employed in the current study, prior work from Chapter 3 indicates that any of the trivalent lanthanide metal cations except promethium and europium would be suitable for sequencing acidic peptides. This is the only study to date that provides a method for obtaining MS/MS spectra for highly acidic peptides. Cationization by trivalent lanthanide cations is a useful and promising tool for analysis of highly acidic biological peptides containing seven or more residues by ETD and ECD.

## References


1. Zubarev, R. A.; Kelleher, N. L.; McLafferty, F. W. Electron Capture Dissociation of Multiply Charged Protein Cations. A Nonergodic Process. *J. Am. Chem. Soc.* **1998**, *120*, 3265-3266.

2. Zubarev, R. A.; Horn, D. M.; Fridriksson, E. K.; Kelleher, N. L.; Kruger, N. A.; Lewis, M. A.; Carpenter, B. K.; McLafferty, F. W. Electron Capture Dissociation for Structural Characterization of Multiply Charged Protein Cations. *Anal. Chem.* **2000**, *72*, 563-573.

3. Ge, Y.; Lawhorn, B.; ElNaggar, M.; Strauss, E.; Park, J.; Begley, T.; McLafferty, F. Top Down Characterization of Larger Proteins (45 kDa) by Electron Capture Dissociation Mass Spectrometry RID G-1783-2010. *J. Am. Chem. Soc.* **2002**, *124*, 672-678.

4. Syka, J. E. P.; Coon, J. J.; Schroeder, M. J.; Shabanowitz, J.; Hunt, D. F. Peptide and Protein Sequence Analysis by Electron Transfer Dissociation Mass Spectrometry. *Proc. Natl. Acad. Sci. USA* **2004**, *101*, 9528-9533.

5. Zubarev, R. A.; Haselmann, K. F.; Budnik, B.; Kjeldsen, F.; Jensen, F. Towards an Understanding of the Mechanism of Electron-capture Dissociation: A Historical Perspective and Modern Ideas. *Eur. J. Mass Spectrom.* **2002**, *8*, 337-349.

6. Biemann, K. Sequencing of Peptides by Tandem Mass-Spectrometry and High-Energy Collision-Induced Dissociation. *Meth. Enzymol.* **1990**, *193*, 455-479.

7. Senko, M. W.; Speir, J. P.; McLafferty, F. W. Collisional Activation of Large Multiply Charged Ions Using Fourier Transform Mass Spectrometer. *Anal. Chem.* **1994**, *66*, 2801-2808.

8. Little, D. P.; Speir, J. P.; Senko, M. W.; O'Connor, P. B.; McLafferty, F. W. Infrared Multiphoton Dissociation of Large Multiply Charged Ions for Biomolecule Sequencing. *Anal. Chem.* **1994**, *66*, 2809-2815.

9. Mirgorodskaya, E.; Roepstorff, P.; Zubarev, R. A. Localization of O-glycosylation Sites in Peptides by Electron Capture Dissociation in a Fourier Transform Mass Spectrometer. *Anal. Chem.* **1999**, *71*, 4431-4436.

10. Shi, S. D. H.; Hemling, M. E.; Carr, S. A.; Horn, D. M.; Lindh, I.; McLafferty, F. W. Phosphopeptide/Phosphoprotein Mapping by Electron Capture Dissociation Mass Spectrometry. *Anal. Chem.* **2001**, *73*, 19-22.

11. Kelleher, N. L.; Zubarev, R. A.; Bush, K.; Furie, B.; Furie, B. C.; McLafferty, F. W.; Walsh, W. T. Localization of Labile Posttranslational Modifications by Electron Capture Dissociation: The Case of γ-Carboxyglutamic Acid. *Anal. Chem.* **1999**, *71*, 4250-4253.

12. Mann, M.; Jensen, O. N. Proteomic Analysis of Post-translational Modifications. *Nat. Biotechnol.* **2003**, *21*, 255-261.

13. Stensballe, A.; Jensen, O. N.; Olsen, J. V.; Haselmann, K. F.; Zubarev, R. A. Electron Capture Dissociation of Singly and Multiply Phosphorylated Peptides. *Rapid Commun. Mass Spectrom.* **2000**, *14*, 1793-2000.

14. Zhao, C.; Sethuraman, M.; Clavreul, N.; Kaur, P.; Cohen, R. A.; O'Connor, P. B. Detailed Map of Oxidative Post-translational Modifications of Human P21Ras Using Fourier Transform Mass Spectrometry. *Anal. Chem.* **2006**, *78*, 5134-5142.

15. Zubarev, R. A.; Kruger, N. A.; Fridriksson, E. K.; Lewis, M. A.; Horn, D. M.; Carpenter, B. K.; McLafferty, F. W. Electron Capture Dissociation of Gaseous Multiply-charged Proteins is Favored at Disulfide Bonds and Other Sites of High Hydrogen Atom Affinity. *J. Am. Chem. Soc.* **1999**, *121*, 2857-2862.

16. Chen, X.; Tureček, F. The arginine anomaly: Arginine Radicals are Poor Hydrogen Atom Donors in Electron Transfer Induced Dissociations. *J. Am. Chem. Soc.* **2006**, *128*, 12520-12530.

17. Syrstad, E. A.; Tureček, F. Toward a General Mechanism of Electron Capture Dissociation. *J. Am. Soc. Mass Spectrom.* **2005**, *16*, 208-224.

18. McLafferty, F. W.; Horn, D. M.; Breuker, K.; Ge, Y.; Lewis, M. A.; Cerda, B. A.; Zubarev, R. A.; Carpenter, B. K. Electron Capture Dissociation of Gaseous Multiply Charged Ions by Fourier Transform Ion Cyclotron Resonance. *J. Am. Soc. Mass Spectrom.* **2001**, *12*, 245-249.

19. Zubarev, R. A. Electron Capture Dissociation LC/MS/MS for Bottom-Up Proteomics. *Methods Mol. Biol.* **2009**, *492*, 413-416.

20. Coon, J. J. Collisions or Electrons? Protein Sequence Analysis in the 21st Century. *Anal. Chem.* **2009**, *81*, 3208-3215.

21. Good, D. M.; Wirtala, M.; McAlister, G. C.; Coon, J. J. Performance Characteristics of Electron Transfer Dissociation Mass Spectrometry. *Mol. Cell Proteomics* **2007**, *6*, 1942-1951.

22. Turecek, F.; Julian, R. R. Peptide Radicals and Cation Radicals in the Gas Phase. *Chem. Rev.* **2013**, *113*, 6691-6733.

23. Dongre, A. R.; Jones, J. L.; Somogyi, A.; Wysocki, V. H. Influence of Peptide Composition, Gas-Phase Basicity, and Chemical Modification on Fragmentation Efficiency: Evidence for the Mobile Proton Model. *J. Am. Chem. Soc.* **1996**, *118*, 8365-8374.

24. Kjeldsen, F.; Giessing, A. M. B.; Ingrell, C. R.; Jensen, O. N. Peptide Sequencing and Characterization of Post-Translational Modifications by Enhanced Ion-Charging and Liquid Chromatography Electron-Transfer Dissociation Tandem Mass Spectrometry. *Anal. Chem.* **2007**, *79*, 9243-9252.

25. Wells, J. M.; Stephenson Jr., J. L.; McLuckey, S. A. Charge Dependence of Protonated Insulin Decompositions. *Int. J. Mass Spectrom.* **2000**, *203*, A1-A9.

26. Madsen, J. A.; Brodbelt, J. S. Comparison of Infrared Multiphoton Dissociation and Collision-Induced Dissociation of Supercharged Peptides in Ion Traps. *J. Am. Soc. Mass Spectrom.* **2009**, *20*, 349-358.

27. Chalkley, R. J.; Medzihradszky, K. F.; Lynn, A. J.; Baker, P. R.; Burlingame, A. L. Statistical Analysis of Peptide Electron Transfer Dissociation Fragmentation Mass Spectrometry. *Anal. Chem.* **2010**, *82*, 579-584.

28. Sharma, V.; Eng, J. K.; Feldman, S.; von Haller, P. D.; MacCoss, M. J.; Noble, W. S. Precursor Charge State Prediction for Electron Transfer Dissociation Tandem Mass Spectra. *J. Proteome Res.* **2010**, *9*, 5438-5444.

29. Marshall, A. G.; Hendrickson, C. L. Charge Reduction Lowers Mass Resolving Power for Isotopically Resolved Electrospray Ionization Fourier Transform Ion Cyclotron Resonance mass spectra. *Rapid Commun. Mass Spectrom.* **2001**, *15*, 232-235.

30. Marshall, A. G.; Hendrickson, C. L. High-Resolution Mass Spectrometers. *Ann. Rev. Anal. Chem.* **2008**, *1*, 579-599.

31. Perry, R. H.; Cooks, R. G.; Noll, R. J. Orbitrap Mass Spectrometry: Instrumentation, Ion Motion and Applications. *Mass Spectrom. Rev.* **2008**, *27*, 661-699.

32. Lapko, V. N.; Jiang, X. Y.; Smith, D. L.; Song, P. S. Posttranslational Modification of Oat Phytochrome A: Phosphorylation of a Specific Serine in a Multiple Serine Cluster. *Biochemistry* **1997**, *36*, 10595-10599.

33. Yagami, T.; Kitagawa, K.; Futaki, S. Liquid Secondary-ion Mass Spectrometry of Peptides Containing Multiple Tyrosine-O-sulfates. *Rapid Commun. Mass Spectrom.* **1995**, *9*, 1335-1341.

34. Chen, Y.; Watson, H. M.; Gao, J.; Sinha, S. H.; Cassady, C. J.; Vincent, J. B. Characterization of the Organic Component of Low-Molecular-Weight Chromium-Binding Substance and Its Binding of Chromium. *J. Nutr.* **2011**, *141*, 1225-1232.

35. Jai-nhuknan, J.; Cassady, C. J. Negative Ion Postsource Decay Time-of-Flight Mass Spectrometry of Peptides Containing Acidic Amino Acid Residues. *Anal. Chem.* **1998**, *70*, 5122-5128.

36. Ganisl, B.; Valovka, T.; Hartl, M.; Taucher, M.; Bister, K.; Breuker, K. Electron Detachment Dissociation for Top-Down Mass Spectrometry of Acidic Proteins. *Chem. Eur. J.* **2011**, *17*, 4460-4469.

37. Kalli, A.; Grigorean, G.; Håkansson, K. Electron Induced Dissociation of Singly Deprotonated Peptides. *J. Am. Soc. Mass Spectrom.* **2011**, *22*, 2209-2221.

38. Huzarska, M.; Ugalde, I.; Kaplan, D. A.; Hartmer, R.; Easterling, M. L.; Polfer, N. C. Negative Electron Transfer Dissociation of Deprotonated Phosphopeptide Anions: Choice of Radical Cation Reagent and Competition Between Electron and Proton Transfer. *Anal. Chem.* **2010**, *82*, 2873-8.

39. Albeck, S.; Aizenberg, J.; Addadi, L.; Weiner, S. Interactions of Various Skeletal Intracrystalline Components with Calcite Crystals. *J. Am. Chem. Soc.* **1993**, *115*, 11691-11697.

40. Hunter, G. K.; Goldberg, H. A. Nucleation of Hydroxyapatite by Bone Sialoprotein. *Proc. Natl. Acad. Sci. U. S. A.* **1993**, *90*, 8562-8565.

41. Hunter, G. K.; Goldberg, H. A. Modulation of Crystal Formation by Bone Phosphoproteins: Role of Glutamic Acid-rich Sequences in the Nucleation of Hydroxyapatite by Bone Sialoprotein. *Biochem. J.* **1994**, *302*, 175-179.

42. Walters, D.; Smith, B.; Belcher, A.; Paloczi, G.; Stucky, G.; Morse, D.; Hansma, P. Modification of Calcite Crystal Growth by Abalone Shell Proteins: An Atomic Force Microscope Study. *Biophys. J.* **1997**, *72*, 1425-1433.

43. Rebar, R. W.; Miyake, A.; Low, T. L.; Goldstein, A. L. Thymosin Stimulates Secretion of Luteinizing Hormone-releasing Factor. *Science* **1981**, *214*, 669-671.

44. Ebert, R. F.; Bell, W. R. Assay of Human Fibrinopeptides by High-Performance Liquid Chromatography. *Anal. Biochem.* **1985**, *148*, 70-78.

45. Voet, D.; Voet, J. G. *Biochemistry;* John Wiley & Sons: New York, 1995.

46. Malinda, K.; Goldstein, A.; Kleinman, H. Thymosin Beta(4) Stimulates Directional Migration of Human Umbilical Vein Endothelial Cells. *Faseb J.* **1997**, *11*, 474-481.

47. Gómez-Márquez, J.; Anadón, R. The Beta-thymosins, Small Actin-binding Peptides Widely Expressed in the Developing and Adult Cerebellum. *The Cerebellum* **2002**, *1*, 95-102.

48. Vincent, J. B. Elucidating a Biological Role for Chromium at a Molecular Level. *Acc. Chem. Res.* **2000**, *33*, 503-510.

49. Speetjens, J. K.; Parand, A.; Crowder, M. W.; Vincent, J. B.; Woski, S. A. Low-molecular Weight Chromium-binding Substance and Biomimetic $[Cr_3O(O_2CH_2CH_3)_6(H_2O)_3]^+$ Do Not Cleave DNA Under Physiologically-relevant Conditions. *Polyhedron* **1999**, *18*, 2617-2624.

50. Davis, C. M.; Vincent, J. B. Isolation and Characterization of a Biologically Active Chromium Oligopeptide from Bovine Liver. *Arch. Biochem. Biophys.* **1997**, *339*, 335-343.

51. Low, T. L.; Hu, S. K.; Goldstein, A. L. Complete Amino Acid Sequence of Bovine Thymosin Beta 4: A Thymic Hormone that Induces Terminal Deoxynucleotidyl Transferase Activity in Thymocyte populations. *Proc. Natl. Acad. Sci. U. S. A.* **1981**, *78*, 1162-1166.

52. Weller, F. E.; Mutchnick, M. G.; Goldstein, A. L.; Naylor, P. H. Enzyme Immunoassay Measurement of Thymosin [beta] 4 in Human Serum. *J. Immunother.* **1988**, *7*, 91-96.

53. Chougnet, C.; Troye-Blomberg, M.; Deloron, P.; Kabilan, L.; Lepers, J. P.; Savel, J.; Perlmann, P. Human immune response in Plasmodium Falciparum Malaria. Synthetic Peptides Corresponding to Known Epitopes of the Pf155/RESA Antigen Induce Production of Parasite-Specific Antibodies in vitro. *J. Immunol.* **1991**, *147*, 2295-2301.

54. Nara, P. L.; Hwang, K. M.; Rausch, D. M.; Lifso, J. D.; Eiden, L. E. CD4 Antigen-based Antireceptor Peptides Inhibit Infectivity of Human Immunodeficiency Virus In Vitro at Multiple Stages of the Viral Life Cycle. *Proc. Natl. Acad. Sci. USA* **1989**, *86*, 7139-7143.

55. Lifson, J. D.; Hwang, K. M.; Nara, P. L.; Fraser, B.; Padgett, M.; Dunlop, N. M.; Eiden, L. E. Synthetic CD4 Peptide Derivatives that Inhibit HIV Infection and Cytopathicity. *Science* **1988**, *241*, 712-716.

56. Chan, D. C.; Kim, P. S. HIV Entry and Its Inhibition. *Cell* **1998**, *93*, 681-684.

57. Fung, Y. M. E.; Liu, H.; Chan, T. W. D. Electron Capture Dissociation of Peptides Metalated with Alkaline-Earth Metal Ions. *J. Am. Soc. Mass Spectrom.* **2006**, *17*, 757-771.

58. Chen, X.; Chan, W. Y. K.; Wong, P. S.; Yeung, H. S.; Chan, T. W. D. Formation of Peptide Radical Cations ($M^{+\cdot}$) in Electron Capture Dissociation of Peptides Adducted with Group IIB Metal Ions. *J. Am. Soc. Mass Spectrom.* **2011**, *22*, 233-244.

59. Liu, H.; Håkansson, K. Electron Capture Dissociation of Tyrosine O-Sulfated Peptides Complexed with Divalent Metal Cations. *Anal. Chem.* **2006**, *78*, 7570-7576.

60. Chen, X.; Fung, Y. M. E.; Chan, W. Y. K.; Wong, P. S.; Yeung, H. S.; Chan, T. W. D. Transition Metal Ions: Charge Carriers that Mediate the Electron Capture Dissociation Pathways of Peptides. *J. Am. Soc. Mass Spectrom.* **2011**, *22*, 2232-2245.

61. Liu, H.; Håkansson, K. Divalent Metal Ion-Peptide Interactions Probed by Electron Capture Dissociation of Trications. *J. Am. Soc. Mass Spectrom.* **2006**, *17*, 1731-1741.

62. Chen, X.; Wang, Z.; Li, W.; Wong, Y. L. E.; Chan, T. W. D. Effect of Structural Parameters on the Electron Capture Dissociation and Collision-induced Dissociation Pathways of Copper(II)-peptide Complexes. *Eur. J. Mass Spectrom.* **2015**, *21*, 649-657.

63. Chen, X.; Liu, G.; Wong, E. Y. L.; Deng, L.; Wang, Z.; Li, W.; Chan, T. W. D. Dissociation of Trivalent Metal Ion ($Al^{3+}$, $Ga^{3+}$, $In^{3+}$ and $Rh^{3+}$)–peptide Complexes Under Electron Capture Dissociation Conditions. *Rapid Commun. Mass Spectrom.* **2016**, *30*, 705-710.

64. Voinov, V. G.; Hoffman, P. D.; Bennett, S. E.; Beckman, J. S.; Barofsky, D. F. Electron Capture Dissociation of Sodium-Adducted Peptides on a Modified Quadrupole/Time-of-Flight Mass Spectrometer. *J. Am. Soc. Mass Spectrom.* **2015**, *26*, 2096-2104.

65. Kleinnijenhuis, A. J.; Mihalca, R.; Heeren, R. M. A.; Heck, A. J. R. Atypical Behavior in the Electron Capture Induced Dissociation of Biologically Relevant Transition Metal Ion Complexes of the Peptide Hormone Oxytocin. *Int. J. Mass Spectrom.* **2006**, *253*, 217-224.

66. van der Burgt, Y. E. M.; Palmblad, M.; Dalebout, H.; Heeren, R. M. A.; Deelder, A. M. Electron Capture Dissociation of Peptide Hormone Changes Upon Opening of the Tocin Ring and Complexation with Transition Metal Cations. *Rapid Commun. Mass Spectrom.* **2009**, *23*, 31-38.

67. Iavarone, A. T.; Paech, K.; Williams, E. R. Effects of Charge State and Cationizing Agent on the Electron Capture Dissociation of a Peptide. *Anal. Chem.* **2004**, *76*, 2231-2238.

68. Flick, T. G.; Donald, W. A.; Williams, E. R. Electron Capture Dissociation of Trivalent Metal Ion-Peptide Complexes. *J. Am. Soc. Mass Spectrom.* **2013**, *24*, 193-201.

69. Dong, J.; Vachet, R. W. Coordination Sphere Tuning of the Electron Transfer Dissociation Behavior of Cu(II)-peptide Complexes. *J. Am. Soc. Mass Spectrom.* **2012**, *23*, 321-329.

70. Asakawa, D.; Takeuchi, T.; Yamashita, A.; Wada, Y. Influence of Metal–Peptide Complexation on Fragmentation and Inter-Fragment Hydrogen Migration in Electron Transfer Dissociation. *J. Am. Soc. Mass Spectrom.* **2014**, *25*, 1029-1039.

71. Asakawa, D.; Wada, Y. Electron Transfer Dissociation Mass Spectrometry of Peptides Containing Free Cysteine Using Group XII Metals as a Charge Carrier. *J Phys Chem B* **2014**, *118*, 12318-12325.

72. Commodore, J. J.; Cassady, C. J. The Effects of Trivalent Lanthanide Cationization on the Electron Transfer Dissociation of Acidic Fibrinopeptide B and its Analogs. *J. Am. Soc. Mass Spectrom.* **2016**, *27*, 1499-1509.

73. Linstrom, P. J.; Mallard, W. G., Eds.; In *NIST Chemistry WebBook, NIST Standard Reference Database Number 69;* Hunter, E.P.; Lias, S. G: National Institute of Standards and Technology, Gaithersburg MD, 20899, (accessed Feb 5, 2016).

74. Chan, W. Y. K.; Chan, T. W. D. Natural Structural Motifs that Suppress Peptide Ion Fragmentation after Electron Capture. *J. Am. Soc. Mass Spectrom.* **2010**, *21*, 1235-1244.

75. Wong, P. S. J.; Chen, X.; Deng, L.; Wang, Z.; Li, W.; Wong, Y. L. E.; Chan, T. W. D. Suppression of Peptide Ion Dissociation Under Electron Capture: Role of Backbone Amide Hydrogen. *Rapid Commun. Mass Spectrom.* **2015**, *29*, 1757-1764.

76. Li, W.; Song, C.; Bailey, D. J.; Tseng, G. C.; Coon, J. J.; Wysocki, V. H. Statistical Analysis of Electron Transfer Dissociation Pairwise Fragmentation Patterns. *Anal. Chem.* **2011**, *83*, 9540-9545.

77. Chan, W. C.; White, P. D. *Fmoc Solid Phase Peptide Synthesis A Practical Approach;* Oxford University Press Inc., New York: 2000.

78. Roepstorff, P.; Fohlman, J. Proposal for a Common Nomenclature for Sequence Ions in Mass Spectra of Peptides. *Biomed. Mass Spectrom.* **1984**, *11*, 601.

79. Biemann, K. Contributions of Mass-Spectrometry to Peptide and Protein-Structure. *Biomed. Environ. Mass Spectrom.* **1988**, *16*, 99-111.

80. Ewing, N. P.; Zhang, X.; Cassady, C. J. Determination of the Gas-Phase Basicities of Proline and its Di- and Tripeptides with Glycine: The Enhanced Basicity of Prolylproline. *J. Mass Spectrom.* **1996**, *31*, 1345-1350.

81. Harrison, A. G. The Gas-phase Basicities and Proton Affinities of Amino Acids and Peptides. *Mass Spectrom. Rev.* **1997**, *16*, 201-217.

82. Martens, J. K.; Grzetic, J.; Berden, G.; Oomens, J. Gas-phase Conformations of Small Polyprolines and their Fragment Ions by IRMPD Spectroscopy. *Int. J. Mass Spectrom.* **2015**, *377*, 179-187.

83. Chalkley, R. J. Improving Peptide Identification Using Empirical Scoring Systems. *Methods Mol. Biol.* **2013**, 173-182.

84. Creese, A. J.; Cooper, H. J. The Effect of Phosphorylation on the Electron Capture Dissociation of Peptide Ions. *J. Am. Soc. Mass Spectrom.* **2008**, *19*, 1263-1274.

85. Mikesh, L. M.; Ueberheide, B.; Chi, A.; Coon, J. J.; Syka, J. E. P.; Shabanowitz, J.; Hunt, D. F. The Utility of ETD Mass Spectrometry in Proteomic Analysis. *Biochim. Biophys Acta.* **2006**, *1764*, 1811-1822.

86. Li, Z.; Matus, M. H.; Velazquez, H. A.; Dixon, D. A.; Cassady, C. J. Gas-phase Acidities of Aspartic Acid, Glutamic Acid, and Their Amino Acid Amides. *Int. J. Mass Spectrom.* **2007**, *265*, 213-223.

87. Feng, C. Electron Transfer Dissociation Mass Spectrometry Studies of Peptides, Ph. D. Dissertation, The University of Alabama, Tuscaloosa, AL, USA, 2014.

88. Fung, Y. M. E.; Duan, L.; Chan, T. W. D. A Comparative Study of the Collision-induced Dissociation and the Electron Capture Dissociation of Model Peptides Using Electrospray Ionization Fourier-Transform Mass Spectrometry. *Eur. J. Mass Spectrom.* **2004**, *10*, 449-457.

89. Pu, D.; Vincent, J. B.; Cassady, C. J. The Effects of Chromium(III) Coordination on the Dissociation of Acidic Peptides. *J. Mass Spectrom.* **2008**, *43*, 773-781.

90. Cooper, H. J.; Hudgkins, R. R.; Håkansson, K.; Marshall, A. G. Characterization of Amino Acid Side Chain Losses in Electron Capture Dissociation. *J. Am. Soc. Mass Spectrom.* **2002**, *13*, 241-249.

91. Xia, Q.; Lee, M.; Rose, C.; Marsh, A.; Hubler, S.; Wenger, C.; Coon, J. Characterization and Diagnostic Value of Amino Acid Side Chain Neutral Losses Following Electron-Transfer Dissociation. *J. Am. Soc. Mass Spectrom.* **2011**, *22*, 255-264.

92. Savitski, M. M.; Nielsen, M. L.; Zubarev, R. A. Side-chain Losses in Electron Capture Dissociation to Improve Peptide Identification. *Anal. Chem.* **2007**, *79*, 2296-2302.

# CHAPTER 5: ELECTRON TRANSFER DISSOCIATION MASS SPECTROMETRY OF ACIDIC PHOSPHORYLATED PEPTIDES CATIONIZED WITH TRIVALENT PRASEODYMIUM

## 5.1 Overview

The lanthanide ion praseodymium, $Pr^{3+}$, was employed to study metal-adducted ion formation and electron transfer dissociation (ETD) of twenty-six biological and model highly acidic phosphorylated peptides. All peptides investigated form metal-adducted ions that can be isolated and studied by ETD to yield useful peptide sequence information. Model acidic phosphorylated hexa- and octa-peptides form predominantly $[M + Pr – H]^{2+}$ by electrospray ionization (ESI). Limited sequence coverage occurs from ETD of $[M + Pr – H]^{2+}$. Biological peptides that form $[M + Pr]^{3+}$ undergo more backbone cleavage than $[M + Pr – H]^{2+}$ and, in some cases, full ETD sequence coverage occurs. Heat shock protein fragment was the only peptide to form 2+, 3+, and 4+ ions. Formation of $[M + Pr + H]^{4+}$ may be due to the presence of at least one residue with a highly basic side chain that may facilitate addition of an extra proton. This 4+ ion yields extensive fragmentation and full sequence coverage. For model hexa- and octapeptides, more sequence coverage occurs when the phosphorylated residue is located in the middle of the sequence than at either the N- or C-terminus. Electron transfer dissociation of $[M + Pr – H]^{2+}$ for AAAAAApTA generates y-ions instead of the z-ions observed for the phosphoseryl and phosphotyrosyl analogs. All peptides studied form exclusively metallated ETD product ions except for PDGF (pTyr Y-8P). The results of this study indicate that ETD is a promising tool for sequencing highly acidic phosphorylated peptides complexed with $Pr^{3+}$.

## 5.2 Introduction

Post-translational modifications are ubiquitous in nature and allow the function of a peptide or protein to be altered via covalent interactions.[1,2] Phosphorylation is a common post-translational modification process that assists in regulation of specific functions in eukaryotic systems. Such processes involve signal transduction, amplification and apoptosis,[3] carcinogenesis,[4] cell differentiation, and cell signaling that alter and direct protein-protein interactions.[5] As many as one third of eukaryotic proteins are phosphorylated.[6,7] Serine, threonine, and tyrosine are the three commonly phosphorylated amino acid residues with hydroxyl groups reversibly replaced by phosphate groups. These phosphorylated amino acid residues are shown in Figure 2.19. About 90% of phosphorylated residues in nature are phosphoseryl (pS), while phosphothreonyl (pT) and phosphotyrosyl (pY) exist in lower abundances collectively contributing to the remaining 10%.[8] A few other amino acid residues including cysteine, histidine, arginine, lysine, aspartic acid, glutamic acid and glycine have been known to undergo phosphorylation although to a much lesser extent than serine, threonine, and tyrosine.[9] According to the database PhosphoNET, about 80% of human coding genes contain phosphorylated proteins.[10]

Several factors contribute to the difficulty encountered when analyzing phosphorylated peptides. Phosphorylated peptides tend to exist in lower abundances in nature than their non-phosphorylated counterparts.[11] In addition, the process is reversible and typically has a short lifetime. A single biomolecule can contain multiple sites for phosphorylation, and the presence of isoforms can further complicate analysis. Mass spectrometry has emerged as an important tool for analysis of phosphopeptides due to its high sensitivity and its ability to locate the site of the phosphorylated residues in the peptide chain.[12,13]

Collison-induced dissociation (CID) is commonly employed as an automated tandem mass spectrometry technique (MS/MS) for phosphorylated peptide analysis in the positive ion mode. The capability of almost every mass spectrometer to perform CID contributes to its widespread use. However, CID may be plagued with loss or migration of the labile phosphate group[11,14,15] as a low energy process upon collisional activation, which hinders identification of phosphorylated sites along the peptide backbone. Electron-induced dissociation techniques, such as electron capture dissociation (ECD) and electron transfer dissociation (ETD), usually preserve the site of phosphorylation due to more random and nonergodic fragmentation. Several studies on protonated peptides and protein ions have demonstrated the ability of ECD and ETD to provide abundant sequence information as well as location of phosphorylated sites.[11,16-24] However, ECD and ETD can be limited by the fact that the processes generally require ions with a charge of 2+ or greater since capture or transfer of an electron to the charged species occurs. Addition of an electron to a singly charged ion (1+) would result in a neutral molecule that cannot be analyzed by mass spectrometry.

Formation of multiply charged ions from phosphorylated peptides can be difficult. Low positive ion mode ionization efficiencies sometimes occur in ESI and matrix-assisted laser desorption ionization (MALDI) involving phosphorylated peptides.[11,25,26] In addition, highly acidic phosphorylated peptides such as those employed in the current study, often contain one or more acidic aspartic and or glutamic acid residues in the same sequence with the phosphorylated residue. Acidic and phosphate groups have a high propensity for deprotonation as represented by their pKa's [27] and gas-phase acidities (GAs)[28,29]. Refer to Table 5.1 for GAs of the phosphorylated amino acid amides. Amide groups at the C-terminus are reflective of an amino acid incorporated within a peptide sequence. The phosphorylated residues are more acidic than

Table 5.1. Experimental GAs ($\Delta G_{acid}$) for acidic and phosphorylated amino acid amides

| Compound | ΔG expt (kJ/mol)[a] |
|---|---|
| **Aspartic acid amide (D)** | 1366 ± 15 |
| **Glutamic acid amide (E)** | 1375 ± 20 |
| **Phosphorylated serine amide (pS)** | 1314 ± 18 |
| **Phosphorylated threonine amide (pT)** | 1319 ± 14 |
| **Phosphorylated tyrosine amide (pY)** | 1285 ± 17 |

[a]Experimental gas-phase acidities (GAs) are from References 28 and 29. A lower numerical GA value indicates a more acidic compound.

aspartic or glutamic acid residues by about 50-90 kJ/mol, so their presence contributes that much more acidic character to any peptide. Therefore, these acidic phosphorylated peptides may be more favorable for negative mode analysis. Several studies have employed negative mode CID[15,30-37] and electron-induced dissociation[38-40]. However, some CID reports[35,41-44] indicate that negative mode analyses may generate product ions that are not sequence informative and involve small neutral molecules and phosphorylated residue losses. Negative mode electron-induced analysis seems to undergo less neutral loss processes than positive mode CID. However, negative electron based analysis can be challenging because Coulomb repulsion limits the ability of an anion and an electron to come into close proximity. This leads to low dissociation efficiencies and lower intensities of product ions.

Complexation of peptides with metal ions can assist in the formation of ions with multiple charges. Work discussed in Chapters 3 and 4[45,46] demonstrates the use of trivalent lanthanide metal ions to facilitate the formation of multiply charged metallated ions by ESI.

These ions undergo abundant fragmentation by ETD to yield full peptide sequence information. For phosphorylated peptides, deprotonation may occur on the phosphate group,[19,28] therefore extra protons may be needed to achieve a positive charge state of 2+ or greater. However, peptide size may restrict addition of three or more protons. A single trivalent lanthanide cation can alleviate the need for several protons by imparting a charge of 3+ that is suitable for ETD and will compensate for the deprotonation of a phosphate group.

Although the use of ionization with metals is not yet routine in proteomics research, there is an increasing body of scientific work involving ECD and ETD of metal-adducted peptides.[38,45-62] These three studies have focused on metal cationization of phosphorylated peptides.[38,61,62] In a report involving metal oxides, Hakansson and Kweon[38] determined the sites of phosphorylation of peptides containing multiple phosphorylated sites using ECD. Mosley and coworkers[61] employed lanthanide metal (III)-ligand complexes to analyze phosphorylated peptides. This group obtained full peptide sequence coverage by ECD as well as unambiguous location of phosphorylated residues. The identity of the lanthanide metal ion also affected the amount of fragmentation obtained, although the easily reduced $Eu^{3+}$ in the Eu(III)-peptide complex provided limited peptide sequence coverage by ECD. In a recent ETD investigation involving zinc (II)-peptide complexes, Asakawa and Osaka[62] observed increased charge states of phosphorylated peptides leading to more sequence coverage and identification of the phosphorylation site.

In the current study, we investigate the effect of metal adduction on ETD of acidic model and biological phosphorylated peptides. In addition, this work probes the effects of location and identity of phosphorylated residue as well as chain length on ETD of metal-adducted acidic

phosphorylated peptides. This complements the work of Chapters 3 and 4, which focus on metal cationization of non-phosphorylated acidic peptides.[45,46]

## 5.3 Experimental

### 5.3.1 Mass spectrometry

All experiments were performed on the Bruker (Billerica, MA, USA) HCTultra PTM Discovery System high capacity quadrupole ion trap (QIT) mass spectrometer equipped with ESI. The needle was held at ground and a high voltage of -3.5 kV was applied to the capillary entrance, the stainless steel end caps, and the capillary entrance cap. Nitrogen gas served as both the drying gas and the nebulizing gas. Drying gas was heated to 260°C and flowed at 5-10 L/min, while the nebulizing gas pressure was optimized between 5 and10 psi. Metal salt and acidic peptide mixtures at a 10:1 $Pr^{3+}$:peptide molar ratio were infused using a KD Scientific (Holliston, MA, USA) syringe pump. The final peptide concentration was 5 μM in a solvent system of acetonitrile: water at a 50:50 volume ratio. All spectra shown are the result of signal averaging 200 scans.

The ETD reagent anion, fluoranthene, was generated in a negative chemical ionization (nCI) source with methane serving as the nCI reagent gas. The anion/cation reaction times were set in the range of 180-250 ms and the lower end m/z cutoff to 120. Reagent anion accumulation was set between 8-12 ms and the ion charge control (ICC) value between 300, 000-400, 000 to maximize transfer of the electron. Immediately following the anion/cation reaction, the "smart decomposition" function was activated to further dissociate any charge reduced (ETnoD) ions. Smart decomposition enhances observed ETD product ions by using resonant excitation to overcome attractive forces (e.g., hydrogen or noncovalent bonding) that may keep peptide

fragments together following the electron transfer process. Smart decomposition is described in more detail in Section 2.4.2.

### 5.3.2 Peptides

Human epidermal growth factor receptor, EGF (988-998) and heat shock protein fragment (hsp) were purchased from Bachem Americas, Inc. (Torrance, CA, USA). The other acidic biological peptides were custom synthesized by Biomatik (Wilmington, Delaware, USA). They are epidermal growth factor receptor (DL-6), platelet-derived growth factor beta-receptor hormone (pTyrY-8P), platelet-derived growth factor beta-receptor hormone (PTyrL-5P), DNA transcription inhibitory peptide and its phosphothreonyl and phosphotyrosyl analogs. All model peptides were synthesized in the Cassady group laboratory with an Advanced ChemTech Model 90 peptide synthesizer (Louisville, KY, USA) using standard Fmoc protocol as discussed in Section 2.6.[63] Praseodymium(III) nitrate salt was purchased from Alfa Aesar (Ward Hill, MA, USA). Ultrapure Milli-Q 18Ω water was produced with a Barnstead (Dubuque, IA, USA) E-pure system.

## 5.4 Results and discussion

Spectra are labeled using the established peptide cleavage nomenclature of Roepstorff and Fohlman[64] as modified by Biemann[65] to keep track of the number of hydrogens incorporated into product ions formed by ETD. A prime symbol to the left indicates loss of a hydrogen (i.e., $^{/}c_n = [c_n - H]^+$) and to the right indicates addition of hydrogen (i.e., $c_n^{//} = [c_n + 2H]^+$). For easier product ion identification, the following colors are used to label spectra: non-metallated z-ions = red, non-metallated c-ions = blue, metal-adducted z-ions = bright pink, metal-adducted c-ions = green, and metal-adducted y-ions = brown. Precursor ion that did not dissociate is labeled in purple with a large purple diamond arrow head. Neutral loss products and electron transfer

without dissociation (ETnoD) ions are labeled in black. The c- and z-ions correspond to N-Cα bond cleavage, which are typically products in ECD[66-70] and ETD[71,72] processes.

### 5.4.1 Biological peptides

The sequences of the acidic phosphorylated biological peptides studied are shown in Table 5.2. These peptides contain a variety of amino acid residues and include one or more aspartic or glutamic acid residues and a phosphoseryl, phosphothreonyl, or phosphotyrosyl residue. Each peptide contains only one phosphorylated amino acid residue. Throughout this chapter, phosphoserine, phosphothreonyl, and phosphotyrosyl are abbreviated as pS, pT, and pY respectively. Phosphorylated residues at specific locations are written in bold and italicized font in the text. Peptide chain lengths vary from 5 to 14 residues.

#### 5.4.1.1. ESI ion formation

The most abundant metallated ions formed by ESI with adduction of $Pr^{3+}$ to the highly acidic biological phosphorylated peptides are $[M + Pr]^{3+}$ and $[M + Pr - H]^{2+}$, as shown in Table 5.2. Only heat shock protein fragment (hsp) also formed $[M + Pr + H]^{4+}$, with protonation undoubtedly occurring due to the presence of two highly basic arginine residues (gas-phase basicity of arginine (GB) = 1006.6 kJ/mol[73]) that can accept protons. The other peptides in this study do not contain an arginine residue. In addition, the greater length of the chain (14 amino acid residues) may allow the peptide to accept both a trivalent lanthanide metal ion and a proton. Conversely, the highly acidic nature of pY in hsp still allows some deprotonation to occur and form $[M + Pr - H]^{2+}$, albeit in lesser abundance than $[M + Pr]^{3+}$ and $[M + Pr + H]^{4+}$.

The hendecapeptide EGF(988-998) forms $[M + Pr - H]^{2+}$ and $[M + Pr]^{3+}$. In Chapter 4,[45] we postulated that a proline residue, which is the fifth most basic amino acid residue[74]

Table 5.2. ESI ion formation and corresponding ETD product ions for acidic phosphorylated biological peptides cationized by $Pr^{3+}$.

| Peptide name | Number of residues | Number of acidic residues[a] | Sequence[b,c] | Metallated ion formed by ESI | $c_n$-ions | $z_n$- ions |
|---|---|---|---|---|---|---|
| **PDGF beta-receptor (pTyrL-5P)** | 5 | 2 | ***pY*$^{1}$VPM**L**$^{5}$** | $[M + Pr - H]^{2+}$ | $[^{/}c_n + Pr]^{+}$, n = 3, 4 | -[d] |
| **Human epidermal growth factor receptor (DL-6)** | 6 | 4 | **D$^{1}$**AN**E$^{4}$*pY*$^{5}$L$^{6}$** | $[M + Pr - H]^{2+}$ | $[^{/}c_n + Pr]^{+}$, n = 5 | $[^{/}z_n + Pr]^{+}$, n = 4, 5 |
| **PDGF beta-receptor (pTyr Y-8P)** | 8 | 3 | ***pY*$^{1}$**MAPY**D$^{6}$**N**Y$^{8}$** | $[M + Pr - H]^{2+}$ | $[^{/}c_n + Pr]^{+}$, n = 6, 7 | - |
| | | | | $[M + Pr]^{3+}$ | $[^{/}c_n + Pr]^{+}$, n = 5-7 | $z_n^{/+}$, n = 2<br>$[^{/}z_n + Pr]^{+}$, n = 6, 7 |
| **DNA transcription inhibitory peptide** | 8 | 8 | **E$^{1}$D$^{2}$D$^{3}$*pS*$^{4}$D$^{5}$E$^{6}$E$^{7}$N$^{8}$** | $[M + Pr - H]^{2+}$ | $[^{/}c_n + Pr]^{+}$, n = 6, 7 | $[^{/}z_n + Pr]^{+}$, n = 6, 7 |
| | | | | $[M + Pr]^{3+}$ | $c_n^{//+}$, n = 1-3<br>$[^{/}c_n + Pr]^{+}$, n = 5-7<br>$[^{/}c_n + Pr]^{2+}$, n = 7 | $z_n^{/+}$, n = 2-4<br>$[^{/}z_n{}^{+} Pr]^{+}$, n = 6, 7 |
| **DNA transcription inhibitory peptide (pT) analog** | 8 | 8 | **E$^{1}$D$^{2}$D$^{3}$*pT*$^{4}$D$^{5}$E$^{6}$E$^{7}$N$^{8}$** | $[M + Pr - H]^{2+}$ | $[^{/}c_n + Pr]^{+}$, n = 6, 7<br>$[^{/}c_n + Pr]^{2+}$, n = 7 | $[^{/}z_n + Pr]^{+}$, n = 6, 7 |
| | | | | $[M + Pr]^{3+}$ | $c_n^{//+}$, n = 1-4<br>$[^{/}c_n + Pr]^{+}$, n = 6, 7<br>$[^{/}c_n + Pr]^{2+}$, n = 7 | $z_n^{/+}$, n = 2-4<br>$[^{/}z_n{}^{+} Pr]^{+}$, n = 6, 7 |
| **DNA transcription inhibitory peptide (pY) analog** | 8 | 8 | **E$^{1}$D$^{2}$D$^{3}$*pY*$^{4}$D$^{5}$E$^{6}$E$^{7}$N$^{8}$** | $[M + Pr - H]^{2+}$ | $[^{/}c_n + Pr]^{+}$, n = 6, 7 | $[^{/}z_n + Pr]^{+}$, n = 6, 7 |
| | | | | $[M + Pr]^{3+}$ | $c_n^{//+}$, n = 1-3<br>$[^{/}c_n + Pr]^{+}$, n = 6, 7 | $z_n^{/+}$, n = 2-4<br>$[^{/}z_n{}^{+} Pr]^{+}$, n = 6, 7 |

Table 5.2, continued.

| Peptide name | Number of residues | Number of acidic residues[a] | Sequence[b,c] | Metallated ion formed by ESI | $c_n$-ions | $z_n$- ions |
|---|---|---|---|---|---|---|
| **Human epidermal growth factor receptor, EGF(988-998)** | 11 | 5 | **D[1]**A**D[3]E[4]*pY*[5]**LIPQQ**G[11]** | $[M + Pr - H]^{2+}$ | $[^{/}c_n + Pr]^{+}$, n = 6 | $z_n^{/+}$, n = 5<br>$[^{/}z_n{}^{+} Pr]^{+}$, n = 7-10 |
| | | | | $[M + Pr]^{3+}$ | $c_n^{//+}$, n = 2-4<br>$[^{/}c_n + Pr]^{+}$, n = 5, 6, 8-10<br>$[^{/}c_n + Pr]^{2+}$, n = 10 | $z_n^{/+}$, n = 2, 3, 5, 6<br>$[^{/}z_n + Pr]^{+}$, n = 7-10<br>$[^{/}z_n + Pr]^{2+}$, n = 9, 10 |
| **Heat shock protein fragment (hsp)** | 14 | 3 | CLNRQL***pS*[7]**SGVS**E[12]**I**R[14]** | $[M + Pr - H]^{2+}$ | $[^{/}c_n + Pr]^{+}$, n = 11-13 | $[^{/}z_n + Pr]^{+}$, n = 11-13 |
| | | | | $[M + Pr]^{3+}$ | $c_n^{//+}$, n = 4-6<br>$[^{/}c_n + Pr]^{+}$, n = 13<br>$[^{/}c_n + Pr]^{2+}$, n = 10, 13 | $z_n^{/+}$, n = 1-4<br>$[^{/}z_n + Pr]^{+}$, n = 8-13<br>$[^{/}z_n + Pr]^{2+}$, n = 8, 9, 11 |
| | | | | $[M + Pr + H]^{4+}$ | $c_n^{//+}$, n = 2-6<br>$[^{/}c_n + Pr]^{+}$, n = 7-13 | $z_n^{/+}$, n = 1-7<br>$[^{/}z_n + Pr]^{+}$, n = 7-13<br>$[^{/}z_n + Pr]^{2+}$, n = 11, 12 |

[a]Acidic residues refer to the number of aspartic acid (D), glutamic acid (E), phosphorylated amino acid (pS, pT, pY), and C-terminal residues in the peptide sequence. If an aspartic acid or glutamic acid residue is located at the C-terminus, then it is counted as only one acidic residue.

[b]Bold font is used to indicate acidic residues. A number immediately following an acidic residue indicates its position in the peptide sequence.

[c]Bold italicized font is used to indicate phosphorylated amino acid residues. A number immediately following a phosphorylated residue indicates its position in the peptide sequence.

[d]- means that no ions were observed.

(GB of proline = 886.0 kJ/mol[73,75]), may accept a proton[76] and facilitate the formation of the $[M + Pr + H]^{4+}$. In previous work,[45] the twelve residue EGF(985-996) with a proline formed the 4+ species. However, EGF(988-998) with a proline, eleven amino acid residues, and a highly acidic pY formed $[M + Pr]^{3+}$ as the highest charge state ion. The facile deprotonation of the phosphorylated residue and possibly the shorter peptide chain length in EGF(988-998) may hinder the formation of $[M + Pr + H]^{4+}$.

The highly acidic octapeptide, DNA transcription inhibitory peptide, and its analogs all form $[M + Pr - H]^{2+}$ and $[M + Pr]^{3+}$. These three peptides have the sequence EDDXDEEN, where X is varied from pS in the main peptide to pT or pY in the analogs. The type of phosphorylated residue had minimal, if any, effect on the ions formed by ESI. This is consistent with the fact that the GAs of the three phosphorylated amino acid amides are very similar and highly acidic.[28] Seven of the eight amino acid residues in the peptides are acidic, which supports the formation of the deprotonated $[M + Pr - H]^{2+}$. More uncertain is the formation of abundant $[M + Pr]^{3+}$ despite the highly acidic nature of all three peptides. In the study discussed in Chapter 4,[45] a heptapeptide with six acidic residues only formed the deprotonated species, $[M + Pr - H]^{2+}$. The increase in chain length from seven to eight amino acid residues may have contributed to the formation of $[M + Pr]^{3+}$.

The peptides with less than seven amino acid residues, PDGF beta-receptor (pTyrL-5P) and human epidermal growth factor receptor (DL-6), generate only $[M + Pr - H]^{2+}$. The pentapeptide pTyrL-5P contains pY, which is the most acidic of the three phosphorylated residues, and undergoes facile deprotonation. In addition, previous work discussed in

Chapter 4[45] involving non-phosphorylated acidic peptides indicates that metal adduction consistently occurs for peptides with chain lengths of seven or greater residues. Lack of formation of 3+ and 4+ for the hexapeptide DL-6 is consistent with the fact that the peptide contains four acidic sites (including the pY residue and the C-terminal carboxyl group) that will easily deprotonate. In addition, the small size of pTyrL-5P may limit the ability of the peptide to coordinate at multiple sites to both a trivalent lanthanide metal ion and a proton.

#### 5.4.1.2 Electron transfer dissociation of biological peptides

Each multiply charged ion generated by ESI was isolated and subjected to ETD. Figure 5.1 shows the ETD spectrum of $[M + Pr + H]^{4+}$ for hsp. As with previous studies discussed in Chapters 3 and 4,[45,46] the 4+ ion yields the most extensive sequence coverage with the same type of c- and z- series. The spectrum contains a high signal-to-noise ratio (S/N) allowing for easy identification of product ions. A mix of complementary non-metallated and metal-adducted c- and z-ions form with $c_n^{//+}$ and $[^{/}c_n + Pr]^+$ as the c-series and $z_n^{/+}$ and $[^{/}z_n + Pr]^+$ as the z-series. All non-metallated c-ions contain two extra hydrogens relative to the direct backbone cleavage site while non-metallated z-ions contain one. All metal-adducted product ions contain the phosphorylated residue suggesting metal interaction with the phosphate group. In metal-based enrichment strategies, the phosphate group acts as a Lewis base and readily binds to a metal carrying a positive charge.[77] Most product ions are singly charged although a few form with a charge of 2+. Both metal-adducted c- and z-ions have one less hydrogen relative to the direct backbone cleavage site (i.e., $^{/}c_n + Pr]^+$ and $[^{/}z_n + Pr]^+$). Cooper and coworkers[18] observed peaks corresponding to $^{/}c_n = [c_n - H]^+$ as well in a phosphorylated study involving a peptide containing arginine and pS. The location of ***pS*** in hsp could be definitively identified at residue 7 by ETD of $[M + Pr + H]^{4+}$. This contrasts CID where loss or migration of the phosphate group

complicate spectra and can prevent unambiguous identification of phosphorylation sites. Definitive localization of phosphorylated residue is a major advantage of analyzing such peptides by ETD rather than by CID.

Electron transfer dissociation of $[M + Pr]^{3+}$ for the biological peptides can also provide full sequence information. For EGF(988-998) as shown in Figures 5.2, most of the c- and z-ions formed are singly charged, although a few are doubly charged. The c- and z-ions correspond to cleavage between all residues except N-terminal to proline and result in full sequence covarage. The side chain of proline forms a ring incorporating the backbone, which prevents dissociation of the peptide into two separate product ions following N-Cα bond cleavage. Previous ECD and ETD studies[11,18,19,78-80] discuss this lack of cleavage N-terminal to proline further. DNA transcription inhibitory peptide and its analogs form both non-metallated and metal-adducted c- and z-ions with mostly a charge of 1+ and a few with 2+, as shown in Figures 5.4, 5.5, and 5.6. Full sequence coverage results in unambiguous identification of the location of the phosphorylated residues in the middle of the peptide sequence. All metallated product ions contain the phosphorylated residue.

For the other biological peptides, ETD of $[M + Pr]^{3+}$ does not generate full sequence coverage. In Figure 5.3, ETD of $[M + Pr]^{3+}$ for hsp results in 71% sequence coverage. The same types of c- and z-series form as observed for previously mentioned peptides. Lack of cleavage between adjacent residues from the C-terminal side of $\boldsymbol{pS^7}$ to the N-terminal side of $V^{10}$ limits identification of the location of phosphorylation. The ETD mass spectrum of octapeptide pTyr Y-8P shown in Figure 5.7 form non-metallated and metal-adducted c- and z-ions resulting in 70% sequence coverage. Cleavages corresponding to the N- and C- terminal backbone sites of $P^4$ are absent. The absence of product ions N-terminal to proline is expected in ETD

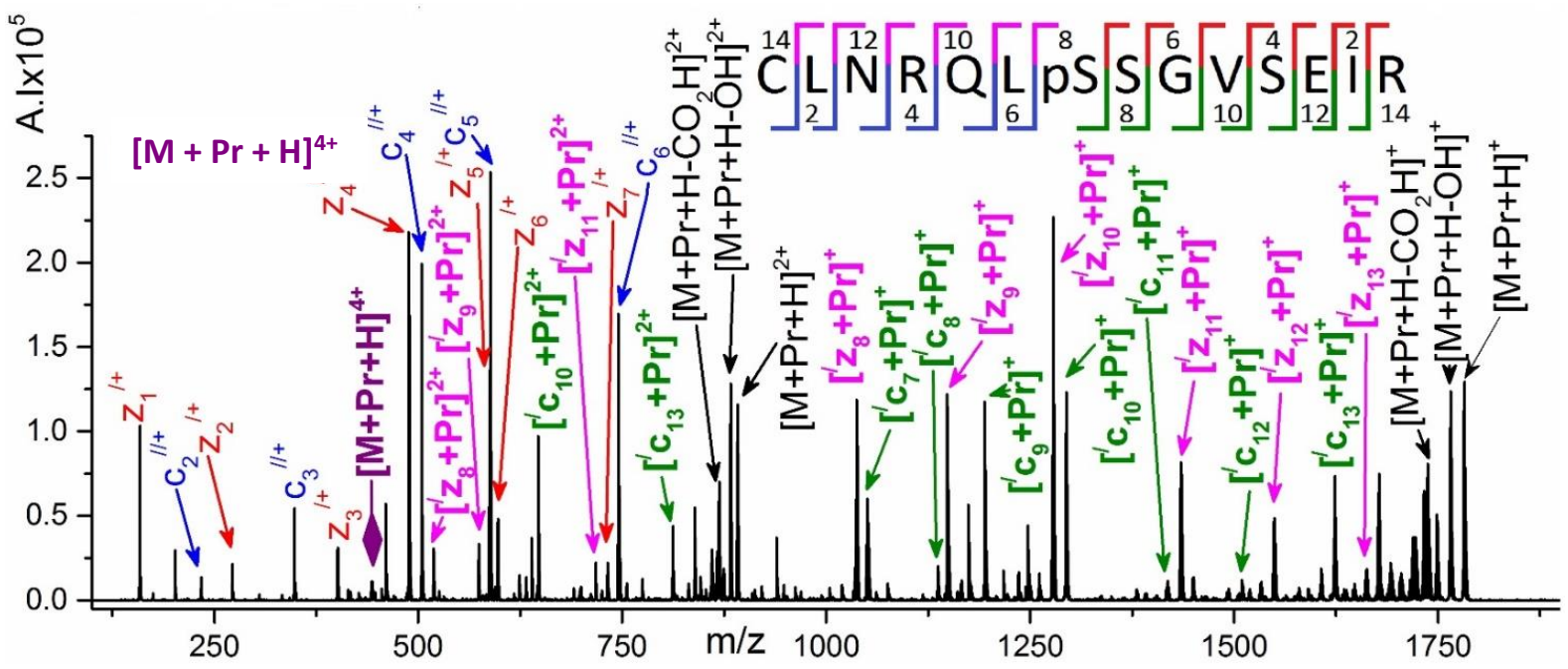


Figure 5.1. ETD mass spectrum of $[M + Pr + H]^{4+}$ for heat shock protein fragment (hsp). In the figure, the following colors are used to label the ions: non-metallated z-ions = red, non-metallated c-ions = blue, metal-adducted z-ions = bright pink, and metal-adducted c-ions = green. Undissociated precursor ion is labeled in purple with a large purple diamond arrow head. Neutral loss products and electron transfer without dissociation (ETnoD) ions are labeled in black. A prime symbol to the left indicates loss of a hydrogen (i.e., $^{/}c_n = [c_n - H]^+$) and to the right indicates the addition of a hydrogen at the cleavage site (i.e., $c_n^{//} = [c_n + 2H]^+$). The spectra have no expansion of the intensity axis; all peaks are shown to scale.

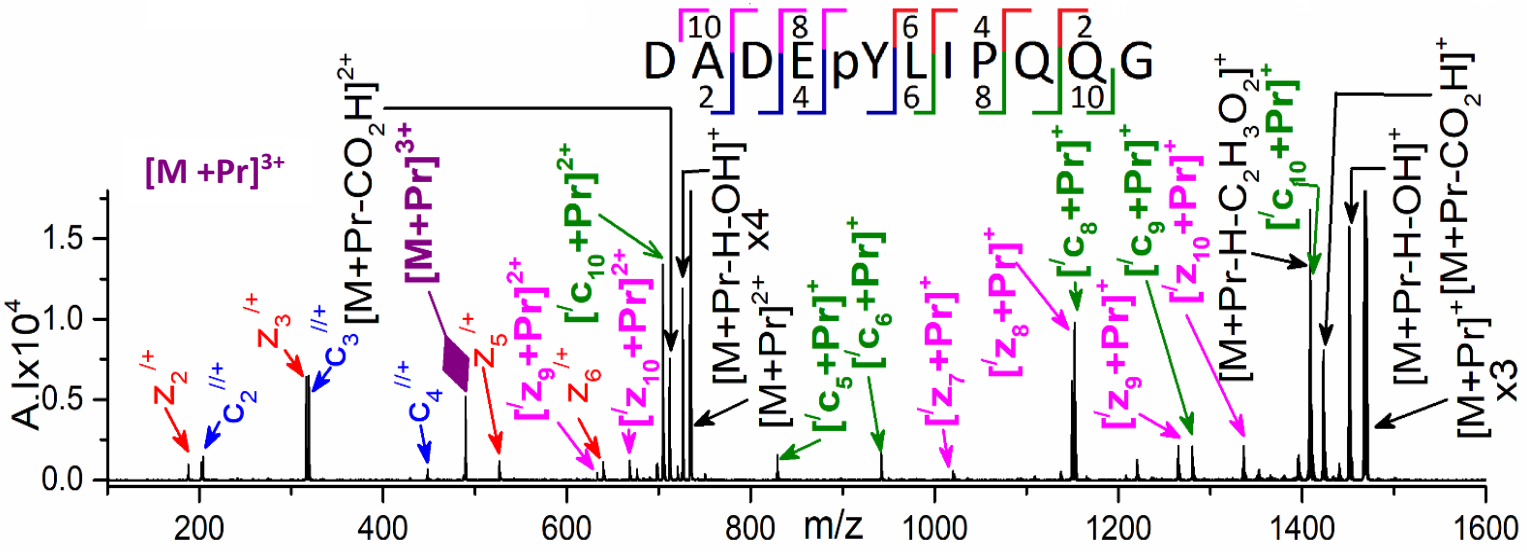


Figure 5.2. ETD mass spectrum of $[M + Pr]^{3+}$ for EGF (988-998). In the figure, the following colors are used to label the ions: non-metallated z-ions = red, non-metallated c-ions = blue, metal-adducted z-ions = bright pink, and metal-adducted c-ions = green. Undissociated precursor ion is labeled in purple with a large purple diamond arrow head. Neutral loss products and electron transfer without dissociation (ETnoD) ions are labeled in black. A prime symbol to the left indicates loss of a hydrogen (i.e., $^{/}c_n = [c_n - H]^+$) and to the right indicates the addition of a hydrogen at the cleavage site (i.e., $c_n^{//} = [c_n + 2H]^+$).

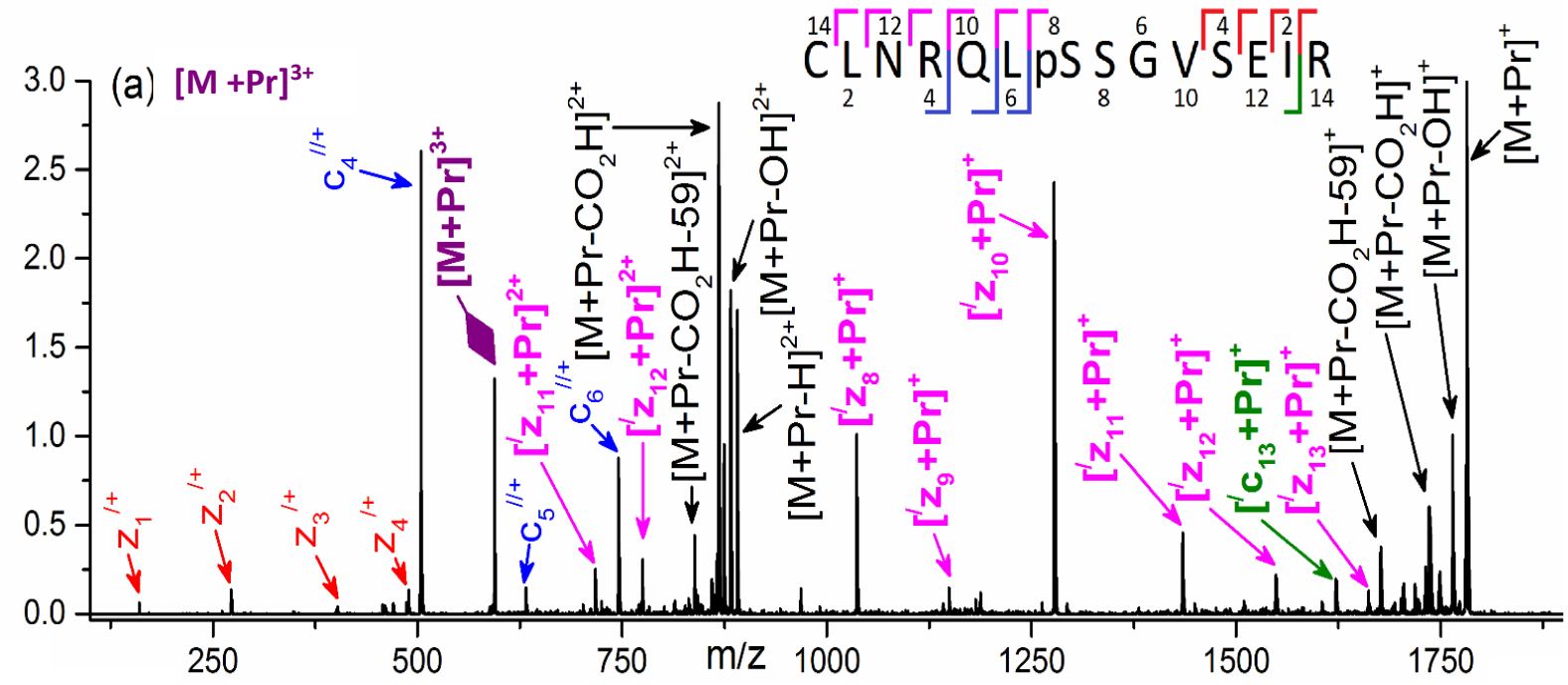


Figure 5.3. ETD mass spectrum of $[M + Pr]^{3+}$ for heat shock protein fragment (hsp). In the figure, the following colors are used to label the ions: non-metallated z-ions = red, non-metallated c-ions = blue, metal-adducted z-ions = bright pink, and metal-adducted c-ions = green. Undissociated precursor ion is labeled in purple with a large purple diamond arrow head. Neutral loss products and electron transfer without dissociation (ETnoD) ions are labeled in black. A prime symbol to the left indicates loss of a hydrogen (i.e., $^{/}c_n = [c_n - H]^+$) and to the right indicates the addition of a hydrogen at the cleavage site (i.e., $c_n^{//} = [c_n + 2H]^+$). The spectra have no expansion of the intensity axis; all peaks are shown to scale.

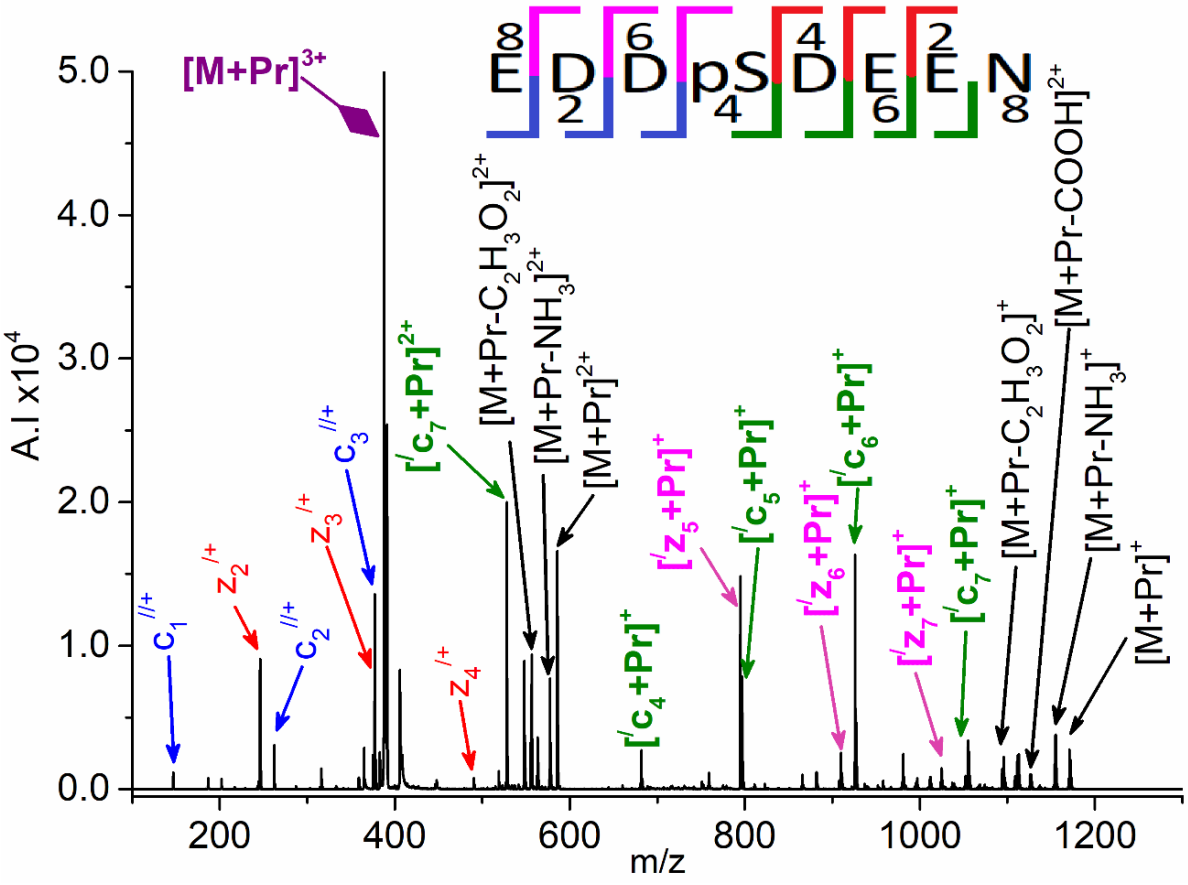


Figure 5.4. ETD mass spectrum of $[M + Pr]^{3+}$ for EDDpSDEEN. ). In the figure, the following colors are used to label the ions: non-metallated z-ions = red, non-metallated c-ions = blue, metal-adducted z-ions = bright pink, and metal-adducted c-ions = green. Undissociated precursor ion is labeled in purple with a large purple diamond arrow head. Neutral loss products and electron transfer without dissociation (ETnoD) ions are labeled in black. A prime symbol to the left indicates loss of a hydrogen (i.e., $^{/}c_n = [c_n - H]^+$) and to the right indicates the addition of a hydrogen at the cleavage site (i.e., $c_n^{//} = [c_n + 2H]^+$). The spectra have no expansion of the intensity axis; all peaks are shown to scale.

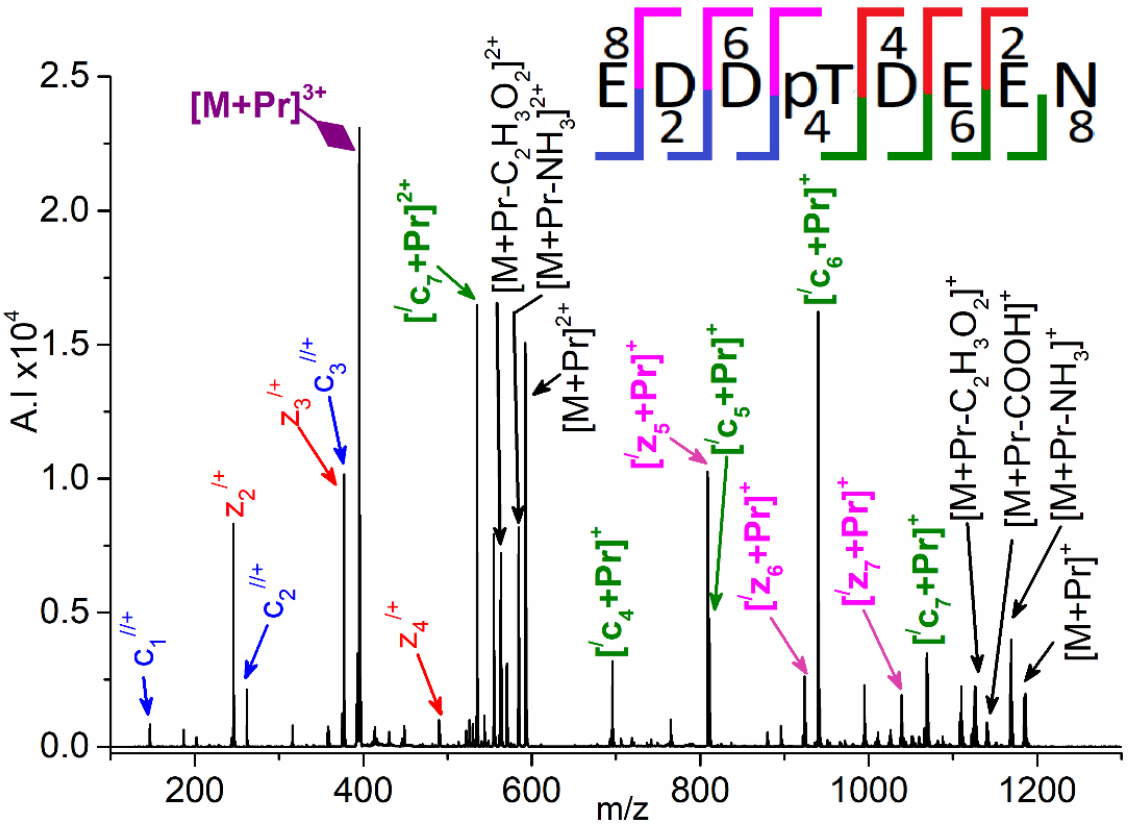


Figure 5.5. ETD mass spectrum of $[M + Pr]^{3+}$ for EDDpTDEEN. In the figure, the following colors are used to label the ions: non-metallated z-ions = red, non-metallated c-ions = blue, metal-adducted z-ions = bright pink, and metal-adducted c-ions = green. Undissociated precursor ion is labeled in purple with a large purple diamond arrow head. Neutral loss products and electron transfer without dissociation (ETnoD) ions are labeled in black. A prime symbol to the left indicates loss of a hydrogen (i.e., $^{/}c_n = [c_n - H]^+$) and to the right indicates the addition of a hydrogen at the cleavage site (i.e., $c_n^{//} = [c_n + 2H]^+$). The spectra have no expansion of the intensity axis; all peaks are shown to scale.

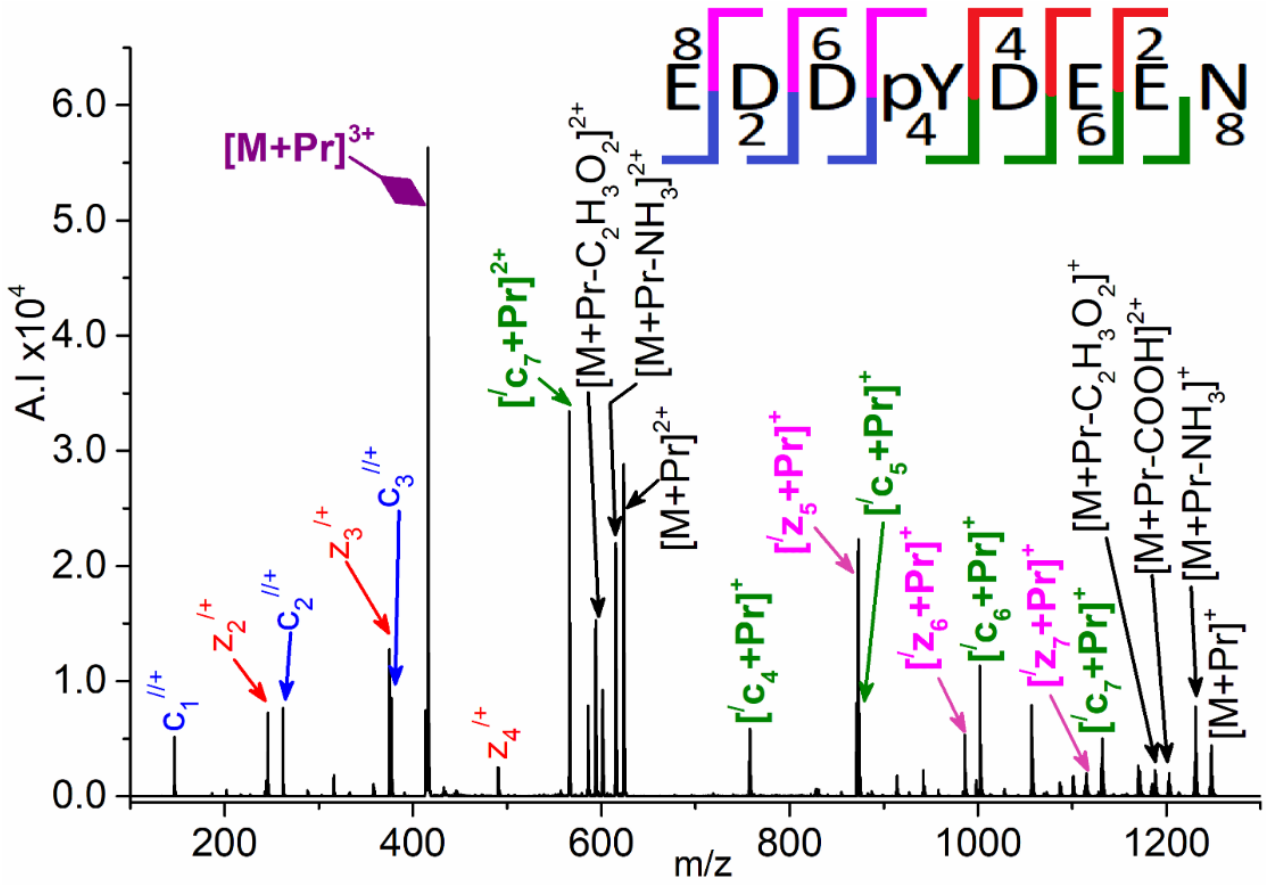


Figure 5.6. ETD mass spectrum of $[M + Pr]^{3+}$ for EDDpYDEEN. In the figure, the following colors are used to label the ions: non-metallated z-ions = red, non-metallated c-ions = blue, metal-adducted z-ions = bright pink, and metal-adducted c-ions = green. Undissociated precursor ion is labeled in purple with a large purple diamond arrow head. Neutral loss products and electron transfer without dissociation (ETnoD) ions are labeled in black. A prime symbol to the left indicates loss of a hydrogen (i.e., $^{/}c_n = [c_n - H]^+$) and to the right indicates the addition of a hydrogen at the cleavage site (i.e., $c_n^{//} = [c_n + 2H]^+$). The spectra have no expansion of the intensity axis; all peaks are shown to scale.

analysis.[19,78-80] Proline contains an aliphatic side chain that incorporates the backbone and the ring holds the two pieces of peptide together following N-Cα bond cleavage. Metal-adducted ions form that do not contain the phosphorylated residue. However, the metal-adducted ions ($^{\prime}z_n$ + Pr, n = 6, 7) contain an acidic aspartic acid residue as well as a C-terminal carboxyl group; i.e., two acidic sites. In addition, the z-ions formed by ETD of $[M + Pr]^{3+}$ for PDGF(pTyr Y-8P), as shown in Figure 5.7, form in low abundance compared to the other peptides possibly indicating that while these z-ions can be generated, the process is not favorable. This may indicate that the $Pr^{3+}$ is favorably attached to the phosphorylated residue and the majority of the electron driven process is directed by attraction at the metal-phosphoresidue location. The $Pr^{3+}$ is able to form structures involving non-phosphorylated acidic residues, but the electron attraction seems to be more favorably directed at the metal-phosphoresidue site instead of to the metal-non-phosphorylated acidic residue. In previous work discussed in Chapter 3,[45] as well as a study by Williams and coworkers[57] with non-phosphorylated acidic peptides, metal-adducted ions form when at least two acidic sites are incorporated into the product.

The least amount of sequence coverage occurs from ETD of $[M + Pr - H]^{2+}$. Figures 5.8-5.12 show ETD spectra of $[M + Pr - H]^{2+}$ for PDGF (pTyrL-5P), EGF (DL-6), PDGF (pTyr Y-8P), EGF(988-998), and hsp, respectively. The spectra contain primarily singly charged metal-adducted c- and z-ions that lose one hydrogen relative to the direct backbone cleavage product. Peptide sequence coverage occurs as follows: PDGF(pTyrL-5P) = 66%, EGF(DL-6) = 60%, PDGF(PTyrY-8P) = 33%, EGF(988-998) = 78%, and hsp = 23%. The site of phosphorylation could not be identified by ETD of $[M + Pr - H]^{2+}$ for any of the peptides due to lack of cleavage on both sides of the modified residue. Similar decreased product ion formation for ETD of $[M + Pr - H]^{2+}$ occurs in previous work discussed in Chapter 3 and 4[45,46]

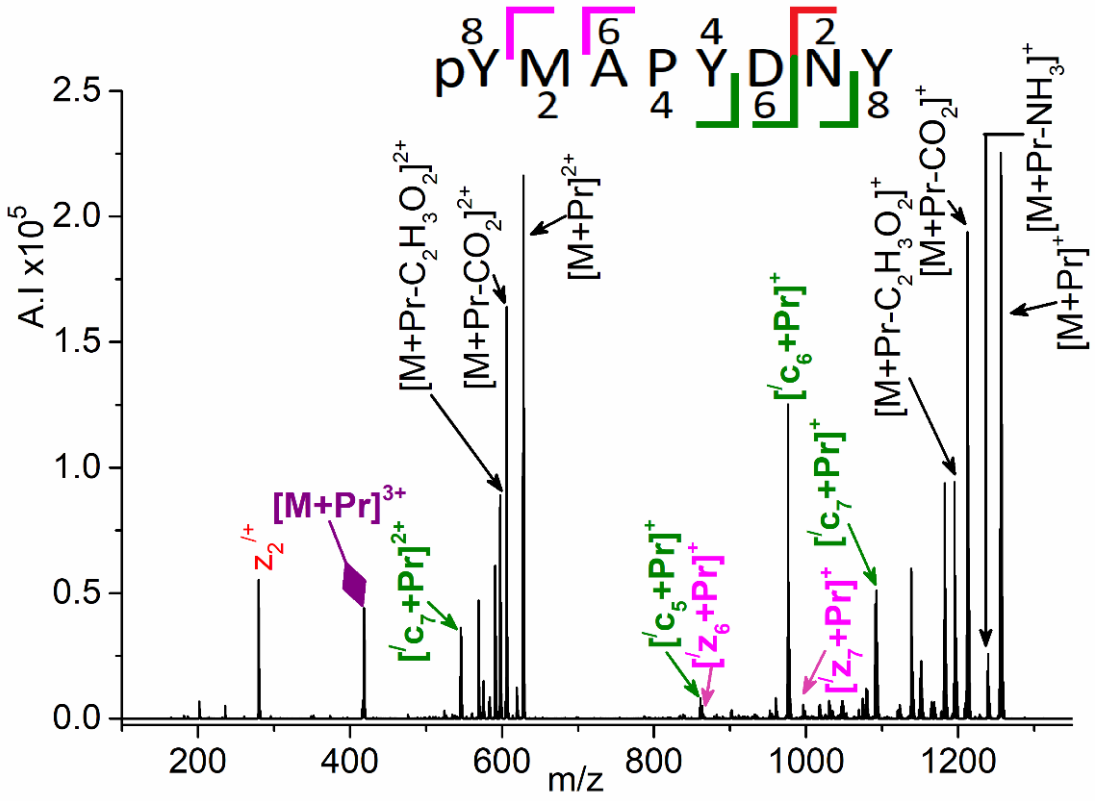


Figure 5.7. ETD mass spectrum of $[M + Pr]^{3+}$ for PDGF (pTyr Y-8P). In the figure, the following colors are used to label the ions: non-metallated z-ions = red, metal-adducted z-ions = bright pink, and metal-adducted c-ions = green. Undissociated precursor ion is labeled in purple with a large purple diamond arrow head. Neutral loss products and electron transfer without dissociation (ETnoD) ions are labeled in black. A prime symbol to the left indicates loss of a hydrogen (i.e., $^{/}c_n = [c_n - H]^+$) and to the right indicates the addition of a hydrogen at the cleavage site (i.e., $c_n^{//} = [c_n + 2H]^+$). The spectra have no expansion of the intensity axis; all peaks are shown to scale.

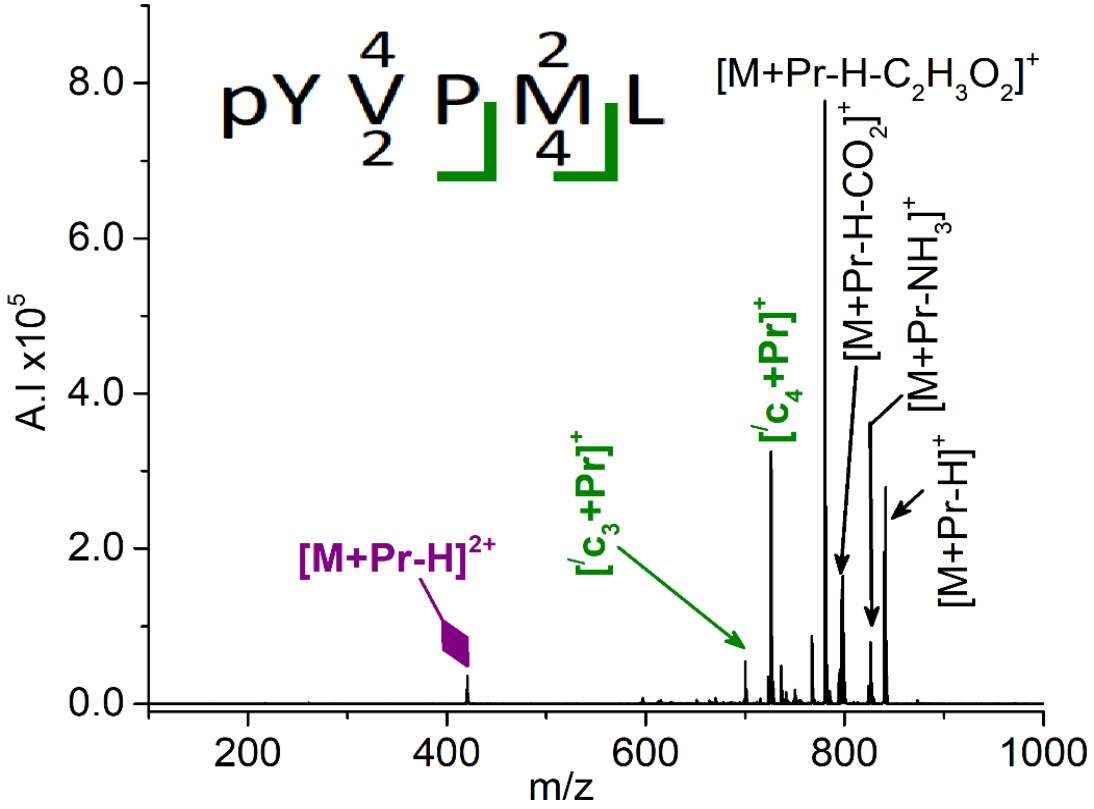


Figure 5.8. ETD mass spectrum of $[M + Pr - H]^{2+}$ for PDGF (pTyrL-5P). In the figure, the following colors are used to label the ions: metal-adducted c-ions = green. Undissociated precursor ion is labeled in purple with a large purple diamond arrow head. Neutral loss products and electron transfer without dissociation (ETnoD) ions are labeled in black. A prime symbol to the left indicates loss of a hydrogen (i.e., $^{/}c_n = [c_n - H]^+$) and to the right indicates the addition of a hydrogen at the cleavage site (i.e., $c_n^{//} = [c_n + 2H]^+$). The spectra have no expansion of the intensity axis; all peaks are shown to scale.

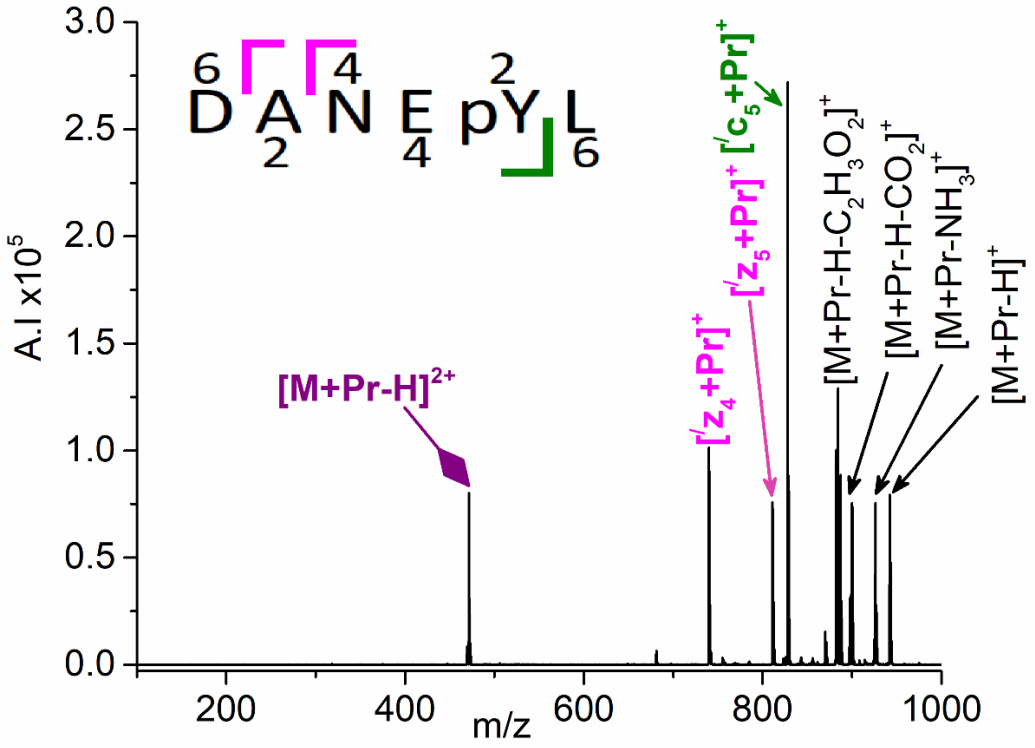


Figure 5.9. ETD mass spectrum of $[M + Pr - H]^{2+}$ for EGF (DL-6). In the figure, the following colors are used to label the ions: metal-adducted z-ions = bright pink, and metal-adducted c-ions = green. Undissociated precursor ion is labeled in purple with a large purple diamond arrow head. Neutral loss products and electron transfer without dissociation (ETnoD) ions are labeled in black. A prime symbol to the left indicates loss of a hydrogen (i.e., $^{/}c_n = [c_n - H]^+$) and to the right indicates the addition of a hydrogen at the cleavage site (i.e., $c_n^{//} = [c_n + 2H]^+$). The spectra have no expansion of the intensity axis; all peaks are shown to scale.

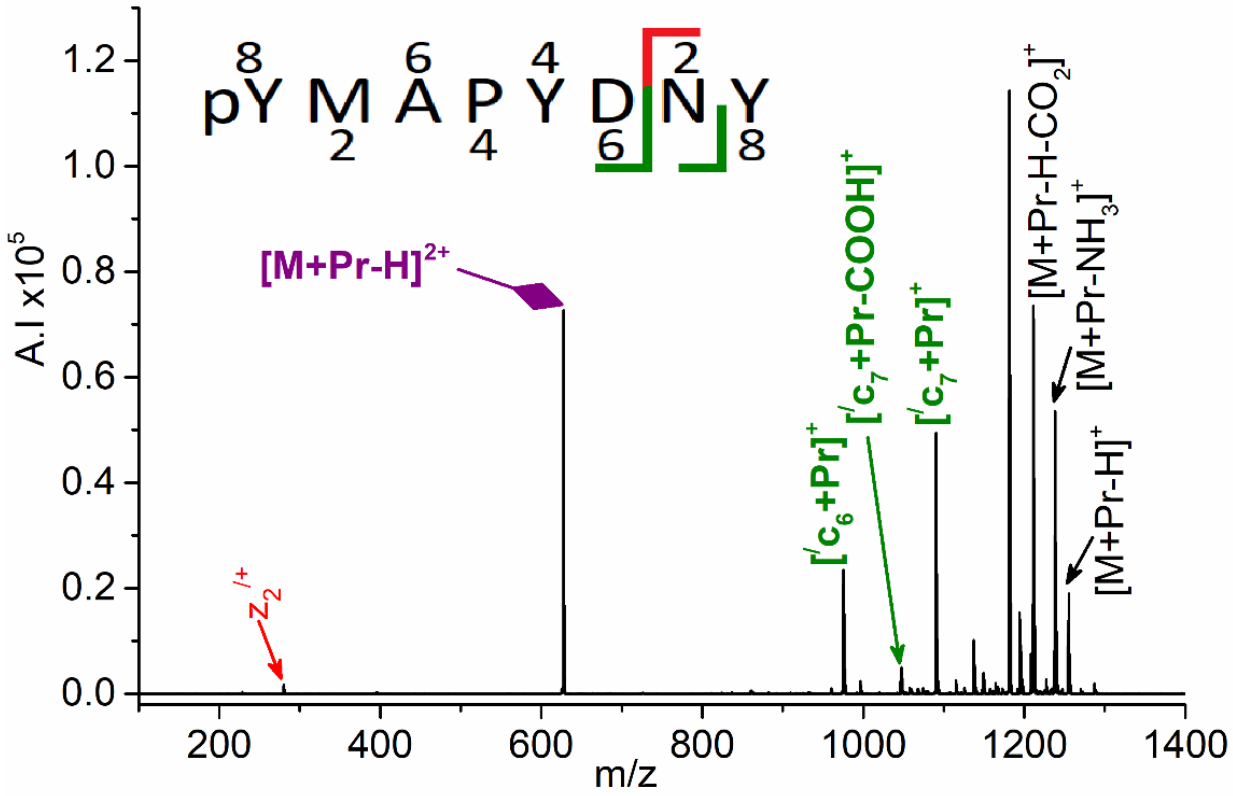


Figure 5.10. ETD mass spectrum of $[M + Pr - H]^{2+}$ for PDGF(pTyr Y-8P. In the figure, the following colors are used to label the ions: non-metallated z-ions = red, and metal-adducted c-ions = green. Undissociated precursor ion is labeled in purple with a large purple diamond arrow head. Neutral loss products and electron transfer without dissociation (ETnoD) ions are labeled in black. A prime symbol to the left indicates loss of a hydrogen (i.e., $^{/}c_n = [c_n - H]^+$) and to the right indicates the addition of a hydrogen at the cleavage site (i.e., $c_n^{//} = [c_n + 2H]^+$). The spectra have no expansion of the intensity axis; all peaks are shown to scale.

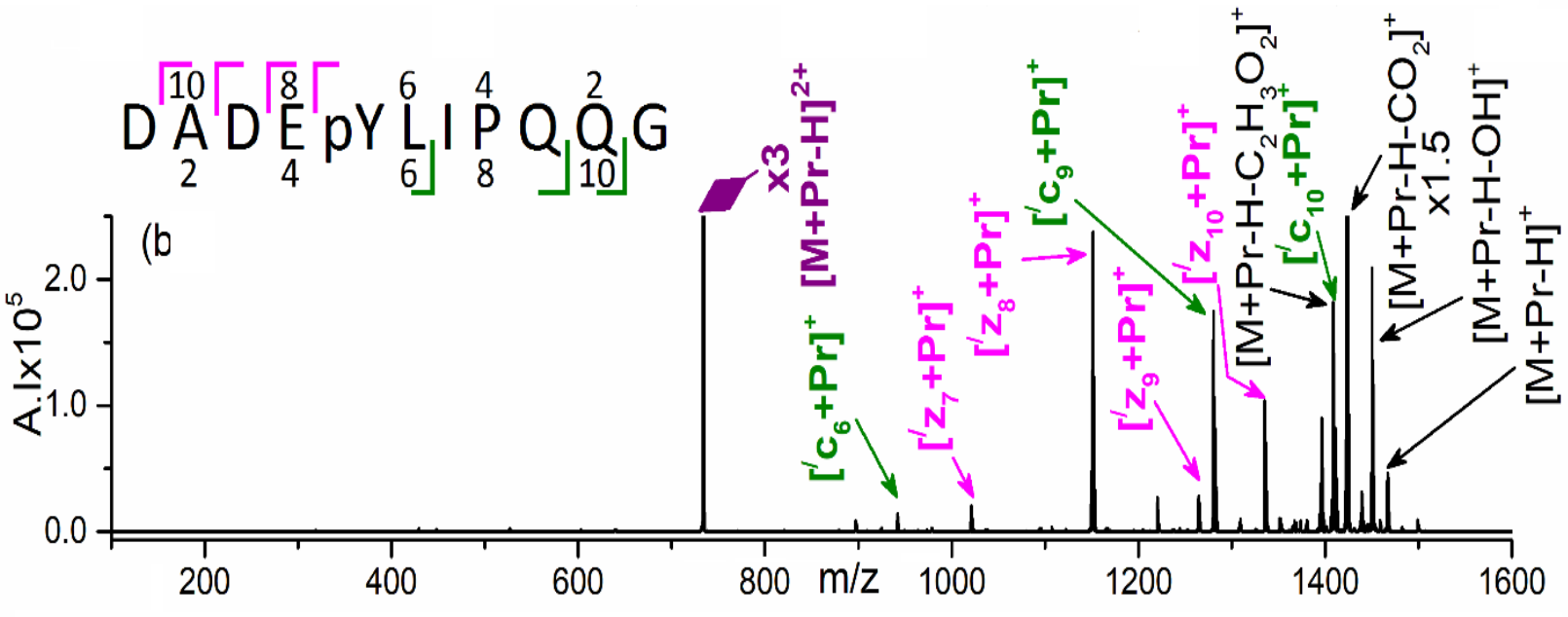


Figure 5.11. ETD mass spectrum of $[M + Pr - H]^{2+}$ for EGF(988-998). In the figure, the following colors are used to label the ions: metal-adducted z-ions = bright pink, and metal-adducted c-ions = green. Undissociated precursor ion is labeled in purple with a large purple diamond arrow head. Neutral loss products and electron transfer without dissociation (ETnoD) ions are labeled in black. A prime symbol to the left indicates loss of a hydrogen (i.e., $^{/}c_n = [c_n - H]^+$) and to the right indicates the addition of a hydrogen at the cleavage site (i.e., $c_n^{//} = [c_n + 2H]^+$).

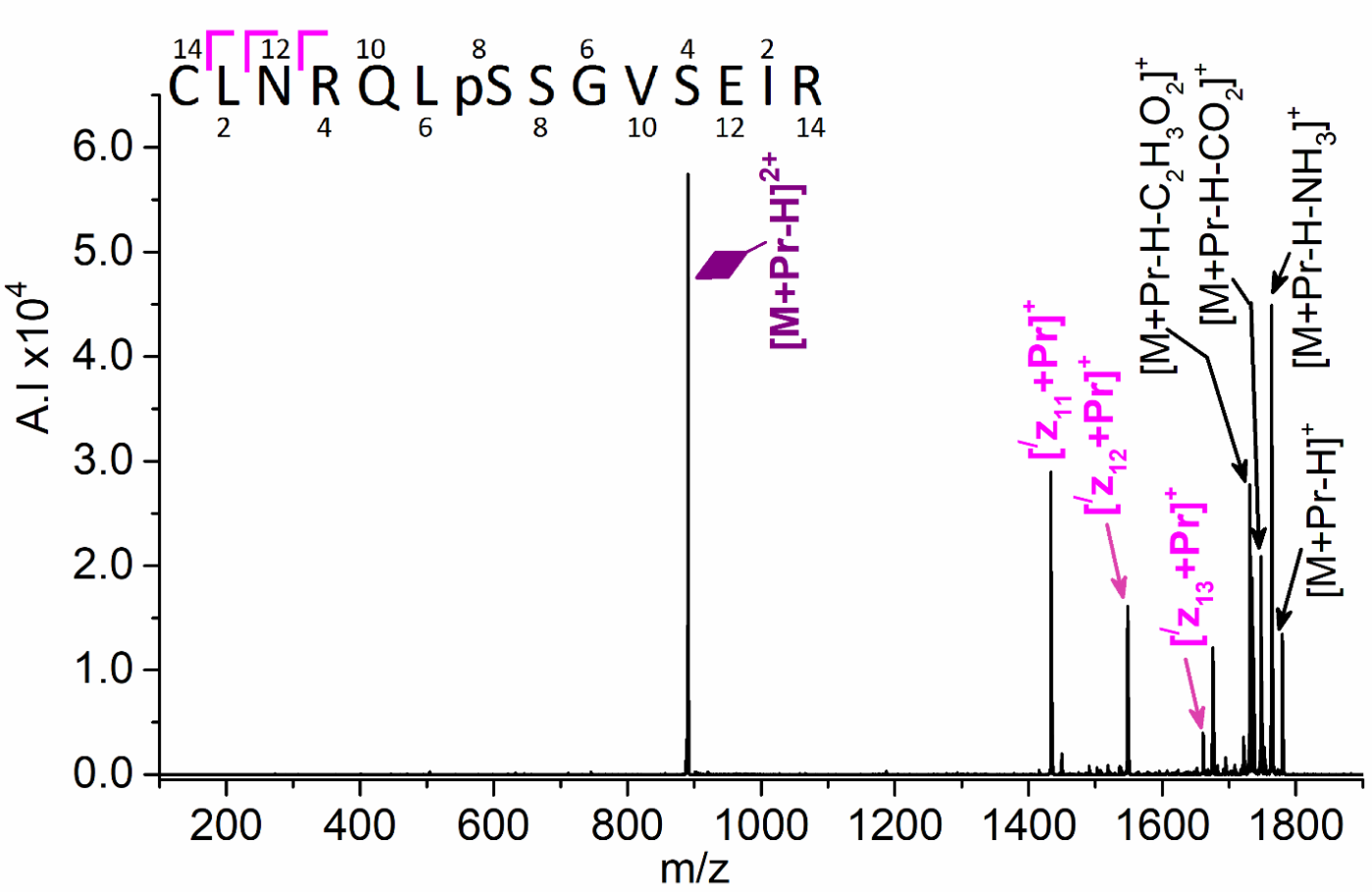


Figure 5.12. ETD mass spectrum of $[M + Pr - H]^{2+}$ for hsp. In the figure, the following colors are used to label the ions: metal-adducted z-ions = bright pink. Undissociated precursor ion is labeled in purple with a large purple diamond arrow head. Neutral loss products and electron transfer without dissociation (ETnoD) ions are labeled in black. A prime symbol to the left indicates loss of a hydrogen (i.e., $^{/}c_n = [c_n - H]^+$) and to the right indicates the addition of a hydrogen at the cleavage site (i.e., $c_n^{//} = [c_n + 2H]^+$). The spectra have no expansion of the intensity axis; all peaks are shown to scale.

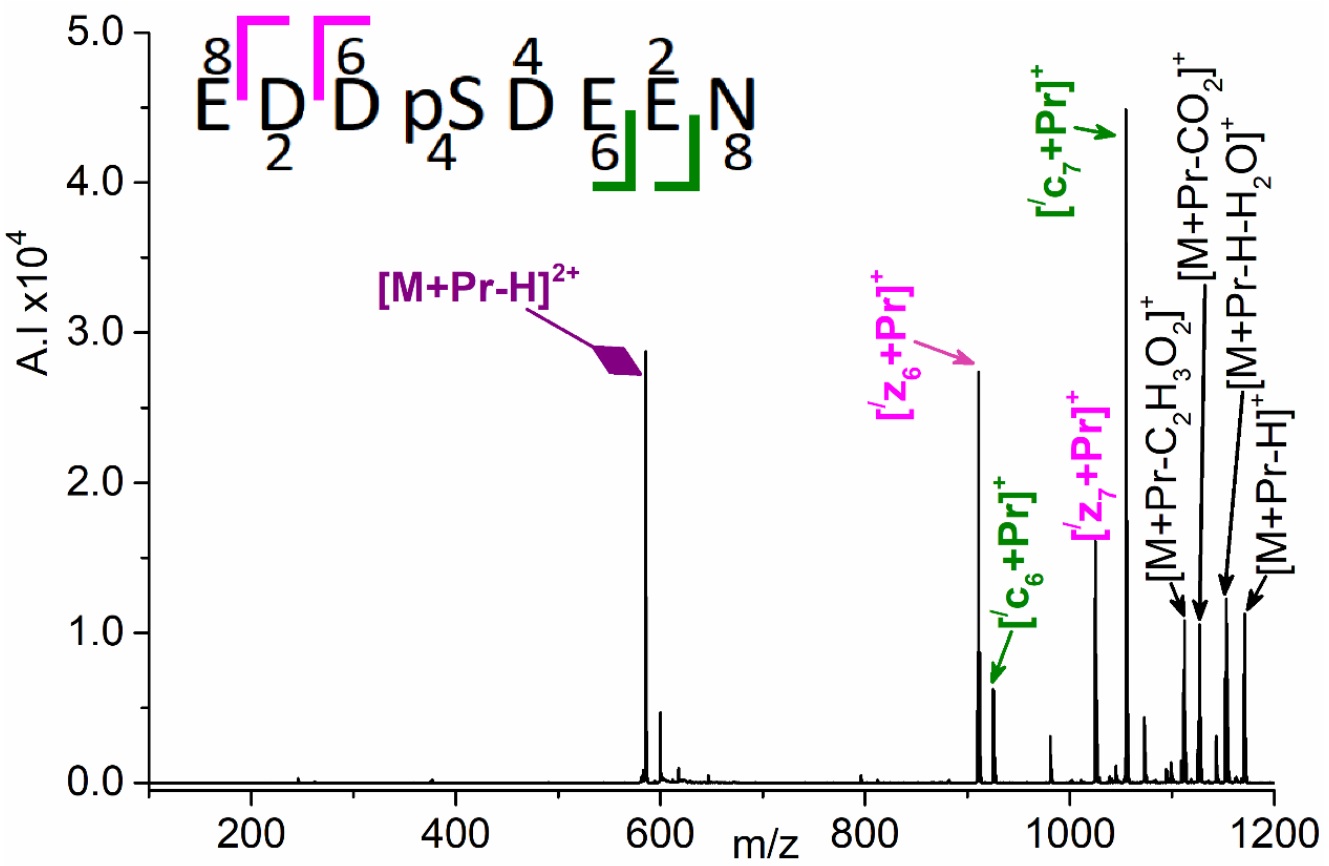


Figure 5.13. ETD mass spectrum of $[M + Pr - H]^{2+}$ for EDDpSDEEN. In the figure, the following colors are used to label the ions: metal-adducted z-ions = bright pink, and metal-adducted c-ions = green. Undissociated precursor ion is labeled in purple with a large purple diamond arrow head. Neutral loss products and electron transfer without dissociation (ETnoD) ions are labeled in black. A prime symbol to the left indicates loss of a hydrogen (i.e., $^{/}c_n = [c_n - H]^+$) and to the right indicates the addition of a hydrogen at the cleavage site (i.e., $c_n^{//} = [c_n + 2H]^+$). The spectra have no expansion of the intensity axis; all peaks are shown to scale.

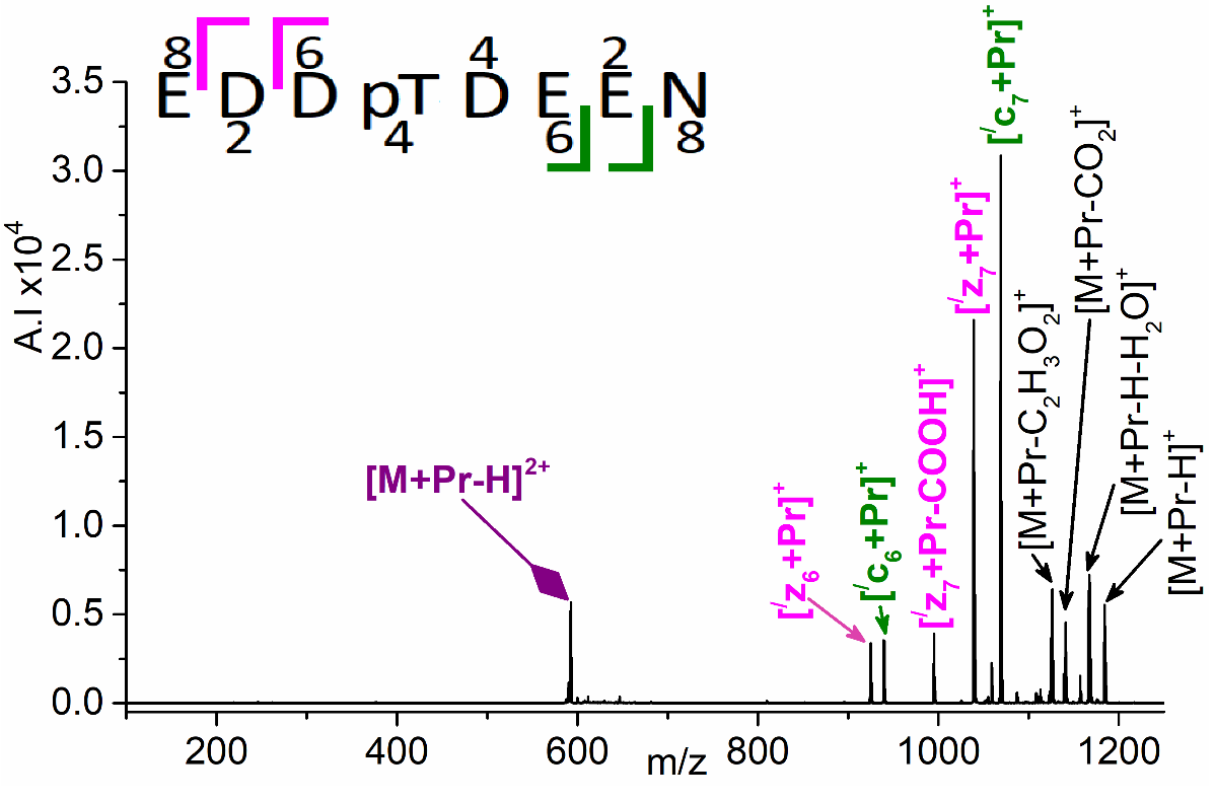


Figure 5.14. ETD mass spectrum of $[M + Pr - H]^{2+}$ for EDDpTDEEN. In the figure, the following colors are used to label the ions: metal-adducted z-ions = bright pink, and metal-adducted c-ions = green. Undissociated precursor ion is labeled in purple with a large purple diamond arrow head. Neutral loss products and electron transfer without dissociation (ETnoD) ions are labeled in black. A prime symbol to the left indicates loss of a hydrogen (i.e., $^{/}c_n = [c_n - H]^+$) and to the right indicates the addition of a hydrogen at the cleavage site (i.e., $c_n^{//} = [c_n + 2H]^+$). The spectra have no expansion of the intensity axis; all peaks are shown to scale.

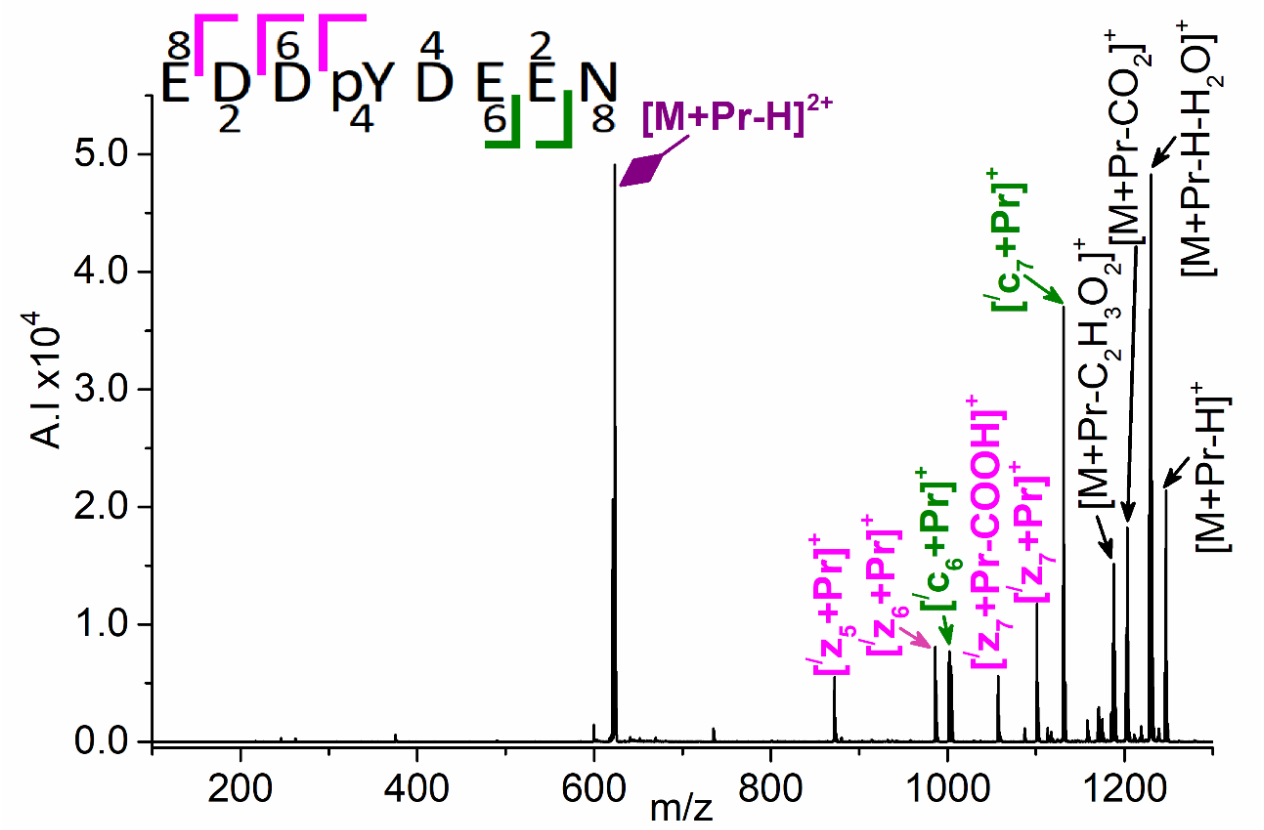


Figure 5.15. ETD mass spectrum of $[M + Pr - H]^{2+}$ for EDDpYDEEN. In the figure, the following colors are used to label the ions: non-metallated z-ions = red, non-metallated c-ions = blue, metal-adducted z-ions = bright pink, and metal-adducted c-ions = green. Undissociated precursor ion is labeled in purple with a large purple diamond arrow head. Neutral loss products and electron transfer without dissociation (ETnoD) ions are labeled in black. A prime symbol to the left indicates loss of a hydrogen (i.e., $^{/}c_n = [c_n - H]^+$) and to the right indicates the addition of a hydrogen at the cleavage site (i.e., $c_n^{//} = [c_n + 2H]^+$). The spectra have no expansion of the intensity axis; all peaks are shown to scale.

for non-phosphorylated acidic peptides as well as in a phosphorylated study by Asakawa and Osaka.[62] ETD of $[M + Pr - H]^{2+}$ of DNA transcription inhibitory peptide and its analogs yields 60% peptide sequence coverage as shown in Figures 5.13-5.15. Only singly charged metal-adducted c- and z- ions form. While cleavage at each backbone site does not occur, the mass of $z_5$ ion in Figure 5.15 indicates that the peptide contains ***pY*** at residue 4.

Neutral losses were also present in ETD spectra of the biological acidic phosphorylated peptides. All peptides exhibit a loss of 59 Da corresponding to $C_2H_3O_2$ from the side chains of aspartic and glutamic residues. The 59 Da loss was also observed in previous work involving non-phosphorylated acidic peptides discussed in Chapters 3 and 4,[45,46] as well as an ECD study to investigate side chain losses by Zubarev and coworkers.[81] Neutral losses corresponding to the phosphate group such as $H_3PO_4$ and $HPO_3$ is common in CID[17,33,82-86] and sometimes in ECD of protonated peptides.[87] However, no peaks corresponding to neutral losses associated with the side chain of the phosphate group were observed for this study.

### 5.4.2 Model peptides

Several model peptides were investigated to determine the effect of structural features on ion formation by ESI and on ETD of acidic phosphorylated peptides adducted to $Pr^{3+}$. Factors considered include the type of phosphorylated amino acid residue, location of the residue within the sequence, and peptide chain length. Nine hexapeptides and nine octapeptides were studied and are listed in Table 5.3. The hexapeptides have the general sequences pXAAAAA (pXA5), AApXAAA (A2pXA3), and AAAApXA (A4pXA), and the octapeptides are pXAAAAAAA (pXA7), AAApXAAAA (A3pXA4), and AAAAAApXA (A6pXA), where A is alanine and pX is pS, pT, or pY. In the Fmoc procedure as discussed in Chapter 2, the peptide is built from the C-terminus on an insoluble polystyrene bead called a Wang resin. No phosphorylated amino

Table 5.3. ESI ion formation and corresponding ETD product ions for phosphorylated model peptides cationized by $Pr^{3+}$.

| Peptide sequence[a] | Number of residues | Number of acidic residues[b,c] | Metallated ion formed by ESI | $c_n$-ions | $z_n$-ions | $y_n$-ions |
|---|---|---|---|---|---|---|
| ***pS*[1]AAAAA[6] (pSA5)** | 6 | 2 | $[M + Pr - H]^{2+}$ | $[^{/}c_n + Pr]^+$, n = 4, 5 | -[d] | |
| ***pT*[1]AAAAA[6] (pTA5)** | 6 | 2 | $[M + Pr - H]^{2+}$ | $[^{/}c_n + Pr]^+$, n = 4, 5 | - | |
| ***pY*[1]AAAAA[6] (pYA5)** | 6 | 2 | $[M + Pr - H]^{2+}$ | $[^{/}c_n + Pr]^+$, n = 4, 5 | - | |
| **AA*pS*[3]AAA[6] (A2pSA3)** | 6 | 2 | $[M + Pr - H]^{2+}$ | $[^{/}c_n + Pr]^+$, n = 4, 5 | $[^{/}z_n + Pr]^+$, n = 5 | |
| **AA*pT*[3]AAA[6] (A2pTA3)** | 6 | 2 | $[M + Pr - H]^{2+}$ | $[^{/}c_n + Pr]^+$, n = 4, 5 | $[^{/}z_n + Pr]^+$, n = 5 | |
| **AA*pY*[3]AAA[6] (A2pYA3)** | 6 | 2 | $[M + Pr - H]^{2+}$ | $[^{/}c_n + Pr]^+$, n = 4, 5 | $[^{/}z_n + Pr]^+$, n = 5 | |
| **AAAA*pS*[5]A[6] (A4pSA)** | 6 | 2 | $[M + Pr - H]^{2+}$ | $[^{/}c_n + Pr]^+$, n = 5 | $[^{/}z_n + Pr]^+$, n = 5 | |
| **AAAA*pT*[5]A[6] (A4pTA)** | 6 | 2 | $[M + Pr - H]^{2+}$ | $[^{/}c_n + Pr]^+$, n = 5 | $[^{/}z_n + Pr]^+$, n = 5 | |
| **AAAA*pY*[5]A[6] (A4pYA)** | 6 | 2 | $[M + Pr - H]^{2+}$ | $[^{/}c_n + Pr]^+$, n = 5 | $[^{/}z_n + Pr]^+$, n = 5 | |
| ***pS*[1]AAAAAAA[8] (pSA7)** | 8 | 2 | $[M + Pr - H]^{2+}$ | $[^{/}c_n + Pr]^+$, n = 5-7 | - | |
| ***pT*[1]AAAAAAA[8] (pTA7)** | 8 | 2 | $[[M + Pr - H]^{2+}$ | $[^{/}c_n + Pr]^+$, n = 5-7 | - | |
| ***pY*[1]AAA[4]AAAA[8] (pYA7)** | 8 | 2 | $[M + Pr - H]^{2+}$ | $[^{/}c_n + Pr]^+$, n = 5-7 | - | |
| **AAA*pS*[4]AAAA[8] (A3pSA4)** | 8 | 2 | $[M + Pr - H]^{2+}$ | $[^{/}c_n + Pr]^+$, n = 5-7 | $[^{/}z_n + Pr]^+$, n = 5-7 | |
| **AAA*pT*[4]AAAA[8] (A3pTA4)** | 8 | 2 | $[M + Pr - H]^{2+}$ | $[^{/}c_n + Pr]^+$, n = 5-7 | $[^{/}z_n + Pr]^+$, n = 5-7 | |
| **AAA*pY*[4]AAAA[8] (A3pYA4)** | 8 | 2 | $[M + Pr - H]^{2+}$ | $[^{/}c_n + Pr]^+$, n = 5-7 | $[^{/}z_n + Pr]^+$, n = 5-7 | |

Table 5.3, continued.

| Peptide sequence[a] | Number of residues | Number of acidic residues[b,c] | Metallated ion formed by ESI | $c_n$-ions | $z_n$-ions | $y_n$-ions |
|---|---|---|---|---|---|---|
| **AAAAAA*pS*$^{7}$A$^{8}$ (A6pSA)** | 8 | 2 | $[M + Pr - H]^{2+}$ | $[^{/}c_n + Pr]^{+}$, n = 7 | $[^{/}z_n + Pr]^{+}$, n = 5-7 | $[^{///}y_n + Pr]^{+}$, n = 6 |
| **AAAAAA*pT*$^{7}$A$^{8}$ (A6pTA)** | 8 | 2 | $[M + Pr - H]^{2+}$ | $[^{/}c_n + Pr]^{+}$, n = 7 | | $[^{///}y_n + Pr]^{+}$, n = 5-7 |
| **AAAAAA*pY*$^{7}$A$^{8}$ (A6pYA)** | 8 | 2 | $[M + Pr - H]^{2+}$ | $[^{/}c_n + Pr]^{+}$, n = 7 | $[^{/}z_n + Pr]^{+}$, n = 5-7 | $[^{///}y_n + Pr]^{+}$, n = 6 |

[a]Acidic residues refer to the number of aspartic acid (D), glutamic acid (E), phosphorylated amino acid (pX), and C-terminal residues in the peptide sequence. If an aspartic acid or glutamic acid residue is located at the C-terminus, then it is counted as only one acidic residue.

[b]Bold font is used to indicate acidic residues. A number immediately following an acidic residue indicates its position in the peptide sequence.

[c]Bold italicized font is used to indicate phosphorylated amino acid residues. A number immediately following a phosphorylated residue indicates its position in the peptide sequence.

[d]- means that no ions were observed

acid Wang resin exists, therefore peptides of the sequence AAAAAAApX could not be synthesized. In addition, tryptic enzymes do not cleave adjacent to phosphorylated residues, so C-terminal phosphorylated residues tend to be absent in nature. Table 5.3 shows the metallated precursor ions formed by ESI and the ETD products for all the model peptides.

#### 5.4.2.1 Ion formation for model peptides

All eighteen model peptides form only $[M + Pr - H]^{2+}$ by ESI. None form $[M + Pr]^{3+}$ or $[M + Pr + H]^{4+}$ indicating that the facile deprotonation of the phosphorylated residue is dominant even in the presence of metallation. In addition, this shows that an N-terminal basic site alone is not sufficient to allow the peptide ions to form in the 3+ or higher charge state. Like the hexapeptides, biological EGF(DL- 6) contains six residues and forms only $[M + Pr - H]^{2+}$. In previous work described in Chapter 4 with non-phosphorylated acidic peptides,[45] the acidic hexapeptides also only form $[M + Pr - H]^{2+}$ with $Pr^{3+}$. The model octapeptides also do not form $[M + Pr]^{3+}$. This is somewhat unexpected because DNA transcription inhibitory peptide and its analogs all contain eight acidic sites including a highly acidic phosphorylated amino acid yet they yield abundant $[M + Pr]^{3+}$ by ESI. The highly acidic nature of these peptides compared to the model peptide would supposedly hinder the formation of the higher 3+ charge state relative to the model peptides.

#### 5.4.2.2 Electron transfer dissociation of model peptides

Structural effects such as position of phosphorylated residue can affect dissociation of peptides.[18,88-91] When the phosphorylated residue is at the N-terminus in the hexapeptides of the type pXA5 (where X = pS, pT, or pY), ETD of $[M + Pr - H]^{2+}$ results in cleavage at only two backbone sites producing $[^{/}c_n + Pr]^{+}$, n = 4, 5 for all three peptides. (See Figures 5.16-5.18). The

same type of ions form for the model octapeptides (pXA7) as seen in Figures 5.19-5.21, where cleavage occurs at three sites yielding only metal-adducted c-ions, $[^{/}c_n + Pr]^+$, n = 5-7. Formation of only c-ions suggests that the metal ion is binding at the phosphorylated residue at the N-terminus. Formation of only N-terminal product ions also supports the hypothesis that a stronger interaction of the phosphorylated residue with the metal ion occurs than a regular acidic amino acid. In my previous work,[45] the location of the aspartic or glutamic acid residues at the N-terminus did not restrict formation of C-terminal ions in non-phosphorylated acidic peptides.

The most extensive sequence coverage occurs when the phosphorylated residue is in the middle of the peptide sequence. Hexapeptides of the type A2pXA3 form singly charged metal-adducted c- and z-ions by ETD of $[M + Pr - H]^{2+}$, as seen in Figures 5.22-5.24. Three backbone cleavage sites occur for A2pSA3, four for A2pTA3, and four for A2pYA3. Lack of cleavage adjacent to the phosphorylated residue makes exact location of phosphorylation site more ambiguous. However, the location can be narrowed down to two residues in the middle of the sequence. Octapeptides with sequences A3pXA4 form metal-adducted c- and z-series with six backbone cleavage sites generated for each peptide, as shown in Figures 5.25-5.27. As with the hexapeptides, the site of phosphorylation can be narrowed down to the two residues in the middle of the sequence. All metal-adducted c- and z- ions contain the phosphorylated amino acid regardless of its location.

Limited sequence information is obtained from the ETD spectra of $[M + Pr - H]^{2+}$ with the phosphorylated residue located penultimate to the C-terminus. As seen in Figures 5.28-5.30 for A4pXA, only two metal-adducted c-and z-ions form: $[^{/}c_n + Pr]^+$, n = 5 and $[^{/}z_n + Pr]^+$, n = 5. Octapeptides (A6pXA) yield singly charged metal-adducted c-, z-, and y- ions corresponding to three cleavage sites for A6pSA, four for A6pTA and four for A6pYA (see Figures 5.31-5.33).

Identification of the exact location of phosphorylated residues is impossible with such limited fragmentation. Regardless of the site of phosphorylation, all metal-adducted c-, z-, and y-ions for the hexa- and octapeptides contain the phosphorylated residue. In addition, no product ions formed involving the loss of the phosphate group.

The three octapeptides with C-terminal phosphorylated residues form y-ions. These y-ions that involve (O=C)-N cleavage are not observed for the other peptides in this study. Octapeptide A6pTA shown in Figure 5.32 form y-ions and one c-ion. The two phosphorylated octapeptide analogs, A6pSA and A6pYA for z-ions with one c- and one y-ion. Formation of y-ions in electron-based techniques such as ECD and ETD has been observed by several groups.[92-94] A Cassady group study observed extensive formation of y-ions in an ETD study of peptides with alkyl side chains.[95] Peptides containing residues with alkyl side chains form b- and y- ions by ETD and ECD,[94,95] and all three peptides (A6pTA, A6pSA, and A6pYA) contain a string of six alanine residues. (The structure of the side chain of alanine is shown in Figure 2.14). Some y-ions form lacking three hydrogens, $^{///}y_n = [y_n\text{-}3H]$, which is unusual and may be due to deprotonation at the phosphoresidue. The ETD study in Chapter 4 involving non-phosphorylated acidic peptides[45] has y-ions.

### 5.4.3 Dissociation trends and structural effects

The type of phosphorylated residue can affect the product ions formed by ECD and ETD.[19,96] In Figure 5.22, hexapeptide A2pSA3 with the central pS undergoes backbone cleavage at one less site ($[^{/}c_4 + Pr]$) than either the pT (A2pTA3 in Figure 5.23) or pY (A2pYA3 in Figure 5.24) analog. Also, octapeptide A6pSA (Figure 5.31) with a pS penultimate to the C-terminus has one less backbone cleavage than the pT (A6pTA in Figure 5.32) or pY (A6pYA in Figure 5.33) analogs. Creese and Cooper[19] observed that pS hampered backbone dissociation.

Peptide chain length can affect ions formed by ETD of metal-adducted peptides. In previous work discussed in Chapter 4 with non-phosphorylated acidic peptides,[45] more cleavage occurs for the same precursor ion type as the peptide chain length increases from six to ten residues. A similar trend is observed when comparing ETD of $[M + Pr - H]^{2+}$ for all model phosphorylated hexapeptides to ETD of octapeptides in the current study. As an example, hexapeptide pSA5 in Figure 5.16 forms $[^{/}c_n + Pr]^{+}$, n = 4 and 5, while octapeptide pSA7 in Figure 5.19 yields cleavage at n = 5-7. However, roughly the same amount of sequence coverage (~ 40%) occurs for both the hexa- and octapeptides. In both cases with the model peptides, roughly 40% of each sequence is deciphered.

The identity of amino acid residues in the peptide sequence and charge state of precursor ions may influence fragmentation patterns. For example, ETD of $[M + Pr - H]^{2+}$ yields 77% sequence coverage for EGF(988-998) with eleven amino acids, but only 23% for fourteen-residue hsp, as observed in Figures 5.11 and 5.12. In two separate studies by Chan and coworkers involving non-phosphorylated peptides,[52,97] researchers found that increased chain length limits backbone cleavage, indicating that residue identity also has an effect. Higher charge states can generate an increased number of product ions and improved sequence coverage with better identification of location of phosphorylated residue.[98-100] Cooper and Creese[19] found increased sequence coverage for triply protonated phosphorylated peptides and their non-phosphorylated analogs compared to the doubly protonated ions. In an ECD study of phosphorylated peptides complexed with divalent zinc by Asakawa and Osaka,[62] precursor ions with higher charge states generate more product ions and provide increased sequence coverage. This trend occurs for several peptides in the current study. Backbone cleavage occurs on both sides of the **pS$^{8}$** in ETD of $[M + Pr + H]^{4+}$ for hsp (Figure 5.1) and allows unambiguous

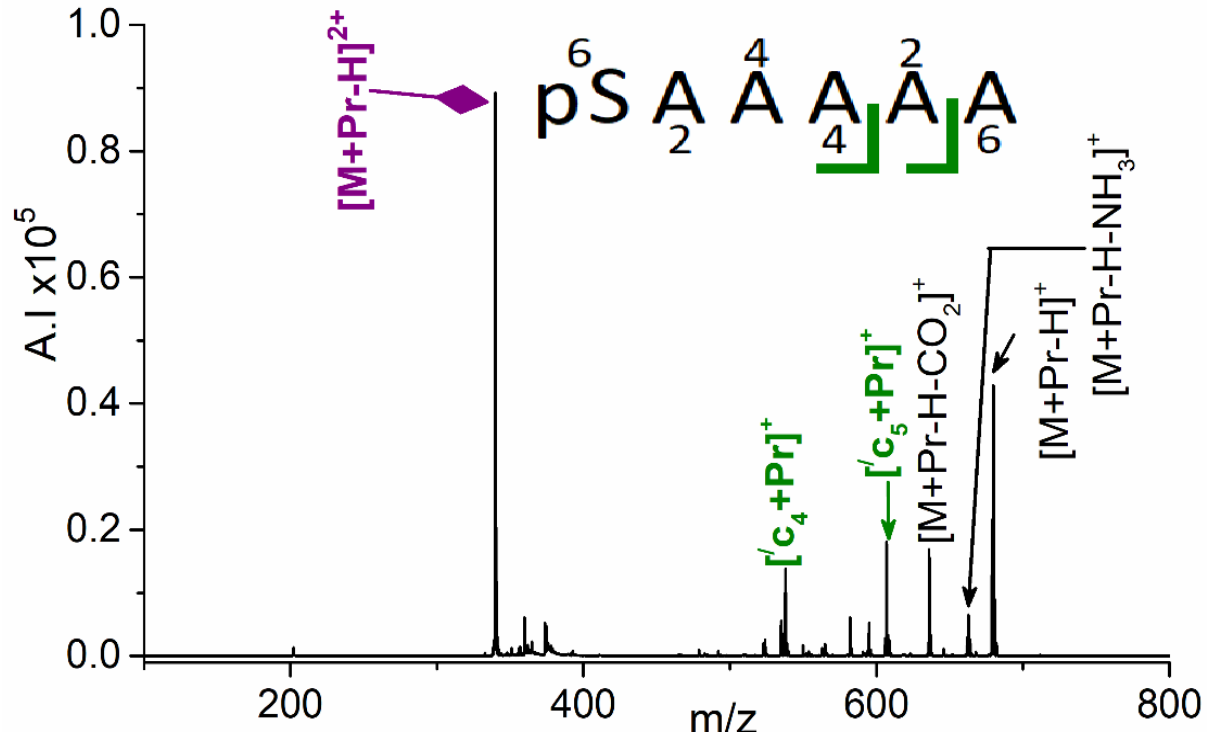


Figure 5.16. ETD mass spectrum of $[M + Pr - H]^{2+}$ for pSAAAAA (pSA5). In the figure, the following colors are used to label the ions: metal-adducted c-ions = green. Undissociated precursor ion is labeled in purple with a large purple diamond arrow head. Neutral loss products and electron transfer without dissociation (ETnoD) ions are labeled in black. A prime symbol to the left indicates loss of a hydrogen (i.e., $^{/}c_n = [c_n - H]^+$) and to the right indicates the addition of a hydrogen at the cleavage site (i.e., $c_n^{//} = [c_n + 2H]^+$). The spectra have no expansion of the intensity axis; all peaks are shown to scale.

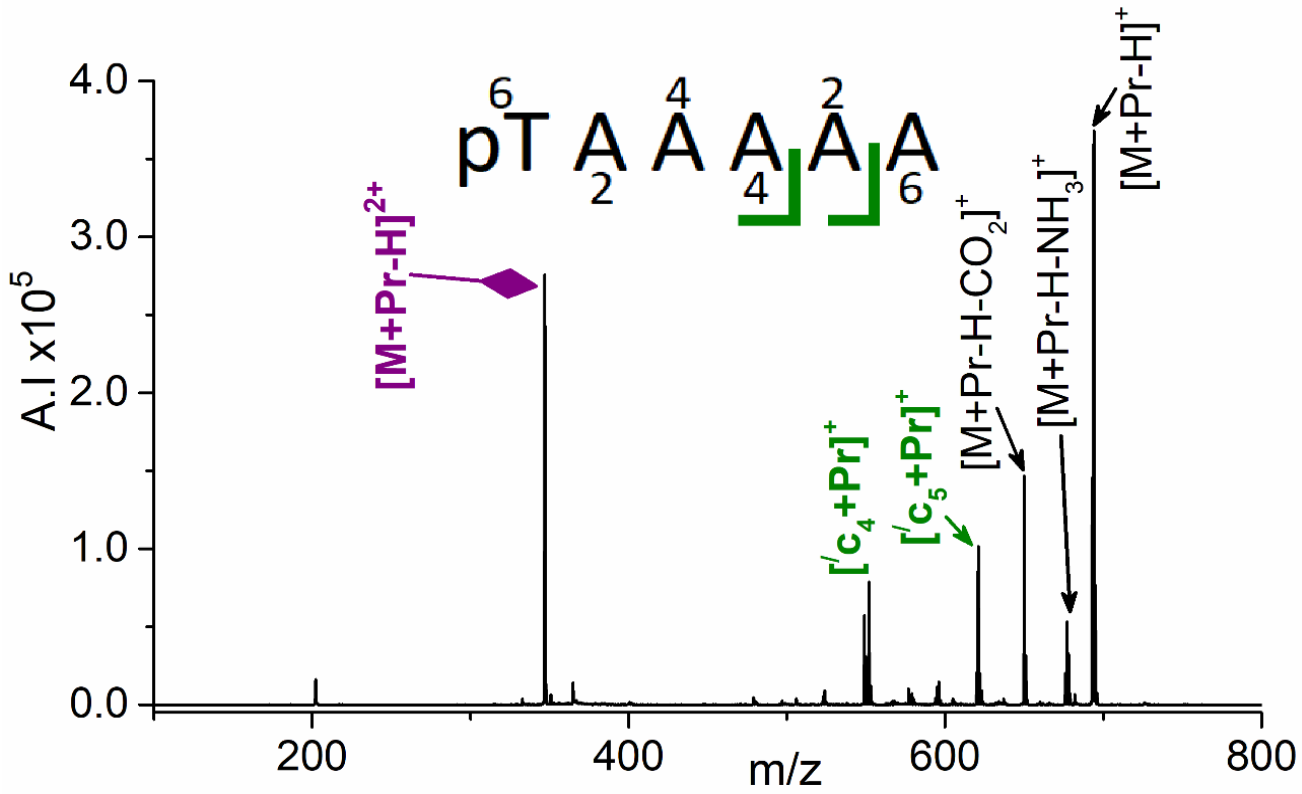


Figure 5.17. ETD mass spectrum of $[M + Pr - H]^{2+}$ for pTAAAAA (pTA5). In the figure, the following colors are used to label the ions: metal-adducted c-ions = green. Undissociated precursor ion is labeled in purple with a large purple diamond arrow head. Neutral loss products and electron transfer without dissociation (ETnoD) ions are labeled in black. A prime symbol to the left indicates loss of a hydrogen (i.e., $^{/}c_n = [c_n - H]^+$) and to the right indicates the addition of a hydrogen at the cleavage site (i.e., $c_n^{//} = [c_n + 2H]^+$). The spectra have no expansion of the intensity axis; all peaks are shown to scale.

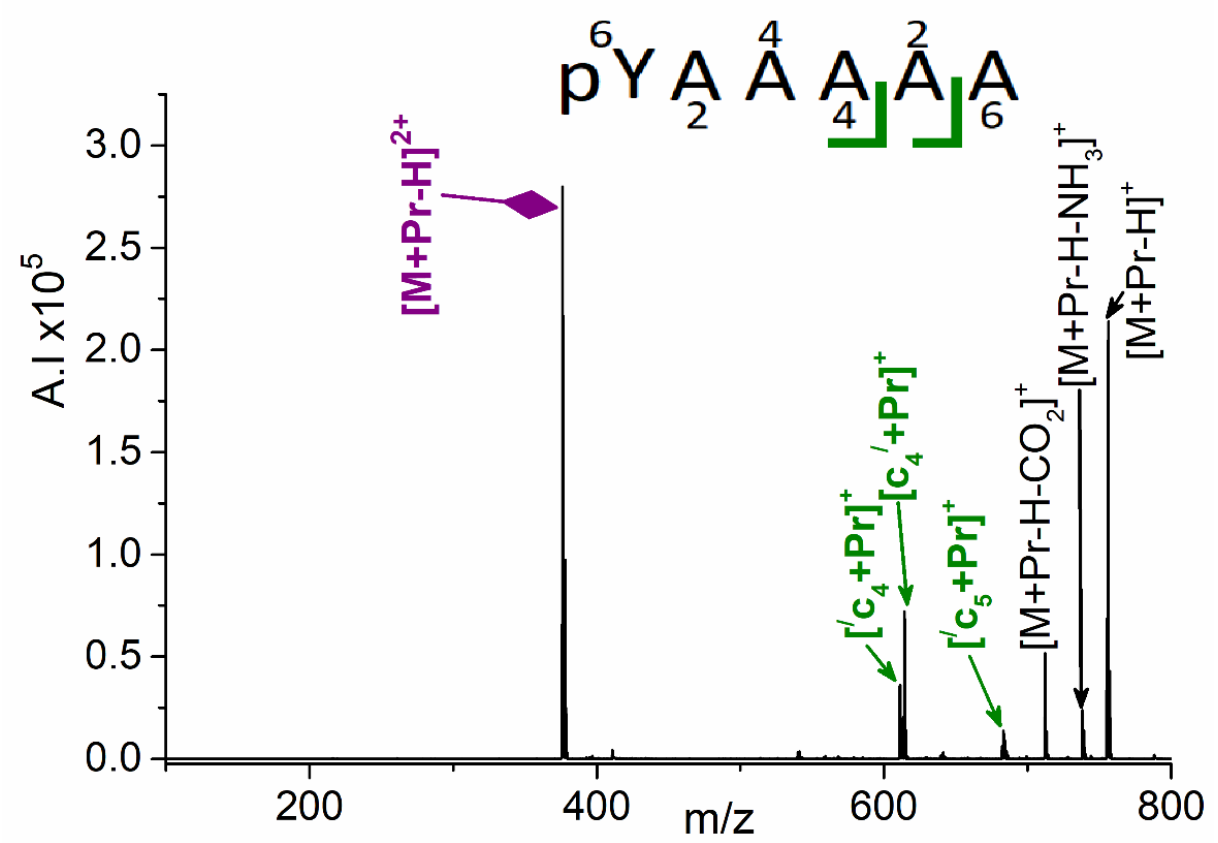


Figure 5.18. ETD mass spectrum of $[M + Pr - H]^{2+}$ for pYAAAAA (pYA5). In the figure, the following colors are used to label the ions: metal-adducted c-ions = green. Undissociated precursor ion is labeled in purple with a large purple diamond arrow head. Neutral loss products and electron transfer without dissociation (ETnoD) ions are labeled in black. A prime symbol to the left indicates loss of a hydrogen (i.e., $^{/}c_n = [c_n - H]^+$) and to the right indicates the addition of a hydrogen at the cleavage site (i.e., $c_n^{//} = [c_n + 2H]^+$). The spectra have no expansion of the intensity axis; all peaks are shown to scale.

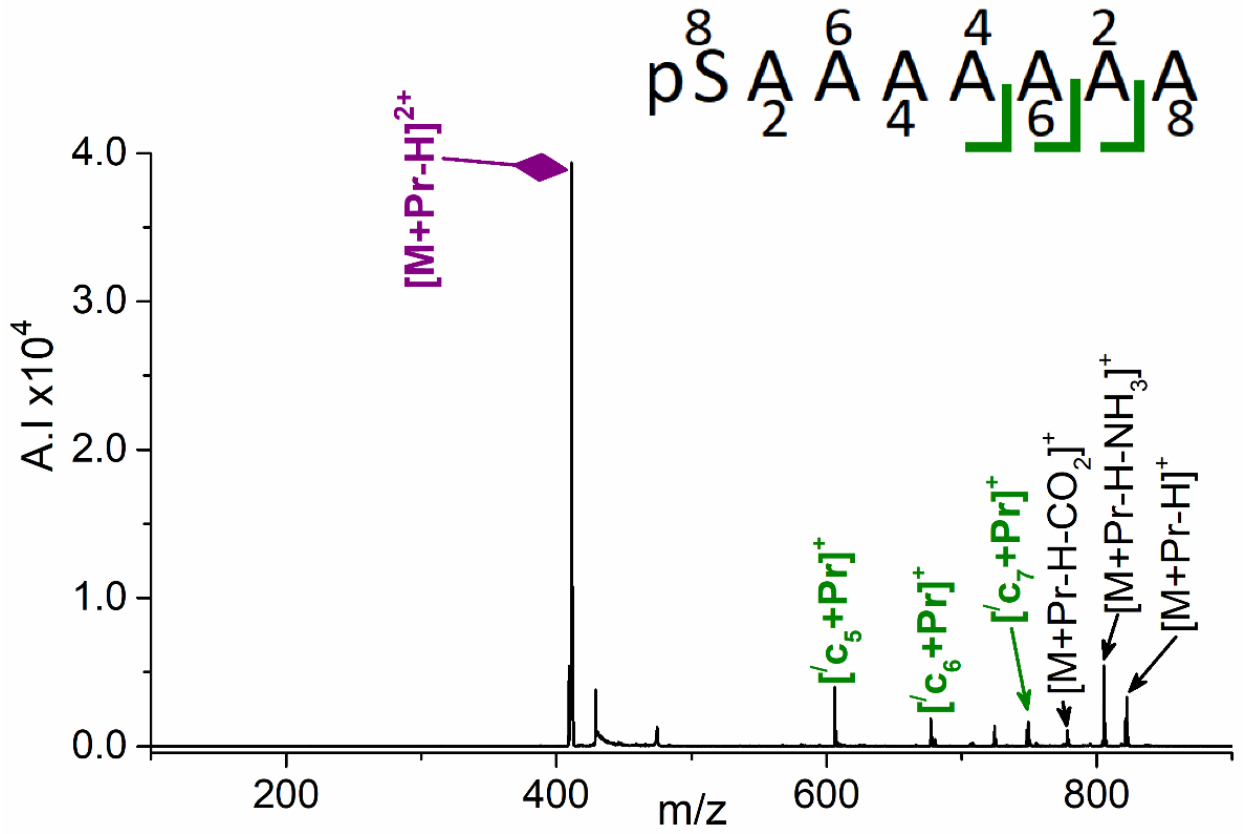


Figure 5.19. ETD mass spectrum of $[M + Pr - H]^{2+}$ for pSAAAAAAA (pSA7). In the figure, the following colors are used to label the ions: metal-adducted c-ions = green. Undissociated precursor ion is labeled in purple with a large purple diamond arrow head. Neutral loss products and electron transfer without dissociation (ETnoD) ions are labeled in black. A prime symbol to the left indicates loss of a hydrogen (i.e., $^{/}c_n = [c_n - H]^+$) and to the right indicates the addition of a hydrogen at the cleavage site (i.e., $c_n^{//} = [c_n + 2H]^+$). The spectra have no expansion of the intensity axis; all peaks are shown to scale.

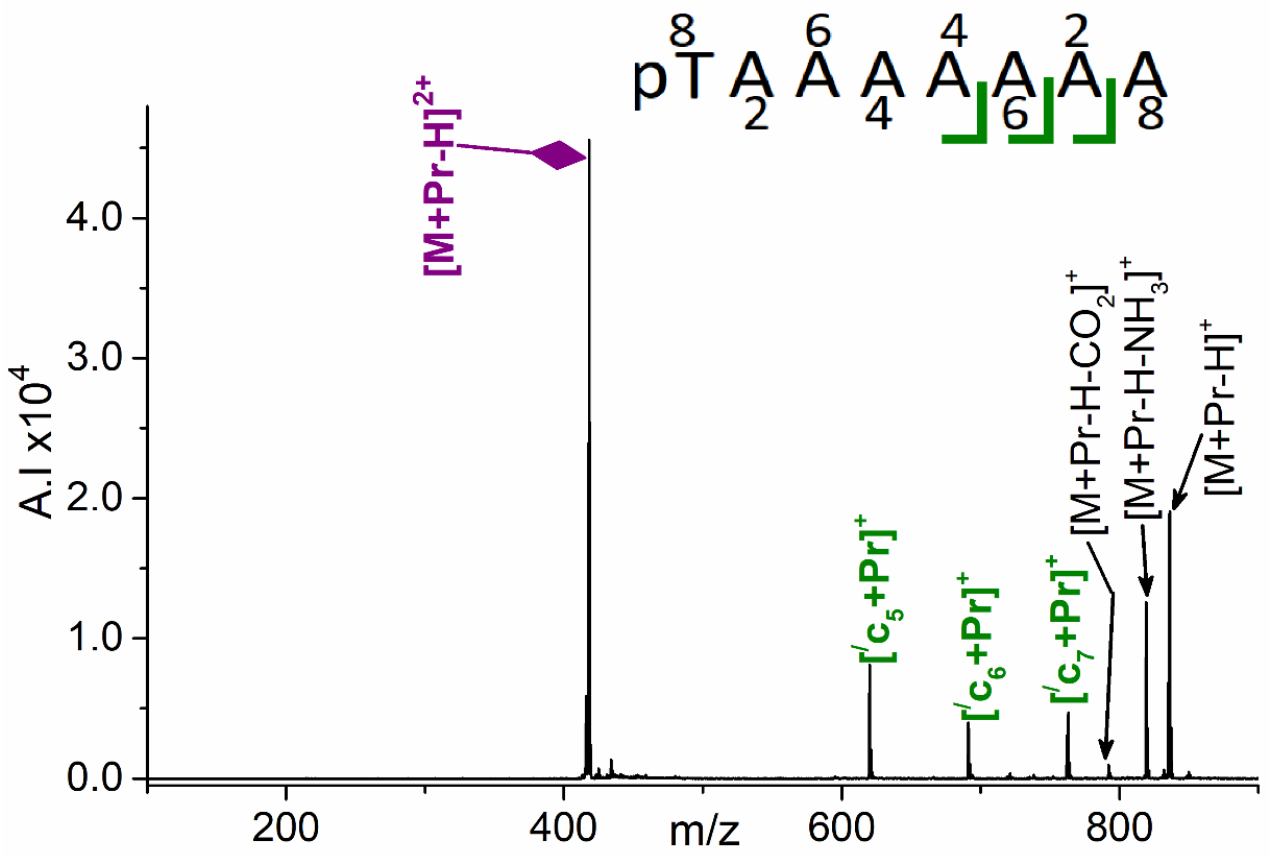


Figure 5.20. ETD mass spectrum of $[M + Pr - H]^{2+}$ for pTAAAAAAA (pTA7). In the figure, the following colors are used to label the ions: metal-adducted c-ions = green. Undissociated precursor ion is labeled in purple with a large purple diamond arrow head. Neutral loss products and electron transfer without dissociation (ETnoD) ions are labeled in black. A prime symbol to the left indicates loss of a hydrogen (i.e., $^{/}c_n = [c_n - H]^+$) and to the right indicates the addition of a hydrogen at the cleavage site (i.e., $c_n^{//} = [c_n + 2H]^+$). The spectra have no expansion of the intensity axis; all peaks are shown to scale.

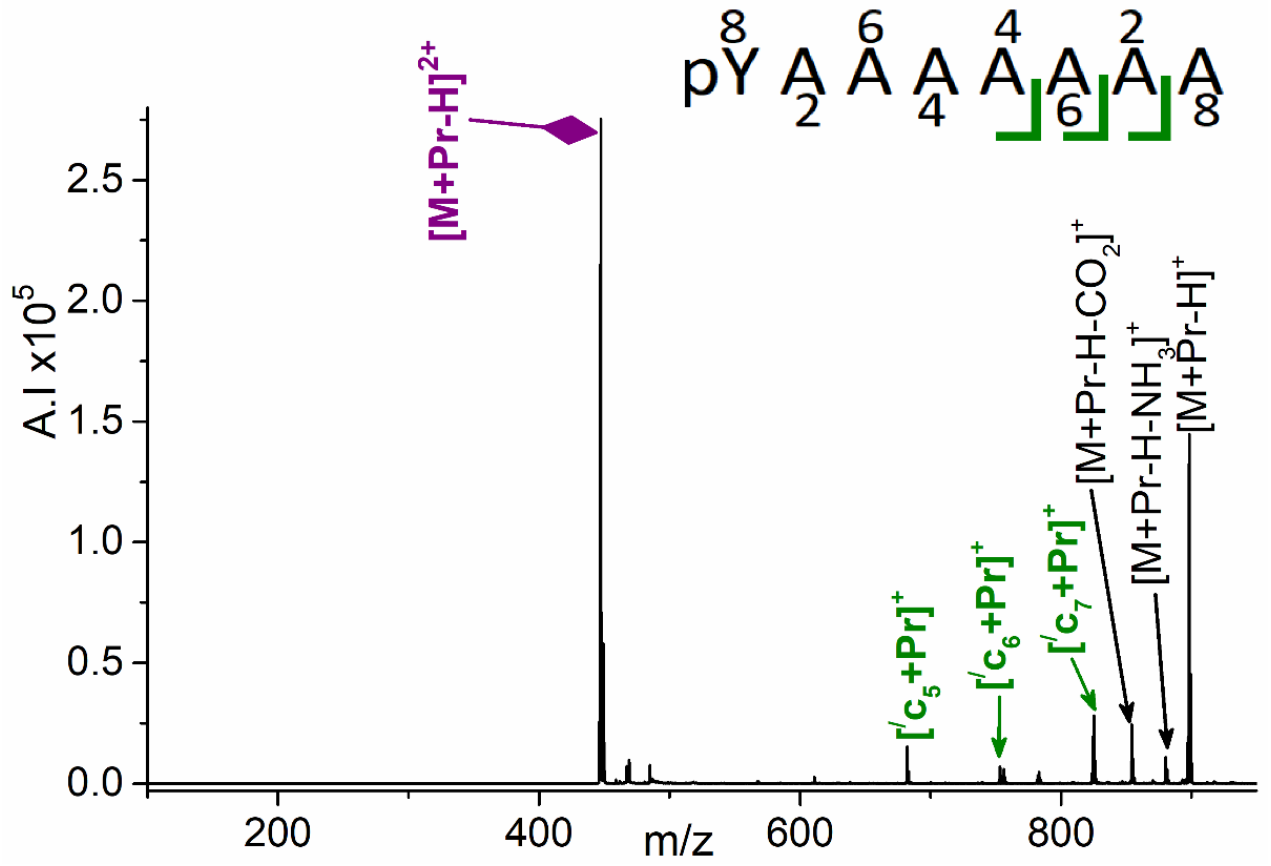


Figure 5.21. ETD mass spectrum of $[M + Pr - H]^{2+}$ for pYAAAAAAA (pYA7). In the figure, the following colors are used to label the ions: metal-adducted c-ions = green. Undissociated precursor ion is labeled in purple with a large purple diamond arrow head. Neutral loss products and electron transfer without dissociation (ETnoD) ions are labeled in black. A prime symbol to the left indicates loss of a hydrogen (i.e., $^{/}c_n = [c_n - H]^+$) and to the right indicates the addition of a hydrogen at the cleavage site (i.e., $c_n^{//} = [c_n + 2H]^+$). The spectra have no expansion of the intensity axis; all peaks are shown to scale.

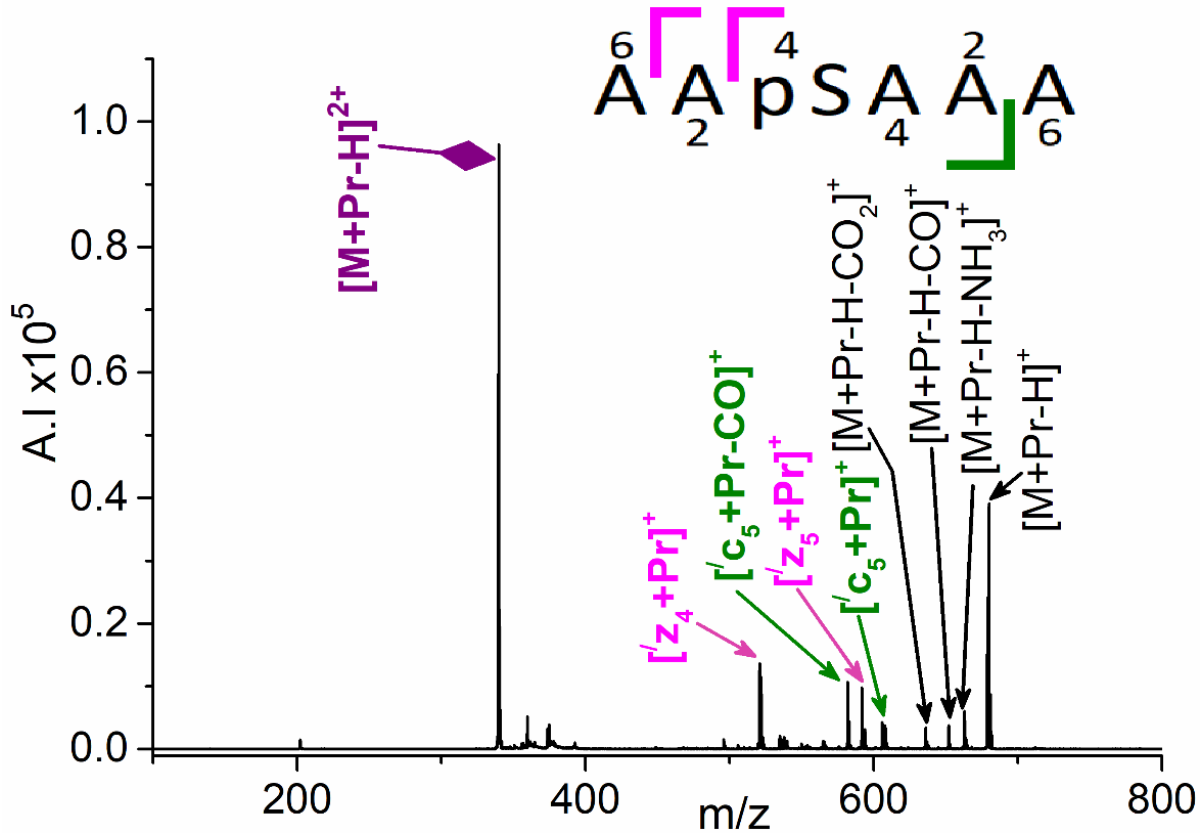


Figure 5.22. ETD mass spectrum of $[M + Pr - H]^{2+}$ for AApSAAA (A2pSA3). In the figure, the following colors are used to label the ions: metal-adducted z-ions = bright pink, and metal-adducted c-ions = green. Undissociated precursor ion is labeled in purple with a large purple diamond arrow head. Neutral loss products and electron transfer without dissociation (ETnoD) ions are labeled in black. A prime symbol to the left indicates loss of a hydrogen (i.e., ${}^{/}c_n = [c_n - H]^+$) and to the right indicates the addition of a hydrogen at the cleavage site (i.e., $c_n^{//} = [c_n + 2H]^+$). The spectra have no expansion of the intensity axis; all peaks are shown to scale.

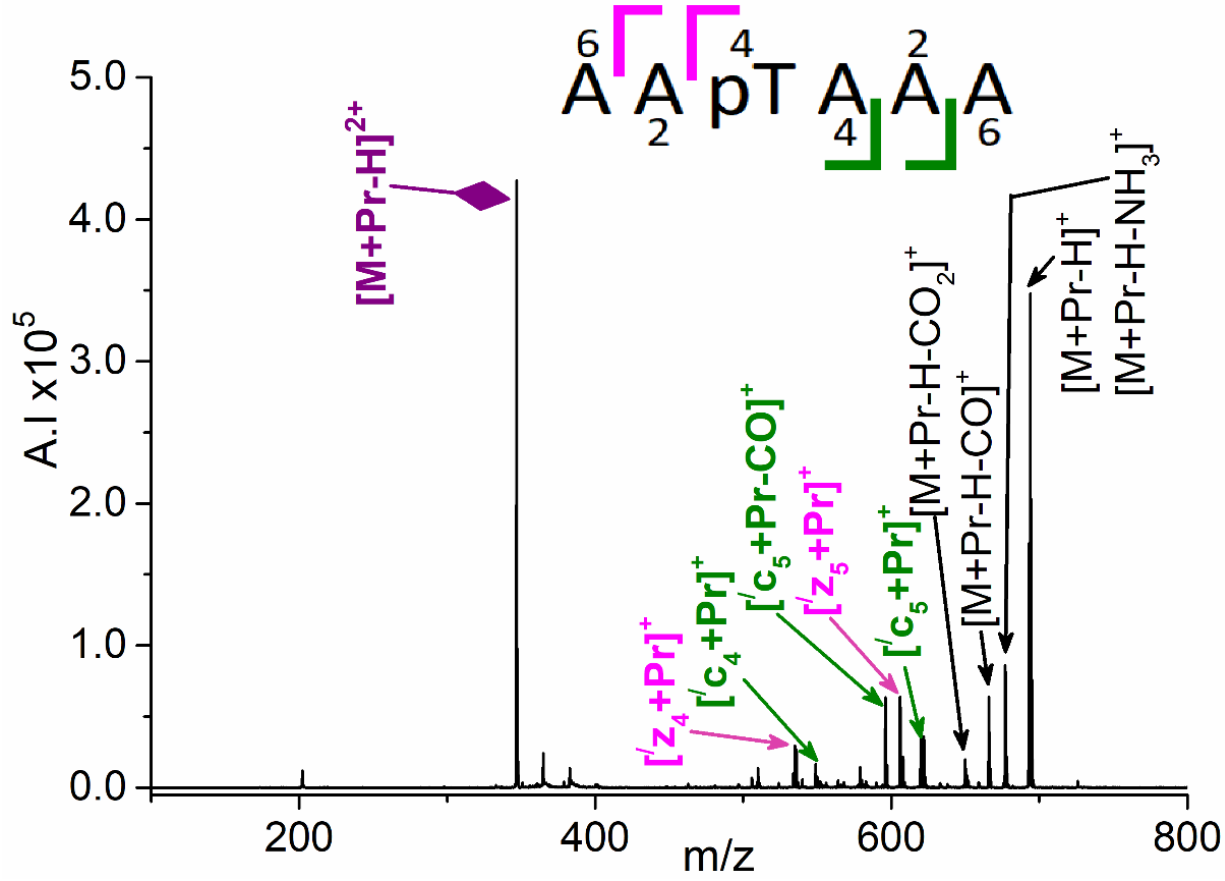


Figure 5.23. ETD mass spectrum of $[M + Pr - H]^{2+}$ for AApTAAA (A2pTA3). In the figure, the following colors are used to label the ions: metal-adducted z-ions = bright pink, and metal-adducted c-ions = green. Undissociated precursor ion is labeled in purple with a large purple diamond arrow head. Neutral loss products and electron transfer without dissociation (ETnoD) ions are labeled in black. A prime symbol to the left indicates loss of a hydrogen (i.e., ${}^{/}c_n = [c_n - H]^+$) and to the right indicates the addition of a hydrogen at the cleavage site (i.e., $c_n^{//} = [c_n + 2H]^+$). The spectra have no expansion of the intensity axis; all peaks are shown to scale.

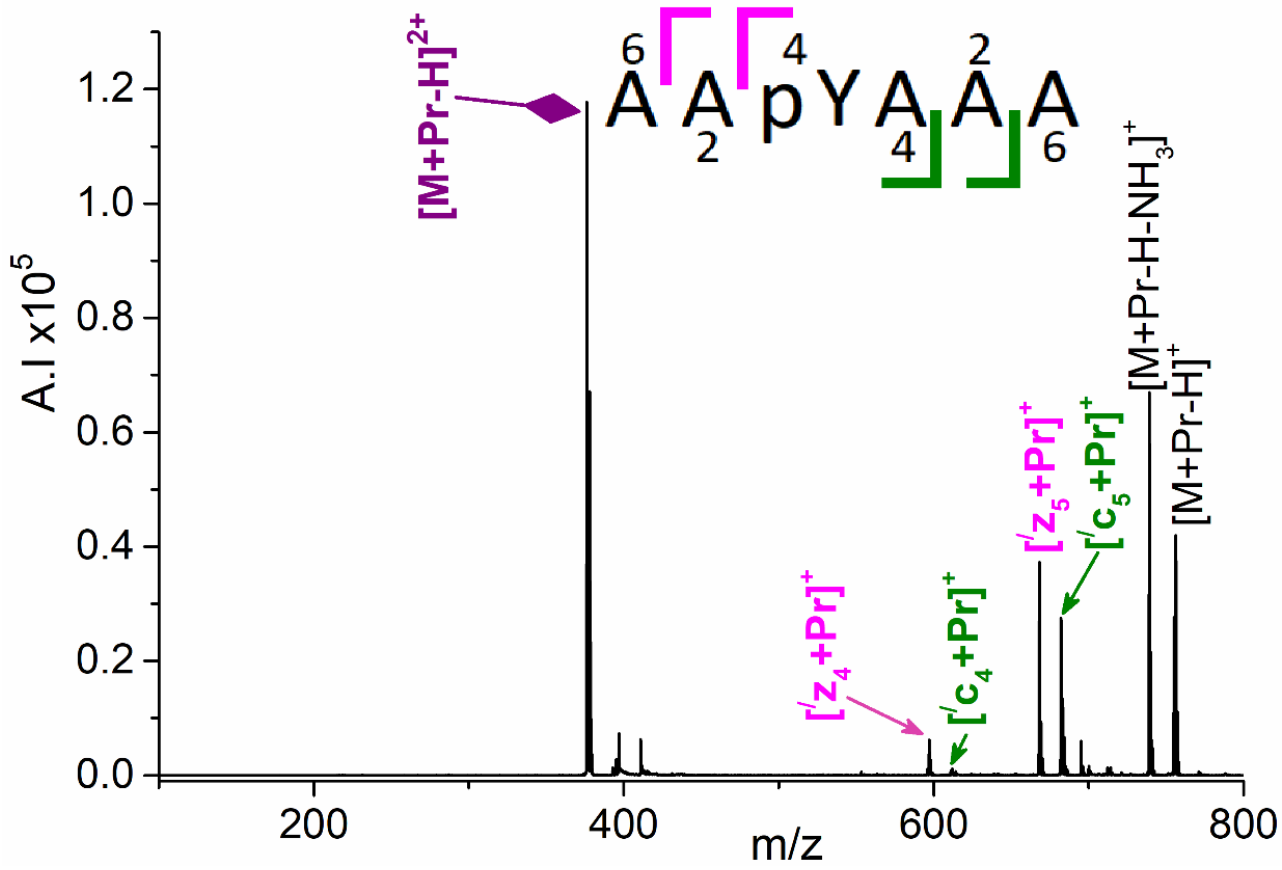


Figure 5.24. ETD mass spectrum of $[M + Pr - H]^{2+}$ for AApYAAA (A2pYA3). In the figure, the following colors are used to label the ions: metal-adducted z-ions = bright pink, and metal-adducted c-ions = green. Undissociated precursor ion is labeled in purple with a large purple diamond arrow head. Neutral loss products and electron transfer without dissociation (ETnoD) ions are labeled in black. A prime symbol to the left indicates loss of a hydrogen (i.e., ${}^{/}c_n = [c_n - H]^+$) and to the right indicates the addition of a hydrogen at the cleavage site (i.e., $c_n^{//} = [c_n + 2H]^+$). The spectra have no expansion of the intensity axis; all peaks are shown to scale.

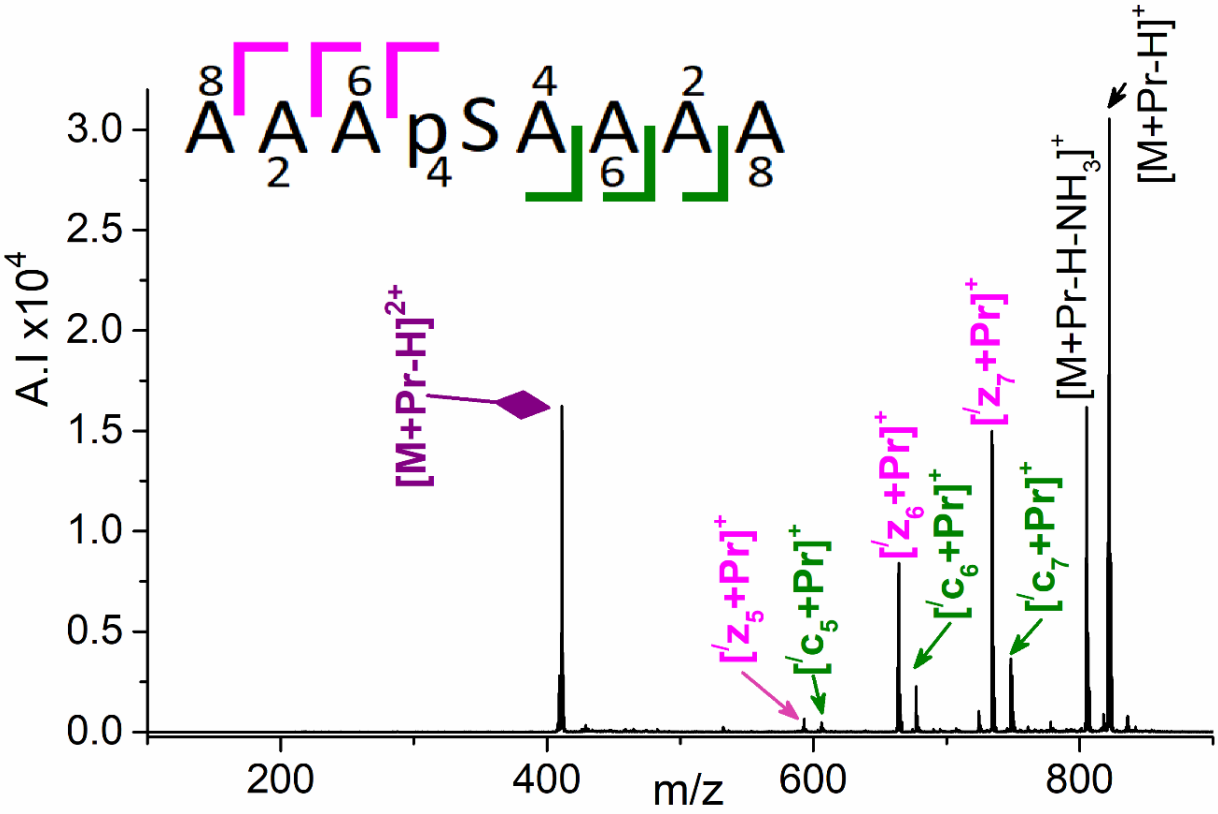


Figure 5.25. ETD mass spectrum of $[M + Pr - H]^{2+}$ for AAApSAAAA (A3pSA4). In the figure, the following colors are used to label the ions: metal-adducted z-ions = bright pink, and metal-adducted c-ions = green. Undissociated precursor ion is labeled in purple with a large purple diamond arrow head. Neutral loss products and electron transfer without dissociation (ETnoD) ions are labeled in black. A prime symbol to the left indicates loss of a hydrogen (i.e., ${}^{/}c_n = [c_n - H]^+$) and to the right indicates the addition of a hydrogen at the cleavage site (i.e., $c_n^{//} = [c_n + 2H]^+$). The spectra have no expansion of the intensity axis; all peaks are shown to scale.

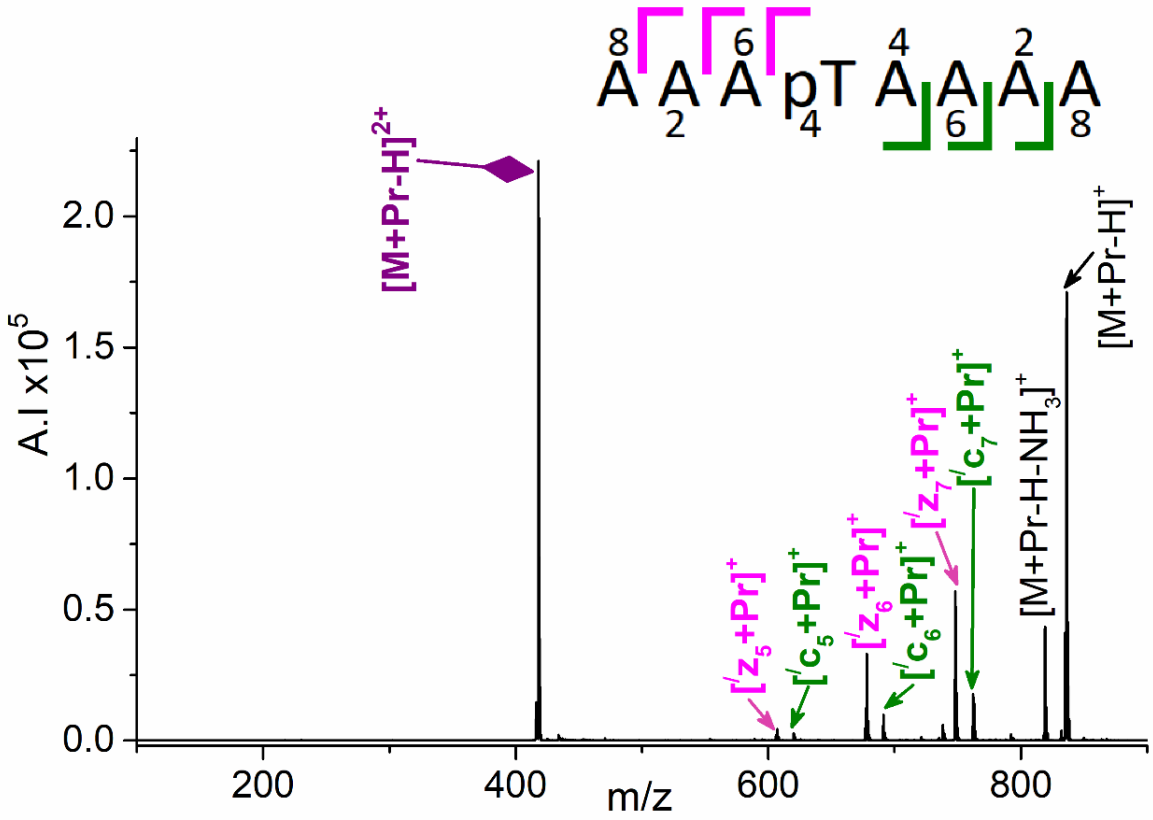


Figure 5.26. ETD mass spectrum of $[M + Pr - H]^{2+}$ for AAApTAAAA (A3pTA4). In the figure, the following colors are used to label the ions: metal-adducted z-ions = bright pink, and metal-adducted c-ions = green. Undissociated precursor ion is labeled in purple with a large purple diamond arrow head. Neutral loss products and electron transfer without dissociation (ETnoD) ions are labeled in black. A prime symbol to the left indicates loss of a hydrogen (i.e., ${}^{/}c_n = [c_n - H]^+$) and to the right indicates the addition of a hydrogen at the cleavage site (i.e., $c_n^{//} = [c_n + 2H]^+$). The spectra have no expansion of the intensity axis; all peaks are shown to scale.

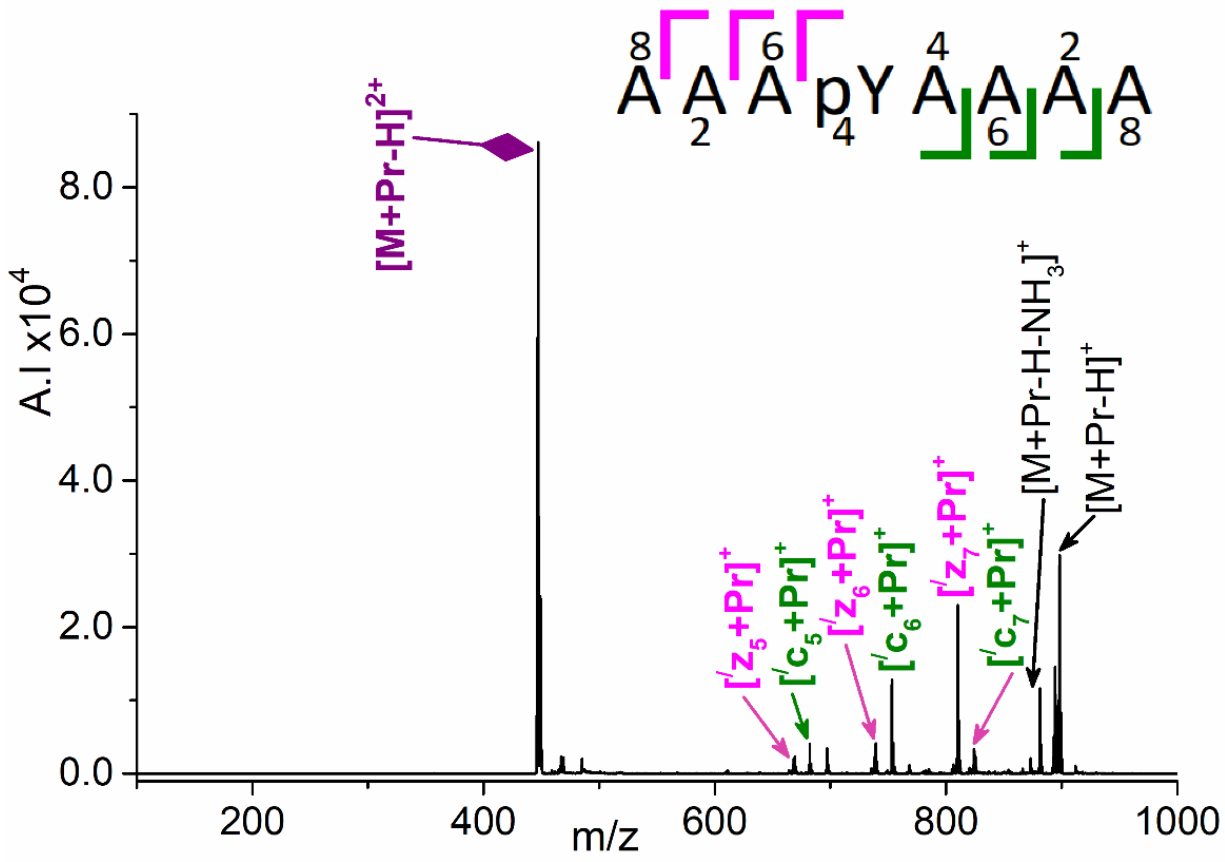


Figure 5.27. ETD mass spectrum of $[M + Pr - H]^{2+}$ for AAApYAAAA (A3pYA4). In the figure, the following colors are used to label the ions: metal-adducted z-ions = bright pink, and metal-adducted c-ions = green. Undissociated precursor ion is labeled in purple with a large purple diamond arrow head. Neutral loss products and electron transfer without dissociation (ETnoD) ions are labeled in black. A prime symbol to the left indicates loss of a hydrogen (i.e., ${}^{/}c_n = [c_n - H]^+$) and to the right indicates the addition of a hydrogen at the cleavage site (i.e., $c_n^{//} = [c_n + 2H]^+$). The spectra have no expansion of the intensity axis; all peaks are shown to scale.

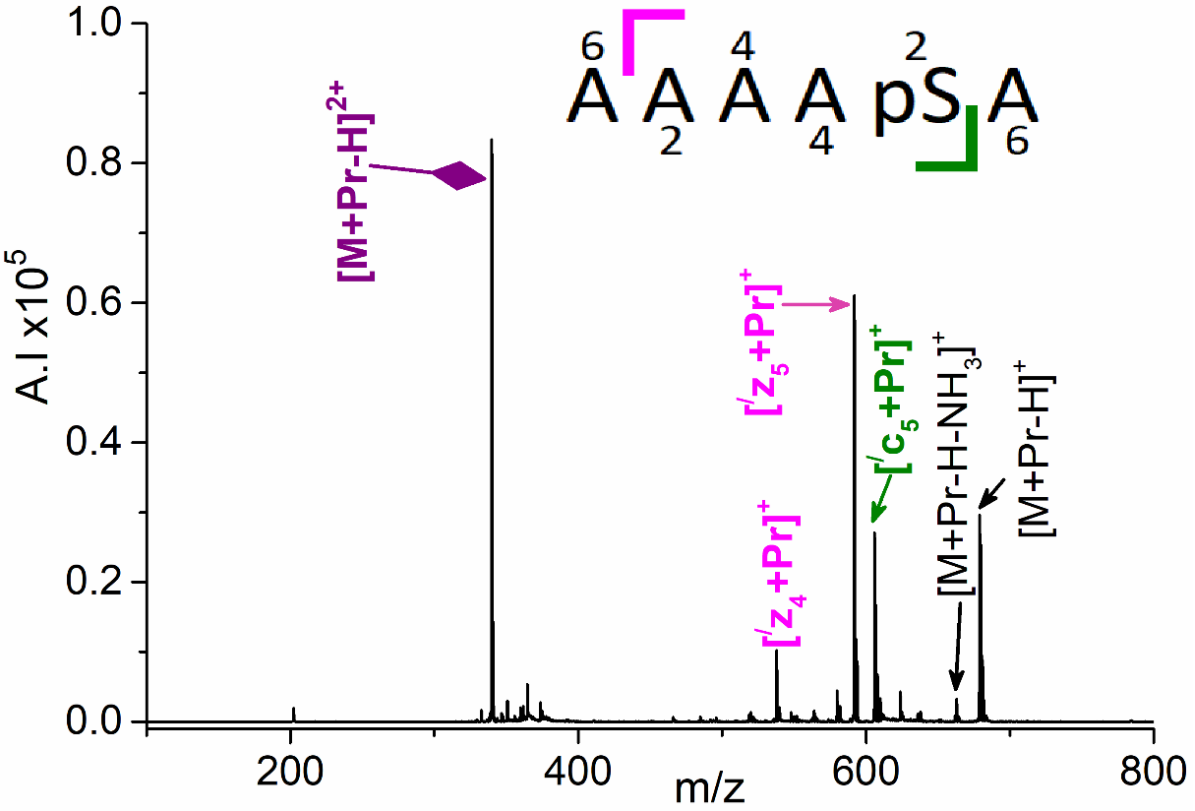


Figure 5.28. ETD mass spectrum of $[M + Pr - H]^{2+}$ for AAAApSA (A4pSA). In the figure, the following colors are used to label the ions: metal-adducted z-ions = bright pink, and metal-adducted c-ions = green. Undissociated precursor ion is labeled in purple with a large purple diamond arrow head. Neutral loss products and electron transfer without dissociation (ETnoD) ions are labeled in black. A prime symbol to the left indicates loss of a hydrogen (i.e., $^{/}c_n = [c_n - H]^+$) and to the right indicates the addition of a hydrogen at the cleavage site (i.e., $c_n^{//} = [c_n + 2H]^+$). The spectra have no expansion of the intensity axis; all peaks are shown to scale.

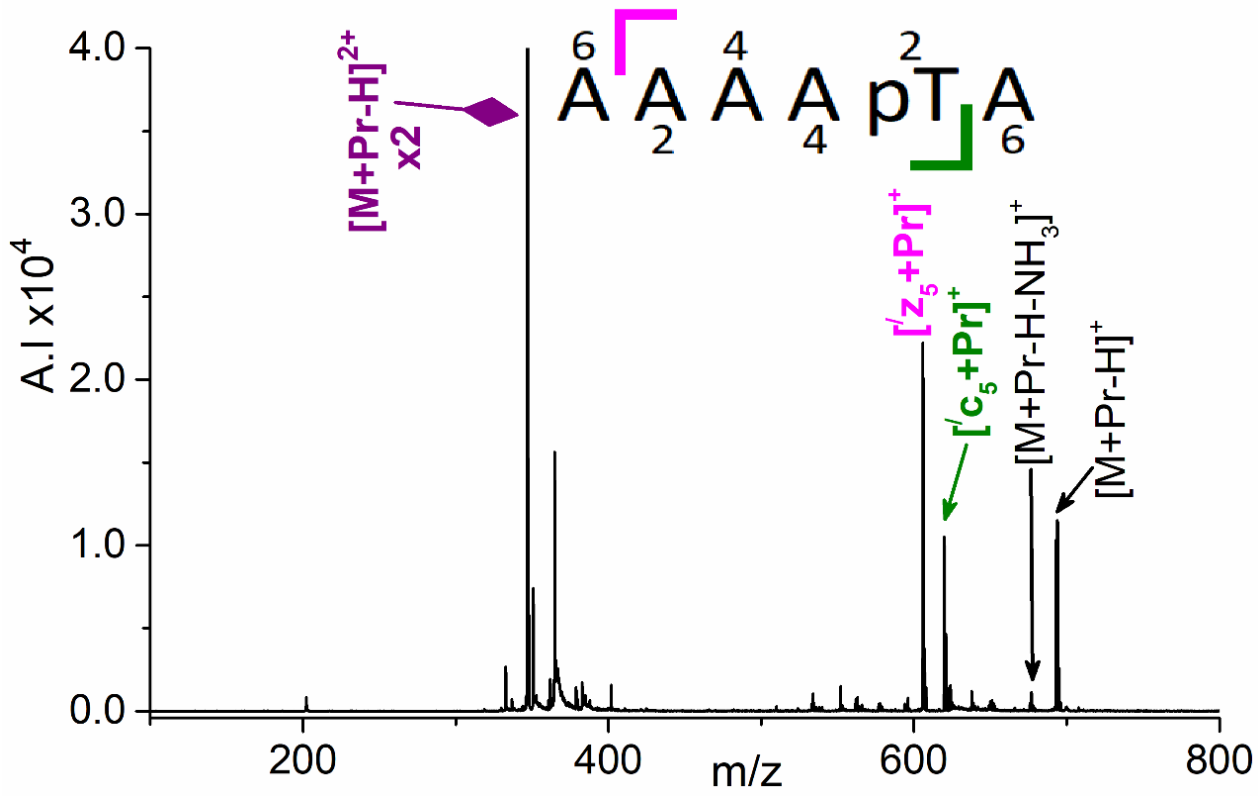


Figure 5.29. ETD mass spectrum of $[M + Pr – H]^{2+}$ for AAAApTA (A4pTA). In the figure, the following colors are used to label the ions: metal-adducted z-ions = bright pink, and metal-adducted c-ions = green. Undissociated precursor ion is labeled in purple with a large purple diamond arrow head. Neutral loss products and electron transfer without dissociation (ETnoD) ions are labeled in black. A prime symbol to the left indicates loss of a hydrogen (i.e., $^{/}c_n = [c_n – H]^+$) and to the right indicates the addition of a hydrogen at the cleavage site (i.e., $c_n^{//} = [c_n + 2H]^+$). The spectra have no expansion of the intensity axis; all peaks are shown to scale.

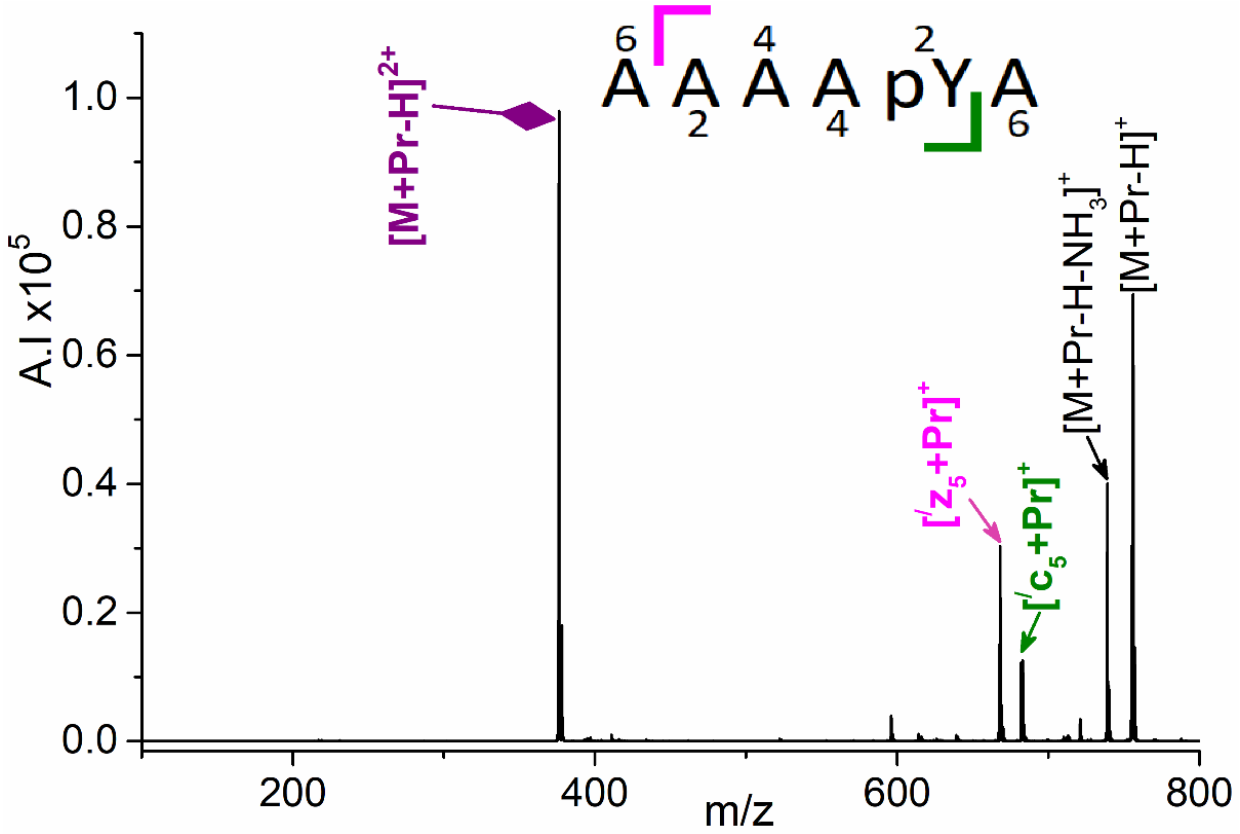


Figure 5.30. ETD mass spectrum of $[M + Pr - H]^{2+}$ for AAAApYA (A4pYA). In the figure, the following colors are used to label the ions: metal-adducted z-ions = bright pink, and metal-adducted c-ions = green. Undissociated precursor ion is labeled in purple with a large purple diamond arrow head. Neutral loss products and electron transfer without dissociation (ETnoD) ions are labeled in black. A prime symbol to the left indicates loss of a hydrogen (i.e., $^{/}c_n = [c_n - H]^+$) and to the right indicates the addition of a hydrogen at the cleavage site (i.e., $c_n^{//} = [c_n + 2H]^+$). The spectra have no expansion of the intensity axis; all peaks are shown to scale.

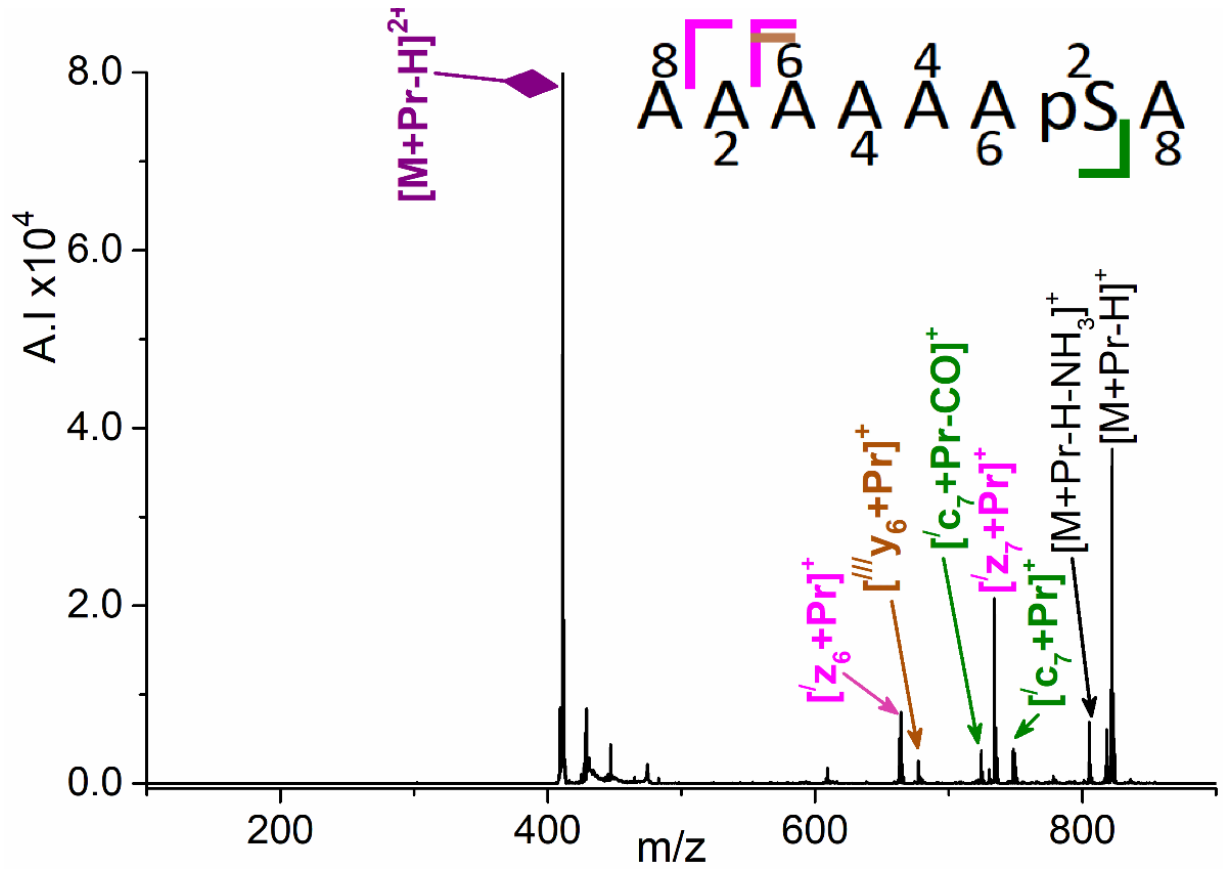


Figure 5.31. ETD mass spectrum of $[M + Pr - H]^{2+}$ for AAAAAApSA (A6pSA). In the figure, the following colors are used to label the ions: metal-adducted z-ions = bright pink, metal-adducted c-ions = green, and metal-adducted y-ions = brown. Undissociated precursor ion is labeled in purple with a large purple diamond arrow head. Neutral loss products and electron transfer without dissociation (ETnoD) ions are labeled in black. A prime symbol to the left indicates loss of a hydrogen (i.e., $^{/}c_n = [c_n - H]^+$) and to the right indicates the addition of a hydrogen at the cleavage site (i.e., $c_n^{//} = [c_n + 2H]^+$). The spectra have no expansion of the intensity axis; all peaks are shown to scale.

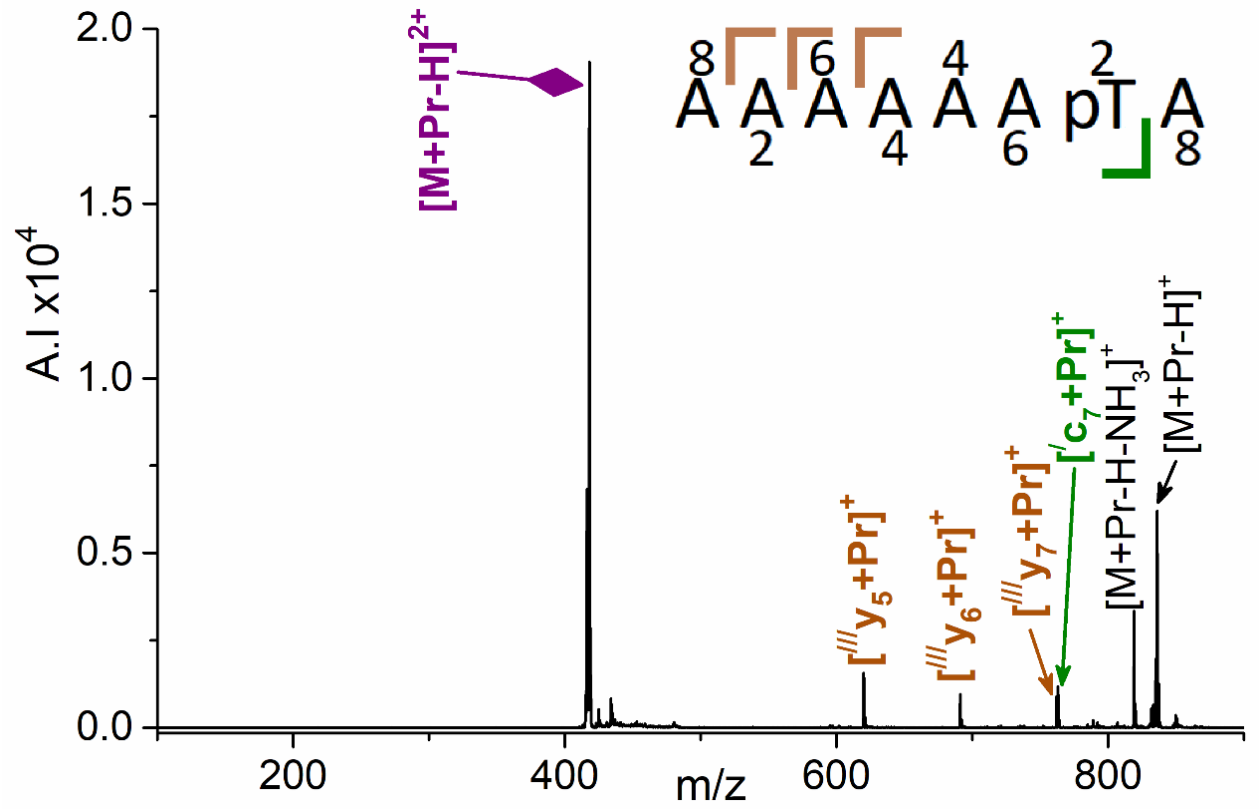


Figure 5.32. ETD mass spectrum of $[M + Pr - H]^{2+}$ for AAAAAApTA (A6pTA). In the figure, the following colors are used to label the ions: metal-adducted c-ions = green, and metal-adducted y-ions = brown. Undissociated precursor ion is labeled in purple with a large purple diamond arrow head. Neutral loss products and electron transfer without dissociation (ETnoD) ions are labeled in black. A prime symbol to the left indicates loss of a hydrogen (i.e., ${}^{/}c_n = [c_n - H]^+$) and to the right indicates the addition of a hydrogen at the cleavage site (i.e., $c_n^{//} = [c_n + 2H]^+$). The spectra have no expansion of the intensity axis; all peaks are shown to scale.

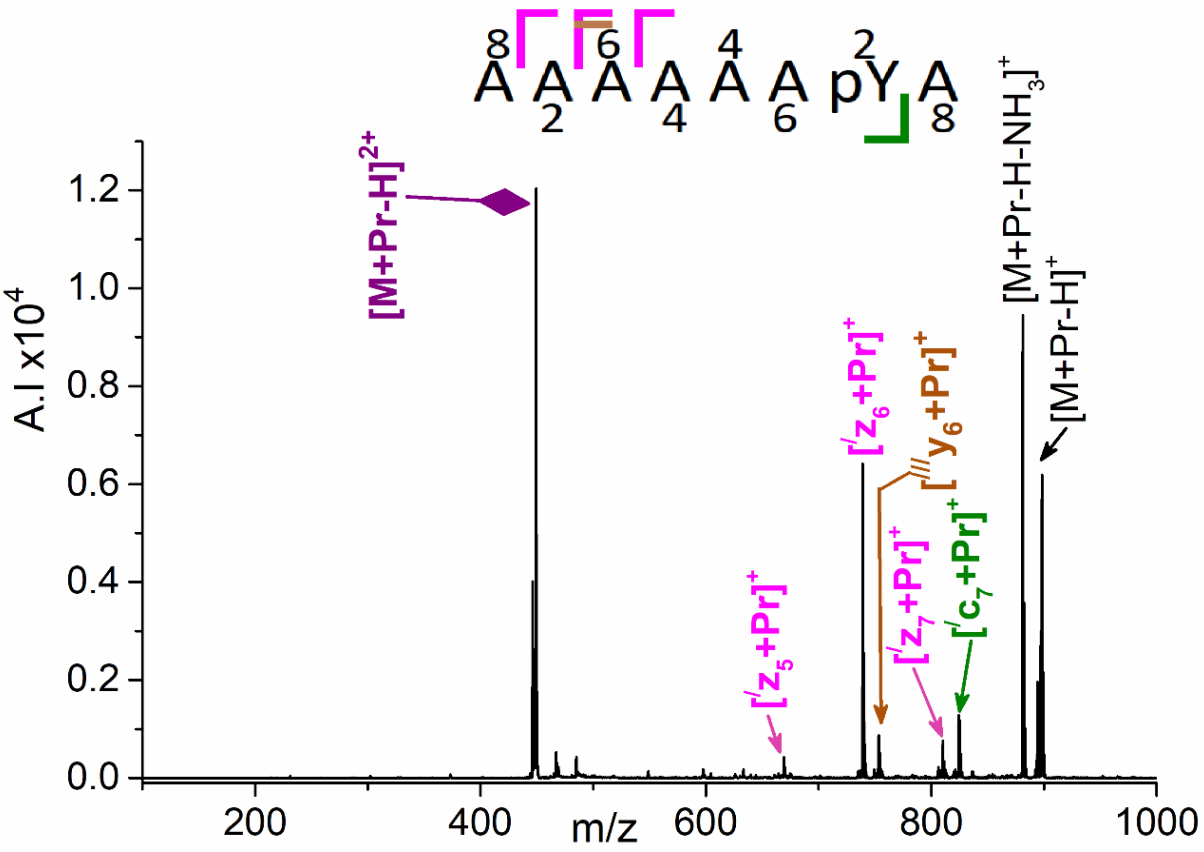


Figure 5.33. ETD mass spectrum of $[M + Pr - H]^{2+}$ for AAAAAApYA (A6pYA). In the figure, the following colors are used to label the ions: metal-adducted z-ions = bright pink, metal-adducted c-ions = green, and metal-adducted y-ions = brown. Undissociated precursor ion is labeled in purple with a large purple diamond arrow head. Neutral loss products and electron transfer without dissociation (ETnoD) ions are labeled in black. A prime symbol to the left indicates loss of a hydrogen (i.e., $^{/}c_n = [c_n - H]^+$) and to the right indicates the addition of a hydrogen at the cleavage site (i.e., $c_n^{//} = [c_n + 2H]^+$). The spectra have no expansion of the intensity axis; all peaks are shown to scale.

identification of the site of phosphorylation. The location of pS could not be determined for the $[M + Met]^{3+}$ (Figure 5.3) or $[M + Pr – H]^{2+}$ (Figure 5.12). Another example is EGF(988-998) where the exact location of ***pY*** at residue 5 can be conclusively determined by ETD of the $[M + Pr]^{3+}$ but not for 2+, as seen in Figures 5.2 and 5.11. For PDGF(pTyr Y-8P), ETD of $[M + Pr]^{3+}$, shown in Figure 5.7, yields more backbone cleavage than $[M + Pr – H]^{2+}$ (Figure 5.10) and allows elucidation of the location of ***pY*** at residue 1. Figures 5.4-5.6 show ETD of $[M + Pr]^{3+}$ for DNA transcription inhibitory peptide and its analogs. Compared to $[M + Pr – H]^{2+}$, a higher number of backbone cleavage sites and full sequence coverage occur with the 3+ ion.

Overall efficiency of fragmentation of precursor ions varies from one peptide to another. For example, in Figure 5.1 showing ETD of $[M + Pr + H]^{4+}$ from hsp, almost all of the precursor ion dissociates. In the ETD spectra shown in Figures 5.2, 5.3 and 5.7, the intensity of the precursor ion, $[M + Pr]^{3+}$, for EGF(988-998), hsp, and PDGF(pTyr Y-8P), is at one third to one half the intensity of the base peak. However, for DNA transcription inhibitory peptide and its analogs, $[M + Pr]^{3+}$ is the most intense peak in their ETD spectra (Figures 5.4-5.6). Nonetheless, full sequence coverage is obtained by ETD of $[M + Pr]^{3+}$ for the highly acidic DNA transcription inhibitory peptide and its analogs. Peptide sequence coverage and efficiency of ETD of the $[M + Pr – H]^{2+}$ for the model hexa- and octapeptides is low with the undissociated $[M + Pr – H]^{2+}$ being the base peak in most spectra. The only exception is for the octapeptide A3pSA4 where the non-dissociated precursor is about half the intensity of the base peak. In that spectrum, however, the base peak is the reduced ion of the precursor, $[M + Pr – H]^{+}$, and is not sequence informative.

## 5.5 Conclusions

The utilization of trivalent metal cationization for the analysis of highly acidic phosphorylated peptides by ETD has been demonstrated. All peptides in the study form multiply charged ions with charge states of 2+ or greater by ESI that can be isolated and investigated further by ETD. For all peptides investigated, ETD of $[M + Pr - H]^{2+}$ provides the least amount of sequence coverage. With the 2+ precursor ion, location of the phosphorylated residue is not possible for any of the acidic phosphorylated peptides studied. In contrast, location of the phosphoresidue and full sequence coverage is possible with both $[M + Pr]^{3+}$ and $[M + Pr + H]^{4+}$. Even highly acidic biological phosphorylated peptides with only acidic residues can be fully sequenced by ETD of $[M + Pr]^{3+}$. While $[M + Pr + H]^{4+}$ yields the most sequence informative fragmentation, generation of the protonated and metallated ion requires the presence of a basic amino acid residue in the peptide chain. In the current ETD study, only $Pr^{3+}$ was employed, but previous work in Chapter 3[46] indicates that any of the trivalent lanthanide metal cations (except radioactive promethium and europium) would be suitable for analysis of acidic phosphorylated peptides.

## References


1. Prabakaran, S.; Lippens, G.; Steen, H.; Gunawardena, J. Post-Translational Modification: Nature's Escape from Genetic Imprisonment and the Basis for Dynamic Information Encoding. *Wires Sys. Biol. Med.* **2012**, *4*, 565-583.

2. Wang, Y.; Peterson, S. E.; Loring, J. F. Protein Post-Translational Modifications and Regulation of Pluripotency in Human Stem Cells. *Cell Res.* **2014**, *24*, 143-160.

3. Hunter, T. Signaling-2000 and Beyond. *Cell* **2000**, *100*, 113.

4. Hunter, T. Oncoprotein Networks. *Cell* **1997**, *88*, 333-346.

5. Manning, G.; Whyte, D. B.; Martinez, R.; Hunter, T.; Sudarsanam, S. The Protein Kinase Complement of the Human Genome. *Science* **2002**, *298*, 1912-1916, 1933-1934.

6. Mann, M.; Ong, S.; Grønborg, M.; Steen, H.; Jensen, O. N.; Pandey, A. Analysis of Protein Phosphorylation using Mass Spectrometry: Deciphering the Phosphoproteome. *Trends Biotechnol.* **2002**, *20*, 261-268.

7. Cohen, P. The Regulation of Protein Function by Multisite Phosphorylation – A 25 Year Update. *Trends Biochem. Sci.* **2000**, *25*, 596-601.

8. Engholm-Keller, K.; Larsen, M. R. Technologies and Challenges in Large-Scale Phosphoproteomics. *Proteomics* **2013**, *13*, 910-931.

9. Ciesla, J.; Fraczyk, T.; Rode, W. Phosphorylation of Basic Amino Acid Residues in Proteins: Important but Easily Missed. *Acta Biochim. Pol.* **2011**, *58*, 137-147.

10. PhosphoNET Human Phosphosite KnowledgeBase. *http://kinexus.ca/* (accessed Feb 19, 2016).

11. Stensballe, A.; Jensen, O. N.; Olsen, J. V.; Haselmann, K. F.; Zubarev, R. A. Electron Capture Dissociation of Singly and Multiply Phosphorylated Peptides. *Rapid Commun. Mass Spectrom.* **2000**, *14*, 1793-2000.

12. Olsen, J. V.; Mann, M. Status of Large-Scale Analysis of Post-Translational Modifications by Mass Spectrometry. *Mol. Cell. Proteomics* **2013**, 3444-3452.

13. Doll, S.; Burlingame, A. L. Mass Spectrometry-Based Detection and Assignment of Protein Posttranslational Modifications. *ACS Chemical Biology* **2015**, *10*, 63-71.

14. Palumbo, A. M.; Reid, G. E. Evaluation of Gas-Phase Rearrangement and Competing Fragmentation Reactions on Protein Phosphorylation Site Assignment Using Collision Induced Dissociation-MS/MS and $MS^3$. *Anal. Chem.* **2008**, *80*, 9735-9747.

15. Edelson-Averbukh, M.; Shevchenko, A.; Pipkorn, R.; Lehmann, W. D. Gas-Phase Intramolecular Phosphate Shift in Phosphotyrosine-Containing Peptide Monoanions. *Anal. Chem.* **2009**, *81*, 4369-4381.

16. Busman, M.; Schey, K. L.; Oatis, J. E.; Knapp, D. R. Identification of Phosphorylation Sites in Phosphopeptides by Postive and Negative Mode Electrospray Ionization Tandem Mass Spectrometry. *J. Am. Soc. Mass Spectrom.* **1996**, *7*, 243-249.

17. Molina, H.; Horn, D. M.; Tang, N.; Mathivanan, S.; Pandey, A. Global Proteomic Profiling of Phosphopeptides using Electron Transfer Dissociation Tandem Mass Spectrometry. *Proc. Natl. Acad. Sci. USA* **2007**, *104*, 2199-2204.

18. Lopez-Clavijo, A. F.; Duque-Daza, C. A.; Creese, A. J.; Cooper, H. J. Electron Capture Dissociation Mass Spectrometry of Phosphopeptides: Arginine and Phosphoserine. *Int. J. Mass Spectrom.* **2015**, *390*, 63-70.

19. Creese, A. J.; Cooper, H. J. The Effect of Phosphorylation on the Electron Capture Dissociation of Peptide Ions. *J. Am. Soc. Mass Spectrom.* **2008**, *19*, 1263-1274.

20. Shi, S. D. H.; Hemling, M. E.; Carr, S. A.; Horn, D. M.; Lindh, I.; McLafferty, F. W. Phosphopeptide/Phosphoprotein Mapping by Electron Capture Dissociation Mass Spectrometry. *Anal. Chem.* **2001**, *73*, 19-22.

21. Bertran-Vicente, J.; Schümann, M.; Hackenberger, C. P.; Krause, E. Gas-Phase Rearrangement in Lysine Phosphorylated Peptides During Electron-Transfer Dissociation Tandem Mass Spectrometry. *Anal. Chem.* **2015**, *87*, 6990-6994.

22. Hayakawa, S.; Hashimoto, M.; Nagao, H.; Awazu, K.; Toyoda, M.; Ichihara, T.; Shigeri, Y. Study of the Dissociation of a Charge-Reduced Phosphopeptide Formed by Electron Transfer from an Alkali Metal Target. *Rapid Commun. Mass Spectrom.* **2008**, *22*, 567-572.

23. Hayakawa, S.; Matsumoto, S.; Hashimoto, M.; Iwamoto, K.; Nagao, H.; Toyoda, M.; Shigeri, Y.; Tajiri, M.; Wada, Y. High-Energy Electron Transfer Dissociation (HE-ETD) Using Alkali Metal Targets for Sequence Analysis of Post-Translational Peptides. *J. Am. Soc. Mass Spectrom.* **2010**, *21*, 1482-1489.

24. Sweet, S. M. M.; Bailey, C. M.; Cunningham, D. L.; Heath, J. K.; Cooper, H. J. Large Scale Localization of Protein Phosphorylation by Use of Electron Capture Dissociation Mass Spectrometry. *Mol. Cell. Proteomics* **2009**, *8*, 904-912.

25. Zhou, W.; Merrick, B. A.; Khaledi, M. G.; Tomer, K. B. Detection and Sequencing of Phosphopeptides Affinity Bound to Immobilized Metal Ion Beads by Matrix-Assisted Laser Desorption/Ionization Mass Spectrometry. *J. Am. Soc. Mass Spectrom.* **2000**, *11*, 273-282.

26. Gunawardena, H. P.; Emory, J. F.; McLuckey, S. A. Phosphopeptide Anion Characterization Via Sequential Charge Inversion and Electron-Transfer Dissociation. *Anal. Chem.* **2006**, *78*, 3788-3793.

27. Lehmann, W. D. *Protein Phosphorylation Analysis by Electrospray Mass Spectrometry: A Guide to Concepts and Practice;* Royal Society of Chemistry, London: 2010.

28. Stover, M. L.; Plummer, C. E.; Miller, S. R.; Cassady, C. J.; Dixon, D. A. Gas-Phase Acidities of Phosphorylated Amino Acids. *J. Phys. Chem. B* **2015**, *119 (46)*, 14604-14621.

29. Li, Z.; Matus, M. H.; Velazquez, H. A.; Dixon, D. A.; Cassady, C. J. Gas-Phase Acidities of Aspartic Acid, Glutamic Acid, and Their Amino Acid Amides. *Int. J. Mass Spectrom.* **2007**, *265*, 213-223.

30. Janek, K.; Wenschuh, H.; Bienert, M.; Krause, E. Phosphopeptide Analysis by Positive and Negative Ion Matrix-Assisted Laser Desorption/Ionization Mass Spectrometry. *Rapid Commun. Mass Spectrom.* **2001**, *15*, 1593-1599.

31. Huddleston, M. J.; Annan, R. S.; Bean, M. F.; Carr, S. A. Selective Detection of Phosphopeptides in Complex -Mixtures by Electrospray Liquid-Chromatography Mass-Spectrometry. *J. Am. Soc. Mass Spectrom.* **1993**, *4*, 710-719.

32. Beck, A.; Deeg, M.; Moeschel, K.; Schmidt, E. K.; Schleicher, E. D.; Voelter, W.; Haring, H. U.; Lehmann, R. Alkaline Liquid Chromatography/Electrospray Ionization Skimmer Collision-Induced Dissociation Mass Spectrometry for Phosphopeptide Screening. *Rapid Commun. Mass Spectrom.* **2001**, *15*, 2324-2333.

33. Neubauer, G.; Mann, M. Mapping of Phosphorylation Sites of Gel-Isolated Proteins by Nanoelectrospray Tandem Mass Spectrometry: Potentials and Limitations. *Anal. Chem.* **1999**, *71*, 235-224.

34. Tholey, A.; Reed, J.; Lehmann, W. D. Electrospray Tandem Mass Spectrometric Studies of Phosphopeptides and Phosphopeptide Analogues. *J. Mass Spectrom.* **1999**, *34*, 117-123.

35. Edelson-Averbukh, M.; Pipkorn, R.; Lehmann, W. D. Analysis of Protein Phosphorylation in the Regions of Consecutive Serine/Threonine Residues by Negative Ion Electrospray Collision-Induced Dissociation. Approach to Pinpointing of Phosphorylation Sites. *Anal. Chem.* **2007**, *79*, 3476-3486.

36. Beck, A.; Moeschel, K.; Deeg, M.; Haring, H.; Voelter, W.; Schleicher, E. D.; Lehmann, R. Identification of an in Vitro Insulin Receptor Substrate-1 Phosphorylation Site by Negative-Ion LC/ES-API-CID-MS Hybrid Scan Technique. *J. Am. Soc. Mass Spectrom.* **2003**, *14*, 401-405.

37. Edelson-Averbukh, M.; Shevchenko, A.; Pipkorn, R.; Lehmann, W. D. Discrimination between Peptide O-Sulfo- and O-Phosphotyrosine Residues by Negative Ion Mode Electrospray Tandem Mass Spectrometry. *J. Am. Soc. Mass Spectrom.* **2011**, *22*, 2256-2268.

38. Kweon, H. K.; Hakansson, K. Metal Oxide-Based Enrichment Combined with Gas-Phase Ion-Electron Reactions for Improved Mass Spectrometric Characterization of Protein Phosphorylation. *J. Proteome Res.* **2008**, *7*, 749-755.

39. Huzarska, M.; Ugalde, I.; Kaplan, D. A.; Hartmer, R.; Easterling, M. L.; Polfer, N. C. Negative Electron Transfer Dissociation of Deprotonated Phosphopeptide Anions: Choice of Radical Cation Reagent and Competition between Electron and Proton Transfer. *Anal. Chem.* **2010**, *82*, 2873-2878.

40. Coon, J. J.; Shabanowitz, J.; Hunt, D. F.; Syka, J. E. P. Electron Transfer Dissociation of Peptide Anions. *J. Am. Soc. Mass Spectrom.* **2005**, *16*, 880-882.

41. Wang, T.; Nha Tran, T.; Andreazza, H. J.; Bilusich, D.; Brinkworth, C. S.; Bowie, J. H. Negative Ion Cleavages of $(M–H)^-$ Anions of Peptides. Part 3. Post-translational Modifications. *Mass Spectrom. Rev.* **2018**, *37*, 3-21.

42. Tran, T. T. N.; Wang, T.; Hack, S.; Hoffmann, P.; Bowie, J. H. Can Collision-Induced Negative-Ion Fragmentations of $[M-H]^-$ Anions be Used to Identify Phosphorylation Sites in Peptides?. *Rapid Commun. Mass Spectrom.* **2011**, *25*, 3537-3548.

43. Edelson-Averbukh, M.; Pipkorn, R.; Lehmann, W. D. Phosphate Group-Driven Fragmentation of Multiply Charged Phosphopeptide Anions. Improved Recognition of Peptides Phosphorylated at Serine, Threonine, or Tyrosine by Negative Ion Electrospray Tandem Mass Spectrometry. *Anal. Chem.* **2006**, *78*, 1249-1256.

44. Andreazza, H. J.; Fitzgerald, M.; Bilusich, D.; Hoffmann, R.; Hoffmann, P.; Eichinger, P. C. H.; Bowie, J. H. Characteristic Negative Ion Fragmentations of Deprotonated Peptides Containing Post-Translational Modifications: Mono-Phosphorylated Ser, Thr and Tyr. A Joint Experimental and Theoretical Study. *Rapid Commun. Mass Spectrom.* **2008**, *22*, 3305-3312.

45. Commodore, J. J.; Cassady, C. J. Effects of Acidic Peptide Size and Sequence on Trivalent Praseodymium Adduction and Electron Transfer Dissociation Mass Spectrometry. *J. Mass Spectrom.* **2017**, *52*, 218-229.

46. Commodore, J. J.; Cassady, C. J. The Effects of Trivalent Lanthanide Cationization on the Electron Transfer Dissociation of Acidic Fibrinopeptide B and its Analogs. *J. Am. Soc. Mass Spectrom.* **2016**, *27*, 1499-1509.

47. Fung, Y. M. E.; Liu, H.; Chan, T. W. D. Electron Capture Dissociation of Peptides Metalated with Alkaline-Earth Metal Ions. *J. Am. Soc. Mass Spectrom.* **2006**, *17*, 757-771.

48. Chen, X.; Chan, W. Y. K.; Wong, P. S.; Yeung, H. S.; Chan, T. W. D. Formation of Peptide Radical Cations ($M^{+\cdot}$) in Electron Capture Dissociation of Peptides Adducted with Group IIB Metal Ions. *J. Am. Soc. Mass Spectrom.* **2011**, *22*, 233-244.

49. Liu, H.; Håkansson, K. Electron Capture Dissociation of Tyrosine O-Sulfated Peptides Complexed with Divalent Metal Cations. *Anal. Chem.* **2006**, *78*, 7570-7576.

50. Chen, X.; Fung, Y. M. E.; Chan, W. Y. K.; Wong, P. S.; Yeung, H. S.; Chan, T. W. D. Transition Metal Ions: Charge Carriers that Mediate the Electron Capture Dissociation Pathways of Peptides. *J. Am. Soc. Mass Spectrom.* **2011**, *22*, 2232-2245.

51. Liu, H.; Håkansson, K. Divalent Metal Ion-Peptide Interactions Probed by Electron Capture Dissociation of Trications. *J. Am. Soc. Mass Spectrom.* **2006**, *17*, 1731-1741.

52. Chen, X.; Wang, Z.; Li, W.; Wong, Y. L. E.; Chan, T. W. D. Effect of Structural Parameters on the Electron Capture Dissociation and Collision-Induced Dissociation Pathways of Copper(II)-Peptide Complexes. *Eur. J. Mass Spectrom.* **2015**, *21*, 649-657.

53. Chen, X.; Liu, G.; Wong, Y. L. E.; Deng, L.; Wang, Z.; Li, W.; Chan, T. W. D. Dissociation of Trivalent Metal Ion ($Al^{3+}$, $Ga^{3+}$, $in^{3+}$ and $Rh^{3+}$)–peptide Complexes Under Electron Capture Dissociation Conditions. *Rapid Commun. Mass Spectrom.* **2016**, *30*, 705-710.

54. Voinov, V. G.; Hoffman, P. D.; Bennett, S. E.; Beckman, J. S.; Barofsky, D. F. Electron Capture Dissociation of Sodium-Adducted Peptides on a Modified Quadrupole/Time-of-Flight Mass Spectrometer. *J. Am. Soc. Mass Spectrom.* **2015**, *26*, 2096-2104.

55. Kleinnijenhuis, A. J.; Mihalca, R.; Heeren, R. M. A.; Heck, A. J. R. Atypical Behavior in the Electron Capture Induced Dissociation of Biologically Relevant Transition Metal Ion Complexes of the Peptide Hormone Oxytocin. *Int. J. Mass Spectrom.* **2006**, *253*, 217-224.

56. Iavarone, A. T.; Paech, K.; Williams, E. R. Effects of Charge State and Cationizing Agent on the Electron Capture Dissociation of a Peptide. *Anal. Chem.* **2004**, *76*, 2231-2238.

57. Flick, T. G.; Donald, W. A.; Williams, E. R. Electron Capture Dissociation of Trivalent Metal Ion-Peptide Complexes. *J. Am. Soc. Mass Spectrom.* **2013**, *24*, 193-201.

58. Asakawa, D.; Takeuchi, T.; Yamashita, A.; Wada, Y. Influence of Metal–Peptide Complexation on Fragmentation and Inter-Fragment Hydrogen Migration in Electron Transfer Dissociation. *J. Am. Soc. Mass Spectrom.* **2014**, *25*, 1029-1039.

59. Dong, J.; Vachet, R. W. Coordination Sphere Tuning of the Electron Transfer Dissociation Behavior of Cu(II)-Peptide Complexes. *J. Am. Soc. Mass Spectrom.* **2012**, *23*, 321-329.

60. Asakawa, D.; Wada, Y. Electron Transfer Dissociation Mass Spectrometry of Peptides Containing Free Cysteine Using Group XII Metals as a Charge Carrier. *J Phys Chem B* **2014**, *118*, 12318-12325.

61. Mosely, J. A.; Murray, B. S.; Parker, D. Electron-Capture Dissociation and Collision-Induced Dissociation of Lanthanide Metal-Ligand Complexes and Lanthanide Metal-Ligand Complexes Bound to Phosphopeptides. *Eur. J. Mass Spectrom.* **2009**, *15*, 145-155.

62. Asakawa, D.; Osaka, I. High-Confidence Sequencing of Phosphopeptides by Electron Transfer Dissociation Mass Spectrometry using Dinuclear Zinc(II) Complex. *Anal. Chem.* **2016**, *88*, 12393-12402.

63. Chan, W. C.; White, P. D. *Fmoc Solid Phase Peptide Synthesis A Practical Approach;* Oxford University Press Inc., New York: 2000.

64. Roepstorff, P.; Fohlman, J. Proposal for a Common Nomenclature for Sequence Ions in Mass Spectra of Peptides. *Biomed. Mass Spectrom.* **1984**, *11*, 601.

65. Biemann, K. Contributions of Mass Spectrometry to Peptide and Protein-Structure. *Biomed. Environ. Mass Spectrom.* **1988**, *16*, 99-111.

66. Zubarev, R. A.; Kelleher, N. L.; McLafferty, F. W. Electron Capture Dissociation of Multiply Charged Protein Cations. A Nonergodic Process. *J. Am. Chem. Soc.* **1998**, *120*, 3265-3266.

67. Zubarev, R. A.; Horn, D. M.; Fridriksson, E. K.; Kelleher, N. L.; Kruger, N. A.; Lewis, M. A.; Carpenter, B. K.; McLafferty, F. W. Electron Capture Dissociation for Structural Characterization of Multiply Charged Protein Cations. *Anal. Chem.* **2000**, *72*, 563-573.

68. Zubarev, R. A.; Haselmann, K. F.; Budnik, B.; Kjeldsen, F.; Jensen, F. Towards an Understanding of the Mechanism of Electron-Capture Dissociation: A Historical Perspective and Modern Ideas. *Eur. J. Mass Spectrom.* **2002**, *8*, 337-349.

69. Zubarev, R. A.; Kruger, N. A.; Fridriksson, E. K.; Lewis, M. A.; Horn, D. M.; Carpenter, B. K.; McLafferty, F. W. Electron Capture Dissociation of Gaseous Multiply-Charged Proteins is Favored at Disulfide Bonds and Other Sites of High Hydrogen Atom Affinity. *J. Am. Chem. Soc.* **1999**, *121*, 2857-2862.

70. Syrstad, E. A.; Tureček, F. Toward a General Mechanism of Electron Capture Dissociation. *J. Am. Soc. Mass Spectrom.* **2005**, *16*, 208-224.

71. Syka, J. E. P.; Coon, J. J.; Schroeder, M. J.; Shabanowitz, J.; Hunt, D. F. Peptide and Protein Sequence Analysis by Electron Transfer Dissociation Mass Spectrometry. *Proc. Natl. Acad. Sci. USA* **2004**, *101*, 9528-9533.

72. Chen, X.; Tureček, F. The Arginine Anomaly: Arginine Radicals are Poor Hydrogen Atom Donors in Electron Transfer Induced Dissociations. *J. Am. Chem. Soc.* **2006**, *128*, 12520-12530.

73. Hunter, E.P., Lias, S.G. Proton Affinity Evaluation. In *NIST Chemistry WebBook, NIST Standard Reference Database Number 69*; Linstrom, P.J., Mallard, W.G., Ed.; NIST: National Institute of Standards and Technology, Gaithersburg MD, 20899, (accessed February 5, 2016), .

74. Harrison, A. G. The Gas-Phase Basicities and Proton Affinities of Amino Acids and Peptides. *Mass Spectrom. Rev.* **1997**, *16*, 201-217.

75. Ewing, N. P.; Zhang, X.; Cassady, C. J. Determination of the Gas-Phase Basicities of Proline and its Di- and Tripeptides with Glycine: The Enhanced Basicity of Prolylproline. *J. Mass Spectrom.* **1996**, *31*, 1345-1350.

76. Martens, J. K.; Grzetic, J.; Berden, G.; Oomens, J. Gas-Phase Conformations of Small Polyprolines and Their Fragment Ions by IRMPD Spectroscopy. *Int. J. Mass Spectrom.* **2015**, *377*, 179-187.

77. Nilsson, C. L. Advances in Quantitative Phosphoproteomics. *Anal. Chem.* **2011**, *84*, 735-746.

78. Li, W.; Song, C.; Bailey, D. J.; Tseng, G. C.; Coon, J. J.; Wysocki, V. H. Statistical Analysis of Electron Transfer Dissociation Pairwise Fragmentation Patterns. *Anal. Chem.* **2011**, *83*, 9540-9545.

79. Chalkley, R. J. Improving Peptide Identification Using Empirical Scoring Systems. *Methods Mol. Biol.* **2013**, 173-182.

80. Mikesh, L. M.; Ueberheide, B.; Chi, A.; Coon, J. J.; Syka, J. E. P.; Shabanowitz, J.; Hunt, D. F. The Utility of ETD Mass Spectrometry in Proteomic Analysis. *Biochim. Biophys Acta.* **2006**, *1764*, 1811-1822.

81. Savitski, M. M.; Nielsen, M. L.; Zubarev, R. A. Side-Chain Losses in Electron Capture Dissociation to Improve Peptide Identification. *Anal. Chem.* **2007**, *79*, 2296-2302.

82. Annan, R. S.; Carr, S. A. Phosphopeptide Analysis by Matrix-Assisted Laser Desoprtion Time-of-Flight Mass Spectrometry. *Anal. Chem.* **1996**, *68*, 3413-3421.

83. Zhang, X.; Herring, C. J.; Romano, P. R.; Brzeska, H. S.; Hinnebusch, A. G. Identification of Phosphorylation Sites in Proteins Separated by Polyacrylamide Gel Electrophoresis. *Anal. Chem.* **1998**, *70*, 2050.

84. Wilm, M.; Neubauer, G.; Mann, M. Parent Ion Scans of Unseparated Peptide Mixtures. *Anal. Chem.* **1996**, *68*, 527-533.

85. Hunter, A. P.; Games, D. E. Chromatographic and Mass Spectrometric Methods for the Identification of Phosphorylation Sites in Phosphoproteins. *Rapid Commun. Mass Spectrom.* **1994**, *8*, 559-570.

86. Schlosser, A.; Pipkorn, R.; Bossemeyer, D.; Lehmann, W. D. Analysis of Protein Phosphorylation by a Combination of Elastase Digestion and Neutral Loss Tandem Mass Spectrometry. *Anal. Chem.* **2001**, *73*, 170-176.

87. Moss, C. L.; Chung, T. W.; Wyer, J. A.; Nielsen, S. B.; Hvelplund, P.; Tureček, F. Dipole-Guided Electron Capture Causes Abnormal Dissociations of Phosphorylated Pentapeptides. *J. Am. Soc. Mass Spectrom.* **2011**, *22*, 731-751.

88. Bielska, A. A.; Zondlo, N. J. Hyperphosphorylation of Tau Induces Local Polyproline II Helix. *Biochemistry (N. Y. )* **2006**, *45*, 5527-5537.

89. Errington, N.; Doig, A. J. A Phosphoserine− Lysine Salt Bridge Within an A-Helical Peptide, the Strongest A-Helix Side-Chain Interaction Measured to Date. *Biochemistry (N. Y. )* **2005**, *44*, 7553-7558.

90. Liu, H.; Yoo, H. J.; Håkansson, K. Characterization of Phosphate-Containing Metabolites by Calcium Adduction and Electron Capture Dissociation. *J. Am. Soc. Mass Spectrom.* **2008**, *19*, 799-808.

91. Settimo, L.; Donnini, S.; Juffer, A. H.; Woody, R. W.; Marin, O. Conformational Changes upon Calcium Binding and Phosphorylation in a Synthetic Fragment of Calmodulin. *Peptide Science* **2007**, *88*, 373-385.

92. van der Rest, G.; Hui, R.; Frison, G.; Chamot-Rooke, J. Dissociation Channel Dependence on Peptide Size Observed in Electron Capture Dissociation of Tryptic Peptides. *J. Am. Soc. Mass Spectrom.* **2011**, *22*, 1631-1644.

93. Bakken, V.; Helgaker, T.; Uggerud, E. Models of Fragmentations Induced by Electron Attachment to Protonated Peptides. *Eur. J. Mass Spectrom.* **2004**, *10*, 625-638.

94. Cooper, H. J. Investigation of the Presence of B Ions in Electron Capture Dissociation Mass Spectra. *J. Am. Soc. Mass Spectrom.* **2005**, *16*, 1932-1940.

95. Feng, C. Electron Transfer Dissociation Mass Spectrometry Studies of Peptides, Ph. D. Dissertation, The University of Alabama, Tuscaloosa, AL, USA, 2014.

96. Kowalewska, K.; Stefanowicz, P.; Ruman, T.; Fraczyk, T.; Rode, W.; Szewczuk, Z. Electron Capture Dissociation Mass Spectrometric Analysis of Lysine-Phosphorylated Peptides. *Biosci. Rep.* **2010**, *30*, 433-443.

97. Wong, P. S. J.; Chen, X.; Deng, L.; Wang, Z.; Li, W.; Wong, Y. L. E.; Chan, T. W. D. Suppression of Peptide Ion Dissociation Under Electron Capture: Role of Backbone Amide Hydrogen. *Rapid Commun. Mass Spectrom.* **2015**, *29*, 1757-1764.

98. Good, D. M.; Wirtala, M.; McAlister, G. C.; Coon, J. J. Performance Characteristics of Electron Transfer Dissociation Mass Spectrometry. *Mol. Cell. Proteomics* **2007**, *6*, 1942-1951.

99. Frese, C. K.; Altelaar, A. F. M.; Hennrich, M. L.; Nolting, D.; Zeller, M.; Griep-Raming, J.; Heck, A. J. R.; Mohammed, S. Improved Peptide Identification by Targeted Fragmentation using CID, HCD and ETD on an LTQ-Orbitrap Velos. *J. Proteome Res.* **2011**, *10*, 2377-2388.

100. Rožman, M.; Gaskell, S. J. Charge State Dependent Top-Down Characterisation using Electron Transfer Dissociation. *Rapid Commun. Mass Spectrom.* **2012**, *26*, 282-286.

# CHAPTER 6: OPTIMIZATION OF ELECTROSPRAY IONIZATION CONDITIONS TO ENHANCE FORMATION OF DOUBLY PROTONATED PEPTIDE IONS WITH AND WITHOUT ADDITION OF CHROMIUM(III)

## 6.1 Overview

Production of multiply protonated ions by electrospray ionization (ESI) is important to the analysis of peptides by mass spectrometry. For small neutral and acidic peptides, addition of chromium(III) greatly increases the intensity of doubly protonated ions. The current study examines instrumental and solution parameters that maximize peptide ion charge by ESI. Nebulizer gas pressure and drying gas flow rate are crucial parameters for production of $[M + 2H]^{2+}$, while drying gas temperature alone has minimal effect. Optimization of the capillary exit and skimmer voltages are important both to maximize $[M + 2H]^{2+}$ and reduce unwanted ion dissociation. Protonation is enhanced and fewer impurity peaks are observed when solutions are prepared in colorless plastic vials that have been rinsed briefly with propan-2-ol (isopropanol). Optimization of instrument and sample preparation factors for enhanced protonation with and without $Cr^{3+}$ is necessary to allow maximum formation of $[M + 2H]^{2+}$. Proteomics researchers should find these procedures to be of use for increasing multiply protonated signal intensity even in the absence of $Cr^{3+}$.

## 6.2 Introduction

The ability to multiply charge can be very important to the analysis of peptides by electrospray ionization (ESI) mass spectrometry. Ions with higher charge states generally require less energy to dissociate and provide more sequence informative fragmentation.[1-6] Collision-induced dissociation (CID), which is the most common tandem mass spectrometry (MS/MS) technique, generally provides more useful biological sequence information with doubly protonated ions, $[M + 2H]^{2+}$, than with singly protonated species, $[M + H]^{+}$.[7-9] For example, in a study of 5,500 CID spectra, two common peptide identification algorithms were found to give much higher peptide identification scores for $[M + 2H]^{2+}$ precursor ions than for $[M + H]^{+}$.[10] Furthermore, multiple charging allows ions to be shifted to a region of the spectrum where resolution is optimal[11] as well as increasing ion intensity for mass spectrometers whose signal detected is proportional to ionic charge.[12,13] Enhanced protonation can also increase the signal-to-noise ratios (S/N) of mass spectra. This is especially useful with automated bioinformatic methods where low ion intensities can result in false-positive peptide identifications due to difficulties in elucidating relevant analyte and MS/MS product ions.[14,15] In addition, multiple charging is necessary for positive mode electron-based MS/MS processes such as electron transfer dissociation (ETD)[16-18] and electron capture dissociation (ECD)[19-21] that involve capture or transfer of electrons. (Addition of an electron to $[M + H]^{+}$ would result in a neutral species and neutral products that are not analyzed and detected by mass spectrometry.)

Recently, the Cassady group reported that the use of chromium(III), $Cr^{3+}$, can enhance the protonation of peptides by ESI.[22] This was first discovered during a CID study of the effect of metalation on peptide fragmentation.[23] While that study focused on metal adduction, Dr. Watson noted that neutral heptaalanine forms $[M + 2H]^{2+}$ upon addition of $Cr^{3+}$ to the peptide

solution. Ten other metal ions were also studied and this effect was found to be unique for $Cr^{3+}$.[22] Neutral and acidic peptides that typically form only $[M + H]^+$ can generate abundant $[M + 2H]^{2+}$ upon addition of $Cr^{3+}$ salts to the solution undergoing ESI. Enhanced protonation of peptide methyl esters does not occur with $Cr^{3+}$, which suggests that the mechanism involves interaction of the metal cation with a carboxylic acid group. In the present work, enhanced protonation was optimized by considering solution parameters, as well as conditions in the ESI source. We compare the protonation of the neutral peptide heptaalanine (A7) using $Cr^{3+}$ to the protonation of the basic peptide AAAKAAA (A3KA3) that forms $[M + 2H]^{2+}$ even in the absence of $Cr^{3+}$. Thus, conclusions are drawn about the best conditions for enhancing the protonation of peptides both with and without addition of $Cr^{3+}$.

## 6.3 Experimental

### 6.3.1 Mass spectrometry

All experiments were performed on a Bruker (Billerica, MA, USA) HCTultra PTM Discovery System high capacity quadrupole ion trap mass spectrometer. The ESI source design has a grounded needle. The high voltage (capillary entrance potential) is applied on the platinum coating at the entrance of the ESI capillary as well as the stainless steel capillary entrance cap and endplate. Refer to Figure 2.2. Parameters altered in the present study included potentials of the capillary entrance and capillary exit shown in Figure 2.2 as well as the potential applied to the skimmer shown in Figure 2.3. Drying gas flow rate and temperature and nebulizing gas pressure were also varied. Values for the capillary entrance ranged from -4.0 to -2.0 kV. Capillary exit potentials were investigated between 0 and -200 V, while skimmer voltages ranged from 0 to -100 V. Experiments were performed in positive ion mode, so all listed voltages are negative to attract the ions into the capillary entrance shown in Figure 2.2. Absolute values for

voltages are used to plot graphs. Single-stage mass spectra were obtained in positive ion mode. Peptide solutions were 10 µM in acetonitrile/water at a volume ratio of 50:50. For experiments involving $Cr^{3+}$, the peptide to metal molar ratio was 1:10, which we have previously optimized.[22] The infused sample flow rate was 3 µL/min using a syringe pump from KD Scientific (Holliston, MA, USA). Experiments were performed in triplicate and each data point involved signal averaging of 300 scans. In all figures, error bars represent a range of ± one standard deviation calculated from the three replicate trials obtained on separate days. All relative ion intensities were normalized to 1.

### 6.3.2 Peptides

The peptide A7 was purchased from Biomatik (Cambridge, Ontario, CA). All other peptides were synthesized in our laboratory with an Advanced ChemTech (Louisville, KY, USA) model 90 automated peptide synthesizer using standard Fmoc procedures.[24] Peptides were used without further purification, which accounts for impurity peaks in the spectra. Peptide synthesis reagents were purchased from VWR International (Radnor, PA, USA). Chromium(III) nitrate and the ESI and rinse solvents, acetonitrile and propan-2-ol (isopropanol = IPA), were purchased from VWR. The distilled and deionized water was produced on an E-pure system (Barnstead, SDubuque, IA, USA).

## 6.4 Results and discussion

The effects of instrument parameters on ESI ion formation will be compared for A7 and A3KA3. With $Cr^{3+}$, A7 forms $[M + 2H]^{2+}$, $[M + Cr – H]^{2+}$ and $[M + H]^{+}$. In the absence of $Cr^{3+}$, A7 forms only $[M + H]^{+}$ as shown in Figure 6.1. With or without addition of $Cr^{3+}$, the basic peptide A3KA3 forms $[M + 2H]^{2+}$ and $[M + H]^{+}$. Analysis of A3KA3 in the absence of $Cr^{3+}$ is used to determine if the effects observed by varying instrument and sample preparation

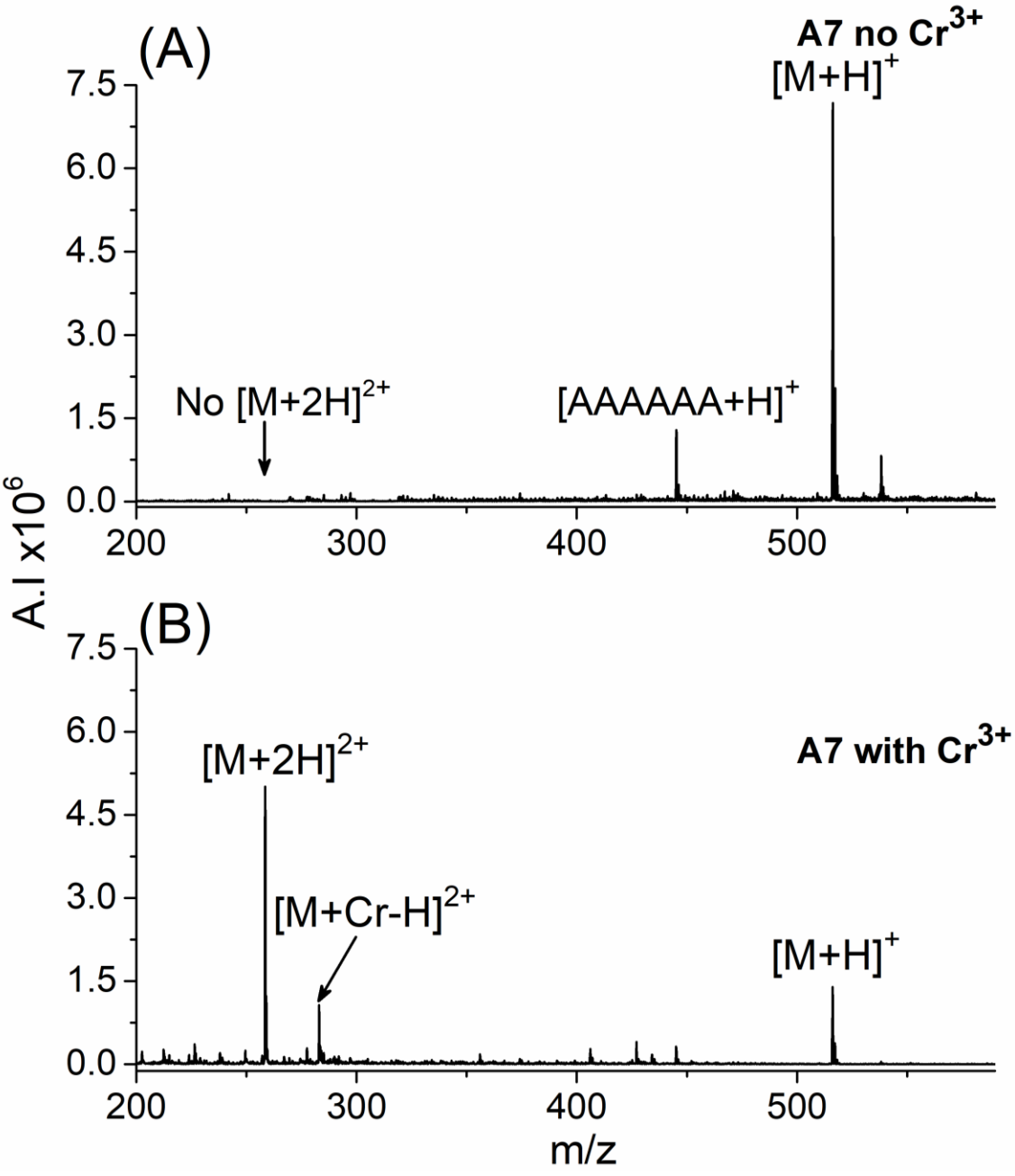


Figure 6.1. ESI mass spectrum of A7 (a) without $Cr^{3+}$ and (b) with $Cr^{3+}$ at a 1:10 molar ratio of A7:Cr. For comparison, (b) shows enhanced protonation at optimized parameters with an $[M + 2H]^{2+}$:$[M + H]^{+}$ intensity ratio of 4:1. AAAAAA (A6) is an impurity from the peptide synthesis.

parameters are related to enhanced protonation with $Cr^{3+}$ or simply relate to "routine" double charging by ESI. Throughout the remainder of this text, experiments involving A7 will include $Cr^{3+}$ addition while experiments with A3KA3 will not include $Cr^{3+}$. Absolute values for voltages are used to plot graphs.

### 6.4.1 Effects of ESI gases

The pressure of the ESI nebulizer gas (nitrogen) was found to be important for increasing the intensity of $[M + 2H]^{2+}$, and this effect is illustrated in Figure 6.2. Nebulizer gas assists in droplet formation as described in Section 2.2 in Chapter 2. Maximum enhanced protonation for A7 occurs at lower nebulizer gas pressures within a narrow range between 8 and 10 psi. For A3KA3, the highest abundance of $[M + 2H]^{2+}$ occurs at a lower nebulizer pressure (~2 psi), which is the lowest pressure that our HCTultra mass spectrometer can achieve. The intensity of $[M + 2H]^{2+}$ from A3KA3 steadily drops as the nebulizer pressure is increased. These results suggest that enhanced protonation with $Cr^{3+}$ is occurring during the spray/desolvation process instead of later at the capillary exit and skimmer region as the Cassady group initially postulated.[22] Protonation of the basic peptide A3KA3 appears to occur, at least to some extent, in solution because it is most abundant at very low nebulizer gas pressure. Two other peptides were studied to confirm these nebulizer gas effects. The neutral peptide AAIAAAA with $Cr^{3+}$ gave a graph similar to that of A7 in Figure 6.2(a), while basic peptide GVAKAAA behaved in a manner similar to A3KA3 in Figure 6.2(b). The intensity of $[M + H]^{+}$ for both peptides, and that of $[M + Cr – H]^{2+}$ for A7, show little fluctuation over the range of nebulizer gas pressures.

Drying gas conditions is also important in the ESI desolvation process, as Fenn and coworkers[25] noted in an early ESI study. Drying gas assists in ion formation by helping to evaporate solvent from mist droplets and is discussed in Figure 2.1. As can be seen in

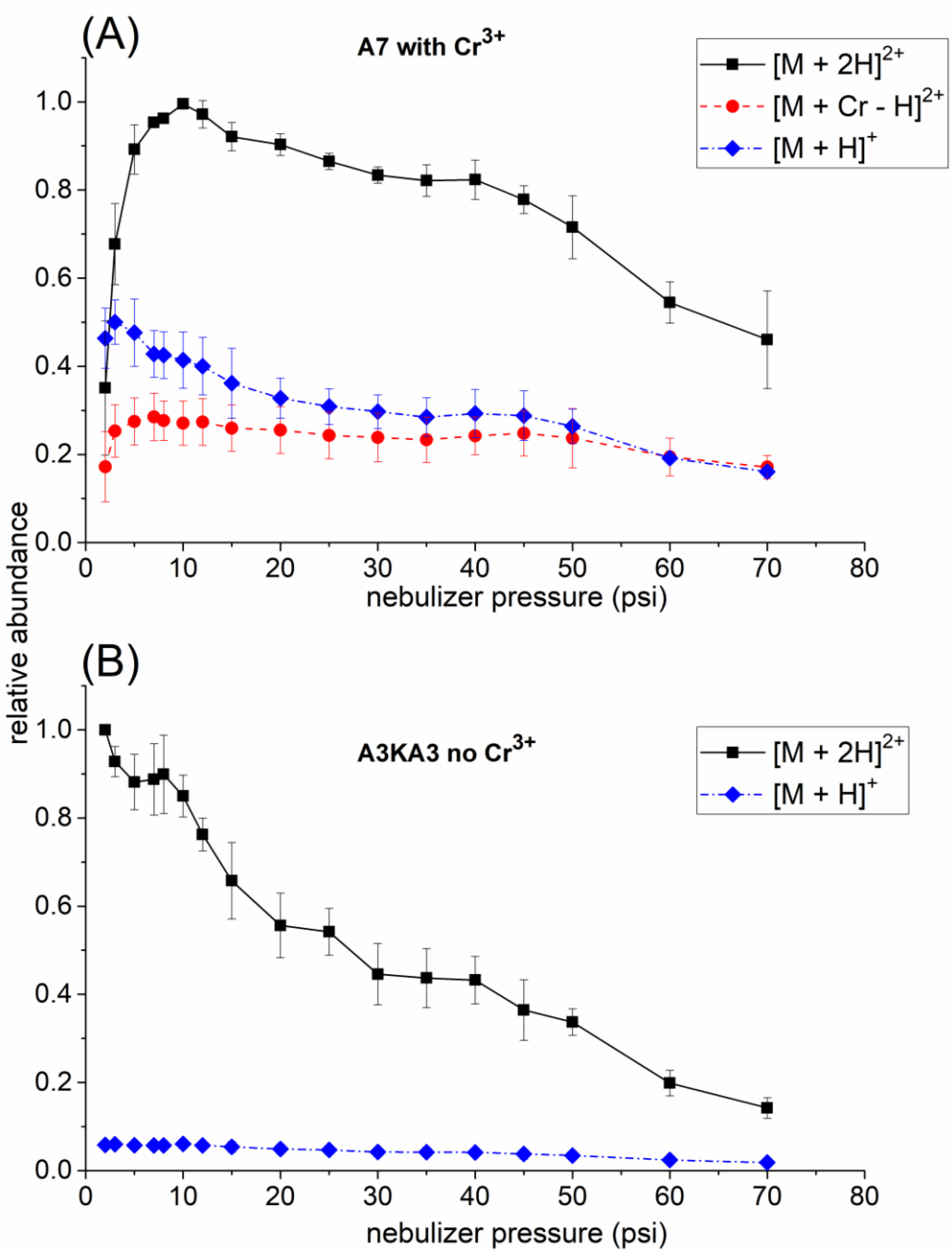


Figure 6.2. Relative intensity of ions formed as a function of nebulizer gas pressure in psi for (a) A7 and (b) A3KA3. The capillary exit and skimmer potentials were fixed at -95 V and -25 V, respectively. $[M + 2H]^{2+}$ is represented by the black solid line with filled black square symbols, $[M + H]^{+}$ by the blue dashed line with filled blue diamond symbols, and $[M + Cr – H]^{2+}$ by the red dashed line with filled red circle symbols.

Figure 6.3, formation of $[M + 2H]^{2+}$ increases with increasing drying gas(nitrogen) flow rate for both A7 and A3KA3. The maximum intensity of $[M + 2H]^{2+}$ occurs between 9 and 10 L/min for A7 and 12 L/min for A3KA3. Drying gas flow rates below about 4 L/min result in great instability of the $[M + 2H]^{2+}$ signal for A7; this effect is less pronounced for A3KA3. These observations again support the importance of the spray/desolvation process in enhanced protonation using $Cr^{3+}$. For A7, formation of $[M + Cr - H]^{2+}$ also increases as a function of increasing drying gas flow rate. The intensity of $[M + H]^{+}$ from A7 steadily decreases with increasing flow rate after a brief peak at ~2 L/min. The decrease in $[M + H]^{+}$ intensity and the increase in $[M + 2H]^{2+}$ intensity for A7 appear to occur simultaneously over the same range of flow rates. This suggests that increasing drying gas flow rate facilitates formation of $[M + 2H]^{2+}$ in place of $[M + H]^{+}$ for A7. In contrast, $[M + H]^{+}$ for A3KA3 shows little fluctuation in its intensity over the range of drying gas flow rates.

Drying gas temperature alone was found to have little effect on protonation once a temperature sufficient for reproducible desolvation was obtained. For A7, as illustrated in Figure 6.4(a), there is little variation in the formation of $[M + 2H]^{2+}$ except for an increase in abundance as the temperature increases from 50°C to 100°C. $[M + Cr - H]^{2+}$ and $[M + H]^{+}$ also show only slight fluctuations in relative abundances with increasing drying gas temperature. For A3KA3, formation of $[M + 2H]^{2+}$ gradually increases with increasing drying gas temperature until leveling off at ~200°C as shown in Figure 6.4(b). The $[M + H]^{+}$ for A3KA3 shows little fluctuation in its intensity over the range of drying gas temperatures. Therefore, drying gas temperature was fixed at 300°C for all other experiments for both peptides (except as noted in the next paragraph).

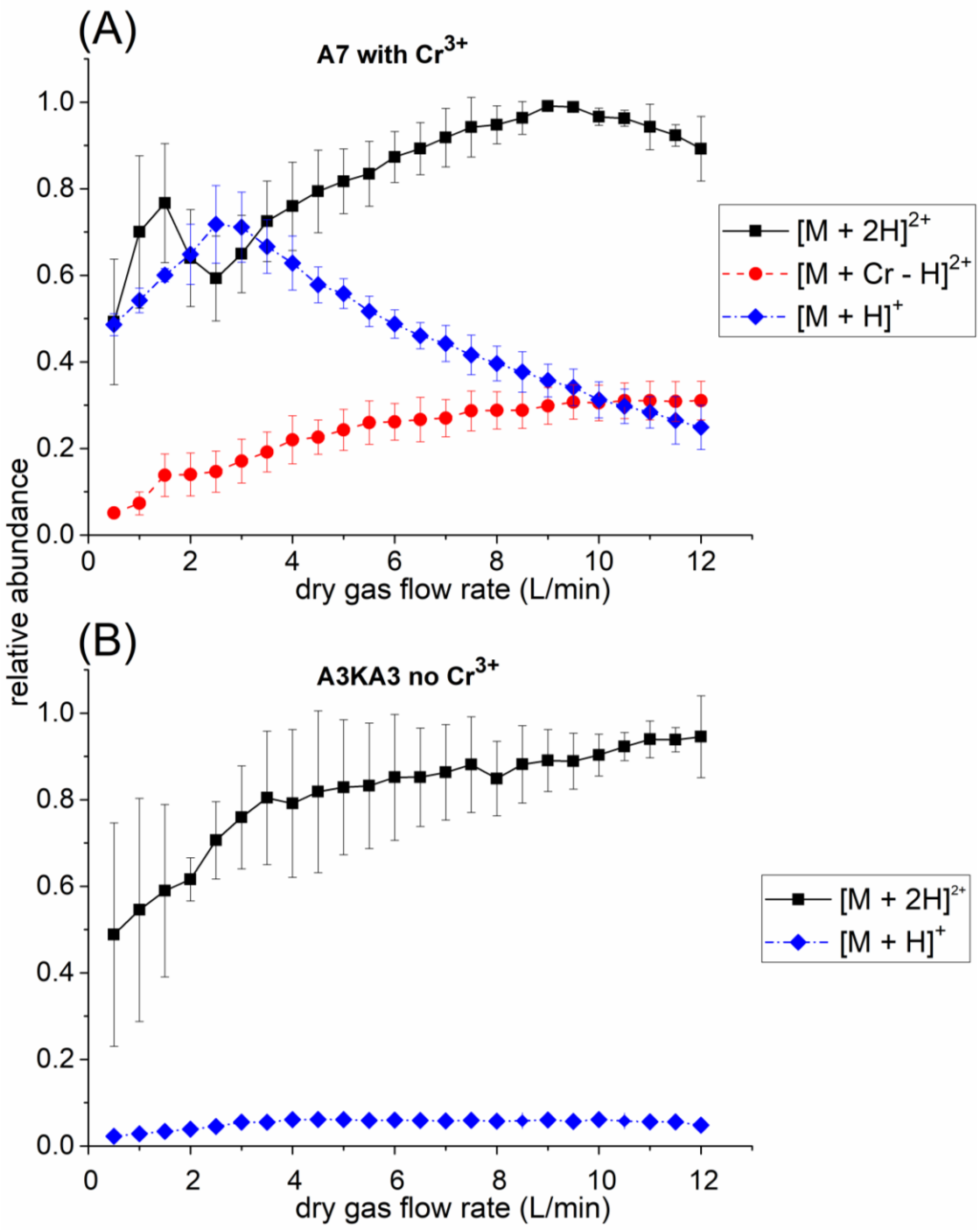


Figure 6.3. Relative intensity of ions formed as a function of drying gas flow rate in L/min for (a) A7 and (b) A3KA3. The capillary exit and skimmer potentials were fixed at -95 V and -25 V, respectively. $[M + 2H]^{2+}$ is represented by the black solid line with filled black square symbols, $[M + H]^{+}$ by the blue dashed line with filled blue diamond symbols, and $[M + Cr – H]^{2+}$ by the red dashed line with filled red circle symbols.

Studies have shown that decreasing drying gas temperature or flow rate/pressure can enhance the formation of solvated analyte ions.[26,27] In the current work, simultaneous lowering of drying gas flow rate and drying gas temperature significantly reduced the intensity of protonated ions formed for A7. However, with these mild desolvation conditions, water-solvated complexes, $[M + Cr – H + nH_2O]^{2+}$, form in sufficient intensities to be isolated and studied by CID. These complex ions with up to four bound water molecules (n = 4) were observed. In our group's previous study,[22] we had proposed that $[M + 2H]^{2+}$ from A7 may be the result of $[M + Cr – H + nH_2O]^{2+}$ undergoing dissociation in the capillary-skimmer region of the ESI source. (The capillary exit-skimmer region can be observed in Figure 2.3). Figure 6.5(a) shows that CID of $[M + Cr – H + 2H_2O]^{2+}$ leads to loss of water molecule(s) to form $[M + Cr – H + H_2O]^{2+}$ and $[M + Cr – H]^{2+}$. Further isolation of $[M + Cr – H + H_2O]^{2+}$ and subsequent $MS^3$, as shown in Figure 6.5(b), generates $[M + Cr – H]^{2+}$. In addition, CID of $[M + Cr – H]^{2+}$ generates a-, b-, x- and y-ions, but no $[M + 2H]^{2+}$ forms. For n = 3 and 4, CID and $MS^3$ also leads to loss of all water molecules to yield the deprotonated chromium-bound peptide species. This suggests (but does not definitely prove) that $[M + Cr – H + nH_2O]^{2+}$ is not the intermediate complex involved in enhanced protonation with $Cr^{3+}$.

### 6.4.2 Effects of ESI potentials

The ESI source design of our Bruker HCTultra has the spray needle at ground and the high voltage placed on the capillary entrance (which is platinum coated), as well as on the stainless steel capillary entrance cap and endplate seen in Figure 2.2. This capillary entrance potential was varied over the range of absolute values 2 to 4 kV. (The positive ion mode uses a negative voltage to attract ions to the capillary entrance, but absolute values are used to plot Figures 6.6, as well as Figures 6.7, and 6.8.) For both A7 and A3KA3, formation of $[M + 2H]^{2+}$

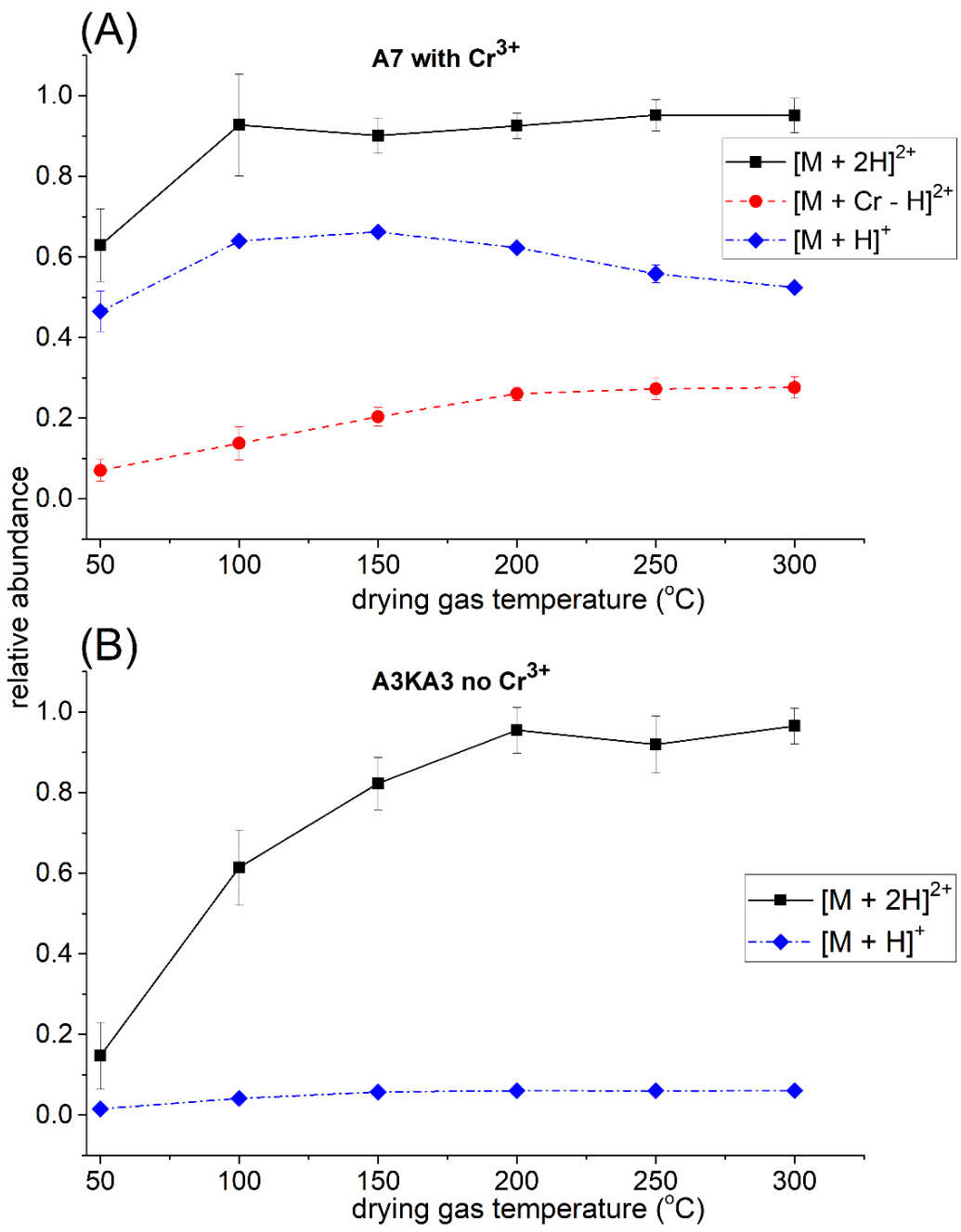


Figure 6.4. Relative intensity of ions formed as a function of drying gas temperature in °C for (a) A7 and (b) A3KA3. The capillary exit and skimmer potentials were fixed at -95 V and -25 V, respectively. $[M + 2H]^{2+}$ is represented by the black solid line with filled black square symbols, $[M + H]^{+}$ by the blue dashed line with filled blue diamond symbols, and $[M + Cr – H]^{2+}$ by the red dashed line with filled red circle symbols.

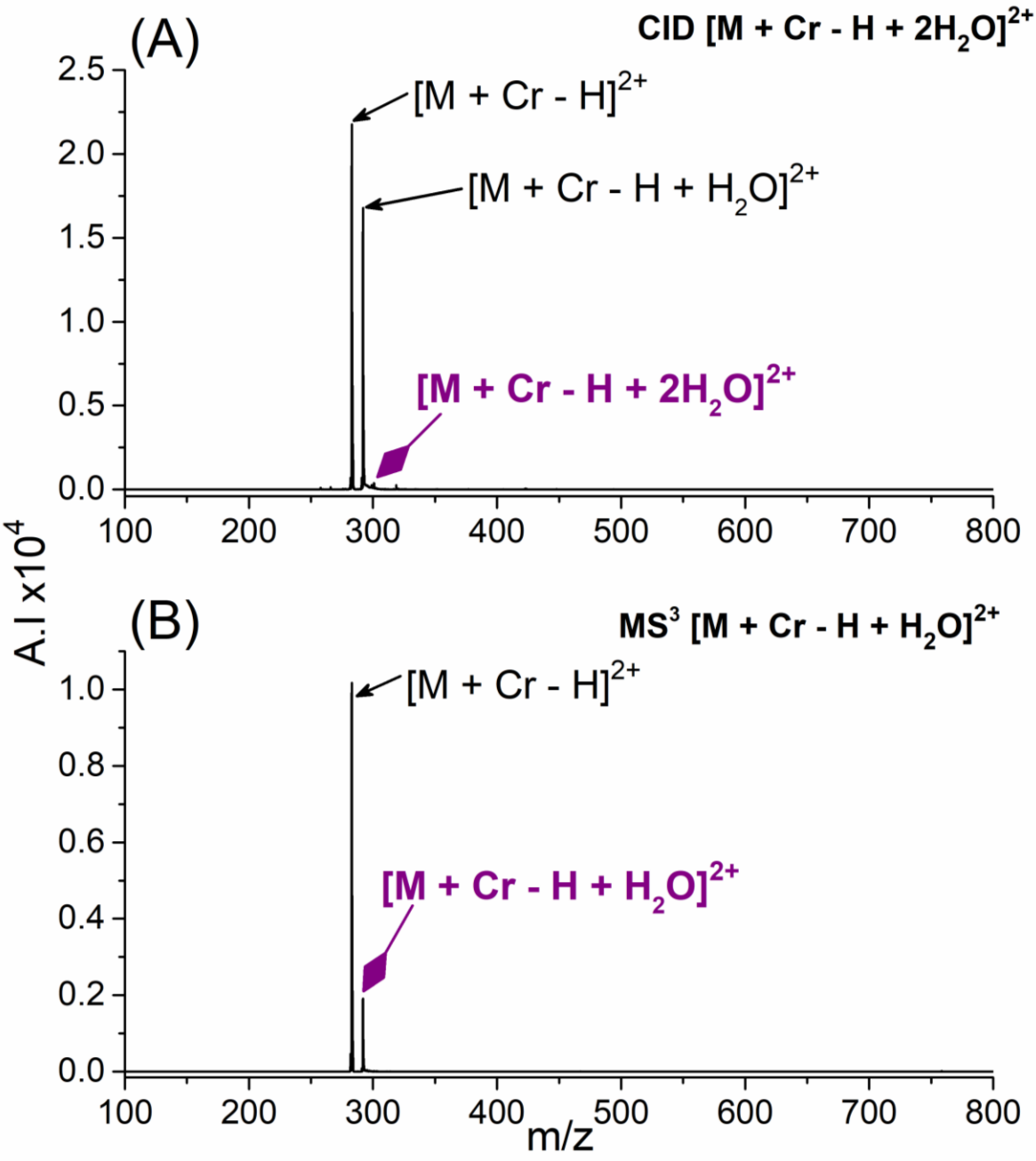


Figure 6.5. Tandem mass spectra of A7 showing (a) CID of $[M + Cr - H + 2H_2O]^{2+}$ and (b) CID $MS^3$ of $[M + Cr - H + H_2O]^{2+}$. Precursor ions are indicated by purple font with a purple arrow with a large diamond head. All product ions are shown in black font with black arrows.

gradually increases with a more intense absolute value of high voltage until a maximum abundance is reached at about an absolute value of 3.5 kV, as shown in Figure 6.6. The pattern of ion formation for both test peptides indicates that variation of the capillary entrance potential has little or no effect on enhanced protonation with $Cr^{3+}$. Therefore, all other experiments used a fixed capillary entrance potential of -4 kV.

The capillary exit potential (located inside of the vacuum chamber and can be seen in Figure 2.3) has a much greater effect on the $[M + 2H]^{2+}$ intensity for A7 and A3KA3 than the entrance potential. In these experiments, the potential of the skimmer (which immediately follows the capillary exit) was maintained at an absolute value of 25 V. As shown in Figure 6.7, production of $[M + 2H]^{2+}$ from A7 is most intense between absolute values of 80 V and 110 V. As the capillary exit potential increases above an absolute value of 110 V (i.e, becomes more negative in positive mode analysis), CID occurs in the source region (known as capillary-skimmer or nozzle-skimmer CID[28-31]) and generally increases with increasing absolute value of the voltage. The intensity of CID product ions directly correlates to decreasing $[M + 2H]^{2+}$ intensity in Figure 6.7(a), indicating that $[M + 2H]^{2+}$ is the primary precursor ion for the CID. This is expected because a greater Coulomb energy causes $[M + 2H]^{2+}$ to dissociate at lower energies than $[M + H]^{2+}$.[5,6] At potentials of higher absolute value (~ 200 V), conditions no longer permit sufficient transfer of ions and a decrease in all ion intensities occurs. For the basic peptide A3KA3, similar trends are observed although there is about a 20 V shift in higher absolute capillary exit voltages for both maximization of $[M + 2H]^{2+}$ and the formation of CID products.

The intensities of $[M + 2H]^{2+}$ for A7 and A3KA3 are also affected by skimmer potential, as shown in Figure 6.8. The capillary exit voltage was maintained at -95 V while the skimmer

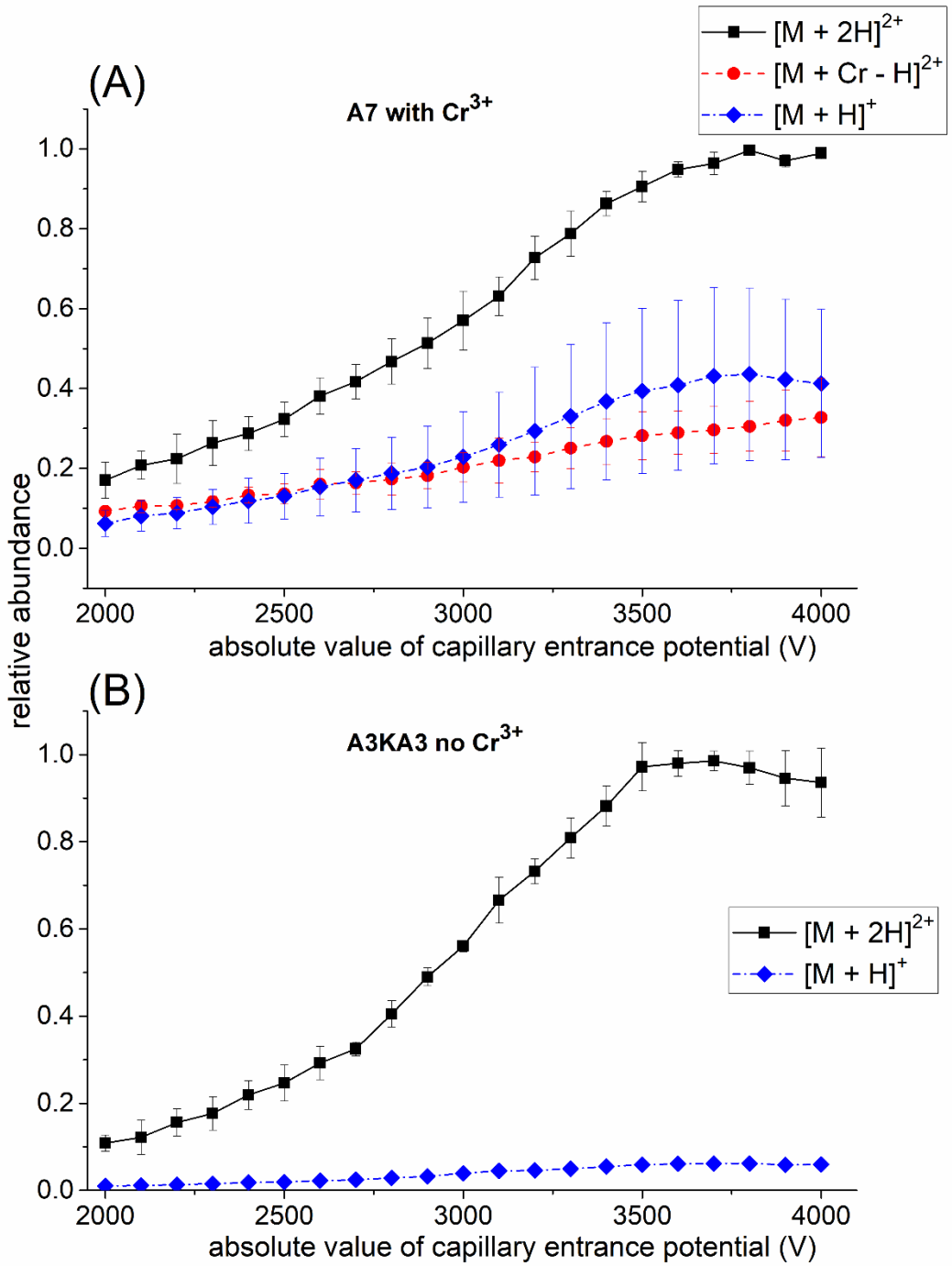


Figure 6.6. Relative intensity of ions formed as a function of the absolute value of the capillary entrance potential in V for (a) A7 and (b) A3KA3. The capillary exit and skimmer potentials were fixed at -95 V and -25V respectively. The $[M + 2H]^{2+}$ is represented by the black solid line with filled black square symbols, $[M + H]^{+}$ by the blue dashed line with filled blue diamond symbols, and $[M + Cr – H]^{2+}$ by the red dashed line with filled red circle symbols.

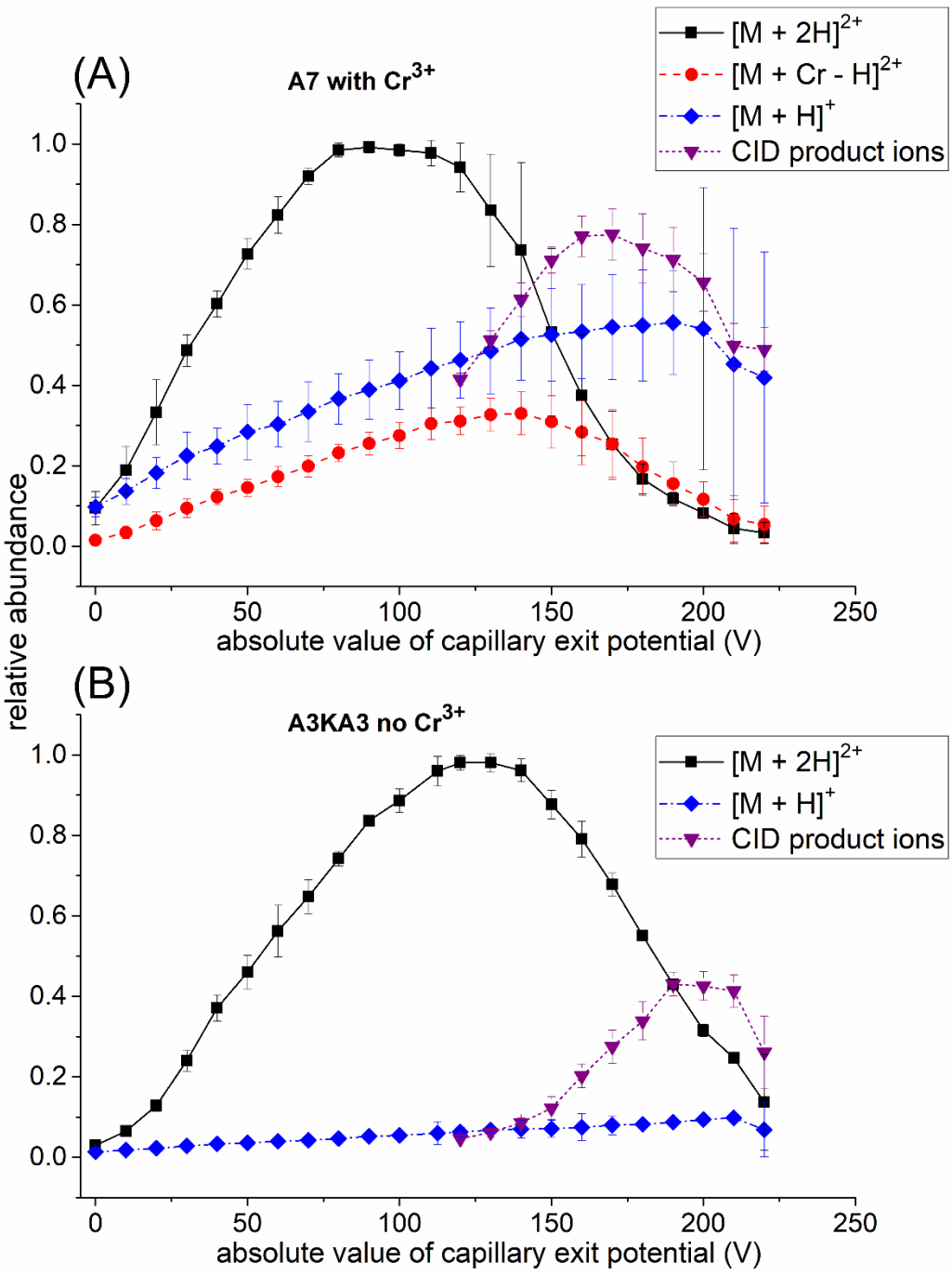


Figure 6.7. Relative intensity of ions formed as a function of the absolute value of the capillary exit potential in V for (a) A7 and (b) A3KA3. The skimmer potential was fixed at -25 V. $[M + 2H]^{2+}$ is represented by the black solid line with filled black square symbols, $[M + H]^{+}$ by the blue dashed line with filled blue diamond symbols, $[M + Cr – H]^{2+}$ by the red dashed line with filled red circle symbols, and CID product ions by a purple dashed line with purple upside down triangle symbols.

potential was altered. In Figure 6.8(a) for A7, maximization of $[M + 2H]^{2+}$ occurs between absolute values of 20 V and 30 V. CID product ions begin to form at absolute 45 V and gradually increase until 75 V. At higher absolute voltages ($\geq$ 80 V, which equates to more negative potentials in positive mode), instrument conditions are no longer optimized and all ion intensities steadily decrease. In Figure 6.8(b), A3KA3 displays a similar effect as A7; that is, maximum $[M + 2H]^{2+}$ intensity occurs within the same voltage range for both peptides. CID product ion formation is less intense for A3KA3 and is incident at a higher absolute value of skimmer potential, which is consistent with the more basic peptide requiring higher activation energies to undergo CID.[32,33] For A7, $[M + Cr – H]^{2+}$ and $[M + H]^{+}$ show small intensity variations over the range of skimmer potentials studied, while for A3KA3 the $[M + H]^{+}$ intensity is generally constant (albeit low) throughout the range of potentials.

Several studies have shown that varying the ratio of potentials between the capillary exit and the skimmer can facilitate dissociation in this region of the ESI source.[28,31,34,35] In the initial report on enhanced protonation using $Cr^{3+}$,[22] the Cassady group hypothesized that the dissociation of water-solvated peptide-Cr(III) complexes, $[M + Cr – H + nH_2O]^{2+}$, in the capillary exit-skimmer region might form $[M + 2H]^{2+}$ and $[M + Cr – H]^{2+}$. Figure 6.9 shows that maximum formation of $[M + 2H]^{2+}$ for both A7 and A3KA3 occurs within a narrow range of capillary exit to skimmer ratios. The highest intensity of $[M + 2H]^{2+}$ occurs when the capillary exit voltage is 3.5-4.5 times greater in absolute value than the skimmer voltage for both A7 and A3KA3. When the capillary exit is 2-3 times greater than that of the skimmer, CID product ions form. Increased dissociation occurs at the lowest ratios; i.e., a greater abundance of capillary-skimmer CID occurs when the values of the capillary exit and skimmer voltages are nearly identical. At potentials where CID occurs, CID product ion intensity increases while the

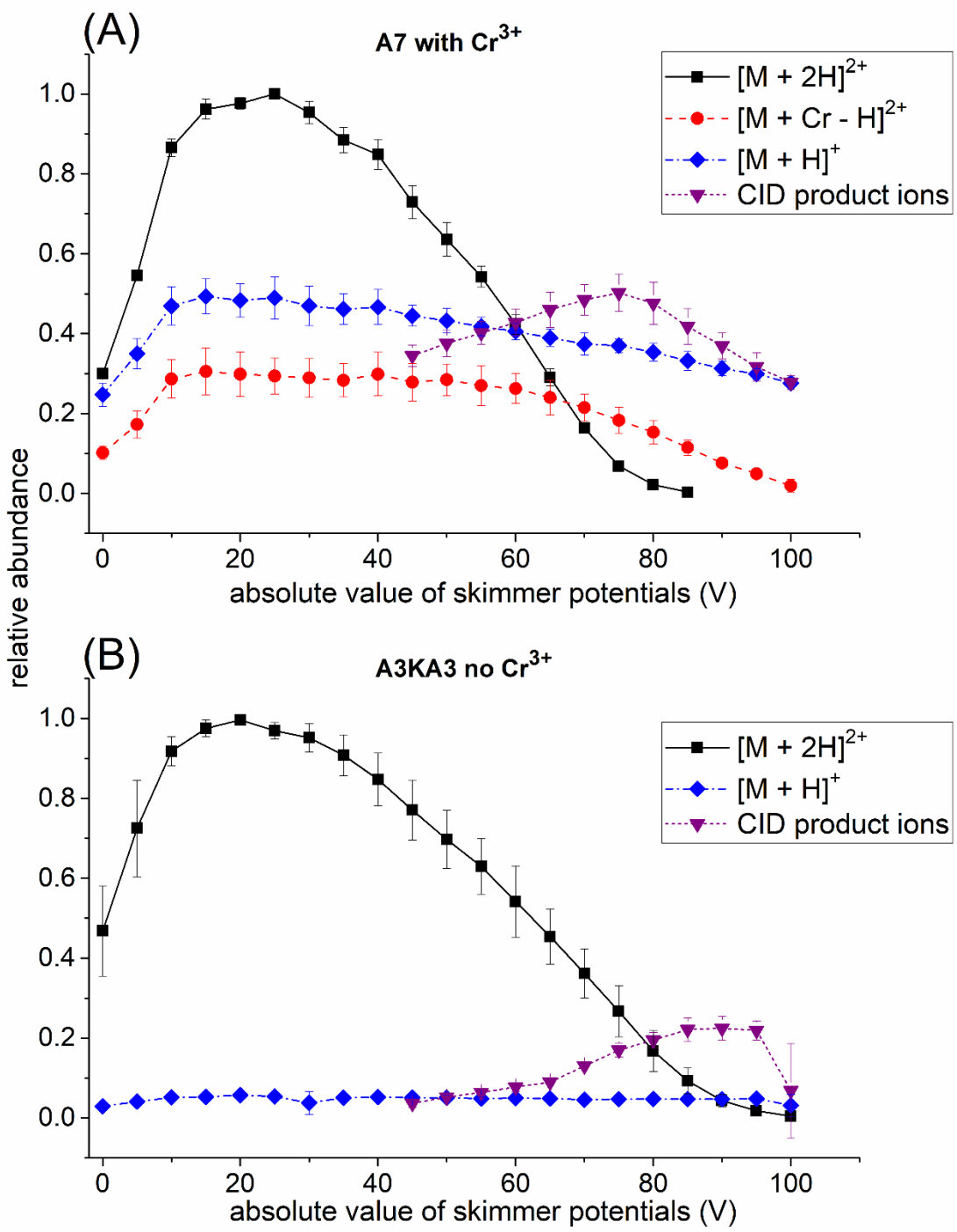


Figure 6.8. Relative intensity of ions formed as a function of skimmer potential in V for (a) A7 and (b) A3KA3. The capillary exit potential was fixed at -95 V. $[M + 2H]^{2+}$ is represented by the black solid line with filled black square symbols, $[M + H]^{+}$ by the blue dashed line with filled blue diamond symbols, $[M + Cr – H]^{2+}$ by the red dashed line with filled red circle symbols, and CID product ions by a purple dashed line with purple upside down triangle symbols.

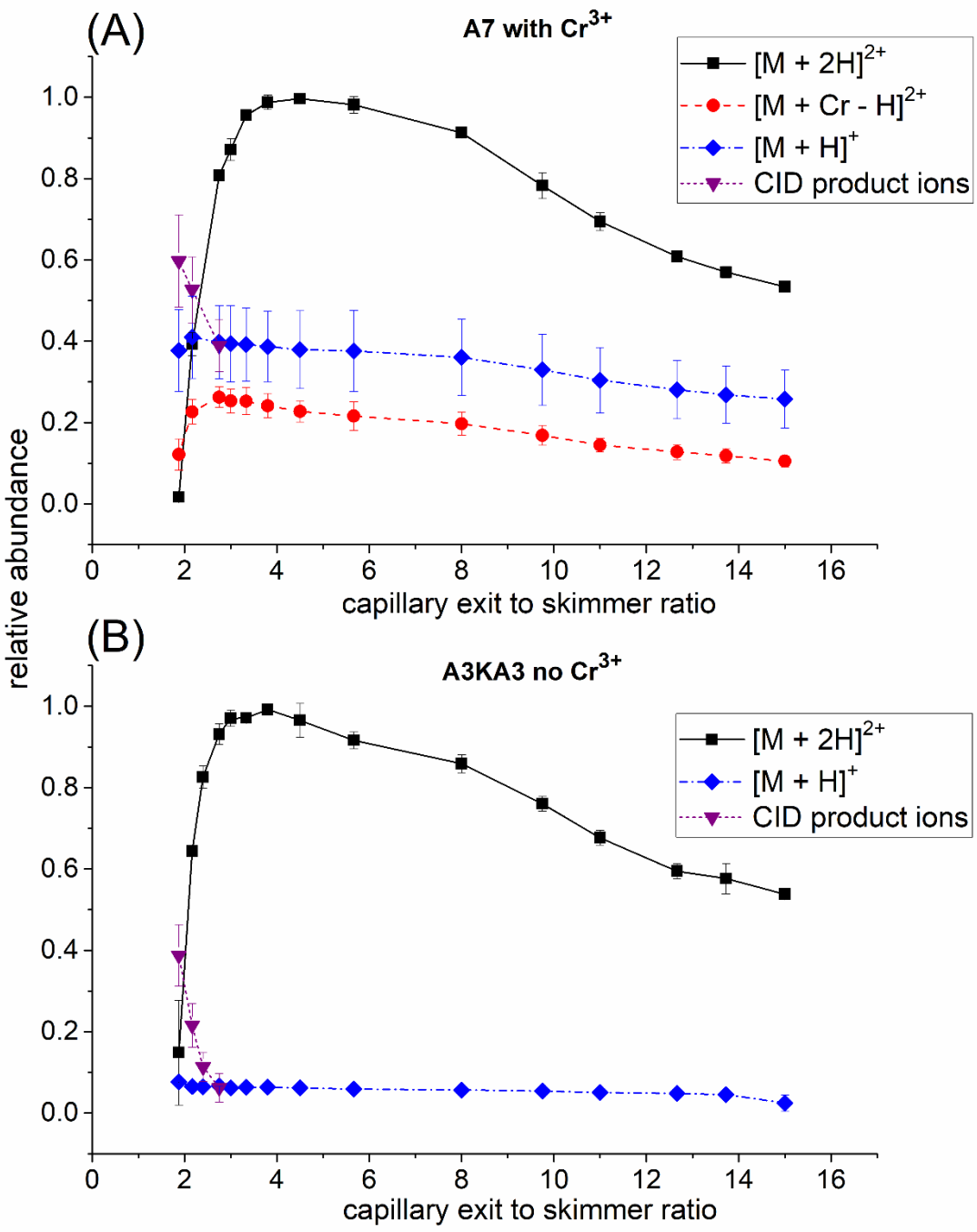


Figure 6.9. Relative intensity of ions formed as a function of capillary exit to skimmer potential ratio for (a) A7 and (b) A3KA3. $[M + 2H]^{2+}$ is represented by the black solid line with filled black square symbols, $[M + H]^{+}$ by the blue dashed line with filled blue diamond symbols, $[M + Cr – H]^{2+}$ by the red dashed line with filled red circle symbols, and CID product ions by a purple dashed line with purple upside down triangle symbols.

intensity of $[M + 2H]^{2+}$ decreases. A study of capillary-skimmer CID by Voyksner and Pack[31] also demonstrated a direct relationship between decreasing precursor ion intensity and increasing CID product ions. In this report, higher ratios (greater than ~5) lead to decreased formation of $[M + 2H]^{2+}$ for both peptides. The intensities of $[M + H]^{+}$ for A7 and A3KA3 are generally unaffected by this voltage ratio. The effects observed here with variation of capillary exit to skimmer ratio are not exclusive to enhanced protonation with $Cr^{3+}$, but this information still proved to be useful for general instrument tuning to maximize $[M + 2H]^{2+}$ intensity.

### 6.4.3 Effects of sample preparation and storage container

The sample preparation and storage containers affect formation of $[M + 2H]^{2+}$ for A7 and A3KA3. The previous study[22] employed ultra-clean glass vials to eliminate plasticizer ions in the ESI spectra that could be enhanced in the presence of $Cr^{3+}$. However, in the current study, solutions prepared and stored for 4 or more hours in glass vials had mass spectra dominated by sodium- and calcium-containing ions and resulted in suppression of $Cr^{3+}$ binding to the peptide. After 4 h of storage in glass vials, formation of $[M + 2H]^{2+}$ from A7 is completely suppressed. In contrast, solution preparation and storage in plasticware microcentrifuge tubes (vials) preserved the intensity of $[M + 2H]^{2+}$ for weeks. Sodium or calcium do not alter formation of $[M + 2H]^{2+}$ with $Cr^{3+}$ in plastic tubes.

The intensity of $[M + 2H]^{2+}$ was affected by the brand of plasticware tubes. Figures 6.10 and 6.11 show ion formation for A7 and A3KA3, respectively, with Eppendorf Safe-Lock Tubes® (Eppendorf, North America, Hauppage, NY, USA), Fisherbrand tubes (Fisher Scientific Company, Hampton, NH, USA), and VWR tubes. Eppendorf Safe-Lock Tubes are marketed as containing fewer contaminants and a more consistent batch-to-batch composition than other plasticware.[36] For the data in Figures 6.10 and 6.11, rinsing involved filling the tubes with our

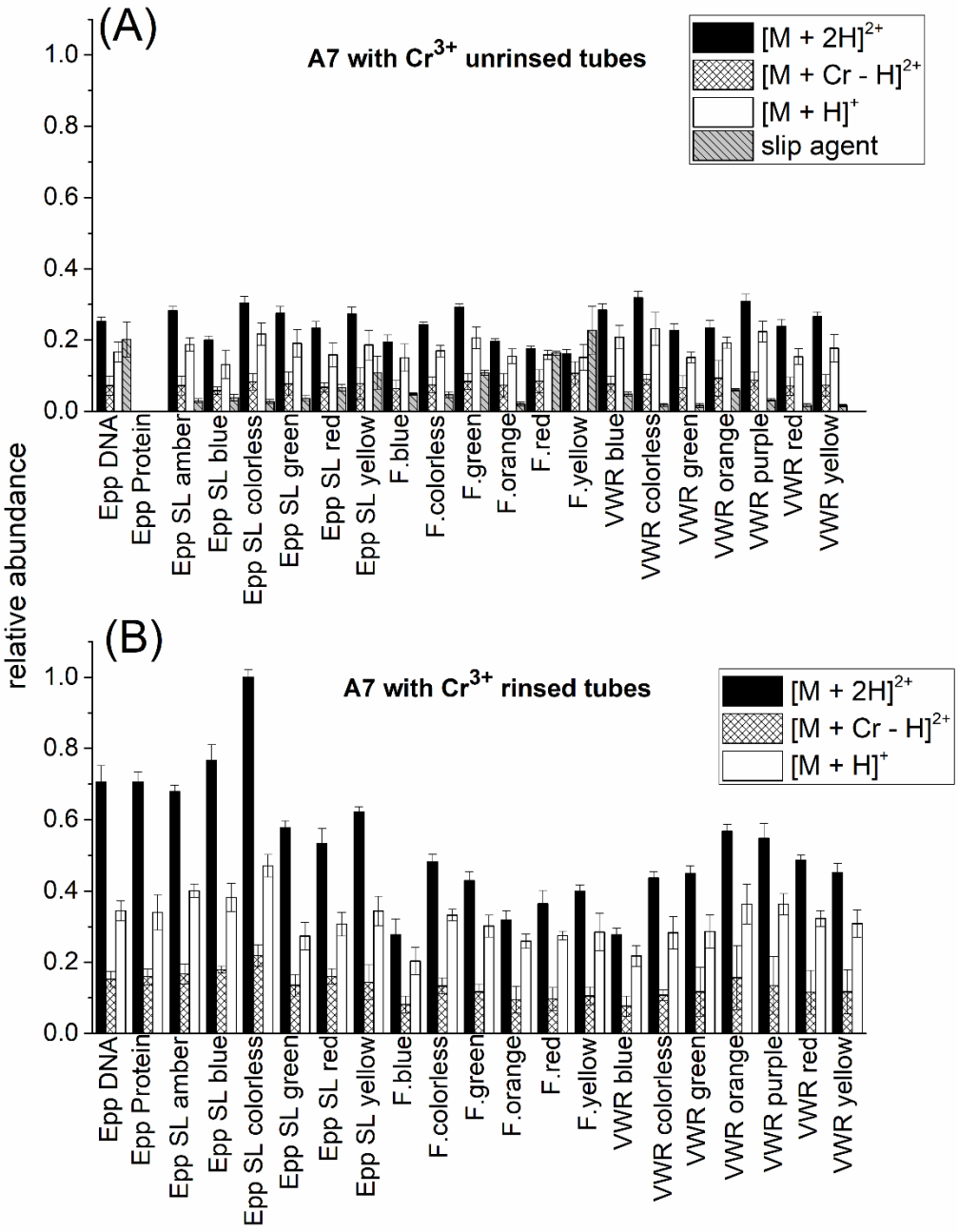


Figure 6.10. Relative intensity of ions formed for A7 with (a) unrinsed and (b) rinsed microcentrifuge tubes with varying vendors and colors. Solid black bars represent $[M + 2H]^{2+}$, white bars with criss-cross stripes represent $[M + Cr – H]^{2+}$, solid white bars represent $[M + H]^{+}$, and grey bars with diagonal stripes represent erucamide (slip agent) found in unrinsed tubes. Epp refers to Eppendorf tubes; SL to Safe-Lock; and F to Fisherbrand tubes. The rinse procedure used here involved exposing the tube to the acetonitrile:water (50:50 v:v) solvent system for 30 minutes, followed by a brief rinse with fresh solvent. Parts (a) and (b) are on the same intensity scale.

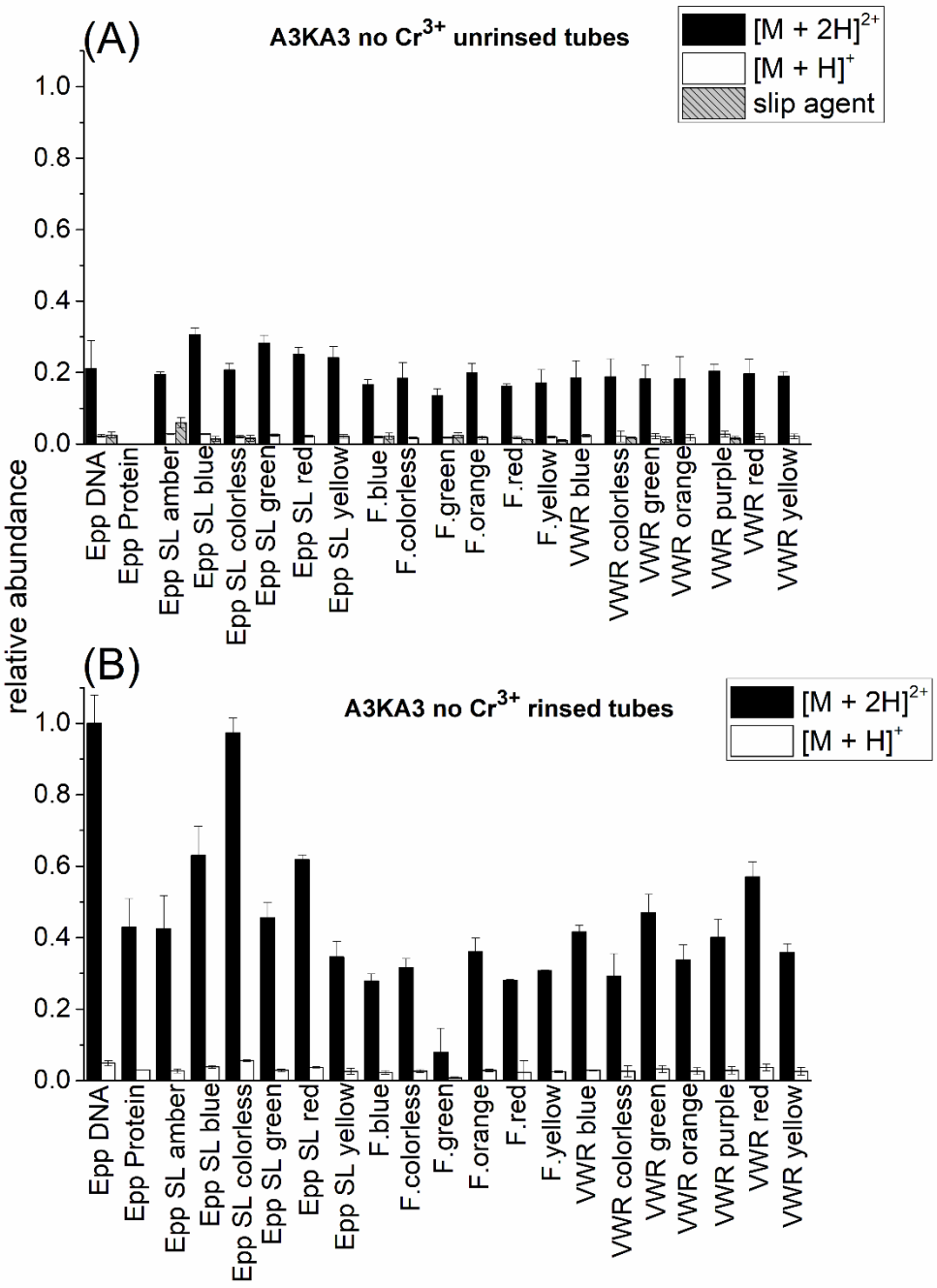


Figure 6.11. Relative intensity of ions formed for A3KA3 with (a) unrinsed and (b) rinsed microcentrifuge tubes with varying vendors and colors. Solid black bars represent $[M + 2H]^{2+}$, solid white bars represent $[M + H]^{+}$, and grey bars with diagonal stripes represent erucamide (slip agent) found in unrinsed tubes. Epp refers to Eppendorf tubes; SL to Safe-Lock; and F to Fisherbrand tubes. The rinse procedure used here involved exposing the tube to the acetonitrile:water (50:50 v:v) solvent system for 30 minutes, followed by a brief rinse with fresh solvent. Parts (a) and (b) are on the same intensity scale.

ESI solvent system of 50:50 (v:v) acetonitrile/water and allowing the filled tubes to sit for 30 minutes (time was optimized to remove maximum impurities), then shaking and pouring out the solvent rinse, followed by a brief final rinse with fresh solvent. For all tubes studied, rinsing before sample preparation was necessary to obtain maximum ion formation by ESI. Overall ion intensity in unrinsed tubes is only one-third of that obtained with rinsed tubes for both A7 and A3KA3. In general, for both peptides, the highest intensity of $[M + 2H]^{2+}$ is recorded for rinsed Eppendorf Safe-Lock Tubes as shown in Figures 6.10(b) and 6.11(b). The most abundant $[M + 2H]^{2+}$ from A7 occurs with rinsed colorless (natural) clear Eppendorf Safe-Lock Tubes, as illustrated in Figure 6.10(b). As shown in Figure 6.11(b), almost equal intensities of $[M + 2H]^{2+}$ from A3KA3 are generated using rinsed colorless Eppendorf Safe-Lock Tubes and using Eppendorf DNA LoBind Tubes®, which have a coating to minimize nuclei acid binding to the tube surface. Interestingly, Eppendorf Protein LoBind Tubes®, which have a coating to minimize protein binding to the tube surface, yield no test peptide ion signal at all unless the tubes are rinsed. Spectra of samples prepared in these unrinsed tubes contain ions at *m/z* 331, 397, and 683 corresponding to Triton X, which is a common detergent in laboratories and a non-ionic surfactant in protein analysis procedures.[37]

The effects of plasticware tube color were studied because anecdotal evidence[38-40] exits to suggest better mass spectrometry performance with colorless tubes. Researchers have suggested that over time dyes may leach from colored tubes and into the sample solutions. In addition, for ultra-clean applications Eppendorf recommends colorless tubes because their colored tubes contain surfactants to bind the dyes to the plastic.[41] These results support the claims that colorless tubes are best for peptide applications. As illustrated in Figures 6.10 and 6.11, rinsed Eppendorf colorless (natural) tubes produce $[M + 2H]^{2+}$ intensities that are 1.4 to 4

times greater than rinsed colored tubes. If use of a colored tube is important, the data in this study suggest that the best results will be obtained with clear blue or clear red rinsed Eppendorf Safe-Lock Tubes.

Rinsing the plastic Eppendorf Safe-Lock Tubes before sample preparation yields the most intense $[M + 2H]^{2+}$ observed by ESI for both peptides. Unrinsed vials from all three manufacturers contain a peak at *m/z* 338.3 corresponding to $[M + H]^{+}$ of the slip agent (Z)-docos-13-enamide, commonly known as erucimide. A slip agent is an additive to prevent polymer films from sticking to each other and to machinery during the manufacturing process.[42] Eppendorf indicates that slip agents, biocides, and plasticizers are not used in the manufacturing of their tubes, tips, and plates.[36,41] Erucimide ions were still observed in multiple trials with various sets of unrinsed tubes from Eppendorf, although to a considerably lesser extent than with VWR and Fisherbrand tubes.

Different solvents, times, and methods of rinsing the tubes were investigated in order to minimize ions from erucimide and other contaminants. Erucamide contains an amide group bound to a linear chain of 21 carbons that is saturated except for one central double bond; thus, a very non-polar chain with one polar end. Consequently, erucamide is insoluble in water and has a detectable solubility measured at less than 0.738 ug/L.[43] However erucimide is soluble in IPA.[44] After considerable trial and error, the most consistent and reliable method for removal of the contaminant is four "quick rinses" with IPA or an IPA:$H_2O$ solvent system at a volume ratio of 50:50. One "quick rinse" involves placing ~1 mL of IPA in the tube and shaking by hand for a few seconds then discarding the rinse solution. A lesser number of IPA rinses than four did not succeed in removing all traces of contaminants. (Still, this is far easier and faster than the 30 minute rinses that we had used to generate the data in Figures 6.10 and 6.11.) Figure 6.12 shows

the decrease in the intensity of erucimide ions formed in the ACN:$H_2O$ (50:50 v:v) solvent system background (no peptide) with increasing number of rinses involving pure IPA. (The ion at *m/z* 360.3, corresponding to $[M + Na]^+$ from erucimide, only appears with solvent background experiments and not with peptide samples.) After four quick rinses, erucamide ions are gone. IPA is soluble in water and most other solvents. Therefore, tubes can be rinsed with the solvent system of choice after the IPA rinses in order to remove traces of IPA. To minimize contamination from erucamide and to enhance ESI protonation (with or without $Cr^{3+}$), periodic rinsing of the ESI tubing and needle with IPA is recommended. Rinses with water, methanol, or acetonitrile are not sufficient to remove erucamide. In addition, for the cleanest system, ESI source cleaning should include a rinse with IPA. It is also noteworthy that plasticware Eppendorf pipettor tips were used without rinsing and did not result in the observation of the erucamide contaminant.

### 6.5 Conclusions

In previous work by the Cassady group,[22] a ratio of 1:1 was achieved for the intensity of $[M +2H]^{2+}$ to $[M +H]^+$ from analysis of a mixture of A7 and $Cr^{3+}$. (Note that in the absence of $Cr^{3+}$ no $[M + 2H]^{2+}$ forms from the neutral peptide A7.) However, using the optimization procedures discussed here, this ratio is greatly improved to 4:1, as shown by Figure 6.13 for a mass spectrum of A7 with $Cr^{3+}$. In addition, previously the ratio of $[M + H]^{2+}$ to $[M + Cr – H]^{2+}$ was 2:1, but with optimized conditions, the ratio is now 4:1. Therefore, the abundance of the 1+ and metal bound species has been minimized and the intensity of $[M + 2H]^{2+}$ has been increased. As an example of the utility of 2+ ions, CID of $[M + 2H]^{2+}$ for A7 (Figure 6.14) generates more peptide backbone cleavage information than CID of $[M + H]^+$

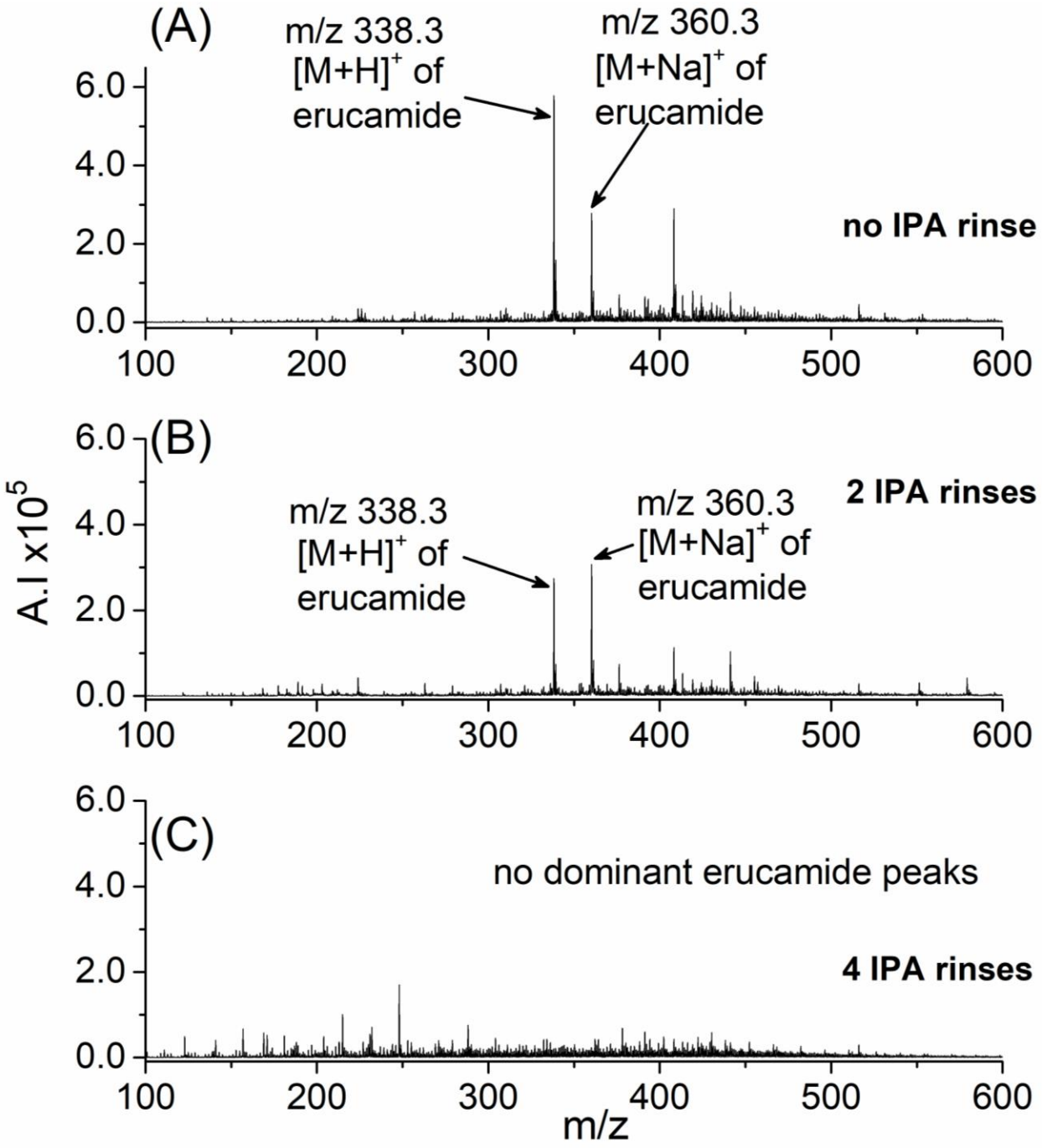


Figure 6.12. ESI mass spectra of the solvent system (ACN:$H_2O$ at 50:50 v:v) with erucimide contaminant in colorless safe-lock microcentrifuge tubes after (a) no rinse, (b) 2 rinses, and (c) 4 rinses with IPA solvent. Note the decrease in intensity of overall background as contaminants become less intense.

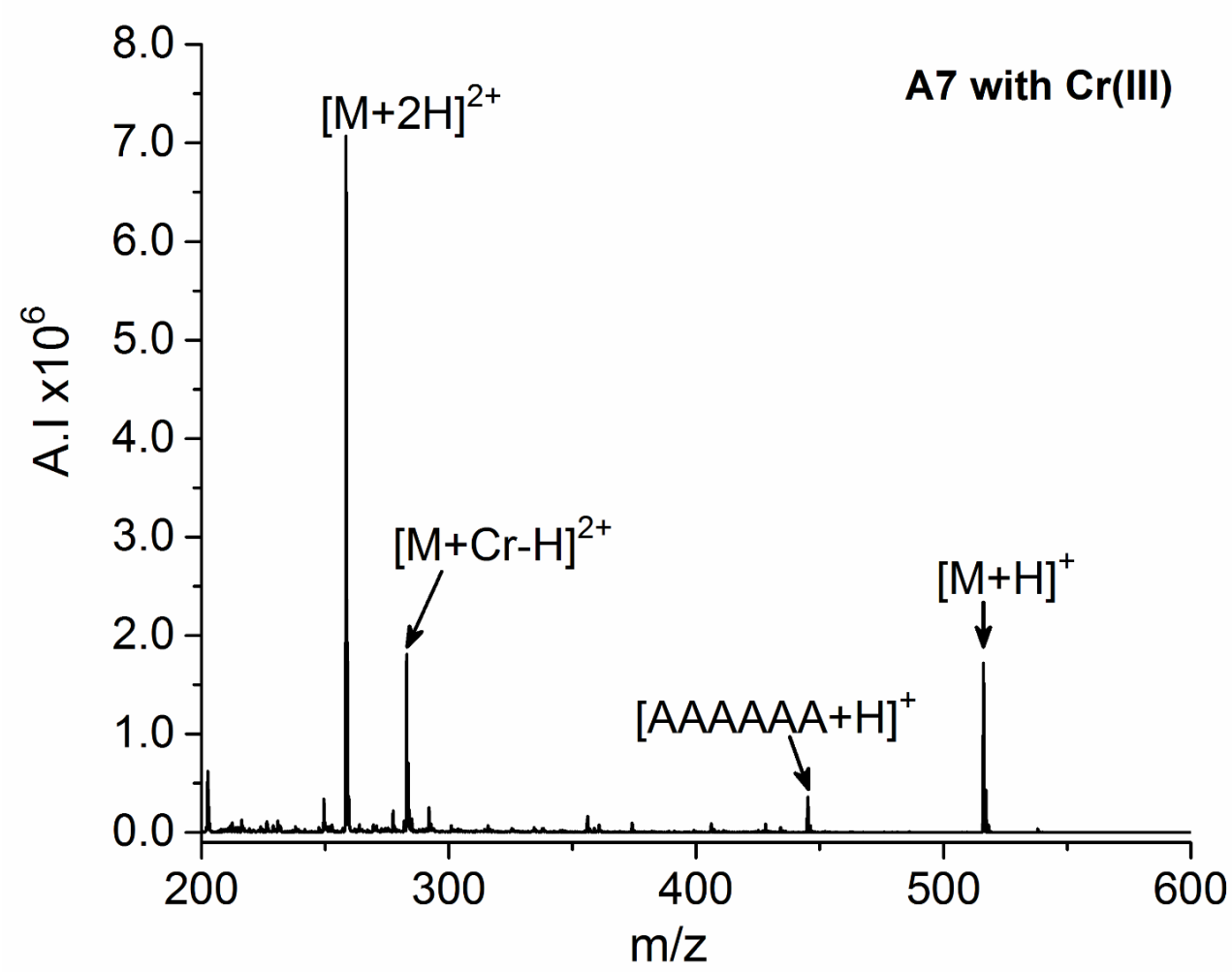


Figure 6.13. ESI mass spectrum of A7 in the presence of $Cr^{3+}$ using optimized parameters. The ratio of $[M + 2H]^{2+}$ intensity to $[M + H]^{+}$ intensity is 4:1.

(Figure 6.15), while ETD of $[M + 2H]^{2+}$ yields even more cleavage sites and full sequence coverage (see Figure 6.16). In addition, a more intense ion signal in ESI leads to increased S/N for MS/MS product ions. This can prove beneficial in MS/MS procedures that utilize data processing software that requires sufficient ion intensity for peak picking and identification. The ETD spectra of $[M + 2H]^{2+}$ could only be acquired due to enhanced protonation of A7 with $Cr^{3+}$. The sample preparation methods investigated in this study can also be useful for general laboratory procedures involving MS. For example, mass spectral analysis involving many sample types and ionization techniques may benefit from our recommendation to minimize contamination by using colorless microcentrifuge plastic tubes briefly rinsed with several aliquots of IPA.

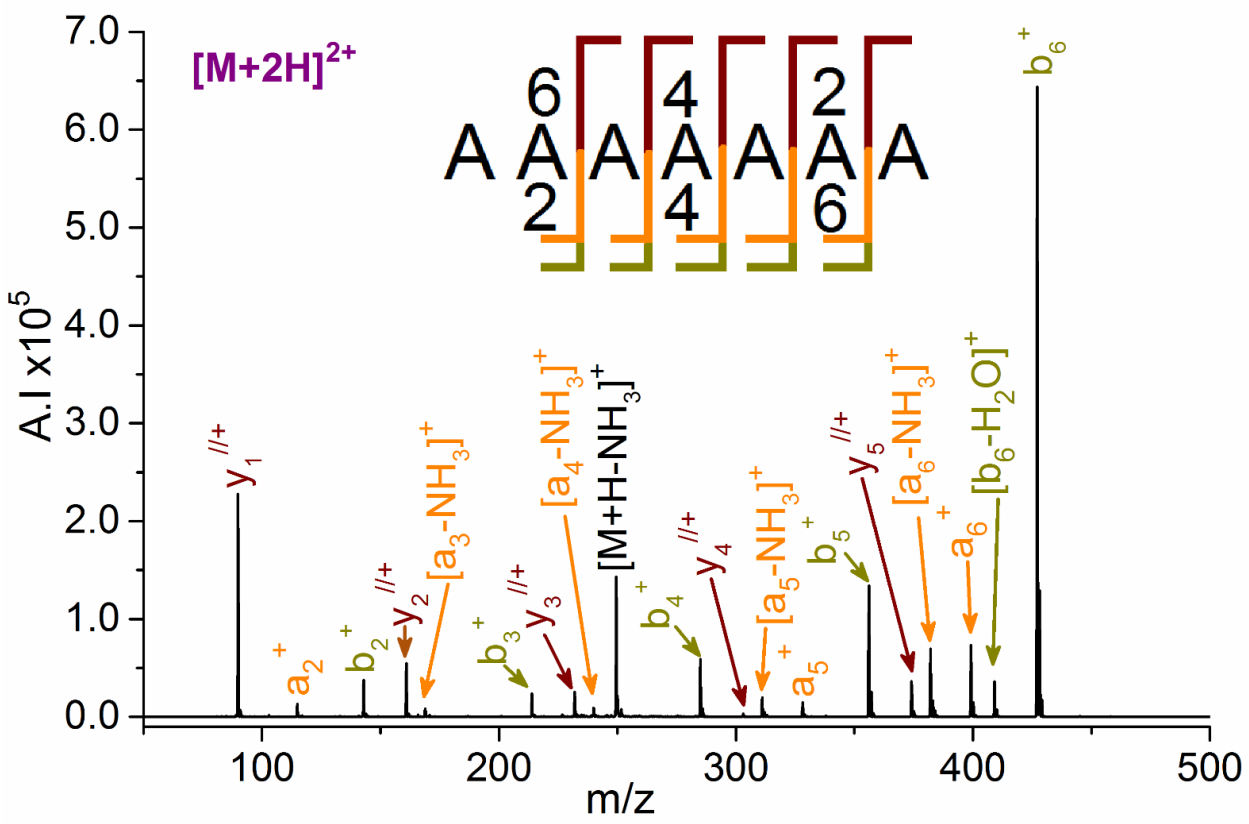


Figure 6.14. CID mass spectrum of $[M + 2H]^{2+}$ for A7. This spectrum could not be obtained without addition of $Cr^{3+}$ to the solution undergoing ESI. In the figures, the following colors are used to label the ions: a-ions = orange, b-ions = olive green, y-ions = burgundy, z-ions = red, and c-ions = blue. Undissociated precursor ion is labeled in purple with a large purple diamond arrow head. A prime symbol to the left indicates loss of a hydrogen (i.e., $^{/}c_n = [c_n - H]^+$) and to the right indicates the addition of a hydrogen at the cleavage site (i.e., $c_n^{//} = [c_n + 2H]^+$). The spectra have no expansion of the intensity axis; all peaks are shown to scale.

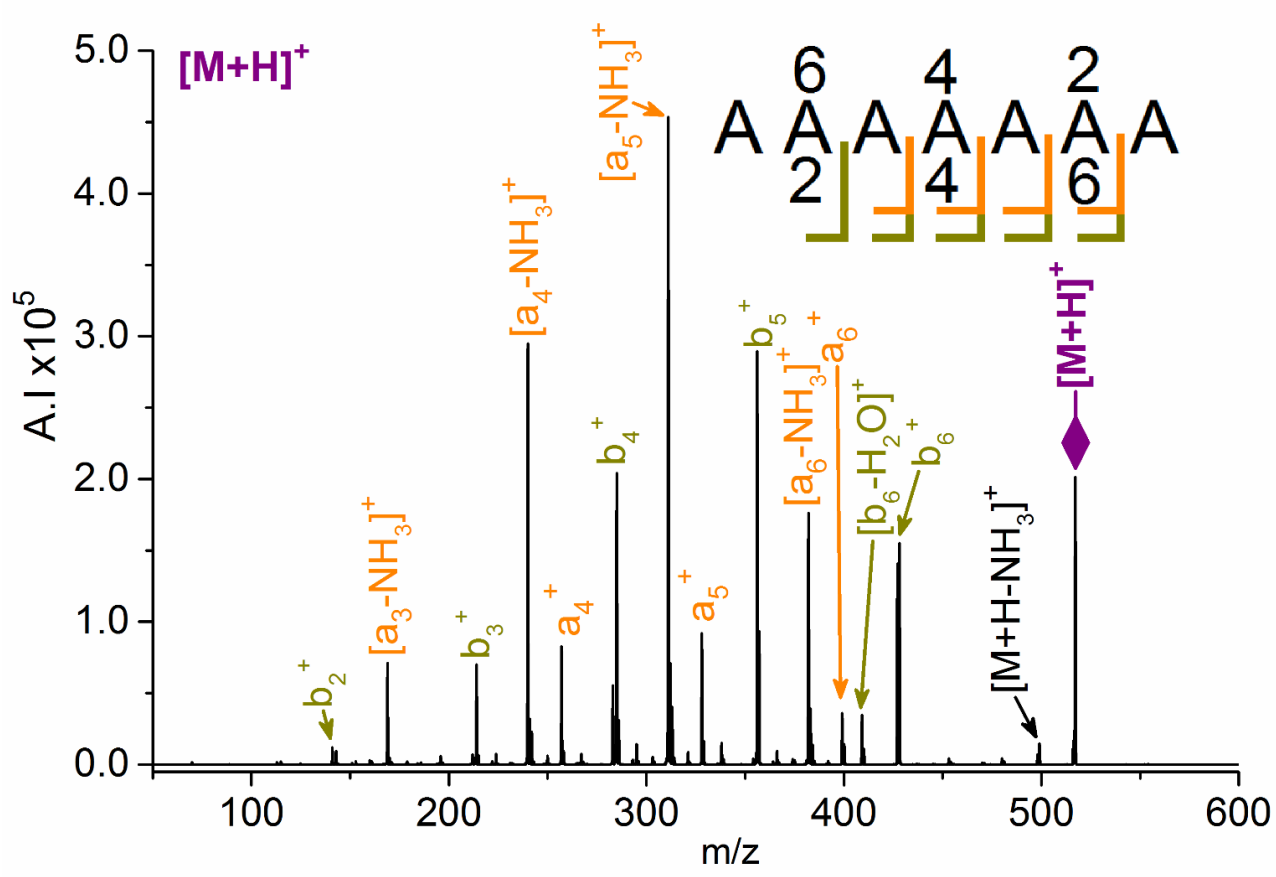


Figure 6.15. CID mass spectrum of $[M + H]^+$ for A7. In the figures, the following colors are used to label the ions: a-ions = orange, b-ions = olive green, y-ions = burgundy, z-ions = red, and c-ions = blue. Undissociated precursor ion is labeled in purple with a large purple diamond arrow head. A prime symbol to the left indicates loss of a hydrogen (i.e., $^{/}c_n = [c_n - H]^+$) and to the right indicates the addition of a hydrogen at the cleavage site (i.e., $c_n^{//} = [c_n + 2H]^+$). The spectra have no expansion of the intensity axis; all peaks are shown to scale.

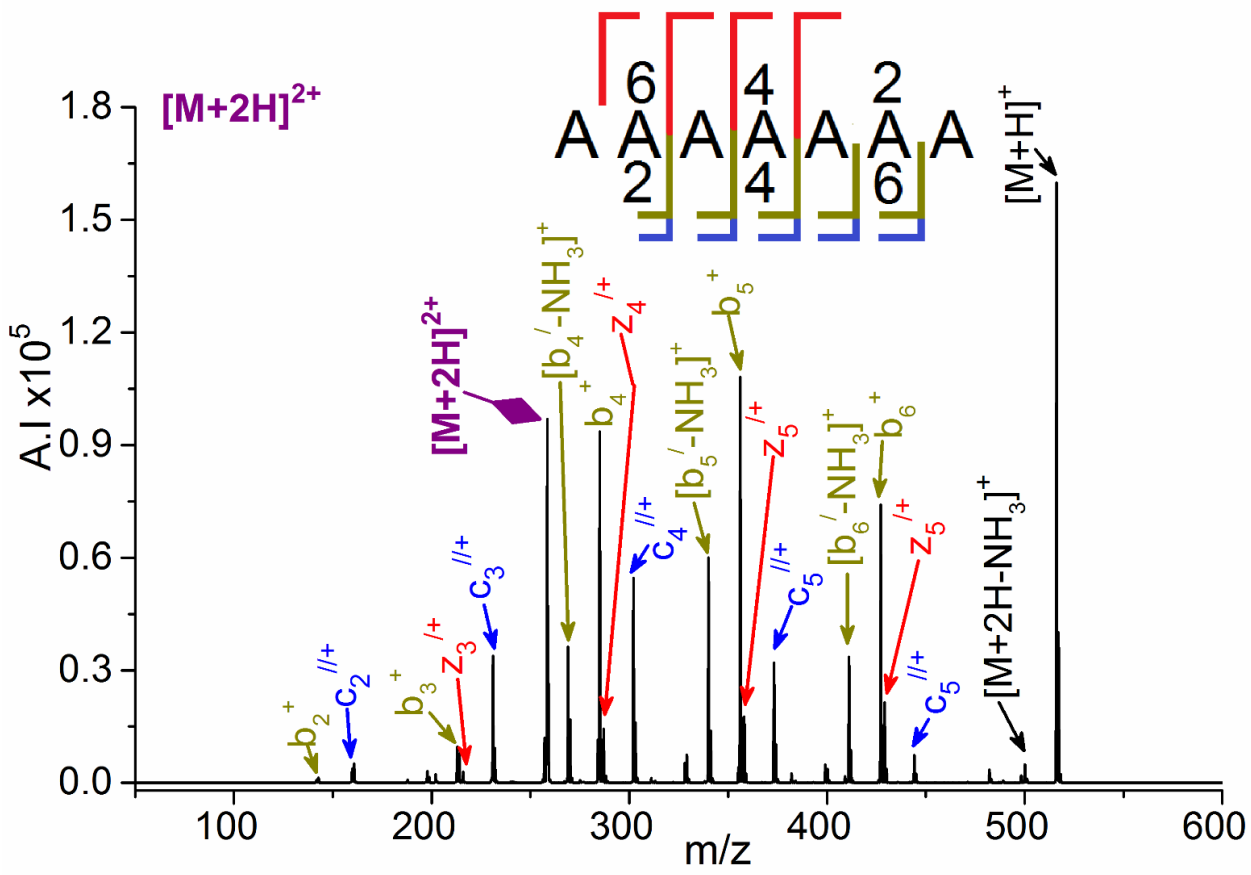


Figure 6.16. ETD mass spectrum of $[M + 2H]^{2+}$ for A7. This spectrum could not be obtained without addition of $Cr^{3+}$ to the solution undergoing ESI. In the figures, the following colors are used to label the ions: a-ions = orange, b-ions = olive green, y-ions = burgundy, z-ions = red, and c-ions = blue. Undissociated precursor ion is labeled in purple with a large purple diamond arrow head. A prime symbol to the left indicates loss of a hydrogen (i.e., $^{/}c_n = [c_n - H]^+$) and to the right indicates the addition of a hydrogen at the cleavage site (i.e., $c_n^{//} = [c_n + 2H]^+$). The $z_n^{/+}$ form at low intensity and overlap with the carbon-13 isotope of $b_n^+$. The spectra have no expansion of the intensity axis; all peaks are shown to scale.

## References


1. Dongre, A. R.; Jones, J. L.; Somogyi, A.; Wysocki, V. H. Influence of Peptide Composition, Gas-Phase Basicity, and Chemical Modification on Fragmentation Efficiency: Evidence for the Mobile Proton Model. *J. Am. Chem. Soc.* **1996**, *118*, 8365-8374.

2. Wells, J. M.; Stephenson Jr., J. L.; McLuckey, S. A. Charge Dependence of Protonated Insulin Decompositions. *Int. J. Mass Spectrom.* **2000**, *203*, A1-A9.

3. Kjeldsen, F.; Giessing, A. M. B.; Ingrell, C. R.; Jensen, O. N. Peptide Sequencing and Characterization of Post-Translational Modifications by Enhanced Ion-Charging and Liquid Chromatography Electron-Transfer Dissociation Tandem Mass Spectrometry. *Anal. Chem.* **2007**, *79*, 9243-9252.

4. Madsen, J. A.; Brodbelt, J. S. Comparison of Infrared Multiphoton Dissociation and Collision-Induced Dissociation of Supercharged Peptides in Ion Traps. *J. Am. Soc. Mass Spectrom.* **2009**, *20*, 349-358.

5. Meot-Ner, M.; Dongre, A. R.; Somogyi, A.; Wysocki, V. H. Thermal Decomposition Kinetics of Protonated Peptides and Peptide Dimers, and Comparison with Surface-induced Dissociation. *Rapid Commun. Mass Spectrom.* **1995**, *9*, 829-836.

6. Yang, Z.; Vorpagel, E.; Laskin, J. Influence of the Charge State on the Structures and Interactions of Vancomycin Antibiotics with Cell-Wall Analogue Peptides: Experimental and Theoretical Studies. *Chem. Eur. J.* **2009**, *15*, 2081-2090.

7. Savitski, M. M.; Faelth, M.; Fung, Y. M. E.; Adams, C. M.; Zubarev, R. A. Bifurcating Fragmentation Behavior of Gas-Phase Tryptic Peptide Dications in Collisional Activation. *J. Am. Soc. Mass Spectrom.* **2008**, *19*, 1755-1763.

8. Faelth, M.; Savitski, M. M.; Nielsen, M. L.; Kjeldsen, F.; Andren, P. E.; Zubarev, R. A. SwedCAD, a Database of Annotated High-Mass Accuracy MS/MS Spectra of Tryptic Peptides. *J. Proteome Res.* **2007**, *6*, 4063-4067.

9. Harrison, A. G. Charge-Separation Reactions of Doubly-Protonated Peptides: Effect of Peptide Chain Length. *J. Am. Soc. Mass Spectrom.* **2009**, *20*, 1890-1895.

10. Kapp, E.; Schutz, F.; Reid, G.; Eddes, J.; Moritz, R.; O'Hair, R.; Speed, T.; Simpson, R. Mining a Tandem Mass Spectrometry Database to Determine the Trends and Global Factors Influencing Peptide Fragmentation. *Anal. Chem.* **2003**, *75*, 6251-6264.

11. Marshall, A. G.; Hendrickson, C. L. Charge Reduction Lowers Mass Resolving Power for Isotopically Resolved Electrospray Ionization Fourier Transform Ion Cyclotron Resonance Mass Spectra. *Rapid Commun. Mass Spectrom.* **2001**, *15*, 232-235.

12. Marshall, A. G.; Hendrickson, C. L. High-Resolution Mass Spectrometers. *Ann. Rev. Anal. Chem.* **2008**, *1*, 579-599.

13. Perry, R. H.; Cooks, R. G.; Noll, R. J. Orbitrap Mass Spectrometry: Instrumentation, Ion Motion and Applications. *Mass Spectrom. Rev.* **2008**, *27*, 661-699.

14. Aebersold, R.; Mann, M. Mass Spectrometry-based Proteomics. *Nature* **2003**, *422*, 198-207.

15. Michalski, A.; Cox, J.; Mann, M. More than 100,000 Detectable Peptide Species Elute in Single Shotgun Proteomics Runs but the Majority is Inaccessible to Data-Dependent LC-MS/MS. *J. Proteome Res.* **2011**, *10*, 1785-1793.

16. Syka, J. E. P.; Coon, J. J.; Schroeder, M. J.; Shabanowitz, J.; Hunt, D. F. Peptide and Protein Sequence Analysis by Electron Transfer Dissociation Mass Spectrometry. *Proc. Natl. Acad. Sci. USA* **2004**, *101*, 9528-9533.

17. Coon, J. J. Collisions or Electrons? Protein Sequence Analysis in the 21st Century. *Anal. Chem.* **2009**, *81*, 3208-3215.

18. Good, D. M.; Wirtala, M.; McAlister, G. C.; Coon, J. J. Performance Characteristics of Electron Transfer Dissociation Mass Spectrometry. *Mol. Cell. Proteomics* **2007**, *6*, 1942-1951.

19. Zubarev, R. A.; Kelleher, N. L.; McLafferty, F. W. Electron Capture Dissociation of Multiply Charged Protein Cations. A Nonergodic Process. *J. Am. Chem. Soc.* **1998**, *120*, 3265-3266.

20. Zubarev, R. A. Electron Capture Dissociation LC/MS/MS for Bottom-Up Proteomics. *Methods Mol. Biol.* **2009**, *492*, 413-416.

21. McLafferty, F. W.; Horn, D. M.; Breuker, K.; Ge, Y.; Lewis, M. A.; Cerda, B. A.; Zubarev, R. A.; Carpenter, B. K. Electron Capture Dissociation of Gaseous Multiply Charged Ions by Fourier Transform Ion Cyclotron Resonance. *J. Am. Soc. Mass Spectrom.* **2001**, *12*, 245-249.

22. Feng, C.; Commodore, J. J.; Cassady, C. J. The Use of Chromium(III) to Supercharge Peptides by Protonation at Low Basicity Sites. *J. Am. Soc. Mass Spectrom.* **2015**, *26*, 347-358.

23. Watson, H. M. Effects of Transition Metal Cationization on Peptide Dissociation by Mass Spectrometry, Ph. D. Dissertation, The University of Alabama, Tuscaloosa, AL, USA, 2011.

24. Chan, W. C.; White, P. D. *Fmoc Solid Phase Peptide Synthesis A Practical Approach;* Oxford University Press Inc., New York: 2000.

25. Fenn, J. B.; Mann, M.; Meng, C. K.; Wong, S. F.; Whitehouse, C. M. Electrospray Ionization for Mass Spectrometry of Large Biomolecules. *Science* **1989**, *246*, 64-71.

26. Rodriguez-Cruz, S. E.; Jockusch, R. A.; Williams, E. R. Hydration Energies of Divalent Metal Ions, $Ca^{2+}(H_2O)_n$ (n=5-7) and $Ni^{2+}(H_2O)_n$ (n=6-8), Obtained by Blackbody Infrared Radiative Dissociation. *J. Am. Chem. Soc.* **1998**, *120*, 5842-5843.

27. Rodriguez-Cruz, S. E.; Jockusch, R. A.; Williams, E. R. Binding Energies of Hexahydrated Alkaline Earth Metal Ions, $M^{2+}(H_2O)(_6)$, M = Mg, Ca, Sr, Ba: Evidence of Isomeric Structures for Magnesium. *J. Am. Chem. Soc.* **1999**, *121*, 1986-1987.

28. Loo, J. A.; Edmonds, C. G.; Udseth, H. R.; Smith, R. D. Collisional Activation and Dissociation of Large Multiply Charged Proteins Produced by Electrospray Ionization. *Anal. Chim. Acta* **1990**, *241*, 167-173.

29. Smith, R. D.; Loo, J. A.; Barinaga, C. J.; Edmonds, C. G.; Udseth, H. R. Collisional Activation and Collision-Activated Dissociation of Large Multiply Charged Polypeptides and Proteins Produced by Electrospray Ionization. *J. Am. Soc. Mass Spectrom.* **1990**, *1*, 53-65.

30. Chien, B. M.; Lubman, D. M. Analysis of the Fragments from Collision-Induced Dissociation of Electrospray-Produced Peptide Ions Using a Quadrupole Ion Trap Storage/Reflectron Time-of-Flight Mass Spectrometer. *Anal. Chem.* **1994**, *66*, 1630-1636.

31. Voyksner, R. D.; Pack, T. Investigation of Collisional-Activation Decomposition Process and Spectra in the Transport Region of an Electrospray Single-Quadrupole Mass-Spectrometer. *Rapid Commun. Mass Spectrom.* **1991**, *5*, 263-268.

32. Johns, J. L.; Dongre, A. K.; Somogyi, A.; Wysocki, V. H. Sequence Dependence of Peptide Fragmentation Efficiency Curves Determined by Electrospray Ionization/Surface-induced Dissociation Mass Spectrometry. *J. Am. Chem. Soc.* **1994**, *116*, 8368-8369.

33. Vekey, K.; Somogyi, A.; Wysocki, V. H. Average Activation Energies of Low-energy Fragmentation Processes of Protonated Peptides Determined by a New Approach. *Rapid Commun. Mass Spectrom.* **1996**, *10*, 911-918.

34. Chen, H.; Tabei, K.; Siegel, M. Biopolymer Sequencing Using a Triple Quadrupole Mass Spectrometer in the ESI Nozzle-Skimmer/Precursor Ion MS/MS mode. *J. Am. Soc. Mass Spectrom.* **2001**, *12*, 846-852.

35. Fuh, M.; Lu, K. Determination of Methylamphetamine and Related Compounds in Human Urine by High Performance Liquid Chromatography Electrospray Mass Spectrometry. *Talanta* **1999**, *48*, 415-423.

36. Chanotiya, C. S.; Pragadhessh, V. S.; Uniyal, G. C. Avoiding Interferences and Contaminants Using Eppendorf Safe-Lock Tubes in Mass Spectrometry Studies of Natural Products. *Eppendorf Application Note* **2013**, *282*.

37. Keller, B. O.; Sui, J.; Young, A. B.; Whittal, R. M. Interferences and Contaminants Encountered in Modern Mass Spectrometry. *Anal. Chim. Acta* **2008**, *627*, 71-81.

38. Border Biomedical Research Center: How to Submit MS Samples. *http://science.utep.edu/bbrc/index.php/center-guidelines/how-to-submit-ms-samples* (accessed February 24, 2017).

39. Protein Identification: Guidelines for Sample Submission. *www.bioms.pitt.edu/Protein%20identification%20submission%20instructions.docx* (accessed February 24, 2017).

40. Research Gate: What are the Best Microcentrifuge Tubes for Mass Spectrometry? *https://www.researchgate.net/post/What_are_the_best_microcentrifuge_tubes_for_mass_spectrometry* (accessed February 24, 2017).

41. Smith, C. Selecting The Right Tubes or Plates for Your Research. *Life Sci* **2011**, (accessed March 13, 2017).

42. Llop, C.; Manrique, A.; Navarro, R.; Mijangos, C.; Reinecke, H. Control of the Migration Behavior of Slip Agents in Polyolefin-Based Films. *Polym. Eng. Sci.* **2011**, *51*, 1763-1769.

43. European Chemical Agency. (Z)-docos-13-enamide: Physical and Chemical Properties. *http://echa.europa.eu/registration-dossier/-/registered-dossier/14899/4/9* (accessed March 12, 2017).

44. Sax, N. I.; Lewis, R. J. *Hawley's Condensed Chemical Dictionary;* Van Nostrand Reinhold Co.: New York, 1987.

# CHAPTER 7: CONCLUDING REMARKS

Mass spectrometry (MS) is constantly adapting and changing and has become an important analytical tool in the field of proteomics. Vast banks of tandem mass spectrometry ($MS^n$ or MS/MS) data generated during high throughput MS processes need special processing software for interpretation. Fundamental studies of dissociation of peptides are therefore required to improve the precision of algorithms for peak picking and peptide sequencing. While an increasing number of proteins of the human proteome have been identified,[1-5] certain types of peptides, including acidic peptides, can be challenging to analyze.

The work presented in this dissertation has provoked many questions. In Chapters 3-5, trivalent lanthanide cationization of acidic non-phosphorylated and phosphorylated peptides produce metal-adducted ions with charges ranging from 2+ to 4+ by electrospray ionization (ESI). These metal-peptide complexes were dissociated by MS/MS and product ions investigated. The identity of the trivalent lanthanide metal cation had minimal, if any, effect on the type and abundance of product ions generated. Full sequence coverage occurred with $[M + Met]^{3+}$ and $[M + Met + H]^{4+}$ and almost complete backbone fragmentation with $[M + Pr - H]^{2+}$ for model peptides containing ten residues. Chapters 3, 4, and 5 described the investigation of a selected number of peptides (3 in Chapter 3, 25 in Chapter 4, and 26 in Chapter 5). To date, there is no literature available that presents a method for routinely analyzing highly acidic peptides. The work presented in this dissertation presents a consistent way to obtain sequence information for highly acidic peptides by MS/MS. In automated methods, entire cell lysate

contents are sometimes investigated. A first extension of this work could involve trivalent lanthanide metal cationization of a mixture of acidic peptides. This research could probe metal binding preferences of the different amino acid residues in the acidic peptides. Mass spectrometry (MS) methods are regularly paired with techniques such as high-performance liquid chromatography (HPLC)[6-8] to separate individual peptides generated from tryptic digests. Further research could investigate the possibility of post column trivalent lanthanide cation adduction to acidic peptides. This may better reflect the type of real-world MS applications performed and improve the chances of automation of the technique. Successful metallation could pave the way for studies to investigate metal adduction to a host of acidic peptides from tryptic digests. At present, no extensive metal adduction data repositories exist for electron based techniques. These studies could contribute to libraries of product ion peaks for metal-peptides complexes.

Chapter 5 is a study involving trivalent lanthanide metal cation adduction of acidic phosphorylated peptides. An interesting result was that the octapeptide A6pTA (spectrum shown in Figure 5.32) formed only y-ions as the C-terminal series, while the phosphoseryl and phosphotyrosyl analogs (A6pSA and A6pYA in Figures 5.33 and 5.44) form z- and y-ions by electron transfer dissociation (ETD) of $[M + Pr - H]^{2+}$. This trend was not observed for the hexapeptide analogs with similar sequences (A4pTA, A4pSA, and A4pYA in Figures 5.28, 5.29, and 5.30). Model peptides containing seven, nine and or ten residues with similar sequence (A5pXA, A7XA and A8XA, where X = pS, pT, and pY) could be investigated to determine if the trend is related to peptide size. Chapter 5 also focuses on peptides containing one phosphorylated residue. Proteins and peptides can have multiple sites of phosphorylation.[9-11] As discussed in Chapter 5, a phosphate group imparts acidic character onto a peptide. Peptides with

phosphorylated sites are highly acidic and even more so than those containing only aspartic and or glutamic acid residues. (See Table 5.1 for comparison of gas-phase acidity values of phosphorylated residues and aspartic or glutamic acid residues.) The study of Chapter 5 can be extended to include biological and model acidic peptides with more than one site of phosphorylation. These experiments would prove to be interesting and provide more insight into some trends observed in Chapters 4 and 5. In Chapter 4, model peptides with 7 amino acid residues and three acidic residues formed $[M + Pr]^{3+}$ and produced abundant backbone cleavage by ETD; just as much as the peptides with 7 residues and one acidic residue. Refer to Figures 4.10 and 4.11. In addition, the biological acidic phosphorylated DNA transcription inhibitory peptide and analogs (EDDpSDEEN, EDDpTDEEN, and EDDpYDEEN) formed abundant $[M + Pr]^{3+}$ despite having only acidic residues. The presence of only acidic residues may facilitate metal binding by providing many acid sites for coordination.

Another type of post-translational modification that adds acidic character to a peptide is sulfonation. Amino acid residues such as serine, threonine, tyrosine, and methionine sulfonate with as much as 1% of all eukaryotic tyrosine residues undergoing sulfonation.[12] In serine, threonine, and tyrosine, a sulfonate group ($-OSO_3H$) replaces the hydroxyl group (-OH). Like phosphorylation, sulfonation is critical to a host of biological functions. One example is in the gastrin family of proteins including sulfonated gastrin and cholecystokinin that are involved in enzyme secretion and growth stimulation in adult gastrointestinal systems.[13,14] Another example is in hirudin protein found in leeches[15] where the last C-terminal sulfonated portion of the protein is essential for performing the blood clotting inhibition activity.[16] Sulfonate groups are acidic and sulfonated peptides often contain aspartic and or glutamic acid residues four or five residues removed from them.[15,17,18] Sulfonated peptides undergo facile deprotonation and can be cleaved

making identification of the site of sulfonation more improbable.[19-22] However, electron capture dissociation (ECD) and ETD metallated studies show that metal adduction helps retain the sulfonate group and allows unambiguous identification of location of site of phosphorylation.[23,24] Electron transfer dissociation studies investigating the effects of trivalent lanthanide metal catitonization on acidic sulfated peptides can be compared to the phosphorylated acidic peptide studies in Chapter 5.

The work presented in Chapter 6 for enhanced protonation of peptides by $Cr^{3+}$ can be explored further involving acidic peptides. The enhanced protonation was observed in a transition metal study by former Cassady group member Dr. Heather Watson.[25] Formation of $[M + 2H]^{2+}$ by ESI would allow these acidic peptides to be analyzed by MS/MS methods just like basic peptides. Previous Cassady group member Dr. Changgeng Feng found that enhanced protonation was more pronounced for acidic peptides than for neutral or basic peptides.[26] Currently, the Cassady group is investigating enhanced protonation of acidic non-phosphorylated peptides by $Cr^{3+}$. This work could be extended to include phosphorylated peptides. Another class of post translationally modified peptides, sulfonated peptides, discussed in the paragraph above can also be included in this study. One challenge would be to keep the sulfonated site from cleaving during ESI. Studies indicate that the sulfonate group is not as robust as the phosphate group and is susceptible to alterations at low pH values and under solution and gas-phase conditions.[27-29] Our previous work indicates that the pH of the solution becomes more acidic with addition of $Cr^{3+}$. Another expansion of Chapter 6 should include investigation of enhanced protonation on acidic peptide mixtures to reflect biological digests and lysates employed in automated MS techniques.

The work in this dissertation presents some information to be added to the field of metallated studies of peptides by mass spectrometry. The contribution will increase knowledge of metal-peptide complex fragmentation by MS/MS techniques. Metallated studies are important since some proteins only become functional in the presence of a metal ion as briefly described in Chapter 1. Classes of peptides that are routinely difficult to protonate by ESI, such as acidic peptides, can benefit from adduction to trivalent lanthanide metal cations. Formation of the multiply positively charged ions will allow electron-based processes such as ETD and ECD to be increasingly utilized for investigation of peptides.

## References


1. Human Proteome Organization: Chromosome-based Human Proteome Project (C-HPP). *https://hupo.org/C-HPP* (accessed on Feb 19, 2018).

2. Omenn, G. S.; Lane, L.; Lundberg, E. K.; Beavis, R. C.; Overall, C. M.; Deutsch, E. W. Metrics for the Human Proteome Project 2016: Progress on Identifying and Characterizing the Human Proteome, Including Post-Translational Modifications. *J. Proteome Res.* **2016**, *15*, 3951-3960.

3. Human Proteome Organization: The Human Proteome Project Mission. *https://hupo.org/human-proteome-project* (accessed on Feb 19, 2018).

4. Omenn, G. S.; Lane, L.; Lundberg, E. K.; Beavis, R. C.; Nesvizhskii, A. I.; Deutsch, E. W. Metrics for the Human Proteome Project 2015: Progress on the Human Proteome and Guidelines for High-Confidence Protein Identification. *J. Proteome Res.* **2015**, *14*, 3452-3460.

5. Cantor, D. I.; Nice, E. C.; Baker, M. S. Recent Findings From the Human Proteome Project: Opening the Mass Spectrometry Toolbox to Advance Cancer Diagnosis, Surveillance and Treatment. *Expert Rev. Proteomics* **2015**, *12*, 279-293.

6. Zhang, Y.; Fonslow, B. R.; Shan, B.; Baek, M.; Yates, J. R. Protein Analysis by Shotgun/Bottom-up Proteomics. *Chem. Rev.* **2013**, *113*, 2343-2394.

7. Ebert, R. F.; Bell, W. R. Assay of Human Fibrinopeptides by High-Performance Liquid Chromatography. *Anal. Biochem.* **1985**, *148*, 70-78.

8. Madsen, J. A.; Xu, H.; Robinson, M. R.; Horton, A. P.; Shaw, J. B.; Giles, D. K.; Kaoud, T. S.; Dalby, K. N.; Trent, M. S.; Brodbelt, J. S. High-throughput Database Search and Large-scale Negative Polarity Liquid Chromatography-Tandem Mass Spectrometry With Ultraviolet Photodissociation for Complex Proteomic Samples. *Mol. Cell. Proteomics* **2013**, *12*, 2604-2614.

9. Cohen, P. The Regulation of Protein Function by Multisite Phosphorylation– A 25 Year Update. *Trends Biochem. Sci.* **2000**, *25*, 596-601.

10. Stensballe, A.; Jensen, O. N.; Olsen, J. V.; Haselmann, K. F.; Zubarev, R. A. Electron Capture Dissociation of Singly and Multiply Phosphorylated Peptides. *Rapid Commun. Mass Spectrom.* **2000**, *14*, 1793-2000.

11. Kyono, Y.; Sugiyama, N.; Tomita, M.; Ishihama, Y. Chemical Dephosphorylation for Identification of Multiply Phosphorylated Peptides and Phosphorylation Site Determination. *Rapid Commun. Mass Spectrom.* **2010**, *24*, 2277-2282.

12. Baeuerle, P. A.; Huttner, W. B. Tyrosine Sulfation of Yolk Protein-1, Protein-2, and Protein-3 in Drosophila-Melanogaster. *J. Biol. Chem.* **1985**, *260*, 6434-6439.

13. Barrowman, J. The Trophic Action of Gastro-intestinal Hormones. *Digestion* **1975**, *12*, 92-104.

14. Rehfeld, J. F.; Vansolinge, W. W. The Tumor Biology of Gastrin and Cholecystokinin. *Advances in Cancer Research, Vol 63* **1994**, *63*, 295-347.

15. Markwardt, F. Pharmacology of Hirudin: One Hundred Years After the First Report of the Anticoagulant Agent in Medicinal Leeches. *Biomed. Biochim. Acta* **1985**, *44*, 1007-1013.

16. Chang, J. The Functional Domain of Hirudin, a Thrombin-specific Inhibitor. *FEBS Lett.* **1983**, *164*, 307-313.

17. Hortin, G.; Folz, R.; Gordon, J. I.; Strauss, A. W. Characterization of Sites of Tyrosine Sulfation in Proteins and Criteria for Predicting Their Occurrence. *Biochem. Biophys. Res. Commun.* **1986**, *141*, 326-333.

18. Lin, W. H.; Larsen, K.; Hortin, G. L.; Roth, J. A. Recognition of Substrates by Tyrosylprotein Sulfotransferase. Determination of Affinity by Acidic Amino Acids Near the Target Sites. *J. Biol. Chem.* **1992**, *267*, 2876-2879.

19. Medzihradszky, K. F.; Darula, Z.; Perlson, E.; Fainzilber, M.; Chalkley, R. J.; Ball, H.; Greenbaum, D.; Bogyo, M.; Tyson, D. R.; Bradshaw, R. A.; Burlingame, A. L. O-Sulfonation of Serine and Threonine: Mass Spectrometric Detection and Characterization of a New Posttranslational Modification in Diverse Proteins Throughout the Eukaryotes. *Mol. Cell. Proteomics* **2004**, *3*, 429-440.

20. Rappsilber, J.; Steen, H.; Mann, M. Labile Sulfogroup Allows Differentiation of Sulfotyrosine and Phosphotyrosine in Peptides. *J. Mass Spectrom.* **2001**, *36*, 832-833.

21. Nemeth-Cawley, J. F.; Karnik, S.; Rouse, J. C. Analysis of Sulfated Peptides Using Positive Electrospray Ionization Tandem Mass Spectrometry. *J. Mass Spectrom.* **2001**, *36*, 1301-1311.

22. Taylor, S. W.; Sun, C.; Hsieh, A.; Andon, N. L.; Ghosh, S. S. A Sulfated, Phosphorylated 7 kDa Secreted Peptide Characterized by Direct Analysis of Cell Culture Media. *J. Proteome Res.* **2008**, *7*, 795-802.

23. Medzihradszky, K.; Guan, S.; Maltby, D.; Burlingame, A. Sulfopeptide Fragmentation in Electron-Capture and Electron-Transfer Dissociation. *J. Am. Soc. Mass Spectrom.* **2007**, *18*, 1617-1624.

24. Liu, H.; Håkansson, K. Electron Capture Dissociation of Tyrosine O-Sulfated Peptides Complexed with Divalent Metal Cations. *Anal. Chem.* **2006**, *78*, 7570-7576.

25. Watson, H. M. Effects of Transition Metal Cationization on Peptide Dissociation by Mass Spectrometry. Ph.D. Dissertation, The University of Alabama, Tuscaloosa, AL, USA, 2011.

26. Feng, C.; Commodore, J. J.; Cassady, C. J. The Use of Chromium(III) to Supercharge Peptides by Protonation at Low Basicity Sites. *J. Am. Soc. Mass Spectrom.* **2015**, *26*, 347-358.

27. Kitagawa, K.; Aida, C.; Fujiwara, H.; Yagami, T.; Futaki, S.; Kogire, M.; Ida, J.; Inoue, K. Facile Solid-phase Synthesis of Sulfated Tyrosine-containing Peptides: Total Synthesis of Human Big Gastrin-II and Cholecystokinin (CCK)-39(1,2). *J. Org. Chem.* **2001**, *66*, 1-10.

28. Seibert, C.; Sakmar, T. P. Toward a Framework for Sulfoproteomics: Synthesis and Characterization of Sulfotyrosine-containing Peptides. *Biopolymers* **2008**, *90*, 459-477.

29. Bettelheim, F. R. Tyrosine-O-Sulfate in a Peptide from Fibrinogen. *J. Am. Chem. Soc.* **1954**, *76*, 2838-2839.